

Advancing Phenotypic Drug Discovery  
for Cardiac Hypertrophy:  
Development and Application of  
a High-Throughput and High-Content  
Screening Platform

**Dissertation**

zur Erlangung des akademischen Grades  
Doktor der Naturwissenschaften  
(Dr. rer. nat.)

Vorgelegt von  
Pia Steinkuhl

Mathematisch-Naturwissenschaftliche Fakultät  
der Christian-Albrechts-Universität zu Kiel  
Kiel, 2025







## **Vorbemerkung**

Die vorliegende Arbeit wurde unter Anleitung von Prof. Dr. Dennis Schade in der Zeit von September 2021 bis Mai 2025 an der Mathematisch-Naturwissenschaftlichen Fakultät der Christian-Albrechts-Universität zu Kiel angefertigt.

1. Gutachter

Prof. Dr. Dennis Schade

2. Gutachter

Prof. Dr. Oliver Müller

Tag der mündlichen Prüfung:

08. Juli 2025

Zum Druck genehmigt:

08. Juli 2025



“cause there were pages turned with the bridges burned,  
everything you lose is a step you take.”

Taylor Swift

**Table of Contents**

<b>Table of Contents.....</b>	<b>I</b>
<b>Abstract .....</b>	<b>III</b>
<b>Kurzzusammenfassung.....</b>	<b>IV</b>
<b>Congress Contributions .....</b>	<b>V</b>
<b>Manuscript in preparation .....</b>	<b>V</b>
<b>Abbreviations .....</b>	<b>VI</b>
<b>1. Introduction.....</b>	<b>1</b>
1.1 Pathophysiology of Cardiac Hypertrophy .....	1
1.2 Therapeutic Strategies to Treat Cardiac Hypertrophy.....	4
1.3 Discovery Approaches for Novel Drug Candidates.....	7
1.4 Current Models in Cardiovascular Drug Discovery .....	9
<b>2. Aims of the Thesis .....</b>	<b>13</b>
<b>3. Materials and Instruments.....</b>	<b>17</b>
3.1 Chemicals .....	17
3.2 Disposable Materials.....	23
3.3 Instruments .....	24
3.4 Software .....	27
<b>4. Methods .....</b>	<b>29</b>
4.1 Cell Culture .....	29
4.2 Protein Analysis .....	33
4.3 mRNA Analysis .....	35
4.4 Immunocytochemistry and Image Analysis .....	37
4.5 Statistical Data Analysis .....	39
<b>5. Results and Discussion.....</b>	<b>41</b>
5.1 Novel Phenotypic Assay for Cardiac Hypertrophy Characterisation .....	41
5.1.1 Establishing a Custom Semi-Automated Image Analysis Pipeline.....	41
5.1.2 Validation of a Mixed Cardiac Cell Culture System .....	46
5.1.3 Mixed Cardiac Culture Compared to Purified Cardiomyocytes .....	52
5.1.4 Comparison of Two Imaging Systems.....	56

5.1.5 Establishing a Confirmatory qPCR Assay .....	58
5.1.6 A “Therapeutic Assay” Approach: Rescue of the Hypertrophy Phenotype .....	60
5.1.7 Summary .....	64
5.2 Targeting GRK5: A Novel Therapeutic Avenue in Cardiac Hypertrophy .....	66
5.2.1 Role of GRKs in Cardiac Hypertrophy and Drug Targeting .....	66
5.2.2 Target Validation of GRK5 .....	69
5.2.3 Assessment of Cellular Efficacy of GRK5 Inhibitors .....	71
5.2.4 Summary .....	79
5.3 L-2HG as a Hypertrophy Driver and Potential Therapeutic Target .....	82
5.3.1 Interplay of L-2HG and Glutamine.....	82
5.3.2 Phenotypic Profiling of L-2HG and Glutamine .....	85
5.3.3 Targeting the Glutamine Metabolism .....	87
5.3.4 Summary .....	94
5.4 Cardiodepressive Effects of Colon Cancer Patients’ Blood Serum.....	97
5.4.1 Translational Research: The Tumour-Heart Axis .....	97
5.4.2 Screening Results of Serum Samples.....	98
5.4.3 Correlation of Patient Data with Cardiac Response .....	104
5.4.4 Summary .....	109
<b>6. Conclusion and Outlook.....</b>	<b>111</b>
<b>7. Appendix .....</b>	<b>115</b>
7.1 Radar Plots Hypertrophy stimulants.....	115
7.2 Declaration of Consent for Blood Serum Biobank .....	116
7.3 Full Data set: Correlation of Patient Data with Cardiac Response.....	118
7.3.1 Mixed Cardiac Cells .....	118
7.3.2 Purified Cardiomyocytes .....	122
<b>8. References .....</b>	<b>127</b>
<b>Erklärung zu §8 der Promotionsordnung.....</b>	<b>i</b>

## Abstract

Cardiovascular diseases (CVDs) remain the leading cause of death globally, with an increasing burden driven by an aging population and the rise of metabolic disorders. Among CVDs, cardiac hypertrophy, a hallmark of heart failure progression, poses a significant clinical challenge. Current therapies often fail to reverse the underlying pathological remodelling, underscoring the need for innovative therapeutic strategies.

This thesis presents a high-throughput, high-content phenotypic screening platform to address this gap in cardiac drug discovery. A mixed cardiac cell culture derived from neonatal rat hearts was established, allowing simultaneous investigation of cardiomyocytes and non-cardiomyocytes within a shared microenvironment. This model better reflects native cardiac tissue than conventional purified cardiomyocyte monocultures. A custom CellProfiler-based image analysis pipeline was implemented to extract multi-parametric morphological data, merged in a robust 'Hypertrophy Score'. An orthogonal qPCR assay was implemented to validate transcriptional changes linked to cardiac remodelling.

The platform was first applied to investigate G protein-coupled receptor kinase 5 (GRK5), an emerging but underexplored target in cardiac hypertrophy. Using a GRK5-focused inhibitor library, the assay platform generated meaningful cellular structure-activity relationships (SAR) to correlate with biochemical IC<sub>50</sub> values and physicochemical features. GRK5 inhibitor **4a** emerged as a highly effective, non-toxic anti-hypertrophic agent, with its inactive optical antipode **4b** serving as an ideal negative control. This data guides further lead optimisation for successful *in vivo*-translation.

Secondly, building on evidence of metabolic rewiring, the role of L-2-hydroxyglutarate (L-2HG) as a novel pro-hypertrophic metabolite was investigated. L-2HG induced robust hypertrophy comparable to adrenergic stimuli. Given its metabolic link to glutamine, small-molecule inhibitors targeting glutaminase (GLS1) and glutamine uptake were systematically profiled in the phenotypic assay platform. GLS1 inhibition effectively suppressed hypertrophy and non-cardiomyocyte proliferation, suggesting a potentially new pharmacological approach for anti-hypertrophic intervention.

Lastly, the screening platform was leveraged to explore the tumour-heart axis by assessing cardiomyocyte responses to serum from colorectal cancer patients. Patient serum induced proliferative effects across cell populations but suppressed hypertrophic markers, suggesting circulating tumour-derived factors with cardiodepressive properties. Correlation analyses linked serum effects to tumour burden, age and sex, providing novel insight into systemic disease impacts on cardiac function.

Collectively, this thesis introduces a novel multiparametric platform for cardiac drug discovery, demonstrating the power of combining high-content phenotyping, translational models and targeted interventions to address unmet clinical needs in cardiac hypertrophy.

## Kurzzusammenfassung

Kardiovaskuläre Erkrankungen (CVDs) sind die häufigste Todesursache weltweit, mit steigender Prävalenz durch Alterung der Bevölkerung und zunehmende Stoffwechselstörungen. Innerhalb der Krankheitsgruppe stellt die kardiale Hypertrophie als zentrales Merkmal der Herzinsuffizienz eine besondere Herausforderung dar. Aktuelle Therapien können die zugrunde liegende pathologische Umstrukturierung oft nicht rückgängig machen, was den Bedarf an neuen therapeutischen Ansätzen hervorhebt.

Diese Arbeit beschreibt eine hochdurchsatzfähige, multiparametrische und phänotypische *Screening*-Plattform für das kardiovaskuläre *Drug Discovery*. Es wurde ein gemischtes kardiales Zellmodell aus neonatalen Rattenherzen etabliert, das die gleichzeitige Untersuchung von Kardiomyozyten und nicht-Kardiomyozyten im gemeinsamen Milieu erlaubt und nativen Gewebeverhältnissen näherkommt als konventionelle Monokulturen von Kardiomyozyten. Eine eigens entwickelte CellProfiler-Bildanalyse extrahiert morphologische Merkmale, die in einem robusten „Hypertrophie-Score“ zusammengefasst werden. Ergänzend dient ein orthogonaler qPCR-Assay zur Validierung transkriptioneller Veränderungen.

Zunächst wurde die Plattform auf die G Protein-gekoppelte Rezeptor Kinase 5 (GRK5) angewendet; ein wenig erforschtes Wirkstoffziel. Eine fokussierte Inhibitor Bibliothek ermöglichte die Korrelation zellulärer Struktur-Wirkungs-Beziehungen mit biochemischen IC<sub>50</sub>-Werten und physikochemischen Parametern. Der GRK5-Inhibitor **4a** zeigte starke anti-hypertrophe Effekte bei guter Verträglichkeit; das inaktive Enantiomer **4b** diente als ideale Negativkontrolle. Diese Ergebnisse dienen der weiteren Leitstrukturoptimierung zur erfolgreichen *in vivo* Translation.

Im zweiten Teil wurde auf Basis der metabolischen Reprogrammierung L-2-Hydroxyglutarat (L-2HG) als neuartiger pro-hypertropher Metabolit untersucht. Aufgrund der metabolischen Verbindung zu Glutamin wurden niedermolekulare Inhibitoren systematisch untersucht, die entweder die Glutaminase 1 (GLS1) oder die Glutaminaufnahme hemmen. Die Hemmung von GLS1 unterdrückte wirksam die Hypertrophie sowie die Proliferation von nicht-Kardiomyozyten und weist damit auf einen potenziell neuen pharmakologischen Ansatz zur anti-hypertrophen Therapie hin.

Abschließend wurde die Plattform genutzt, um Serumeffekte kolorektaler Krebspatienten auf kardiale Zellen zu untersuchen. Das Patientenserum förderte die Zellproliferation, unterdrückte jedoch Hypertrophie-assoziierte Marker, was auf kardiodepressive, tumorderivierte Faktoren hinweist. Die Wirkung korrelierte mit Tumorlast, Alter und Geschlecht und liefert neue Einblicke in systemische Effekte auf die Herzfunktion.

Zusammengefasst stellt diese Arbeit eine neuartige, multiparametrische Plattform für die kardiologische Wirkstoffforschung vor und zeigt, wie die Kombination aus hochinhaltsbasierter Phänotypisierung, translationalen Modellen und gezielten Interventionen helfen kann, therapeutische Lücken bei kardialer Hypertrophie zu schließen.



## Congress Contributions

Parts of this work were presented as:

### **A semi-automated high-content assay in neonatal cardiomyocytes for high-throughput profiling of hypertrophy phenotypes**

Pia Steinkuhl\*, Carmen Carrillo García, Axel Choidas, Matthias Baumann, Oliver J Müller, Dennis Schade

EFMC-ISMIC **2024**, Rome, 01.09.2024 – 05.09.2024, scientific poster

EMFC-YMCS **2024**, Rome, 05.09.2024 – 06.09.2024, scientific poster and flash poster presentation

\* Presenting author

## Manuscript in preparation

### **High-throughput cardiac hypertrophy phenotyping supports lead optimization of GRK5 inhibitors**

Pia Steinkuhl, Anca Kliesow Remes, Carmen Carrillo García, John J G Tesmer, Oliver J Müller, Dennis Schade

Original Article (*in preparation*)

## Abbreviations

<b>A</b>	ACE	Angiotensin-converting enzyme
	AI	Artificial intelligence
	$\alpha$ -KG	$\alpha$ -ketoglutarate
	Ang. II	Angiotensin II
	ANP	Atrial natriuretic peptide
	APS	Ammonium peroxydisulfate
	ARB	Angiotensin II receptor blocker
	ARNI	Angiotensin receptor neprilysin inhibitor
	AT1	Angiotensin II receptor
<b>B</b>	BCA	Bicinchoninic acid
	BMB	Biomaterial bank
	BNP	B-type natriuretic peptide
	BPTES	Bis-2-(5-phenylacetamido-1,3,4thiadiazol-2-yl) ethyl sulfide
	BSA	Bovine serum albumin
<b>C</b>	CCC	Comprehensive Cancer Center
	cDNA	Complementary DNA
	CM	Cardiomyocyte
	CRT	Cardiac resynchronisation therapy
	CVD	Cardiovascular disease
<b>D</b>	DMEM	Dulbecco's modified Eagle's medium
	DMSO	Dimethyl sulfoxide
<b>E</b>	ECL	Enhanced chemiluminescence
	EDTA	Ethylenediaminetetraacetic acid
	EHT	Engineered heart tissues
	EMA	European Medicines Agency
	ESC	European Society of Cardiology
	ET-1	Endothelin-1
<b>F</b>	FA	Formaldehyde
<b>G</b>	GAC	Glutaminase C
	GDH	Glutamate dehydrogenase
	GLS	Glutaminase
	GPCR	G protein-coupled receptor
	GRK	G protein-coupled receptor kinase
	GSK3 $\beta$	Glycogen synthase kinase 3 $\beta$
<b>H</b>	HCM	Hypertrophic cardiomyopathy
	HDAC	Histone deacetylases

	HEPES	4-(2-hydroxyethyl)-1-piperazineethanesulfonic acid
	hERG	Ether-à-go-go-related gene
	HRP	Horseradish peroxidase
	HTS	High-throughput screening
<b>I</b>	IDH	Isocitrate dehydrogenase
	iPSC-CM	Induced pluripotent stem cell-derived cardiomyocytes
<b>K</b>	KGA	Kidney isoform of glutaminase
<b>L</b>	LDH	Lactate dehydrogenase
	LIF	Leukemia inhibitory factor
	LVAD	Left ventricular assist devices
<b>M</b>	MDH	Malate dehydrogenase
	MEF2	Myocyte enhancer factor-2
	MHC	Myosin heavy chain
	MIPDD	Mechanism-informed phenotypic drug discovery
	MoA	Mode of action
	MRA	Mineralocorticoid receptor antagonists
	MTBST	Milk TRIS buffered saline with TritonX
<b>N</b>	NE	Norepinephrine
	NRCM	Neonatal rat cardiomyocyte
<b>P</b>	P/S	Penicillin/streptomycin
	P1-3	Postnatal day 1-3
	P2N	Popgen 2.0 network
	P5	Postnatal day 5
	PAGE	Polyacrylamide gel electrophoresis
	PBS	Phosphate buffered saline
	PCR	Polymerase chain reaction
	PDD	Phenotypic drug discovery
	PE	Phenylephrine
	PVDF	Polyvinylidene difluoride
<b>Q</b>	qPCR	Quantitative real time PCR
<b>R</b>	RAAS	Renin-angiotensin-aldosterone system
	ROS	Reactive oxygen species
<b>S</b>	SAR	Structure-activity relationship
	SB	Staining buffer
	SDS	Sodium dodecyl sulfate
	SGLT2	Sodium-glucose co-transporter 2
	siRNA	Small interfering RNA

	SLC1A5	Solute carrier family 1 neural amino acid transporter member 5
<b>T</b>	TAC	Transverse aortic constriction
	TBST	TRIS buffered saline with TritonX
	TCE	2,2,2-Trichloroethanol
	TEMED	<i>N,N,N',N'</i> -Tetramethylethylenediamine
	TGF $\beta$	Transforming growth factor $\beta$
	TML	Timolol
	TRIS	Tris-(hydroxymethyl)-amino methane
<b>U</b>	UKSH	University Hospital Schleswig-Holstein
	UV	Ultraviolet light



## 1. Introduction

### 1.1 Pathophysiology of Cardiac Hypertrophy

Cardiovascular diseases (CVDs) encompass a broad spectrum of disorders affecting the heart and blood vessels, making them a leading cause of morbidity and mortality worldwide<sup>[1, 2]</sup>. Their multifactorial aetiology includes genetic predisposition, environmental influences and lifestyle-related risk factors such as hypertension, obesity and smoking. With an aging population and increasing prevalence of metabolic disorders, the incidence of CVDs continues to rise in many European countries<sup>[1]</sup>. Despite significant advances in therapeutic strategies, the persistently high mortality rates highlight the urgent need for more effective and targeted treatment options<sup>[3]</sup>.

One key pathological adaptation in many CVDs is cardiac hypertrophy, a compensatory response of the heart characterised by an increase in cardiomyocyte size. During embryonic development, this is accompanied by cell proliferation<sup>[4]</sup>. However, soon after birth, cardiomyocytes exit the cell cycle and lose the ability to proliferate, leaving hypertrophic growth as the predominant mechanism of postnatal cardiac development<sup>[5]</sup>. When the heart is subjected to increased demands, for example during pregnancy or in athletes, physiological hypertrophic growth occurs. This type of growth is characterised by a reversible increase in cardiomyocyte size accompanied by the maintenance of physiological architecture and structure<sup>[6]</sup>. In contrast, chronic alterations in cardiovascular stress can lead to pathological cardiac hypertrophy, an adaptive response to increased wall tension<sup>[7]</sup>. To compensate for these demands, the ventricular wall thickens according to Laplace's law, initially maintaining stroke volume and functionality<sup>[8, 9]</sup>. However, if the underlying cause of the increased workload persists, the heart undergoes irreversible remodelling, resulting in dysfunction and ultimately leading to heart failure<sup>[8, 9]</sup>.

Pathological cardiac hypertrophy can arise from conditions that impose pressure overload on the heart, like hypertension or aortic stenosis. Additionally, diseases causing volume overload, like aortic or mitral regurgitation and septal defects, can also induce hypertrophic growth<sup>[10]</sup>. When hypertrophy arises from genetic mutations in sarcomere proteins or from non-genetic factors unrelated to abnormal loading, such as inflammation or multisystem diseases, it is classified as hypertrophic cardiomyopathy (HCM)<sup>[11]</sup>.

In addition to biomechanical stress, several neurohumoral systems contribute to the development of hypertrophy<sup>[10, 12]</sup>. Cardiovascular reflexes originating from various baroreceptors and chemoreceptors activate neurohumoral systems to compensate for impaired cardiac function by modifying heart rate, contractility and blood pressure. The latter is achieved through salt and water retention and the constriction of peripheral blood vessels<sup>[13]</sup>.

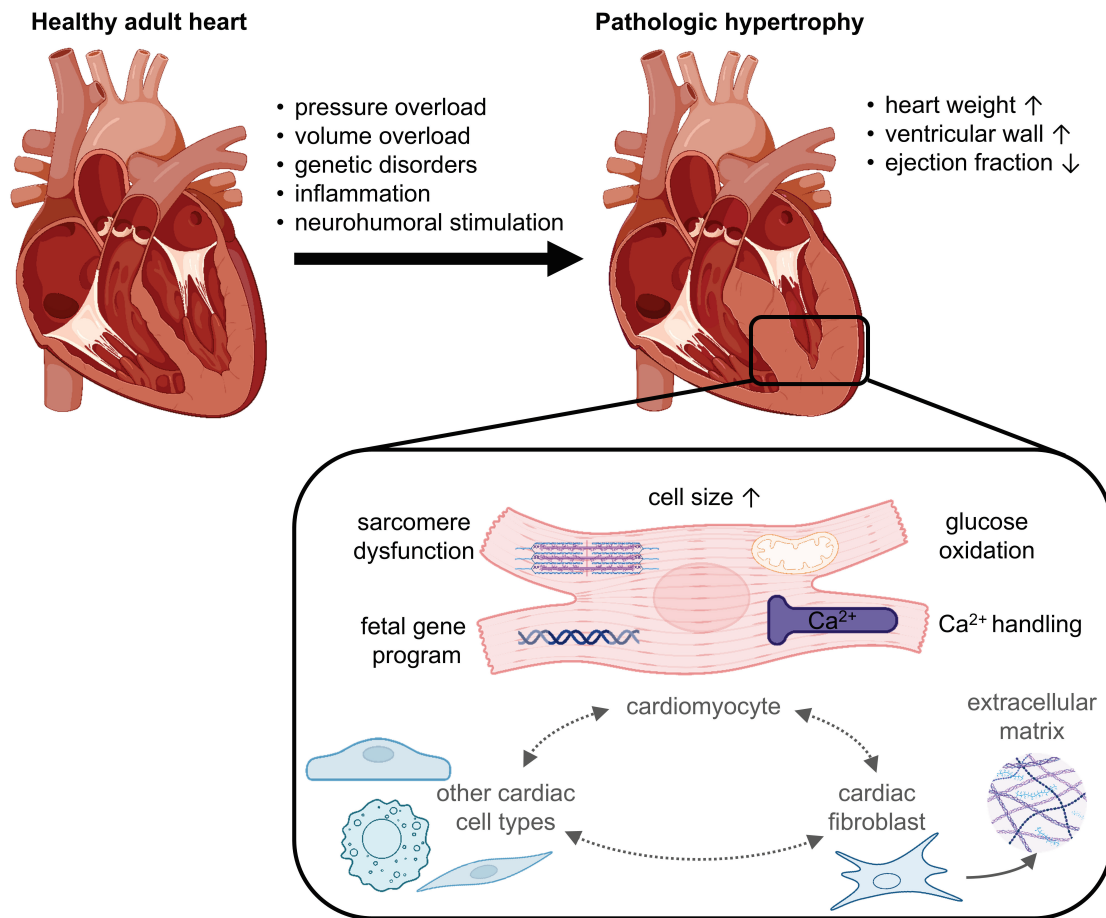


**Figure 1: Pathology of cardiac hypertrophy.** Multifactorial aetiology leads to the development of cardiac hypertrophy, characterised by distinct morphometric, molecular and metabolic changes.

One of these activated systems is the sympathetic nervous system, which releases the catecholamines norepinephrine and epinephrine. These neurotransmitters bind to G protein-coupled receptors (GPCRs) on cell surfaces, activating intracellular signalling pathways. In cardiac cells, this activation increases heart rate (positive chronotropy), contractility (positive inotropy), cardiac relaxation (positive lusitropy) and impulse conduction (positive dromotropy). In vascular cells, it promotes constriction of smooth muscle cells, further increasing blood pressure<sup>[14]</sup>.

The renin-angiotensin-aldosterone system (RAAS) also plays a significant role by increasing salt and water retention as well as promoting vasoconstriction. Both the angiotensin II receptor (AT1) and aldosterone receptors are expressed in cardiomyocytes and cardiac fibroblasts, promoting hypertrophic and fibrotic responses, inflammation and oxidative stress<sup>[15, 16]</sup>. Renal adrenergic  $\beta$ -receptors stimulate the release of renin, thereby linking the sympathetic nervous system to RAAS<sup>[13]</sup>.

Moreover, several cytokines, chemokines and inflammatory mediators have been identified as key players in hypertrophy and heart failure. Persistent low-grade inflammation, triggered

by continuous tissue damage or stress, attempts to restore homeostasis. Adrenergic and RAAS activation exacerbate cardiac inflammation, highlighting the multifactorial aetiology of cardiac hypertrophy, which involves distinct but interrelated origins<sup>[17, 18]</sup>.

At the cellular level, the disease is characterised by an increase in cardiomyocyte size, an upregulation of protein synthesis and a regression to the fetal gene program<sup>[19]</sup>. This reversion includes a shift back to the fetal protein expression, affecting metabolism, sarcomere organisation and hormone production<sup>[20]</sup>. Increased oxygen consumption leads to hypoxia in cardiac tissue, prompting a shift to glucose consumption as a more efficient energy source compared to fatty acid oxidation<sup>[21]</sup>. To maintain adequate contractility, a decrease of sarcomere protein  $\alpha$ -myosin heavy chain (MHC) expression occurs, while  $\beta$ -MHC production increases<sup>[22]</sup>. Concurrently, a dysregulation of  $\text{Ca}^{2+}$ -handling proteins influences intracellular  $\text{Ca}^{2+}$ -concentration and myofilament sensitivity, thereby further altering the hearts contractility<sup>[8, 23]</sup>. In response, the heart produces higher levels of cardioprotective hormones, namely atrial natriuretic peptide (ANP) and B-type natriuretic peptide (BNP). These hormones regulate blood pressure through natriuresis, vasodilatation and RAAS inhibition. They also induce metabolic changes, like increased lipid oxidation and improved insulin sensitivity<sup>[24]</sup>. Thereby, they protect the heart against hypertrophy progression, fibrosis and heart failure<sup>[8, 9]</sup>.

Other cardiac cell types also contribute to hypertrophic development. For example, cardiac fibroblasts proliferate in response to biochemical and neurohumoral stimulation, promoting fibrosis by accelerating extracellular matrix production<sup>[25]</sup>. On the other hand, crosstalk between endothelial cells and cardiomyocytes induces the expression of protective factors and cytokines by both cell types<sup>[26]</sup>.

These alterations in cardiac tissue, combined with the systemic effects of multiple stimulatory pathways, lead to irreversible remodelling, ventricular chamber dilation and further impairment of cardiac function. If untreated, this deterioration ultimately results in arrhythmias, heart failure and sudden death<sup>[8, 24]</sup>.



### 1.2 Therapeutic Strategies to Treat Cardiac Hypertrophy

Heart failure has an estimated global prevalence of 17 per 1,000 individuals, with over 39 per 1,000 affected in Germany during 2018-2019<sup>[27]</sup>. Furthermore, cardiac hypertrophy represents the leading risk factor for cardiovascular morbidity and mortality, emphasising the urgent need for novel and effective treatment strategies to prevent its progression to heart failure<sup>[2]</sup>.

The heterogeneous nature of cardiac hypertrophy presents a significant challenge for an effective therapy. For that reason, accurate diagnosis and identification of underlying causes are crucial for selecting the most appropriate treatment approach. Additionally, secondary complications, like arrhythmias or left ventricular outflow tract obstructions, further influence therapeutic decisions. The primary objectives of treatment are to reduce mortality, prevent hospitalisation and improve clinical outcomes, ultimately enhancing the quality of life<sup>[28]</sup>.

Standard therapy for cardiac hypertrophy and heart failure comprises a three-pillar regimen: dual inhibition of RAAS and additional inhibition of the sympathetic nervous system. Angiotensin-converting enzyme (ACE) inhibitors as well as angiotensin II receptor (AT1) blockers (ARB) are pivotal in treating hypertension and heart failure<sup>[28]</sup>. These agents reduce fluid retention, blood pressure and left ventricular preload and afterload. In the heart, AT1 and aldosterone receptors are expressed on both cardiomyocytes and cardiac fibroblasts, where their activation promotes hypertrophic and fibrotic responses. By inhibiting these receptors, ACE-inhibitors, ARBs or mineralocorticoid receptor antagonists (MRA) alleviate cardiac wall stress, improve left ventricular filling and partially reverse cardiac remodelling<sup>[15, 16]</sup>.

Novel combination therapy of ARBs with neprilysin inhibitor (ARNI) sacubitril has shown superior efficacy compared to monotherapy with ACE inhibitors or ARBs. This combination reduces hypertrophy and lowers plasma levels of hypertrophic biomarker pro-BNP<sup>[2]</sup>. Neprilysin, a metalloprotease, degrades numerous peptides including cardiac natriuretic peptides ANP and BNP. Inhibition of neprilysin increases circulating levels of ANP and BNP, enhancing their cardioprotective effects, which include natriuresis, vasodilatation and RAAS inhibition<sup>[29]</sup>.

Dual inhibition of RAAS with ACE inhibitor, ARBs or ARNI combined with MRA have shown the most effect in treating cardiac hypertrophy and heart failure<sup>[16]</sup>.

The third pillar of standard therapy involves  $\beta$ -blockers, which counteract chronic sympathetic nervous system activation.  $\beta$ -blockers protect the heart from overstimulation, restore downregulated receptor expression and improve contractility. By their negative chronotropic and negative inotropic effect, they improve left ventricular ejection fraction. While  $\beta$ -blocker therapy does not induce reverse remodelling, its combination with RAAS inhibitors enhances clinical outcomes<sup>[2, 14, 15]</sup>.

For patients intolerant to  $\beta$ -blockers, the European Society of Cardiology (ESC) guidelines recommend calcium channel blockers (CCBs) [28, 30]. Non-dihydropyridine CCBs, like verapamil and diltiazem, have similar negative inotropic and chronotropic effects while also reducing atrioventricular node conduction speed (negative dromotropic). These agents block L-type calcium channels in the heart, restoring impaired calcium handling in cardiomyocytes. In contrast, dihydropyridine CCBs predominantly induce vasodilatation by targeting vascular calcium channels, which is contraindicated for obstructive disease forms of hypertrophy or heart failure [15]. CCBs demonstrate short-term efficacy but limited long-term benefits, restricting their use to add-on therapy with RAAS inhibitors or diuretics [2, 27, 31].

As antihypertensive treatment, low dose loop or thiazide diuretics may be used to alleviate dyspnoea. However, hypovolemia must be avoided to prevent exacerbation of obstructive disease forms, requiring regular disease progression evaluation [28, 30].

For non-responsive or insufficiently responsive patients, additional treatments may include the class IA antiarrhythmic agent disopyramide. By blocking cardiac sodium channels, disopyramide reduces sodium influx and decreases excitability (negative bathmotropy). It also inhibits the Ether-à-go-go-related gene (hERG) potassium channel, prolonging action potential duration. Hence, treatment with disopyramide is contraindicated in patients with prolonged QT interval [15]. Other anti-arrhythmic drugs, along with anticoagulation therapy, may be used to address secondary arrhythmias and reduce thromboembolic risks [28, 30].

Another emerging add-on therapy is the use of sodium-glucose co-transporter 2 (SGLT-2) inhibitors. Initially developed for diabetes mellitus by inhibiting glucose reabsorption in the renal proximal tubule, these agents have demonstrated efficacy in improving cardiac function in heart failure patients. The mechanisms remain unclear but may involve mild natriuresis, osmotic diuresis, reduced preload and afterload as well as improved myocardial bioenergetics [16].

In 2023, the European Medicines Agency (EMA) approved mavacamten, the first-in-class cardiac myosin adenosine triphosphatase (ATPase) inhibitor, for the treatment of inherited HCM. By inhibiting myosin ATPase activity, mavacamten reduces the number of myosin heads available for ATP-dependent interactions with actin, thereby lowering energy consumption, reducing maximal tension in cardiac muscle fibres and reversing impaired mechanical and energetic properties of cardiac hypertrophy [15]. The ESC guidelines recommend mavacamten as co-treatment with  $\beta$ -blockers or CCBs at the maximum tolerated dose, since the monotherapy lacks sufficient clinical evidence [28, 30].

In summary, significant advancements in recent years have expanded the therapeutic landscape for cardiac hypertrophy and heart failure. While combinational therapy with RAAS inhibitors and  $\beta$ -blockers can alleviate symptoms and slow disease progression in some patients, a substantial proportion fails to achieve meaningful clinical benefits with these long-

established treatments. Complete regression of left ventricular mass remains rare and the risk of terminal heart failure or lethal arrhythmias persist<sup>[32]</sup>. Apart from mavacamten, few first-in-class drugs have entered the market in recent years, highlighting the need for innovative approaches targeting novel signalling pathways. Consequently, many pathophysiological mechanisms remain unaddressed, emphasising the necessity for new drug discovery efforts<sup>[33]</sup>.

For patients unresponsive to pharmacological therapy, mechanical support devices, like cardiac resynchronisation therapy (CRT) with dual-chamber pacemakers or left ventricular assist devices (LVADs), may be required. For refractory HCM patients, invasive septal reduction can alleviate disease symptoms. However, while these interventions offer additional management strategies, they also carry inherent risks, including infection and procedural complications. Ultimately, heart transplantation remains the final option for patients who respond to neither pharmacological nor invasive treatments, yet it is limited by a shortage of donor organs and is associated with a reduced life expectancy<sup>[2, 28, 30]</sup>.

### 1.3 Discovery Approaches for Novel Drug Candidates

Despite significant progress in the treatment of cardiovascular diseases (CVDs) over recent years, the decline in global mortality rates has plateaued, and CVDs remain the leading cause of death worldwide<sup>[1, 2]</sup>. While advancements in pharmacological and interventional therapies have improved patient outcomes, they have not been sufficient to counteract the growing burden of CVDs, particularly in aging populations. Additionally, drug innovation in cardiology has lagged behind other medical fields, such as oncology, resulting in a weak pipeline for novel cardiovascular therapeutics<sup>[34]</sup>. Many existing treatments focus on symptom management rather than targeting the underlying disease mechanisms, leaving a substantial gap in effective and curative options<sup>[35]</sup>.

To overcome these limitations, there is an urgent need to develop therapeutic agents that act on novel and previously unexplored pathways in cardiac hypertrophy and heart failure. Identifying innovative drug targets and modes of action (MoA) will be crucial in addressing the unmet medical needs in these conditions. Consequently, the exploration of new tools and approaches for drug discovery is essential to advance treatment strategies and improve clinical outcomes for affected patients.

Uncovering new therapeutic modalities in drug discovery relies on two primary approaches: target-based drug discovery (TDD) and phenotypic drug discovery (PDD). When a well-defined molecular target is implicated and validated in a disease, TDD serves as a powerful tool for identifying potential drug candidates. These targets are typically proteins, such as enzymes, ion channels, receptors or transporters<sup>[36]</sup>. However, recent advances in the field have expanded the scope of druggable targets to include lipids, carbohydrates, DNA and RNA, broadening the spectrum of possible therapeutic interventions<sup>[37]</sup>. With a clearly identified target, TDD allows for the direct investigation of molecular hypotheses, facilitating rational drug design through methods such as molecular docking and computational modelling<sup>[38]</sup>. Furthermore, the approach is well-suited for mostly biochemical, high-throughput screening, increasing the likelihood of identifying active compounds from extensive chemical libraries. This makes TDD particularly effective for optimising and improving existing drug classes by discovering follow-up candidates with enhanced efficacy and safety profiles<sup>[39]</sup>.

However, a key limitation of TDD is its reliance on prior knowledge of disease mechanisms and specific molecular targets. If a crucial target has not yet been identified, this approach may overlook potential therapeutic candidates. Additionally, focusing on a single molecular interaction might not be sufficient to achieve the desired clinical outcome, particularly for diseases with complex or multifactorial pathophysiology. TDD also carries the risk of missing drugs that act through unconventional or unknown mechanisms, as compounds that do not directly affect the chosen target are excluded from the screening process. As a result, issues such as poor translation from *in vitro* to *in vivo* efficacy and unforeseen off-target effects often

emerge at later stages of development, contributing to the high failure rates in drug discovery [39, 40, 41].

In contrast, PDD takes a broader, more holistic approach by identifying compounds that shift a disease phenotype toward a healthier state, without requiring prior knowledge of a specific molecular target. This makes it particularly advantageous for discovering first-in-class drugs that act on previously unknown pathways or through multi-target mechanisms [42]. Moreover, since phenotypic assays are typically designed to better replicate the complexity of disease biology, they offer a higher likelihood of translating *in vitro* findings into clinically relevant outcomes.

Despite these advantages, PDD presents its own challenges. Developing robust, physiologically relevant assay systems that faithfully mimic disease conditions can be technically demanding, particularly when integrating high-throughput capabilities. Additionally, while PDD enables the identification of promising drug candidates, understanding their precise mechanism of action requires subsequent target deconvolution, a challenging and resource-intensive process [39, 40, 42, 43].

To overcome the limitations of both TDD and PDD, mechanism-informed phenotypic drug discovery (MIPDD) has emerged as a promising hybrid approach. MIPDD aims to combine the unbiased, phenotypic screening of PDD with a mechanistic understanding of drug action typically associated with TDD. This approach enhances drug discovery success by integrating disease-relevant, physiologically complex assay systems while incorporating molecular insights that improve the identification of drug targets and pathways [44, 45].

However, the pharmaceutical industry still faces significant challenges, as a large proportion of drug candidates fail during the transition from preclinical development to clinical trials. This high attrition rate, often due to insufficient efficacy, unforeseen toxicity, poor pharmacokinetics or a lack of translatability from preclinical models to human physiology, coupled with the immense costs associated with drug development, underscores the urgent need for improved strategies to enhance efficiency and success rates. Given that the drug discovery and development process can take up to 12 years and cost approximately \$1.8 billion [46], while only 10-20% of clinical trial candidates receive approval [47], it is essential to develop robust assays with high predictive and translatable value. A key factor in this effort is the selection of appropriate *in vitro* models, which must accurately mimic the pathophysiological features of the disease while remaining cost-effective and balancing simplicity with complexity to generate meaningful insights.

## 1.4 Current Models in Cardiovascular Drug Discovery

For contemporary cardiovascular research, numerous assays have been established to study cardiac hypertrophy. *In vivo* models offer a superior physiological relevance in a systemic context compared to *in vitro* models<sup>[48, 49]</sup>. Rodents are commonly used due to their genetic tractability, cost effectiveness and well-established methodologies. However, larger animals, such as pigs and rabbits, have a higher translational value because their cardiovascular system more closely resembles that of humans<sup>[49, 50]</sup>. Cardiac hypertrophy is typically induced invasively through transverse aortic constriction (TAC), mimicking pressure overload hypertension<sup>[51]</sup>. In addition, genetically modified *in vivo* models are employed to investigate specific hypertrophic pathways, while spontaneously hypertensive rats are widely used to explore general effects without inter-individual genetic variation<sup>[50, 52, 53]</sup>. Lastly, pharmacological models involve the administration of biochemical hypertrophic agents like angiotensin II, phenylephrine or isoproterenol<sup>[53]</sup>.

Experimental outcomes in these hypertrophic models include morphometric changes like heart weight to tibia length or body mass, cardiomyocyte size and fibrosis. Functional alterations are assessed using echocardiography to measure ventricular wall thickness, contractility, cardiac output and ejection fraction<sup>[54]</sup>. Additionally, molecular biomarkers like ANP and BNP are analysed in plasma<sup>[55]</sup>.

*In vivo* models offer greater physiological relevance by enabling the study of organ-level and systemic interactions. However, ethical considerations and compliance with the 3Rs principles (reduction, refinement, replacement) necessitate minimising animal use<sup>[56]</sup>. Additionally, the high costs, demanding maintenance and complex experimental readouts make *in vivo* studies impractical for high-throughput screening in the early stages of drug discovery.

Here, models with higher throughput and reduced complexity are required. Consequently, a variety of *in vitro* models have been developed to facilitate the drug development process, ranging from high-throughput screening to detailed investigations of molecular interactions in specific cell types<sup>[48]</sup>. Permanent cell lines like H9C2 or HL1<sup>[57]</sup> are easy to culture and manipulate, but overall less frequently used as they do not exhibit the full functionality of bona fide cardiomyocytes<sup>[58]</sup>. More commonly, neonatal rats are used to isolate neonatal rat cardiomyocytes (NRCM) for primary cell culture. First described in 1960<sup>[59]</sup>, the dissociation of cardiac cells from neonatal rodent hearts has since been further refined<sup>[57, 60]</sup>. After tissue dissociation, the cardiomyocytes usually are purified from other cardiac cell types. Since cardiomyocytes attach slower to surfaces, they can be separated by differential attachment technique<sup>[61]</sup>, however protocols and purification efficiency vary in the literature<sup>[62]</sup>. Alternatively, Percoll gradient centrifugation is performed to separate cardiomyocytes from other cell types. While this method enables the targeted analysis of cardiomyocyte biology

without interference from other cell types<sup>[63]</sup>, it does not fully capture the complex composition of the *in vivo* heart. Crucial aspects of intercellular communication, such as direct cell-cell interactions and paracrine signalling, are not replicated<sup>[64]</sup>. Nevertheless, NRCMs remain the most widely used model due to their high availability and the reproducibility of dissociation and isolation. Unlike immortalised cell lines, NRCMs retain key functional properties, including contractility<sup>[58]</sup>.

Hypertrophy can be induced in NRCMs via biochemical stimulation, most commonly using either angiotensin II, endothelin-1, phenylephrine<sup>[65]</sup>, or by applying mechanical stress. For the latter, cardiomyocytes are cultured on silicone rubber slips, which can be stretched to a defined extent<sup>[66]</sup>. Hypertrophic effects are assessed by analysing morphological changes, the hallmark being an increase in cell size<sup>[57, 67]</sup>, as well as alterations in the expression of hypertrophy markers like ANP, BNP or  $\beta$ -MHC<sup>[68, 69]</sup>. Functional assays, including the measurements of contractility<sup>[69]</sup> and calcium transients<sup>[70]</sup>, are also commonly employed. Recent advancements in artificial intelligence (AI) and computational capabilities have allowed researchers to move beyond oversimplified, one-dimensional models, driving the evolution toward more comprehensive phenotypic systems. Few assays now encompass automated measurement of cell size<sup>[71]</sup> or even concurrent assessments of multiple phenotypic parameters, like size, perimeter, solidity and texture<sup>[68]</sup>, ranging up to in-depth single-cell morphological analysis with extended data processing protocols<sup>[67]</sup>.

Despite their advantages, NRCMs have notable limitations. These include their non-human origin and neonatal state, which differs from the mature cardiomyocytes in patients. Furthermore, the drive to reduce animal use in research has spurred the development of alternative systems for characterising hypertrophy *in vitro*. Induced pluripotent stem cell-derived cardiomyocytes (iPSC-CMs) offer a means of studying drug candidates in a human context<sup>[57, 67]</sup>, and even enable personalised approaches with patient-derived iPSCs<sup>[72]</sup>. However, iPSC-CMs remain immature and exhibit limited contractile functionality compared to adult cardiomyocytes<sup>[73]</sup>. The differentiation protocol varies in the literature, showing the lack of reproducibility and uniformity of the model. Furthermore, to overcome the constraints of two-dimensional cell culture, engineered heart tissues (EHTs) have been developed. These three-dimensional scaffolds support the culture of either neonatal rat cells<sup>[74]</sup> or iPSC-CMs<sup>[73]</sup> to create cardiac patches for sophisticated studies of contractility and remodelling. Recent breakthroughs in generating cardiac organoids with multiple chambers<sup>[75]</sup> herald a future where *in vitro* investigations might be conducted on highly advanced three-dimensional heart models, closely mimicking human cardiac physiology.

NRCMs remain the most widely used model for screening novel drug candidates against cardiac hypertrophy. Their reproducibility, cost-effectiveness and relatively high physiological relevance make them particularly well-suited for phenotypic drug discovery and finding first-in-

class drug candidates. Moreover, novel drug targets or mechanisms of action (MoA) typically require early *in vivo* efficacy studies for validation, studies that are predominantly conducted in rodent models. Therefore, improving the *in vitro* models based on rodent cells, like NRCMs, used for prior drug screening and functional assessment is crucial to enhance translational relevance and ultimately increase the success rate of preclinical drug development. Hence, further advancements in readouts and high-throughput capabilities are essential. Relying solely on manual cardiomyocyte size measurements provides only an incomplete and potentially biased assessment of drug effects. By leveraging modern computational tools, more comprehensive data can be extracted from cell images, enabling a deeper understanding of phenotypic changes. Additionally, enhancing the model's high-throughput capacity will enable the screening of a greater number of potential drug candidates. This ultimately increases the likelihood of identifying effective treatments for cardiac hypertrophy and paving the way for improved patient outcomes.





## 2. Aims of the Thesis

Traditional *in vitro* models in drug discovery often use monocultures or transformed cell lines that lack the cellular diversity and complex signalling of native cardiac tissue<sup>[57, 76]</sup>, limiting their predictive value and contributing to high failure rates in later development stages<sup>[39, 40, 41]</sup>. Most assays focus solely on cardiomyocytes, overlooking key roles of non-cardiomyocytes like fibroblasts in cardiac remodelling. Additionally, standard hypertrophy assays often suffer from low throughput, reducing their suitability for large-scale screening<sup>[77, 78, 79]</sup>. Since novel drug targets or mechanisms of action (MoA) require early *in vivo* validation, typically in rodent models, optimising preceding *in vitro* systems based on rodent cells such as neonatal rat cardiomyocytes (NRCMs) is essential to enhance translational success.

To address these limitations, this thesis aims to establish an improved *in vitro* model that more accurately reflects the cardiac cellular environment. A mixed cardiac cell culture system will be developed for quantitative assessment of hypertrophic responses. To enable high-throughput screening, the assay will be scaled to a 384-well format, increasing efficiency and reproducibility. A custom image analysis pipeline using the CellProfiler software will support high-content morphological analysis, providing detailed phenotypic characterisation of hypertrophy.

The model will be validated using different hypertrophic stimuli to assess sensitivity and define a reliable positive control. This high-content, high-throughput platform will serve as a versatile tool for investigating anti-hypertrophic compounds and studying cardiac pathological mechanisms, with proof-of-concept demonstrated in three subsequent research applications.

### Targeting GRK5: A Novel Therapeutic Avenue in Cardiac Hypertrophy

In recent years, attention has increasingly focused on the molecular mechanisms underlying pathological hypertrophic signalling, with G protein-coupled receptor kinase 5 (GRK5) emerging as a critical regulator. Beyond its classical role in desensitising G protein-coupled receptors (GPCRs) at the membrane<sup>[80]</sup>, GRK5 translocates to the nucleus, where it modulates transcriptional programs promoting maladaptive cardiac remodelling<sup>[81, 82]</sup>. These dual functions position GRK5 as a highly attractive therapeutic target for interventions aimed at preventing or reversing hypertrophic progression at an early disease stage. Despite evidence supporting the role of GRK5 in cardiac pathology, the development of specific pharmacological inhibitors remains at an early stage<sup>[83, 84, 85]</sup>. Therefore, there is a pressing need for chemical biology approaches to deliver small-molecule inhibitors suitable for translational research and potential therapeutic application.

The aim of this project is to explore GRK5 inhibition as a therapeutic strategy for cardiac hypertrophy in the high-content assay system to provide a valid tool that guides GRK5-centric

lead optimisation programs for effective *in vivo* translation. The impact of GRK5 perturbation in the new assay setup will be evaluated by genetic methods and profiling of a collection of small-molecule GRK5 inhibitors, selected based on reported GRK5 inhibitory potency, drug-likeness and pharmacological profiles.

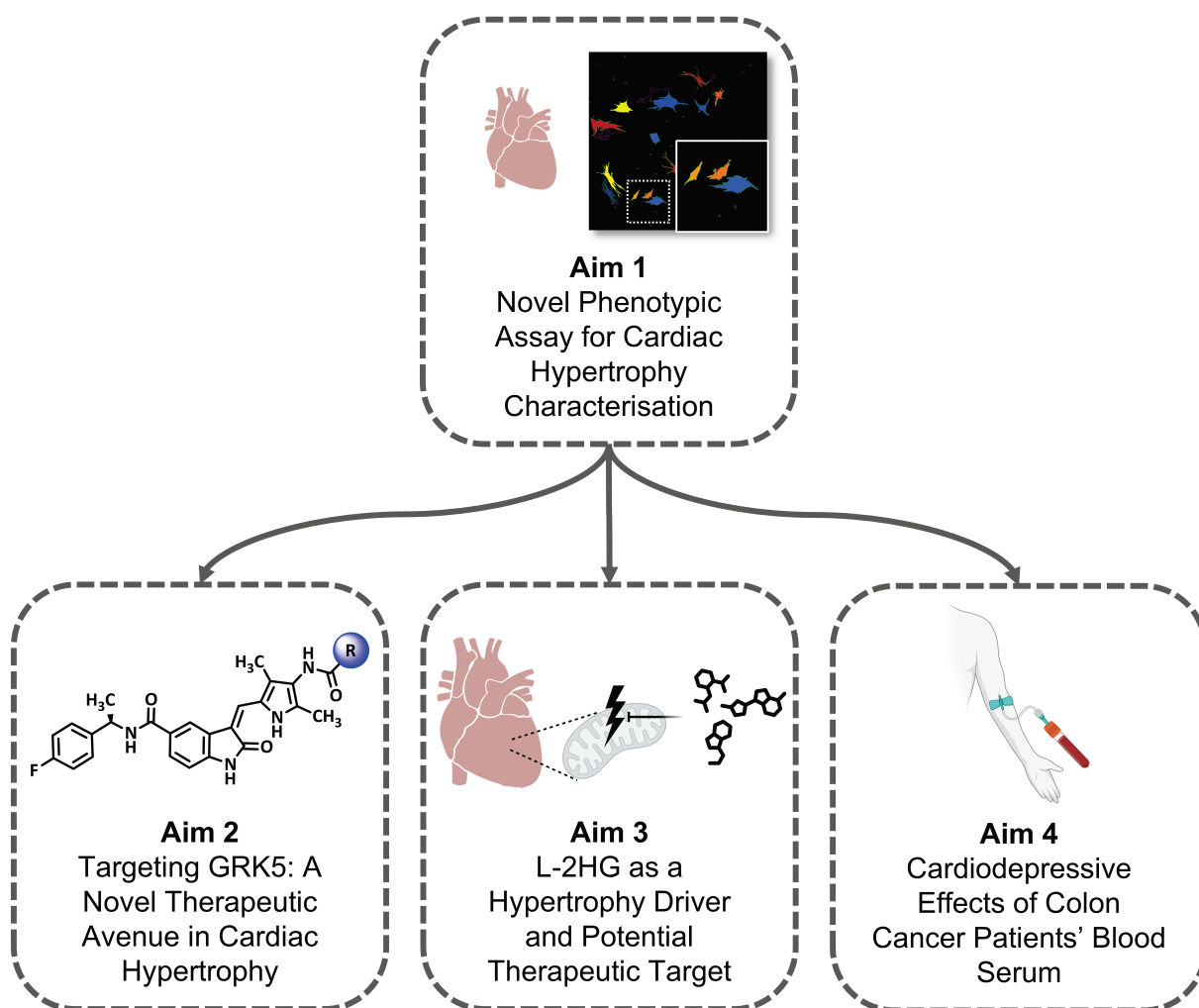


**Figure 2: Aims of the thesis.** A high-throughput, high-content screening assay for cardiac hypertrophy will be established (Aim 1) for three distinct applications (Aims 2-4).

### L-2HG as a Hypertrophy Driver and Potential Therapeutic Target

In the context of cardiac hypertrophy, altered cardiac metabolism has emerged as a hallmark of disease progression, offering new opportunities for therapeutic intervention<sup>[20]</sup>. Recent metabolomics studies have identified elevated levels of L-2-hydroxyglutarate (L-2HG) as a significant metabolic alteration in hypertrophic hearts<sup>[86]</sup>. However, the functional contribution of L-2HG to the development of cardiac hypertrophy remains poorly understood. Since L-2HG biosynthesis is tightly linked to glutamine metabolism, the potential of targeting glutamine pathways to modulate hypertrophic remodelling represents a promising strategy<sup>[87]</sup>.

This project aims to evaluate whether the established high-content screening assay can reliably capture the L-2HG-induced hypertrophic phenotype within the novel mixed cell culture system. Building on this, a panel of small-molecule inhibitors targeting glutamine metabolism is tested for their ability to prevent or reverse L-2HG-driven hypertrophic growth.

By investigating this metabolism-based mechanism, the study provides new insight into the contribution of L-2HG to pathological cardiac remodelling and supports the potential of glutamine metabolism inhibitors as a novel therapeutic strategy for cardiac hypertrophy.

### **Cardiodepressive Effects of Colon Cancer Patients' Blood Serum**

To improve patient outcomes in cardiac hypertrophy and heart failure, early identification of patients at risk of disease manifestation is essential. Accordingly, cardiovascular research increasingly focuses on biomarkers and risk factors that enable timely detection and intervention<sup>[88]</sup>. In this context, the interplay between different disease states, such as the emerging link between cancer and cardiovascular health, has gained growing interest. Recent studies suggest that malignancies may directly contribute to cardiac dysfunction. Epidemiological studies indicate that colon cancer patients have a higher incidence of CVDs, however, the mechanisms underlying this association remain poorly understood. One potential explanation is that tumour-derived circulating factors influence cardiac function by altering cardiomyocyte morphology and viability. However, direct experimental evidence remains limited<sup>[89, 90]</sup>.

Therefore, this project aims to illuminate this relationship by investigating the effects of blood serum from colon cancer patients on cardiomyocytes. The herein established cardiac hypertrophy assay seeks to characterise morphological changes in cardiomyocytes after exposure to patient serum, focusing on potential cardiodepressive effects. To further strengthen the clinical relevance of these findings, patient-specific data will be correlated with cardiomyocyte responses. Identifying statistical associations between cancer progression and cardiac remodelling could provide further evidence for a tumour-induced impact on cardiovascular health and help identify subgroups of patients at higher risk for developing CVDs.



### 3. Materials and Instruments

#### 3.1 Chemicals

All liquid and solid chemicals used in this study are listed below, divided by their function:

**Table 1: List of buffers with their composition.**

Buffers	Composition
Buffer A (10x)	34 g NaCl 2 g KCl 0.5 g MgSO <sub>4</sub> 6.5 g NaH <sub>2</sub> PO <sub>4</sub> 5 g glucose 23.5 g HEPES, pH 7.4
ECL reagent A	7.88 g TRIS HCl in 400 ml <i>aqua bidest.</i> 125 mg luminol sodium salt Ad 500 ml <i>aqua bidest.</i> Adjusted to pH 8.6 with KOH
ECL reagent B	27.5 mg <i>p</i> -coumaric acid 25 ml DMSO
Laemmli buffer (4x)	2.5 ml TRIS (1 M, pH 6.8) 0.4 g SDS 2 ml 2-mercaptoethanol 6 ml glycerol (86%) 2 mg bromophenol blue sodium salt Ad 10 ml <i>aqua dem.</i>
Lysis buffer (pH 7.5)	59.6 mg HEPES 18.6 mg KCl 0.9 mg Na <sub>2</sub> -EDTA 3.9 mg Dithiothreitol 0.125 mg nonidet-P40 ad 25 ml <i>aqua bidest.</i> Phosphatase inhibitor cocktail Protease inhibitor cocktail
MTBST	2.5 g milk powder ad 50 ml TBST buffer

### 3. Materials and Instruments

---

<b>Buffers</b>	<b>Composition</b>
Running buffer (10x)	30.28 g TRIS 1144.1 g glycine 10 g SDS Ad 1000 ml <i>aqua bidest.</i>
Separating gel	2.4 ml <i>aqua dem.</i> 1 ml separating gel buffer 0.6 ml acrylamide 6 µl TEMED 25 µl APS (10%)
Separating gel buffer (4x)	90.9 g TRIS 2 g SDS Ad 500 ml <i>aqua bidest.</i> Adjusted to pH 8.8 with HCl
Stacking gel	3.94 ml <i>aqua dem.</i> 3 ml stacking gel buffer 5 ml acrylamide (30%) 10 µl TEMED 80 µl APS (10%) 60 µl TCE
Stacking gel buffer	30.25 g TRIS 2 g SDS Ad 500 ml <i>aqua bidest.</i> Adjusted to pH 6.8 with HCl
Staining buffer	0.1 ml TritonX 2.5 ml FBS Ad 50 ml PBS buffer
TBS buffer (10x)	2.43 g TRIS 8 g NaCl ad 1000 ml <i>aqua bidest.</i> Adjusted to pH 7.6 with HCl
TBST buffer	900 ml <i>aqua bidest.</i> 100 ml TBS buffer (10x) 1 ml tween 20

---

Buffers	Composition
Transfer buffer	100 ml transfer buffer (10x) 200 ml methanol 700 ml <i>aqua bidest.</i>
Transfer buffer (10x)	30,3 g TRIS 144,1 g glycine ad 1000 ml <i>aqua bidest.</i>

Table 2: Cell culture media and supplements.

Media and Supplements	Company
DMEM, low glucose, pyruvate, no glutamine, no phenol red	Gibco
Fetal bovine serum (FBS)	Gibco
Opti-MEM, reduced serum	Gibco
Penicillin streptomycin 10,000 U/ml (P/S)	Gibco

Table 3: List of stimulants, inhibitors and other reagents.

Chemical	Company
1,4-Dithiothreitol	Carl Roth GmbH
2,2,2-Trichloroethanol (TCE)	Thermo Fisher Scientific Inc.
2-Mercaptoethanol	Gibco
4',6-Diamidino-2-phenylindole (DAPI)	Carl Roth GmbH
Ammonium peroxydisulfate (APS)	Carl Roth GmbH
Angiotensin II (Ang. II)	Sigma-Aldrich
Bovine serum albumin (BSA)	Carl Roth GmbH
Bromphenole blue	Carl Roth GmbH
CB-839	Sigma-Aldrich
Collagenase type II	Sigma-Aldrich
Complete, EDTA-free protease inhibitor cocktail	Roche
Compound 968	Sigma-Aldrich
Dimehtylsulfoxide (DMSO)	Fisher BioReagents



### 3. Materials and Instruments

---

<b>Chemical</b>	<b>Company</b>
Dulbecco's balanced salt solution (DPBS), no calcium, no magnesium	Gibco
Endothelin-1 (ET-1)	Sigma-Aldrich
Ethanol (DNase-free, RNase-free, protease-free)	Carl Roth GmbH
Ethylenediamine tetraacetic acid disodium salt dihydrate (Na <sub>2</sub> -EDTA)	Carl Roth GmbH
Formaldehyde solution 37%	neoFroxx GmbH
Gelatine 0.1%, DPBS	PAN-Biotech
Glycerol (86%)	Carl Roth GmbH
Glycine	Carl-Roth GmbH
GRL018-21	MedChemExpress
Hydrocortisone	Sigma-Aldrich
IPN60090	Sigma-Aldrich
Isopropanol	Carl-Roth GmbH
L- (-)-Norepinephrine (+)-bitartrate monohydrate (NE)	Sigma-Aldrich
Leukemia inhibitory factor (LIF)	Dortmund Protein Chemistry Facility, Germany
L-Glutamine 200 mM, 100X	Gibco
Lipofectamine RNAiMAX Transfection Reagent	Invitrogen
Luminol natrium	Sigma-Aldrich
Luminol sodium salt	Sigma-Aldrich
L- $\alpha$ -Hydroxyglutaric acid disodium salt	Sigma-Aldrich
Magnesium sulfate (MgSO <sub>4</sub> )	Carl-Roth GmbH
Methanol	Carl-Roth GmbH
<i>N,N,N',N'</i> -Tetramethyl ethylenediamine (TEMED)	Carl Roth GmbH
<i>N</i> -2-Hydroxyethylpiperazine- <i>N'</i> -2-ethane sulphonic acid (HEPES)	Carl Roth GmbH
No ROX SYBR 2X MasterMix blue dTTP	Takyon

Chemical	Company
Nonidet-P40	BioChemica
PageRuler plus prestained protein ladder (10-250 kDa)	Thermo Fisher Scientific Inc.
Pancreatin from porcine pancreas	Sigma-Aldrich
<i>p</i> -coumaric acid	Sigma-Aldrich
Percoll density gradient media	Cytiva
Phosphatase inhibitor cocktail	Sigma-Aldrich
Pierce bovine serum albumin standard	Thermo Fisher Scientific Inc.
Potassium chloride (KCl)	Carl Roth GmbH
Powdered milk	Carl Roth GmbH
qScript cDNA SuperMix	QuantaBio
( <i>R</i> )-(-)-Phenylephrine hydrochloride (PE)	Sigma-Aldrich
Rnase-free water	VWR
RotiFair PBS 7.4 powder	Carl Roth GmbH
Rotiphorese NF-acrylamid/bis-solution 40 (29:1)	Carl Roth GmbH
Sodium Chloride (NaCl)	Carl Roth GmbH
Sodium dihydrogen phosphate (NaH <sub>2</sub> PO <sub>4</sub> )	Carl-Roth GmbH
Sodium dodecyl sulfate (SDS)	Carl Roth GmbH
TGFβ-1	Sigma-Aldrich
Timolol (TML)	Sigma-Aldrich
Tris-(hydroxymethyl)-amino methane (TRIS)	Carl Roth GmbH
TritonX-100	Sigma-Aldrich
Trypan blue solution	Thermo Fisher Scientific Inc.
Trypsin 0.25% / 1 mM EDTA	PAN-Biotech GmbH
Tween 20	Carl Roth GmbH
V-9302	Sigma-Aldrich
Water, sterile, pyrogen-free, hypotonic	Carl Roth GmbH

**Table 4: List of primary and secondary antibodies and their respective dilutions.**

<b>Antibodies</b>	<b>Company</b>	<b>Dilution</b>
Goat anti-mouse IgG (H+L) cross-adsorbed secondary antibody, alexa fluor™ 568	Invitrogen (A11004)	1:1,000
Goat anti-mouse IgG (H+L) cross-adsorbed secondary antibody, alexa fluor™ 488	Invitrogen (A11001)	1:1,000
Goat anti-mouse IgG (H+L), HRP-conjugated antibody	Proteintech (SA00001-1)	1:1,000
Goat anti-rabbit IgG, HRP-conjugated antibody	Abcam (ab79051)	1:1,000
Mouse anti-GRK5 antibody, monoclonal	Santa Cruz Biotechnology (Sc-518005)	1:500
Mouse anti- $\alpha$ -cctinin (sarcomeric) antibody, monoclonal	Sigma-Aldrich (A78119)	1:800
Rabbit anti-ANP antibody, polyclonal	Invitrogen (PA5-29559)	1:500

Primers were purchased from Integrated DNA Technologies as custom DNA oligonucleotides (25 nmole) after sequences were generated using the National Library of Medicines Primer-BLAST:

**Table 5: List of primer sequences used for qPCR.**

<b>Primer</b>	<b>Sequence</b>
<i>Nppa</i>	forward: 5'-CCTCGGAGCCTGCGAAGGTCA-3' reverse: 5'-TGTGACACACCGCAAGGGCTTG-3'
<i>Nppb</i>	forward: 5'- GACGGGCTGAGGTTGTTTTA-3' reverse: 5'- ACTGTGGCAAGTTTGTGCTG-3'
<i>RPL32</i>	forward: 5'- GGGAGCAACAAGAAAACCAA-3' reverse: 5'- ATTGTGGACCAGGAAGTTGC-3'

Silencer Select siRNA for knockdown experiments were purchased from Thermo Fisher Scientific.

**Table 6: siRNA sequences for knockdown experiments.**

<b>siRNA</b>	<b>Catalog Number</b>
GAPDH	4390849
GRK5	s133076
Scrambled	4390843

**Table 7: List of assay and reagent kits.**

<b>Kits</b>	<b>Company</b>
Clarity Max Western ECL Substrate	Bio-Rad Laboratories, Inc.
Neonatal Heart Dissociation Kit, mouse and rat	Miltenyi Biotec
Pierce Bicinchoninic Acid Protein Assay (BCA)	Thermo Fisher Scientific Inc.
RNase-Free DNase Set (250)	Qiagen
RNeasy Mini Kit (250)	Qiagen

### 3.2 Disposable Materials

In the following, all consumables and general laboratory materials used in this study are listed.

**Table 8: List of disposable materials.**

<b>Material</b>	<b>Company</b>
Cell culture microplate, 384 well, PS, F-bottom, µclear, black	Greiner Bio-One GmbH
Cell culture plate (6-well, 96-well)	Sarstedt AG & Co. KG
Cell strainer (100 µm)	Corning Incorporated
Cell strainer (70 µm)	Sarstedt AG & Co. KG
Countess 3 standard slide	Thermo Fisher Scientific Inc.
Deep well 96-well plate, 2 ml	Starlab GmbH
Falcon tube (15 ml, 50 ml)	Sarstedt AG & Co. KG
Hard-shell PCR paltes, 96-well	Bio-Rad Laboratories, Inc.

<b>Material</b>	<b>Company</b>
Immuno blot PVDF membrane	Bio-Rad Laboratories, Inc.
Microseal 'B' adhesive seals for PCR	Bio-Rad Laboratories, Inc.
Parafilm M sealing film	Heathrow Scientific LLC
PCR single tube, 0.2 ml	Sarstedt AG & Co. KG
Pipette tips (1000, 300, 200, 10 µl)	Sarstedt AG & Co. KG
Pipette tips Biosphere plus (1000, 300, 200, 20 µl)	Sarstedt AG & Co. KG
Pipette tips for E1-ClipTip (2-125 µl)	Thermo Fisher Scientific Inc.
Pipette tips for Viaflo (125 µl)	Integra Biosciences GmbH
Pipette tips gel loader (200 µl)	Sarstedt AG & Co. KG
Precision wipes	Kimberly-Clark Worldwide, Inc.
Reaction tube (0.2, 0.5, 1.5, 2.0 ml)	Sarstedt AG & Co. KG
Reservoir	Carl Roth GmbH
Serological pipette (50 ml)	Greiner Bio-One GmbH
Serological pipettes (25, 10, 5 ml)	Sarstedt AG & Co. KG
Whatman blotting paper	Cytiva

### 3.3 Instruments

This list includes all equipment and instruments from the laboratory that were required to perform the experiments.

**Table 9: List of instruments required for all experiments.**

<b>Application</b>	<b>Device</b>	<b>Company</b>
Autoclave	HST 4x6x6	Zirbus
Centrifugation	Fresco 21	Thermo Fisher Scientific Inc.
	Mega Star 3.0R	VWR
	Sunlab mini centrifuge SU1550	neoLab Migge GmbH
Gel electrophoresis	ChemoStar 21 TS	Intas Science Imaging Instruments GmbH

Application	Device	Company
	Mini Trans Blot Module	Bio-Rad Laboratories, Inc.
	Mini-PROTEAN Tetra System	Bio-Rad Laboratories, Inc.
	PeqPower power supply	VWR Peqlab
	PowerPac Universal power supply	Bio-Rad Laboratories, Inc.
Incubation	Heracell Vios 160i CO2 Incubator	Thermo Fisher Scientific Inc.
Microscopy	Echo Rebel	Bio Convergence Company
	Evos XL Core	Thermo Fisher Scientific Inc.
	ImageXpress Micro XL Widefield High Content Screening System	Molecular Devices
	Keyence BZ-X810 Fluorescence Microscope	Keyence Corporation
	Olympus CKX53	Olympus K.K.
	Olympus DP74 (camera)	
	Olympus HGLGPS (light source)	
	Olympus SZ61	Olympus K.K.
	Olympus SC50 (camera)	
Miscellaneous	Countess 3	Thermo Fisher Scientific Inc.
	Digital heating shaking drybath	Thermo Fisher Scientific Inc.
	pH electrode 1100L	VWR
	Purelab Flex water purification system	Veolia Water Technologies Deutschland GmbH
	Tecan Spark	Tecan Trading AG
	WB2 water bath	VWR
Mixing	Corning LSE Platform Rocker	Corning
	Sunlab mini vortex mixer SU1900	neoLab Migge GmbH

### 3. Materials and Instruments

<b>Application</b>	<b>Device</b>	<b>Company</b>
Pipettes	E1-ClipTip electronic 16-channel pipette	Thermo Fisher Scientific Inc.
	Electronic Transferpette-8 (10-200 µl)	Brand GmbH+ Co KG
	Electronic Viaflo 16- channel pipette (5-125 µL)	Integra Biosciences GmbH
	Electronic Viaflo single- channel pipette (5-125 µL)	Integra Biosciences GmbH
	Manual 8-channel pipette (1-10, 10-100, 30-300 µL)	Thermo Fisher Scientific Inc. (Finnpipette F2)
	Manual single-channel pipette (1000, 200, 100, 20, 10, 2.5 µl)	Brand GmbH+ Co KG (Transferpette S)
	Pipette controller accu-jet pro	Brand GmbH+ Co KG
	Sunlab digital pipette controler	neoLab Migge GmbH
Plate Washer	Biotek 405 TS Plate Washer	Biotek
	Vacuum pump ME8	Vacuubrand GmbH + Co. KG
Polymerase chain reaction (PCR)	CFX Opus 96 Real-Time PCR System	Bio-Rad Laboratories, Inc.
	Nanodrop OneC	Thermo Fisher Scientific Inc.
	C1000 Touch Thermal Cycler	Bio-Rad Laboratories, Inc.
Scale	Analytic balance CP225D	Sartorius AG
	Precision balance L2200P	Sartorius AG
Sterile working	BVC professional fluid aspiration system	Vacuubrand GmbH + Co. KG
	Herasafe 2025 1.5	Thermo Fisher Scientific Inc.

Application	Device	Company
	Herasafe KS 12	Thermo Fisher Scientific Inc.
	Herasafe KS 15	Thermo Fisher Scientific Inc.
	Stainless stell manifolds (16, 24 pins)	Drummond Scientific Company

### 3.4 Software

This section includes all software used in this study, including instrument-specific software for data acquisition and analysis software for processing and evaluation.

**Table 10: List of used software for data acquisition and analysis.**

Software	Company
BioRad CFX Maestro	Bio-Rad Laboratories GmbH
BioRender	Science Suite
BZ-X800 Analyzer 1.03.00.01	Keyence Corporation
BZ-X800 Viewer 1.03.00.1	Keyence Corporation
CellProfiler 4.2.1	Broad Institute, Inc.
cellSens Software	Olympus K.K.
ChemoStarTS	Intas Science Imaging Instruments GmbH
ChemSketch 2023.2.4	Advanced Chemistry Development, Inc.
Citavi 6	Swiss Academic Software GmbH
Echo Pro 1.0.3-f4	Bio Convergence Company
GraphPad Prism 8.4.2	Dotmatics
ImageJ 1-52a	National Institutes of Health, USA
MetaXpress	Molecular Devices
NanoDrop 2000	Thermo Fisher Scientific
Origin 2020	OriginLab Corporation
Primer-BLAST	National Center for Biotechnology Information
SparkControl 2.3	Tecan Trading AG





## 4. Methods

### 4.1 Cell Culture

#### Isolation of Mixed Cardiac Cells

Mixed cardiac cells were isolated from neonatal rat hearts as previously described by our group<sup>[91]</sup>. Five-day-old (P5, postnatal day 5) Wistar rats were sacrificed by decapitation and fixed at all extremities on a Styrofoam pad with needles. The rat's body was sterilised by spraying it with 70% ethanol and the abdomen was opened between stomach and ribcage using scissors (see Figure 3). After cutting the diaphragm, the ribcage was opened by making a cut on each side. The heart was exposed, harvested by tweezers and immediately placed in sterile PBS buffer on ice. Residual tissue or blood was removed with tweezers under the microscope.

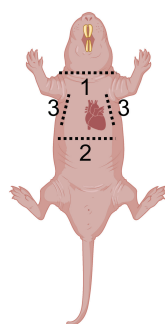


**Figure 3: Preparation of P5 rats.** Rats were decapitated, abdomen was opened with a horizontal cut between ribcage and stomach and diaphragm was cut. Ribcage was then opened with two vertical cuts to expose the heart.

Subsequently, enzymatic and mechanical digestion of the organ was performed using Miltenyi's Neonatal Heart Dissociation Kit as described in the manufacturer's protocol. Briefly, digestion mix A was prepared and incubated for 15 min at 37 °C, afterwards mix A and B were combined. Each heart was placed in 1 ml of combined digestion mix in a 1.5 ml microtube and thoroughly minced with scissors. The contents of two microtubes were pooled in one Falcon tube, followed by three steps of incubation (each 15 min, 37 °C) accompanied by intermittent dissociation by slowly pipetting up and down. Digestion was stopped by adding DMEM media with high serum (DMEM, 10% FBS, 1% penicillin/streptomycin (P/S)) and remaining cell and tissue clumps were removed by filtering the suspension through a 70 µm cell strainer. Changing to growth medium, cells were centrifuged at 500 rpm for 15 min and supernatant was aspirated and replaced with DMEM (DMEM, 2% FBS, 1% penicillin/streptomycin).

Either black 384-well plates with µclear bottom or standard 6-well plates for cell culture were coated with 0.1% gelatine using 20 µl and 800 µl per well, respectively. Gelatine was aspirated after 30 min of incubation at 37 °C and cells were seeded on the plates. For

immunocytochemistry either 1,500 or 4,000 cells were suspended in 25  $\mu$ l DMEM (DMEM, 2% FBS, 1% penicillin/streptomycin) and dispensed into 384-well plates. For siRNA knockdown and protein analysis 750,000 to 1,000,000 cells were suspended in 1.5 ml DMEM and seeded on 6-well plates.

### Isolation of Purified Cardiomyocytes

One to three-day-old (P1-3, postnatal day 1-3) Wistar rats were sacrificed by decapitation. With one central cut at the sternum, the thorax was opened and hearts were uncovered by gently pushing on the stomach (see Figure 4). Similar to the isolation of mixed cardiac cells, hearts were removed using tweezers and placed in sterile buffer A. It is worth noting that this quicker extraction method of rat hearts was not feasible for P5 rats, as their ribcages were more developed.



**Figure 4: Preparation of P1-3 rats.** Preparation of P1-3 neonatal rats was performed by decapitation and one vertical cut into the sternum. By gently pressing onto the rat's stomach, the heart was uncovered.

After mechanical dissociation with scissors, hearts were digested using a mix of pancreatin and collagenase type II in three cycles for 20 min at 37 °C while shaking. After each cycle, the dissociation solution was replaced and the isolated cells were pooled, strained with a 100  $\mu$ m cell strainer and 10 ml FBS was added to halt the dissociation. Cells were centrifuged at 1,000 rpm for 5 min and the pellet was resuspended in buffer A.

To purify cardiomyocytes from stromal cells (fibroblasts, endothelia, smooth muscle cells and immune cells), Percoll gradient centrifugation was performed [76]. The top layer with 40.5% Percoll in buffer A and phenol red was added first, followed by the bottom layer with 58.5% Percoll in buffer A, which was carefully pipetted below the top layer in a 50 ml Falcon tube. Last, the cell suspension was added above the top layer and the tube was centrifuged at 2,400 rpm at 4 °C for 30 min. The upper layer enriched with fibroblasts was aspirated and the interphase containing cardiomyocytes (see Figure 5) was washed twice with buffer A and resuspended in DMEM. Cells were seeded as described above for the isolation of mixed cardiac cells.

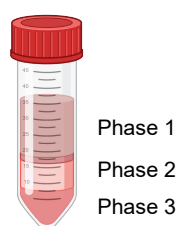


**Figure 5: Percoll gradient.** Percoll density gradient centrifugation is performed to purify cardiomyocytes from stromal cells. After centrifugation, fibroblasts are enriched in phase 1, cardiomyocytes in phase 2 and erythrocytes form a pellet at the bottom of phase 3.

### Hypertrophic Stimulation and Compound Treatment

For immunocytochemistry experiments, either mixed cardiac cells or purified cardiomyocytes were treated one day after seeding, while siRNA knockdown plates were treated one day after the second knockdown step (see Figure 7).

The cell treatment consisted of two steps: Firstly, a hypertrophic stimulant was added, typically using a combination of phenylephrine (PE) at 20  $\mu$ M and leukemia inhibitory factor (LIF) at 50 ng/ml. Stimulation and DMSO control were prepared in DMEM. For qPCR, cells were stimulated with a higher concentration of 100  $\mu$ M PE along with 50 ng/ml LIF to increase the dynamic range, as the stimulation period for qPCR experiments was limited to 24 h.

Secondly, a 96-well source plate with anti-hypertrophic compounds at different concentrations with technical triplicates was prepared. After the addition of DMEM, the source plate was transferred to three 384-well plates containing NRCMs by an electronic 8-channel pipette (see Figure 6), yielding plate triplicates. Since all compound stocks were dissolved in DMSO, at least three DMSO control wells with a final DMSO concentration of 0.1% were included on each 384-well plate. For 384-well plates, both treatment steps were added with 25  $\mu$ l each, while 1.5 ml was used for 6-well plates.

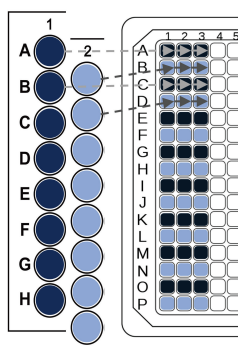


**Figure 6: 96-well source plate.** Preparation of anti-hypertrophic treatment was carried out in a 96-well source plate. Each well served as a reservoir for three technical replicates on the final 384-well plate. Treatment was transferred from 96-well plate using an electronic 8-channel pipette.

### siRNA Knockdown

The knockdown protocol was newly implemented for this project, adapting a previously described protocol by Schlegel et al. using neonatal rat ventricular cardiomyocytes<sup>[92]</sup> according to the manufacturer's protocol of Lipofectamine RNAiMAX Reagent by Invitrogen.

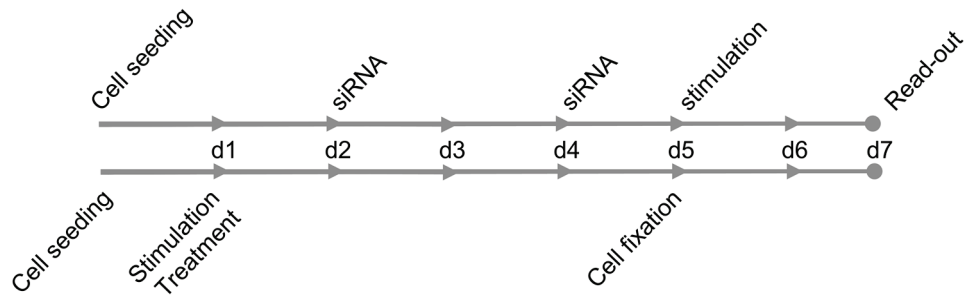


**Figure 7: Protocol timelines.** Overview of the timeline for immunocytochemistry (below) and siRNA (above) protocols.

In 6-well plates, mixed cardiac cells were cultured in 1.5 ml of DMEM (2% FBS, 1% P/S) the day after seeding to ensure viability, as the stress from knockdown and hypertrophic stimulation could lead to cell death in freshly isolated cells. Knockdown was performed twice, 48 h and 96 h after seeding, by diluting siGRK5, siScrambled and Lipofectamine RNAiMAX, each in Opti-MEM-Media. siRNA (final amount of 25 pmol) and Lipofectamine were then mixed and incubated for 5 min at room temperature. Finally, the mix was added to the respective wells and plates were gently shaken to ensure quick distribution.

One day after the last knockdown, cells were treated with either 1.5 ml PE-LIF or DMSO dissolved in DMEM, in this step P/S was omitted to reduce stress on the cells. 48 h later, cells were fixed for immunocytochemistry (see Chapter 4.4) or total protein was extracted (see Chapter 4.2) to confirm knockdown efficiency via Western blotting.

## 4.2 Protein Analysis

### Protein Extraction

For protein analysis, mixed cardiac cells from 6-well plates were lysed 48 h after treatment. First, the media was aspirated and cells were washed twice with warm sterile PBS. Then, 700  $\mu$ l of trypsin was added to each well and incubated for 5 min at 37 °C. To detach remaining adherent cells, plates were gently tapped. To stop the activity of trypsin, 700  $\mu$ l DMEM containing 2% FBS were added and mixed thoroughly. The content of each well was transferred to 1.5 ml microtubes and centrifuged for 3 min at 1,300 rpm at 4 °C. The supernatant was quickly aspirated and the cell pellet was resuspended in 30  $\mu$ l of lysis buffer (10 mM 4-(2-hydroxyethyl)-1-piperazineethanesulfonic acid (HEPES), 10 mM KCl, 0.1 mM ethylenediaminetetraacetic acid (EDTA), 1 mM dithiothreitol, 0.5% Nonidet-P40, pH 7.5, phosphatase inhibitor cocktail and complete protease inhibitor cocktail). During 20 min of incubation on ice, the suspension was mixed by pipetting up and down. The final centrifugation step was performed for 10 min at 4 °C and 12,000 *g* and the supernatant containing proteins was transferred to a new 1.5 ml microtubes. Protein samples were stored at -80 °C for no longer than one week before quantification and immunoblotting.

### Protein Quantification

The total amount of protein was quantified using Thermo Scientific's Pierce Bicinchoninic Acid (BCA) Protein Assay. Protein samples were thawed completely before being diluted to a suitable concentration with a final volume of 50  $\mu$ l. Then, 500  $\mu$ l of BCA-working reagent was added and mixed before incubation of 20 min in a 60 °C shaking water bath. Standard solution of bovine serum albumin for calibration was diluted and mixed with BCA-working reagent to final concentration in a range of 1.25-10.00 mg/ml. Samples and standards were distributed on a 96-well plate and absorbance was measured at 562 nm using a Tecan Spark plate reader. Calibration with  $R^2 > 0.98$  and all sample measurements within the calibration range were accepted.

### Immunoblotting

Protein expression was evaluated by sodium dodecyl sulfate polyacrylamide gel electrophoresis (SDS-PAGE) followed by Western blotting, according to standard procedures.

The discontinuous denaturing approach established by Laemmli<sup>[93]</sup> was used to separate proteins by molecular weight. All samples were diluted to the same concentration and mixed with 4x Laemmli buffer. Samples were then heated for 5 min at 95 °C and allowed to cool down before loading the polyacrylamide gel. For GRK5 expression analysis, separation gels with a concentration of 12% and 10-well comb were used to enable a protein loading amount of

150 µg in 60 µl. First, proteins were focused in a 4% stacking gel at 100 V for 10 min, afterwards proteins were separated for 1.5-2 h in a self-cast 12% separation gel at 120 V. For normalisation, 0.5% of 2,2,2-Trichloroethanol (TCE) was incorporated in all separation gels for fluorescent visualisation<sup>[94]</sup>. TCE binds under ultraviolet-light (UV) exposure to tryptophan resulting in a covalent modification in the indole ring. The shift of fluorescent emission into the visible spectrum can then be detected. For this purpose, gels were activated under UV-light for 5 min in a ChemoStar Touch ECL & Fluorescence Imager, afterwards fluorescence was imaged in the GFP-channel at 508 nm.

For identification of specific proteins, Western blotting was subsequently performed. Here, separated proteins are transferred from polyacrylamide gel to a polyvinylidene difluoride (PVDF) membrane using wet electroblotting. Blotting was performed at 110 V for 2 h with cooling. The membrane was removed and TCE fluorescence was imaged in a ChemoStar Touch ECL & Fluorescence Imager to evaluate successful blotting. Afterwards, the membrane was blocked in 5% MTBST buffer for 1 h while shaking at room temperature. The membrane was incubated with primary antibody diluted in MTBST at 4 °C overnight with shaking. Primary antibody was washed off with 10 ml TBST buffer three times for 10 min each before the membrane was stained with secondary antibody conjugated with horseradish peroxidase (HRP) in MTBST for 1 h at room temperature. Secondary antibody was similarly washed off three times before detection. For this, enhanced chemiluminescence (ECL) substrate was mixed with 37% hydrogen peroxide and pipetted onto the membrane. The ECL-signal was imaged using a ChemoStar Touch ECL & Fluorescence Imager at 428 nm.

Quantification of lane intensity was performed using ImageJ and ECL signal of specific proteins was normalised to total protein from TCE signal.

### 4.3 mRNA Analysis

#### mRNA Extraction

RNA was extracted from either mixed cardiac cells or purified cardiomyocytes cultured in 6-well plates after 24 h of treatment. After aspirating the media, cells were washed twice with warm PBS, lysed and RNA was extracted using RNeasy Mini Kit with the RNase-Free DNase Set (Qiagen), following the manufacturer's instructions. The purified RNA was eluted in 30  $\mu$ l of RNase-free water and its concentration was measured using the NanoDrop One<sup>C</sup> spectrophotometer. For quality control, the absorbance ratios at 260/280 nm (acceptable range of 1.9-2.1) and 260/230 nm (acceptable range of 1.8-2.2) were evaluated to confirm RNA purity.

#### Reverse Transcription of mRNA

Complementary DNA (cDNA) synthesis was carried out using the qScript cDNA Synthesis Kit on the C1000 Touch Thermal Cycler. RNA samples were first diluted to a concentration of 25-50 ng/ $\mu$ l in RNase-free water and 8  $\mu$ l were subsequently mixed with 2  $\mu$ l of the qScript solution. The reverse transcription was conducted with 5 min at 25 °C, 30 min at 42 °C and 5 min at 85 °C. Samples were then cooled and kept at 4 °C until further preparation for qPCR.

#### Quantitative real-time PCR (qPCR)

The qPCR reaction mix was prepared with a total volume of 15  $\mu$ l per sample. This included 7.5  $\mu$ l of Takyon SYBR Master Mix, 1.5  $\mu$ l of forward and reverse primer mix (final concentration of 500 nM) and 0.75  $\mu$ l of cDNA diluted with 5.25  $\mu$ l RNase-free water. Diluted cDNA was first added to a 96-well qPCR plate, then the Master Mix with the respective primers was added. The plate was sealed and briefly centrifuged.

The qPCR was performed on the Bio-Rad CFX Opus 96 thermocycler using the following temperature program:

**Table 11: qPCR temperature program.**

Cycles	Steps	Time	Temperature
1x	Heat-activation	3 min	95 °C
	Denaturation	3 s	95 °C
44x	Annealing	20 s	60 °C
	Elongation	20 s	72 °C



As a final step, a melting curve analysis was performed to verify the specificity of the amplified products. The plate was held at 65 °C for 1 min, followed by a continuous temperature increment of 1 °C per second up to 95 °C. The first derivative of the melting curve for each sample was analysed to confirm the presence of a single peak. Samples displaying multiple peaks were excluded from further analysis. Gene expression was calculated using the  $\Delta\Delta C_q$  method<sup>[95]</sup> with *Rp132* used as a housekeeping gene. Unstimulated DMSO-treated samples served as the control group for normalisation.

## 4.4 Immunocytochemistry and Image Analysis

### Staining

For 384-well plates, the media was aspirated and washed automatically using a BioTek 405 TS Plate Washer, while 6-well plates were handled manually. Firstly, cells were fixed for 10 min using 20  $\mu$ l and 800  $\mu$ l of 4% formaldehyde (FA) in PBS for 384-well and 6-well plates, respectively. Subsequently, plates were washed thrice with PBS to reduce noise caused by FA and stored at 4 °C. Cells were then permeabilised using 0.2% TritonX and blocked using 5% FBS in sterile PBS (staining buffer, SB) for 20 min at room temperature. SB was aspirated and replaced by primary antibody diluted in SB for 1.5 h at room temperature or overnight at 4 °C. Primary antibody was washed off three times with PBS before fluorescence-labelled secondary antibody and DAPI, both diluted in PBS, were added for 1 h at room temperature in the dark. Finally, plates were washed three times with PBS before imaging.

### Imaging

All plates were imaged using an ImageXpress Micro XL Widefield High Content Screening System (Molecular Devices). Capture settings consisted of a 10x Plan Fluor objective, 25 °C and laser auto-focus. Each well was imaged at 4 sites in both DAPI and Texas red channel.

For higher resolution and magnification, the Keyence B7-X810 Fluorescence Microscope was used with a Plan Apo 10x objective. Similarly, 4 sites per well in both channels were captured, however, a z-stack was compiled from 7 images to enhance image quality.

### CellProfiler Analysis

The CellProfiler pipeline shown in Table 12 was specifically designed for this project. Images acquired with the ImageXpress or Keyence microscope were loaded into the pipeline and the correct extraction of metadata from file names was ensured. The first pipeline was built to calculate an illumination correction function for all images. The correction function was exported as “.npz” file and subsequently loaded along with images into the second pipeline. Module settings for nucleus and cell segmentation were adjusted for each experiment to account for changes in image quality.

All measurements were finally exported to a “.csv” file as means per well. Data from “.csv” file was extracted and copied to the analysis template. Metadata concerning culture conditions (for example hypertrophic stimulation, anti-hypertrophic treatment, concentration, cell density) were assigned to each well. Every measurement was reviewed and outliers of technical triplicates were excluded from the analysis. The mean of technical triplicate for each condition and each measurement was automatically summarised for graphic representation or merged with experimental replicates.

**Table 12: CellProfiler pipelines.** The calculated illumination function from the first pipeline is afterwards applied in the second pipeline, followed by nucleus and cell segmentation and phenotypic measurements.

Modules	Description
Images, Metadata, NamesAndTypes	Upload of images; metadata extraction from file names, assigning images either to DAPI or $\alpha$ -actinin channel
CorrectIlluminationCalculate	Calculation of illumination function for $\alpha$ -actinin images
SaveImages	Saving illumination function as .npy file
CorrectIlluminationApply	Applying illumination function to all $\alpha$ -actinin images
IdentifyPrimaryObjects	Identification of nuclei in the DAPI channel
MeasureObjectSizeShape	Measuring equivalent diameter for nuclei
FilterObjects	Eliminating nuclear debris or identified nuclear clumps
IdentifyPrimaryObjects	Identification of cardiomyocytes in the $\alpha$ -actinin channel
MeasureObjectSizeShape	Measuring equivalent diameter for cardiomyocytes
FilterObjects	Eliminating cell debris or wrongly identified cell clumps
MaskObjects	Cardiomyocytes are masked with nuclei to identify whole cells and eliminate wrongly segmented cells.
MaskObjects	Nuclei are masked with cardiomyocytes to identify cardiomyocytes' nuclei.
MaskObjects	Nuclei are invertedly masked with cardiomyocytes to identify stromal nuclei.
RelateObjects	Relate nuclei to the corresponding cardiomyocyte.
FilterObjects	Create a sub-population of mononucleated cardiomyocytes.
MeasureObjectSizeShape	Measurements for the area of nuclei and cardiomyocytes
MeasureTexture	Measurements for the texture of cardiomyocytes
MeasureObjectIntensity	Measurements for the intensity of cardiomyocytes
ExportToDatabase	Exporting measurements to an Excel file

#### **4.5 Statistical Data Analysis**

All statistical analyses were calculated using GraphPad Prism 8.4.2 software. Comparisons of three or more groups were assessed using one-way ANOVA, followed by Dunnett's multiple comparisons test for specific pairs of groups. An unpaired t-test was used for comparison of two groups. p-values  $\leq 0.05$  were considered significant (\*  $p \leq 0.05$ , \*\*  $p \leq 0.01$ , \*\*\*  $p \leq 0.001$ , \*\*\*\*  $p \leq 0.0001$ ). All experiments were tested in experimental triplicate, each consisting of plate triplicate and technical triplicate on each plate. Data are presented as mean  $\pm$  SEM.



## 5. Results and Discussion

### 5.1 Novel Phenotypic Assay for Cardiac Hypertrophy Characterisation

#### 5.1.1 Establishing a Custom Semi-Automated Image Analysis Pipeline

The persistently high global mortality rate of cardiovascular diseases highlights the urgent need for novel and effective therapeutic options<sup>[1]</sup>. To increase the likelihood of drug candidates advancing through the stages of drug discovery and ultimately reaching clinical application, robust *in vitro* assays with high translatability are essential. This is particularly important for first-in-class drugs or novel molecular targets, which require early target validation in *in vivo* models. These validation studies are commonly conducted in mice or rats, making it crucial that preceding target-centric *in vitro* assays are based on rodent cells with a well-designed method and biologically meaningful readouts. Strong potency in such models increases the translational probability of success in subsequent *in vivo* studies and supports informed decision-making in early preclinical development. However, many current methods in cardiovascular research still rely on manual cardiomyocyte size measurement<sup>[77, 78, 79]</sup>, which limits data collection to a subset of cells, provides only a single output parameter and introduces the risk of subjective bias. Advances in computational tools have enabled more comprehensive immunocytochemistry analyses, like the “C-MORE” (cellular morphology recognition) pipeline developed by Furkel et al<sup>[67]</sup>. However, the extensive data processing using a custom R package requires specialised computational expertise and resources, restricting the accessibility of this method.

To address these limitations, the herein presented thesis aimed to establish a new phenotypic assay for cardiac hypertrophy with an enhanced and more comprehensive image analysis approach. The method was designed to be widely accessible, ensuring that research groups could implement it regardless of their computational resources and imaging equipment. To further increase its usability and scalability, the analysis process was intended to be as automated as possible.

A fundamental image analysis protocol for neonatal rat cardiomyocytes had already been developed within our group<sup>[91]</sup>, primarily focusing on nuclear count and cell area measurements. Building upon this foundation, the objective was to expand the range of extractable features from immunocytochemistry images, allowing for a more detailed characterisation of hypertrophic stimulation and potential anti-hypertrophic treatments beyond merely assessing cardiomyocyte size.

The previously established method utilised Molecular Devices' MetaXpress software to quantify cardiomyocyte count and area. However, this software offers limited options for morphological measurements, lacks flexibility and accessibility for external research groups. To overcome these constraints, CellProfiler, an open-source image analysis software

developed by the Broad Institute, was selected [96, 97, 98]. CellProfiler operates on a modular framework, allowing high-throughput quantitative and morphological analysis of cell images. With a library of 89 customisable modules, it enables flexible pipeline design for various applications, including image correction, segmentation and feature extraction. A key advantage of CellProfiler is its ability to analyse each cell individually, providing a more robust and detailed assessment, particularly useful for addressing inhomogeneous cell responses.

For the new image analysis protocol, additional hypertrophic features were incorporated to extend the phenotypic readout beyond cardiomyocyte area. To assess viability, cells were stained with DAPI, while cardiomyocytes were specifically labelled with an anti- $\alpha$ -actinin antibody, a structural protein enabling precise cellular measurements. To account for the cellular complexity of cardiac tissue, the analysis was designed to distinguish cardiomyocyte and stromal cell nuclei (including fibroblasts, smooth muscle and endothelial cells) by co-localising DAPI and  $\alpha$ -actinin signals. This approach enables a more precise evaluation of heterogeneous cell responses. Since cardiomyocytes frequently exhibit binucleation as part of their growth process, nuclearity (the number of nuclei per cardiomyocyte) was included as a parameter. Furthermore, while cell area is a commonly used parameter, this analysis also incorporated novel measurements of texture and intensity in the  $\alpha$ -actinin channel, providing a more comprehensive assessment of hypertrophic changes.

The complete analysis pipeline is outlined in Figure 8. Every CellProfiler pipeline begins with an image upload module, followed by metadata extraction and the assignment of images to groups, here the DAPI and  $\alpha$ -actinin channels. This step ensures that images from the same well, site and acquired wavelengths are correctly associated. Metadata extraction is achieved by defining a regular expression (see Table 13), which only needs to be generated once, provided a consistent file-naming convention is maintained.

**Table 13: Exemplary Image Metadata Extraction.**

File Name	20220121 NRCM 9 Plt 1_B02_s1_w1
Regular Expression	^(?P<Date>[0-9]{1,8}) (?P<Experiment>[A-Z]{1,4} [0-9]{1,2}) Plt (?P<Plate>[0-9]{1})_(?P<Well>[A-P][0-9]{1,2})_s(?P<Site>[0-9]{1})_w(?P<Wavelength>[0-2]{1})

To optimise efficiency, the analysis was divided into two separate pipelines. The first pipeline was dedicated to calculating an illumination function for all  $\alpha$ -actinin images. This step needed to be handled separately because computing the illumination function across all images runs in a single-threaded mode, utilising only one CPU core. By performing this calculation beforehand and then importing the resulting illumination function into the second pipeline, the subsequent analysis could be executed in a multi-threaded mode, utilising up to

six CPU cores simultaneously. This approach significantly improved processing speed and reduced susceptibility to network errors.

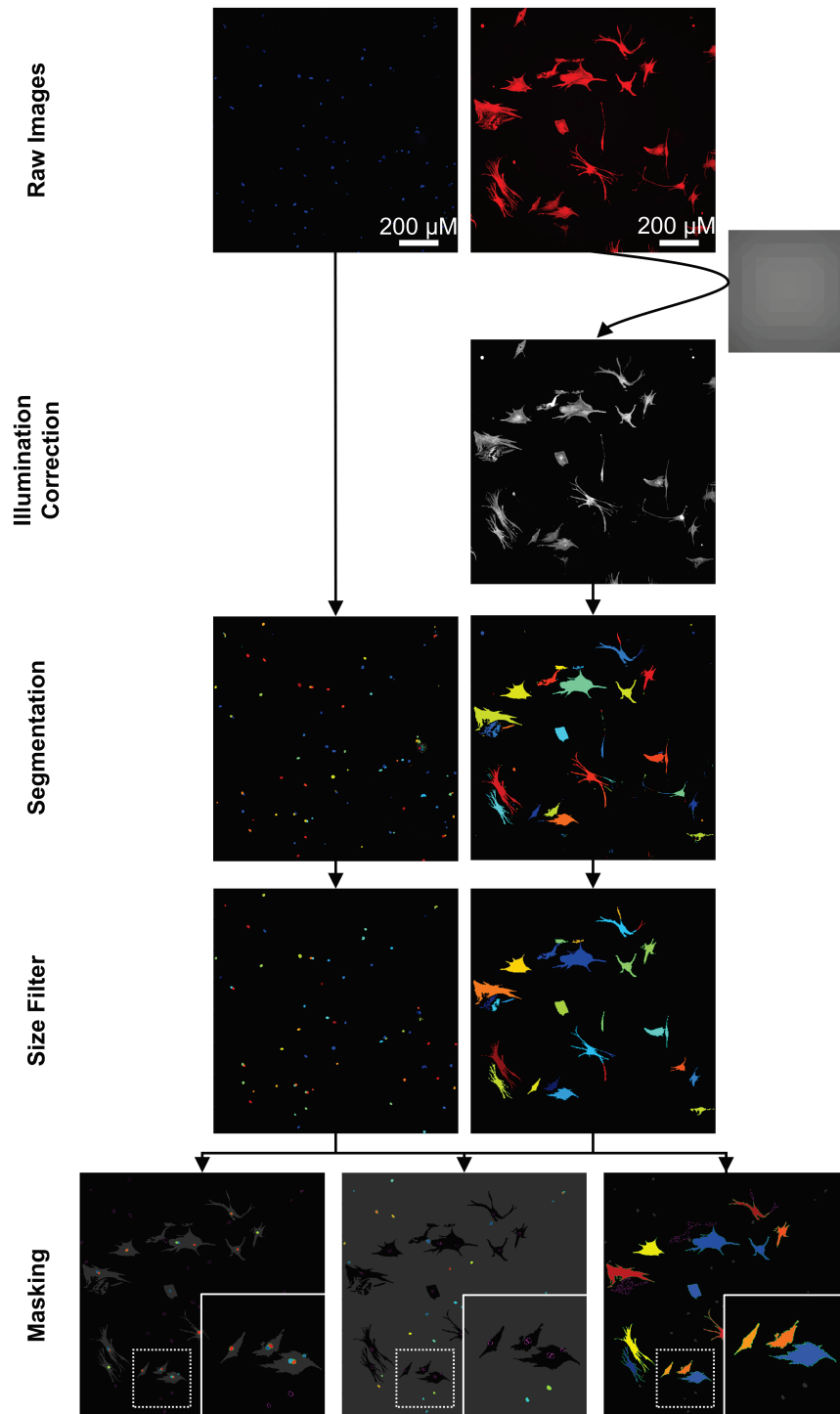


**Figure 8: Illustration of CellProfiler pipeline.** The illumination for images of cardiomyocytes stained with anti- $\alpha$ -actinin antibody is corrected to facilitate object segmentation. DAPI-stained nuclei and cardiomyocytes are then identified separately, accounting for binucleated cardiomyocytes. After filtering for incorrectly identified clumped objects or cytoplasmic projections, nuclei and cardiomyocytes are masked to create subpopulations of cardiomyocytes and stromal objects.



The illumination function served two key purposes for  $\alpha$ -actinin images. First, it corrected uneven lighting caused by the microscope, which typically results in images with a brighter centre and darker edges. Second, it minimised background noise, thereby enhancing the contrast between the cell signal and background, which improved both cell segmentation and thresholding accuracy. The module responsible for this function identified minimum pixel intensities in image sections of defined dimensions and then subtracted the background signal. It was crucial to appropriately adjust the image section size (set to 50-80 px in this study) to ensure optimal performance. If sections were entirely occupied by cell signals without background, the module could mistakenly subtract the weakest cell signal instead of the actual background, leading to a loss of cellular information. The computed illumination function for all images of the  $\alpha$ -actinin channel was then saved as an ".npy"-file and later imported into the second pipeline. To apply the correction, this file was added as a third channel alongside DAPI and  $\alpha$ -actinin in the "NamesAndTypes" module before processing.

Following illumination correction, nuclear and cellular segmentation were performed. Given that cardiomyocytes frequently contain multiple nuclei, particularly in more mature P5 rat models, the standard propagation-based method was not suitable. Such an approach would incorrectly separate binucleated cardiomyocytes into two distinct cells. To avoid this, nuclei and cardiomyocyte segmentation were carried out individually.

CellProfiler offers multiple configuration options for the "IdentifyPrimaryObjects" module, including various thresholding strategies, object distinction methods and size parameters. Since nuclei are relatively homogeneous in size and morphology and DAPI staining provides a strong signal with minimal background noise, segmentation was performed using the Otsu two-class method. This method effectively classifies pixels into foreground and background categories based on an optimal threshold. Additionally, given the consistent nuclear morphology, clumped nuclei could be accurately distinguished based on shape rather than intensity distribution. The size range was set narrowly (14-17 px) to improve the identification of clumped nuclei. Rather than excluding out-of-range objects immediately, all objects were measured, and those falling outside the acceptable diameter range (16-45 px) were filtered out to prevent misidentification of nuclear clusters or inaccurate segmentations.

A similar approach was applied to segment cardiomyocytes from illumination-corrected  $\alpha$ -actinin images. However, due to the more heterogeneous morphology of cardiomyocytes and the higher background noise from staining, segmentation posed a greater challenge. The "robust background" thresholding method was selected, as it assumes a Gaussian distribution for background signal and removes an adjustable fraction of the highest and lowest intensities. The threshold is then determined by calculating the mean and standard deviation of the remaining pixels and adding an adaptable number of standard deviations to the mean. To effectively distinguish clumped cells, identification based on shape, combined with division by

intensity, proved to be the most suitable approach. The initial size range was set to 40-200 px to ensure the differentiation of touching cardiomyocytes while minimising the misidentification of cytoplasmic projections as separate objects. After object measurement, a final accepted diameter range of 30-250 px was applied to further refine the segmentation.

Then the "MaskObjects" module was applied three times to distinguish cardiomyocytes from stromal nuclei. This module overlays objects with images or other objects to exclude those outside the specified regions. First, cardiomyocytes were masked with nuclei to eliminate incorrectly identified cells, cell debris or cytoplasmic projections without nuclei. Next, nuclei were masked with the remaining cardiomyocytes to specifically identify nuclei within cardiomyocytes. Finally, for stromal nuclei, the same masking process was performed, but with an inverted mask, ensuring that only nuclei outside cardiomyocytes were retained.

To determine cardiomyocyte nuclearity, the "RelateObjects" module was used to assign all nuclei within a single cardiomyocyte as child objects of that cell. This also enabled the creation of subpopulations, such as filtering for mononucleated cells.

Once segmentation and object relationships were established, various measurements could be performed on either individual cells or entire images. Measurements could be calculated per cell or as mean values for all cells in an image along with the standard deviation. Data were then exported as a ".csv"-file. To optimise file size and facilitate downstream analysis, only relevant measurements and image means were selected for export. Additionally, metadata were included to ensure proper assignment of measurements to the correct location on the cell culture plates.

Given the large volume of data generated (spanning multiple measurement types, a 384-well format and four images per well across two wavelength channels, resulting in approximately 33,000 individual data points), a custom Excel analysis file was created. This file integrated CellProfiler data with metadata, automatically calculated means across technical triplicates, and provided a flexible template that could easily be adapted for future experiments with varying compounds, concentrations and conditions.

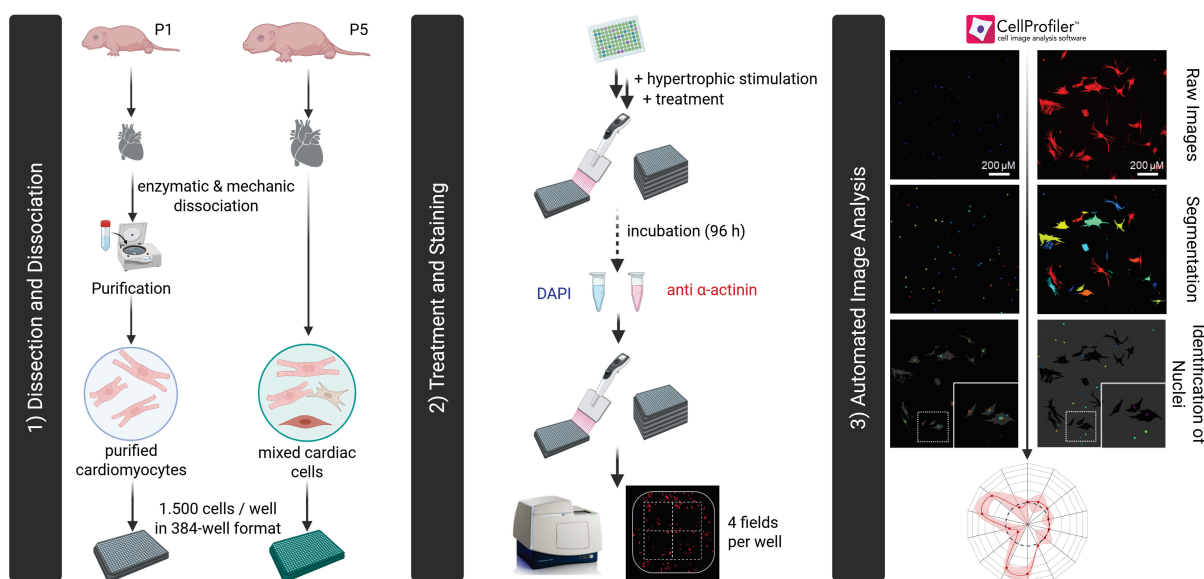
On the first sheet of the designed template, raw data from CellProfiler's ".csv"-file can be inserted. Metadata, such as hypertrophic stimulation, anti-hypertrophic compounds and their respective concentrations, is then automatically assigned to each well. The template organises the data for each measurement in a separate sheet, displaying it as a plate layout for easy visualisation. This allows for quick data review and the identification of outliers among technical replicates, which can be excluded from further analysis if necessary. The remaining data is then processed, calculating the mean and standard deviation for each replicate, and compiled into a final output sheet. From this sheet, data can easily be copied for graphical representation or merged with additional experimental replicates for further analysis.

In summary, the newly developed assay significantly expands the analytical capabilities and throughput of cardiac hypertrophy screening. By incorporating a broader set of phenotypic readouts, it enables a more comprehensive characterisation of cellular responses. The integration of automated image analysis with open-source software ensures high reproducibility and the unbiased measuring of compound effects while maintaining accessibility for various research groups. Additionally, the high-throughput approach allows for the efficient screening of large compound libraries, ultimately increasing the likelihood of identifying promising drug candidates for cardiac hypertrophy.

### 5.1.2 Validation of a Mixed Cardiac Cell Culture System

With the newly developed image analysis pipeline enabling a more comprehensive phenotypic characterisation, the next goal was to enhance the physiological relevance of the underlying assay system. In primary cell culture, NRCMs are typically purified to eliminate non-cardiomyocyte populations, allowing for a focused analysis of cardiomyocyte-specific responses while preventing fibroblast overgrowth. However, this does not fully reflect the complex *in vivo* environment of the heart, which consists of various cell types, including fibroblasts, smooth muscle cells, endothelial cells and immune cells. These cellular interactions and paracrine signalling mechanisms play a crucial role in cardiac function but are not represented in a purified cardiomyocyte culture. Therefore, a mixed cardiac cell culture was used, following a protocol previously established in our group by Dr. Carmen Carrillo García<sup>[91]</sup>. This approach preserved the physiological cellular composition of the neonatal rodent heart while enabling a cardiomyocyte-focused analysis by selective immunocytochemistry.

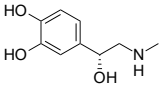
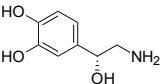
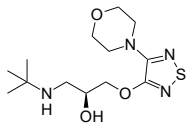
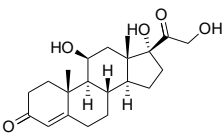
To validate the new CellProfiler pipeline and assess the impact of cell culture composition, a selection of well-characterised hypertrophic stimulants<sup>[65]</sup> targeting different signalling pathways was tested. This included the adrenergic agonists phenylephrine (PE) and norepinephrine (NE), given that excessive adrenergic stimulation is a key driver of pathological cardiac hypertrophy. Additionally, the endogenous peptides endothelin-1 (ET-1) and angiotensin-II (Ang II) were included, both of which are elevated in patients with cardiac hypertrophy and commonly used for *in vitro* stimulation. Furthermore, the cytokines leukemia inhibitory factor (LIF) and transforming growth factor beta 1 (TGF $\beta$ -1), along with cortisol, were tested for their hypertrophic effects. Each stimulant was applied at three different concentrations (see Table 14), except for timolol (TML), which was tested as a  $\beta$ -antagonist in combination with PE to evaluate whether  $\alpha$ -adrenergic stimulation remains dominant when  $\beta$ -adrenergic signalling is blocked. LIF was also tested individually and in combination with PE, a condition previously investigated by Dr. Carmen Carrillo García.



**Figure 9: Established high-throughput and high-content assay platform for hypertrophic phenotype screening.** Neonatal rat hearts are enzymatically dissociated, and cells are either purified via Percoll gradient centrifugation to isolate cardiomyocytes or used as a mixed cardiac cell population, retaining all cardiac cell types. Cells are seeded into 384-well plates and stimulated with pro-hypertrophic agents, followed by treatment with test compounds after 24 h. After 96 h, cells are fixed and stained for  $\alpha$ -actinin and nuclei. High-content imaging (4 fields/well) and automated phenotypic analysis via a custom CellProfiler pipeline enable quantitative evaluation of cardiomyocyte hypertrophy and cell viability.

For each condition, the new CellProfiler pipeline provided a wide range of phenotypic measurements. In addition to the custom cell area analysis, further morphological alterations associated with hypertrophy were examined. Given that cellular enlargement is a hallmark of hypertrophy, previous studies have shown that nuclear size typically increases in parallel with cell growth<sup>[99]</sup>. However, nuclear area is rarely utilised as a parameter for characterising hypertrophy *in vitro*. Accordingly, it was investigated whether this morphological feature could also be reliably captured using the herein established assay. Since hypertrophic cardiomyocytes undergo structural remodelling, changes in  $\alpha$ -actinin staining intensity, indicative of sarcomere composition and density, were analysed along with alterations in cellular texture. Additionally, as cardiomyocytes tend to become binucleated during maturation, the relationship between hypertrophy and nuclearity was explored. Specifically, it was assessed whether hypertrophic stimulation promotes an increase in nuclearity and whether mononucleated and binucleated cells respond differently to hypertrophic stimulants. Lastly, to account for potential cardiotoxic effects, cell viability was assessed by measuring the total number of detected nuclei and cardiomyocytes.

**Table 14: Overview of tested hypertrophic stimulants.**

Stimulants	Compound Structure	Target	Concentrations
Phenylephrine (PE)		Alpha-1 adrenergic agonist (GPCR)	10; 20; 50 $\mu$ M
Norepinephrine (NE)		Alpha- and beta-adrenergic agonist (GPCR)	1; 2; 5 $\mu$ M
Timolol (TML)		Beta-adrenergic antagonist (GPCR)	2 $\mu$ M (+ PE 20 $\mu$ M)
Cortisol		Cortisol receptor (nuclear receptor, transcription factor)	1; 2; 5 $\mu$ M
Endothelin-1 (ET-1)	Cys-Ser-Cys-Ser-Ser-Leu-Met-Asp-Lys-Glu-Cys-Val-Tyr-Phe-Cys-His-Leu-Asp-Ile-Ile-Trp	Endothelin-1 receptor (GPCR)	50; 100; 200 nM
Angiotensin II (Ang. II)	Asp-Arg-Val-Tyr-Ile-His-Pro-Phe	Angiotensin II receptor (GPCR)	50; 100; 200 nM
Leukemia inhibitor factor (LIF)	[cytokine of IL-6 family]	Gp130 receptor associated to LIF receptor	20; 50; 100 ng/ml
TGF $\beta$ -1	[cytokine of TGF $\beta$ family]	TGF $\beta$ receptor (transmembrane serine/threonine kinase)	50; 100; 200 ng/ml

Representative results for one concentration of each stimulant are shown in Figure 10, results from further concentrations are shown in the Appendix 7.1. All tested conditions induced measurable changes in the selected phenotypic parameters, although to varying extents. As expected, cardiomyocyte area increased significantly in response to most hypertrophic

stimulants. Additionally, the nuclear area expanded slightly in cardiomyocytes but remained unchanged in stromal cells (non-cardiomyocytes), supporting the hypothesis that cellular growth is accompanied by nuclear enlargement.

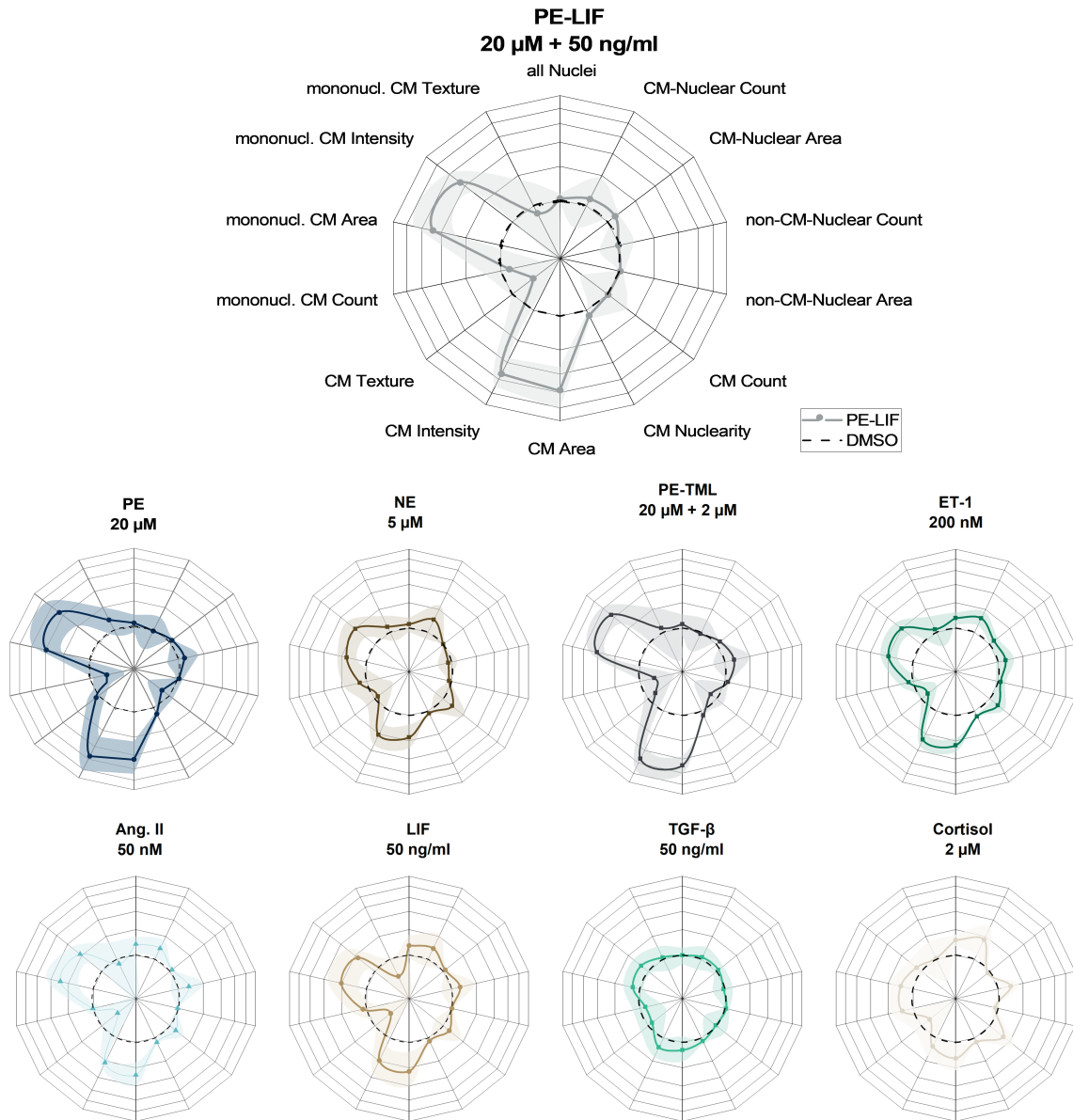


**Figure 10: Overview of hypertrophy phenotypes induced by distinct stimuli.** Phenylephrine (PE), norepinephrine (NE), timolol (TML), endothelin-1 (ET-1), angiotensin-II (Ang. II), leukemia inhibitory factor (LIF), transforming growth factor beta 1 (TGF $\beta$ -1) and cortisol are shown in one representative concentration. The total dataset is shown in Appendix 7.1. (n = 3, normalised to DMSO, axis range from 50-350%, mean  $\pm$  SEM)

Since  $\alpha$ -actinin is a key structural protein of the sarcomere, its staining intensity and distribution reflect changes in sarcomere organisation during hypertrophy. As expected, hypertrophic remodelling led to alterations in  $\alpha$ -actinin intensity, indicating structural reorganisation. In some conditions, a decrease in texture measurements was also observed,

suggesting disruptions in sarcomere composition. However, this effect was not consistent across all hypertrophic phenotypes, such as those induced by PE and NE, and exhibited high variability, including susceptibility to outliers.

Regarding cardiomyocyte nuclearity, only a slight yet consistent increase was detected across all stimulants. Interestingly, the response patterns of mononucleated cardiomyocytes closely mirrored those of the total cardiomyocyte population (including both mono- and binucleated cells), indicating that nuclearity did not provide additional discriminatory power in assessing hypertrophic stimulation.

To assess potential cardiotoxic effects, total nuclear counts, as well as the individual subpopulations of cardiomyocytes and non-cardiomyocytes nuclei, were analysed alongside cardiomyocyte numbers. As expected, none of the hypertrophic stimulants led to a significant reduction in cell populations, indicating an absence of cytotoxicity. This aligns with previous reports, as all tested stimulants are physiological substances known to induce hypertrophy rather than exert toxic effects<sup>[65]</sup>. However, stimulation with NE, ET-1, Ang. II and Cortisol resulted in a slight increase in object counts. This increase can be attributed to the proliferative capacity of cardiac fibroblasts. In contrast, cardiomyocytes typically lose their proliferative ability shortly after birth, making their increased object count intriguing. Possible explanations include residual proliferative capacity at postnatal day 5, an increase in binucleation (although nuclearity was only marginally elevated) or potential segmentation inaccuracies.

Among all measured parameters, three exhibited the most pronounced and consistent changes across all tested stimulants: cardiomyocyte area, nuclear area and  $\alpha$ -actinin staining intensity. To facilitate direct comparisons between different hypertrophic stimulants and to evaluate subsequent pharmacological inhibition, these parameters were integrated into a single metric, the 'Hypertrophy Score', calculated as follows:

$$\text{Hypertrophy Score} = (\text{CM-Nuclear Area}) * (\text{CM Area}) * (\text{CM Intensity}) * 10^{-4}$$

The Hypertrophy Scores for all stimulants at various concentrations are presented in Figure 11. Although adrenergic receptors are activated by the same catecholamines, differences in their expression patterns and downstream signalling cascades result in distinct cellular effects. Cardiac contractility is primarily regulated by  $\beta$ -adrenergic signalling, whereas chronic overstimulation of this pathway has been associated with cellular stress and maladaptive remodelling. In contrast,  $\alpha$ -adrenergic receptors are more closely involved in the regulation of cardiomyocyte growth and play a comparatively minor role in modulating cardiac output<sup>[100]</sup>. The effect of  $\alpha$ -adrenergic receptors is well reflected in the results of the Hypertrophy Score, where the  $\alpha_1$ -adrenergic agonist PE exhibited the strongest hypertrophic response, both when applied alone and in a previously reported combination with the  $\beta$ -antagonist TML, which was

used to isolate  $\alpha$ -adrenergic stimulation, or the IL-6 family cytokine LIF<sup>[99]</sup>. Across all tested conditions, PE significantly increased the Hypertrophy Score compared to the DMSO control. The combination of PE and LIF induced the most pronounced hypertrophic effect, establishing it as the positive control for subsequent experiments.

Interestingly, NE, a non-selective adrenergic agonist activating both  $\alpha$ - and  $\beta$ -adrenergic receptors, elicited a weaker hypertrophic response than PE. This observation, together with the potent effect of PE in combination with TML, highlights the dominant role of  $\alpha$ -adrenergic signalling in driving hypertrophic growth *in vitro*, compared to  $\beta$ -adrenergic pathways.

ET-1 and Ang. II also demonstrated robust hypertrophic effects, reinforcing their known roles in cardiac remodelling<sup>[65]</sup>.

LIF, as previously mentioned, is a cytokine of the IL-6 family that has been shown to induce cardiac hypertrophy through activation of the gp130 receptor subunit<sup>[101]</sup>. In addition to activating JAK/STAT and MAPK signalling pathways<sup>[102]</sup> (both of which are closely associated with hypertrophic remodelling<sup>[103]</sup>) LIF also upregulates L-type  $\text{Ca}^{2+}$  channels, thereby increasing calcium influx. This rise in intracellular  $\text{Ca}^{2+}$  levels activates  $\text{Ca}^{2+}$ -dependent kinases such as calcineurin and calmodulin, ultimately promoting the expression of hypertrophic genes<sup>[104]</sup>.

Due to its engagement of multiple pro-hypertrophic pathways, the combination of LIF with adrenergic stimulation (PE) may lead to a broader and more robust induction of hypertrophy, enhancing the dynamic range of the assay. Furthermore, the activation of JAK/STAT signalling is closely linked to inflammatory processes<sup>[105]</sup>, thereby LIF mimics another hallmark of pathological cardiac hypertrophy and increases the biological relevance and complexity of the *in vitro* disease model. In line with these expectations, LIF elicited a pronounced hypertrophic response in the assay, which was further amplified when administered in combination with PE.

To assess the influence of cell density on hypertrophic responses, experiments were conducted at two different seeding densities: 1,500 or 4,000 cells per well in a 384-well plate. The phenotypic changes were comparable across both conditions; however, the dynamic range of hypertrophy was greater at lower cell densities (see Figure 11). This suggests that cardiomyocytes require sufficient space in 2D culture to exhibit hypertrophic growth. At the lower density of 1,500 cells per well, the cells were more isolated, while at the higher density of 4,000 cells per well, confluency increased, leading to a higher probability of cell-cell contacts. The confluency plays a crucial role, as reduced cell density likely enhances the drive for cardiomyocytes to grow toward neighbouring cells. From a technical perspective, a lower cell density also improves segmentation accuracy, as the reduced occurrence of cell clumping facilitates more precise segmentation of individual cardiomyocytes.



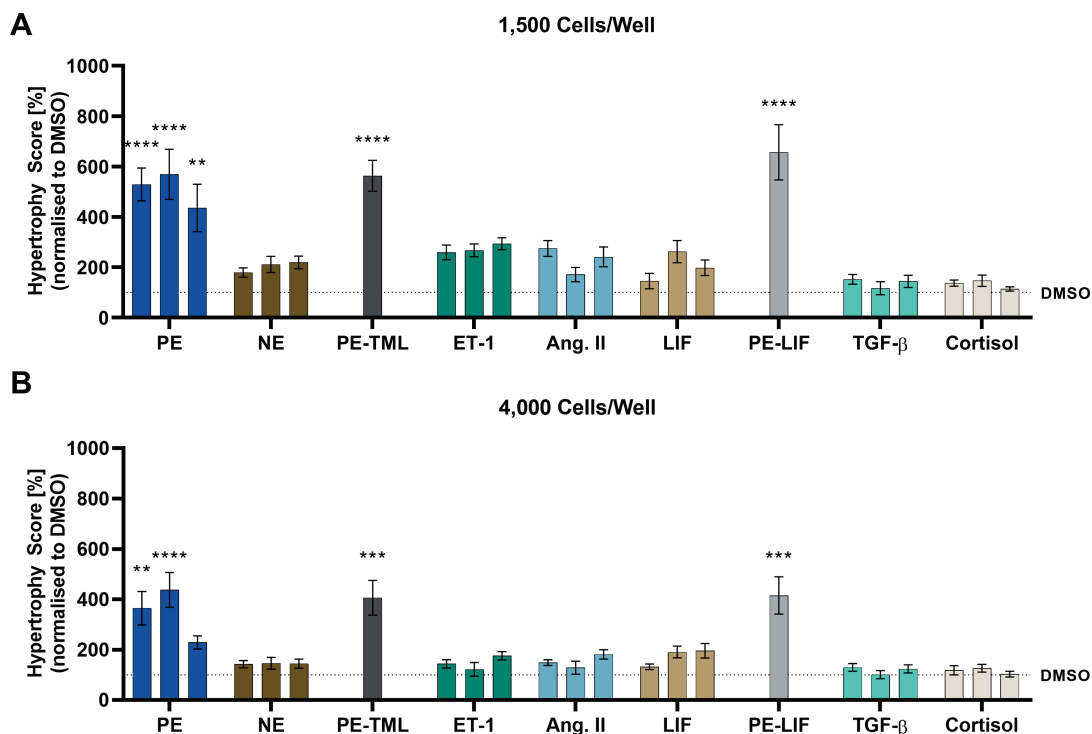


**Figure 11: Characterisation of hypertrophy induction at two cell densities.** Hypertrophic stimulants were incubated on mixed cardiac cells for four days, using two different cell densities: **(A)** 1,500 cells per well and **(B)** 4,000 cells per well. Each stimulant was tested at three increasing concentrations (left to right), except for the combination of PE with LIF and TML, which was only tested in one fixed combination. Specific concentrations are provided in Table 14. Consequently, image analysis was performed and results for the Hypertrophy Score are shown. (n = 3, normalised to DMSO, mean  $\pm$  SEM, one-way ANOVA, \*  $p \leq 0.05$ , \*\*  $p \leq 0.01$ , \*\*\*  $p \leq 0.001$ , \*\*\*\*  $p \leq 0.0001$ )

In this chapter, a high-throughput image analysis pipeline was applied to a mixed cardiac cell culture, allowing for a quantitative and unbiased assessment of hypertrophic responses. By evaluating multiple phenotypic parameters, including cellular and nuclear area as well as  $\alpha$ -actinin intensity, a Hypertrophy Score was established to facilitate direct comparisons between stimulants and treatment effects. The analysis revealed that PE alone and in combination with LIF or TML induced the strongest hypertrophic response, confirming the importance of  $\alpha$ -adrenergic signalling *in vitro*. Furthermore, testing at two different cell densities showed that a lower density increased the dynamic range of hypertrophic responses, likely due to enhanced space for cellular expansion. These findings highlight the robustness of the image-based phenotypic assay, providing a sensitive and scalable platform for studying hypertrophic mechanisms and potential therapeutic interventions.

### 5.1.3 Mixed Cardiac Culture Compared to Purified Cardiomyocytes

By culturing the physiological mix of cardiac cells, the newly established approach enhances the translational relevance of the assay by preserving intercellular signalling and

paracrine interactions. However, many standard protocols purify primary cardiomyocytes after dissociation to focus exclusively on cardiomyocyte biology and to prevent fibroblast overgrowth, which can complicate long-term analysis. To evaluate the advantages and limitations of the mixed cardiac cell approach, the next step involved directly comparing this model to a protocol that enriches cardiomyocytes through purification. The goal was to determine whether the mixed cardiac cell culture achieves a similar dynamic range and exhibits comparable phenotypic responses to hypertrophic stimulation.

For this comparison, a well-established cardiomyocyte purification protocol from the group of Oliver Müller at the University Hospital Schleswig-Holstein was implemented<sup>[106]</sup>. This method employs Percoll gradient centrifugation following enzymatic heart dissociation to enrich cardiomyocytes based on their density. Stromal cells, which accumulate in the upper or lower gradient phases, are effectively removed.

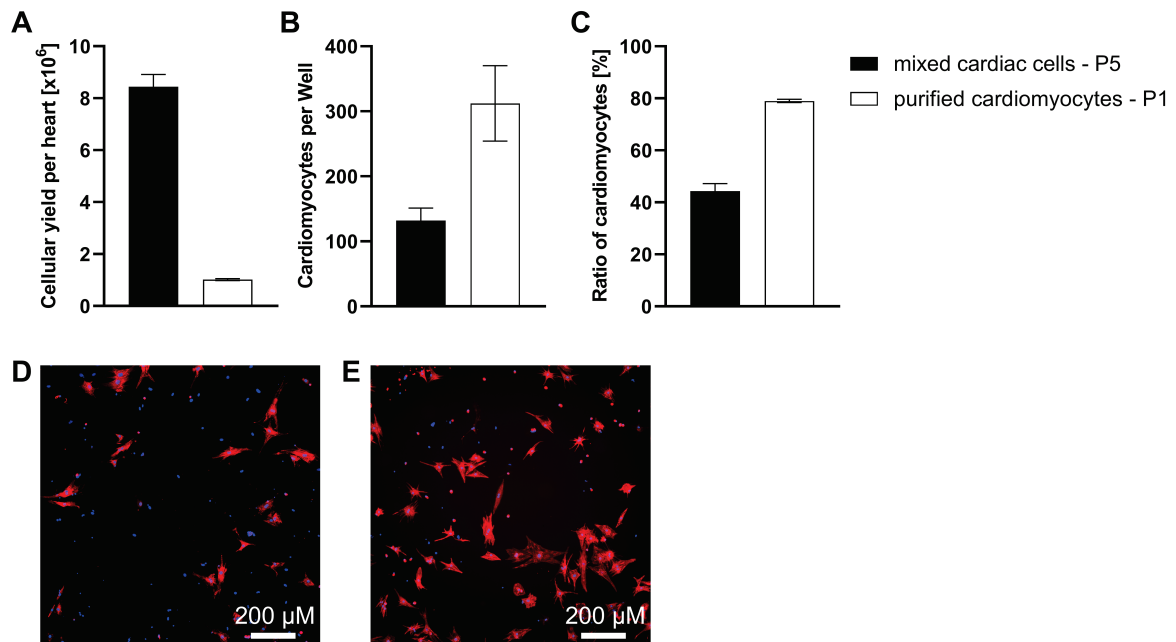


**Figure 12: Comparison of mixed cardiac cells and purified cardiomyocytes protocols.** (A) The cellular yield after dissociation shows that more cells are obtained by the mixed cardiac cell protocol, since stromal cells remain in culture. (B) Comparing the number of identified cardiomyocytes per well for both protocols revealed a higher number of cardiomyocytes for the purified protocol at the same seeding density. (C) The ratio of cardiomyocytes in culture shows the purification efficiency of the Percoll gradient centrifugation, resulting in roughly double the number of cardiomyocytes. Representative images are shown for (D) mixed cardiac cells and (E) purified cardiomyocytes treated with PE-LIF (20  $\mu$ M / 50 ng/mL), stained with DAPI (nuclei, blue) and  $\alpha$ -actinin (cardiomyocytes, red). (n $\geq$ 5, mean  $\pm$  SEM)

One key distinction between the two protocols is the age of the neonatal rats. The purification protocol relies on one-day-old (P1) rats, whereas the mixed cardiac cell culture is derived from five-day-old (P5) rats. P1 cardiomyocytes exhibit a more immature protein

expression profile and a lower tendency for binucleation, potentially influencing hypertrophic responses. To ensure a robust comparison, the same panel of hypertrophic stimulants was tested in both models, allowing for a direct assessment of their respective phenotypic responses.

Altering the cellular composition not only affects the cellular response to stimulation but also impacts the baseline characteristics of the assay. A direct comparison of both protocols is shown in Figure 12. Using P5 rats resulted in a yield of  $8.4 \times 10^6$  cells per heart after dissociation, whereas P1 rats, with their smaller and less developed hearts, produced only  $1.0 \times 10^6$  cells per heart after dissociation and purification. From a high-throughput perspective, P5-derived cultures are advantageous as they generate a significantly higher cellular yield per animal, reducing the number of animals required for experiments.

However, the purification step increases the cardiomyocyte ratio in culture. At a seeding density of 1,500 cells per well, the mixed cardiac cell culture contained approximately 132 cardiomyocytes per well, while the purified protocol yielded 312 cardiomyocytes per well. This translates to a cardiomyocyte ratio of 44% in the mixed culture compared to 79% in the purified culture. By incorporating Percoll gradient centrifugation, the ratio of cardiomyocytes per well is roughly doubled, thereby enhancing the statistical power of the analysis, as the mean values per well are derived from a larger number of cardiomyocytes. Of note, flow cytometry is generally considered the method of choice for quantifying cell population compositions due to its high throughput and precision. However, in this study, the use of neonatal rat cardiomyocytes posed significant challenges for flow cytometric analysis. The elongated morphology of cardiomyocytes, combined with their sensitivity to mechanical stress, resulted in substantial cell loss during the multiple washing and centrifugation steps required for sample preparation. As an alternative, image-based quantification was employed to estimate purification efficiency. While this method is less precise due to the smaller sample size and limited statistical power compared to flow cytometry, it provided a practical solution given the technical difficulties associated with cardiomyocyte handling in suspension-based assays<sup>[107]</sup>.

Comparing the effects of hypertrophic stimulants between mixed cardiac cell cultures and purified cardiomyocytes (see Figure 13) revealed that PE induced the highest Hypertrophy Score in both approaches. In both cases, combining PE with TML or LIF further enhanced its hypertrophic effect.

A closer look at the dynamic range shows that purified cardiomyocytes exhibited a stronger hypertrophic response to PE, NE, ET-1 and Ang. II stimulation compared to mixed cardiac cell cultures. Interestingly, the tested cytokines LIF and TGF $\beta$ -1 had little to no effect in the mixed culture, whereas in purified cardiomyocytes, LIF significantly increased the Hypertrophy Score, reaching a level comparable to PE stimulation.

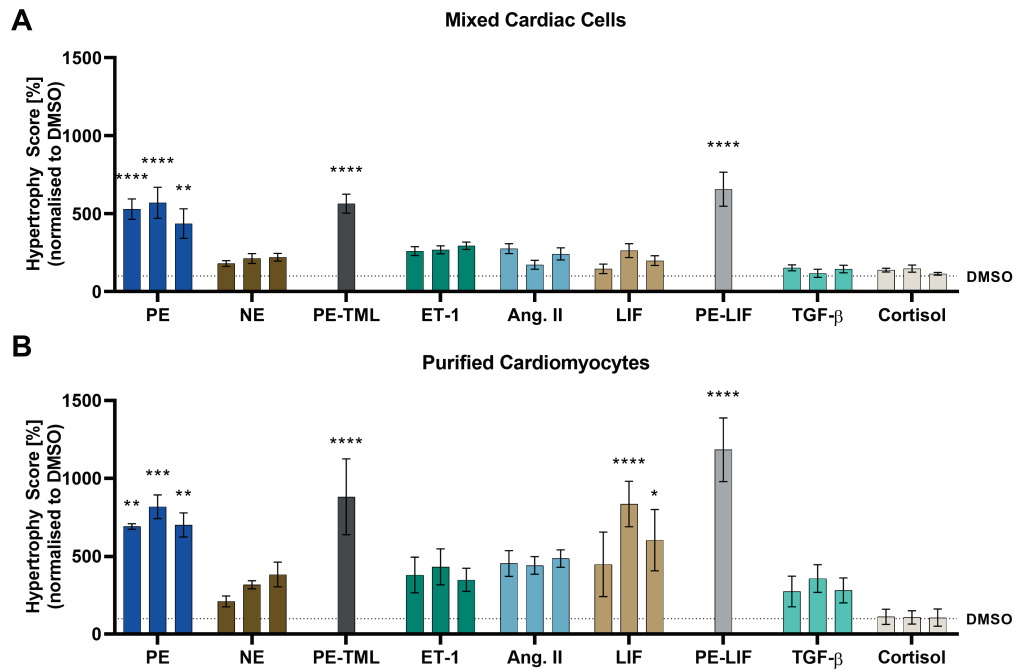


**Figure 13: Hypertrophy Scores for mixed cardiac cells and purified cardiomyocytes.** Hypertrophic stimulants were incubated for four days on (A) P5 mixed cardiac cells and (B) P1 purified cardiomyocytes. Each stimulant was tested at three different concentrations (see Table 14), except for the combination of PE with LIF and TML, which was only tested in one fixed combination. Specific concentrations are provided in Table 14. Consequently, image analysis was performed and results for the Hypertrophy Score are shown. ( $n = 3$ , normalised to DMSO, mean  $\pm$  SEM, one-way ANOVA, \*  $p \leq 0.05$ , \*\*  $p \leq 0.01$ , \*\*\*  $p \leq 0.001$ , \*\*\*\*  $p \leq 0.0001$ )

One possible explanation for this discrepancy is the lack of cell-cell communication in purified cardiomyocyte cultures. In the absence of paracrine signalling from non-cardiomyocyte populations, cytokines may exert a stronger direct effect on cardiomyocytes than in a co-culture. This highlights the importance of assay selection, as it directly influences the experimental outcome. Evaluating treatment options that target cytokine signalling in mixed cardiac cultures could lead to false-negative results if the effect is masked by intercellular interactions. However, if a potential treatment only affects isolated cardiomyocytes but not co-cultured, its *in vivo* relevance becomes questionable, given the complexity of the three-dimensional cardiac environment and its diverse cellular composition.

This comparative analysis demonstrates that both mixed cardiac cell cultures and purified cardiomyocytes offer distinct advantages and their selection should be guided by the specific research question. While purified cardiomyocytes provide a higher dynamic range and a stronger hypertrophic response, they lack the physiological complexity of intercellular communication present in mixed cultures. The latter, by maintaining the native cellular composition of the heart, better reflects *in vivo* conditions, making it particularly valuable for studying paracrine signalling and cell-cell interactions. Moreover, certain stimulants, such as cytokines, may have an exaggerated impact in purified cultures due to the absence of

competing signals. These findings emphasise the importance of assay design in determining experimental outcomes and highlight the necessity of carefully selecting the most suitable model system for drug screening, mechanistic studies and translational research.

### 5.1.4 Comparison of Two Imaging Systems

The characterisation of the hypertrophic phenotypes relies heavily on image analysis, making image quality a crucial factor in achieving accurate and reproducible results. Poor image quality should intuitively lead to a reduced dynamic range or even the loss of important phenotypic information. The group of B. A. Cimini previously validated the robustness of the Cell Painting assays using multiple imaging systems with a subsequent CellProfiler analysis, demonstrating that while certain imaging parameters were essential for optimal results, the assay remained broadly applicable across different devices<sup>[108]</sup>.

To assess whether this phenotypic assay is similarly robust across different imaging systems, two representative plates from the hypertrophic stimulant experiment were analysed using two different microscopy platforms: the ImageXpress (the standard system for this study) and the Keyence BZ-X810 Fluorescence Microscope. While the Keyence system is not equipped with an automated plate handler or high-throughput imaging capabilities, it offers several advantages in terms of image quality. As a newer model, the BZ-X810 supports a higher interpolated pixel resolution (up to 12.5 MP) and employs an LED light source, allowing for sharper imaging and enhanced fluorescence signal detection. In contrast, the ImageXpress Micro XL uses a 4.66 MP scientific CMOS sensor and a solid-state light engine, prioritising speed and reproducibility for high-throughput workflows. Furthermore, the ImageXpress offers high stage precision and robust support for automated plate handling, making it the more suitable option for large-scale screening applications. In the Keyence-based imaging workflow, four images per well were acquired and stitched together, rather than capturing multiple individual sites as done with the ImageXpress, which resulted in fewer total images and a faster downstream analysis pipeline in this smaller-scale context.

As shown in Figure 14, both imaging systems exhibited strong correlations for hypertrophic parameters. Cardiomyocyte area and intensity measurements correlated well, with  $R^2$  values of 0.8527 and 0.9310, respectively. However, the correlation for nuclear area was unexpectedly lower ( $R^2 = 0.3741$ ). This may be due to the fact that nuclei are relatively small objects, making their segmentation more sensitive to slight differences in image resolution, magnification or stitching. Even minor variations in how nuclear boundaries are detected can significantly affect area measurements. In contrast, larger structures like cardiomyocytes are less affected by these subtle discrepancies, resulting in more consistent measurements across imaging systems. Despite this, the Hypertrophy Score itself maintained a strong correlation

( $R^2 = 0.8806$ ), confirming that both imaging systems can effectively characterise hypertrophic phenotypes.

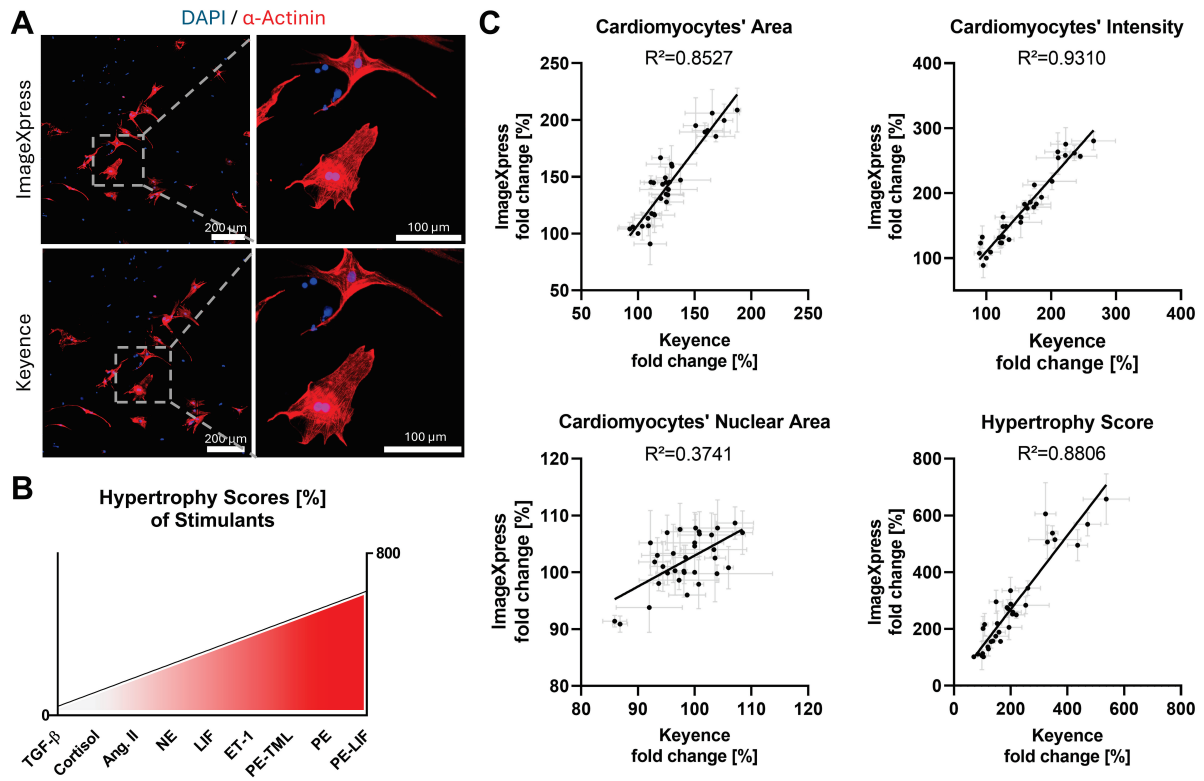


**Figure 14: Cross-platform comparison of hypertrophic phenotype analysis using two imaging systems.**

**(A)** Representative immunofluorescence images of PE-LIF (20  $\mu$ M and 50 ng/mL) stimulated cells were acquired using the ImageXpress XL (Molecular Devices) and BZ-X800 (Keyence) imaging platforms. **(B)** Overview of Hypertrophy Score results from the previous hypertrophic stimulant screening, illustrating the range of phenotypic responses across different stimulants. These data form the basis for the correlation analyses shown in **(C)**. **(C)** Images were taken from screening plates containing various hypertrophic stimulants to ensure analysis across a range of stimulation conditions. Cardiomyocyte area and intensity show strong correlations ( $R^2 = 0.85$  and  $0.93$ ), while nuclear area correlates less robustly ( $R^2 = 0.37$ ), likely due to sensitivity in nuclear segmentation. The overall Hypertrophy Score remained consistent between systems ( $R^2 = 0.88$ ), supporting reliable phenotype assessment across platforms. ( $n = 2$ , normalised to DMSO, mean  $\pm$  SEM)

This comparison highlights the robustness and adaptability of the phenotypic hypertrophy assay across different imaging platforms. While image quality and segmentation differences can slightly affect certain parameters, the core phenotypic measurements and overall Hypertrophy Score remain consistent. This indicates that the assay can be successfully applied across different laboratory setups, making it a versatile tool for high-content screening and phenotypic analysis of cardiac hypertrophy.

### 5.1.5 Establishing a Confirmatory qPCR Assay

Screening assays in drug discovery are designed to achieve high physiological relevance, strong translational power and a direct link to the pathophysiology of the investigated disease. By implementing a mixed cardiac cell culture, which retains the natural cellular composition of the heart, and by expanding the image analysis beyond simple cell area measurements, the original assay was significantly improved, increasing its robustness and predictive value. However, to ensure the reliability and reproducibility of observed effects, each screening assay requires an orthogonal confirmation assay. This validation step helps eliminate false positives, making the process more cost-effective, reducing unnecessary follow-up experiments and ultimately enhancing the translation of *in vitro* findings into clinically relevant outcomes.

For this phenotypic hypertrophy assay, quantitative real-time PCR (qPCR) was established as an orthogonal confirmatory assay to analyse cardiac hypertrophy-related gene expression. qPCR is a powerful and widely accepted method for quantifying gene expression changes, offering high sensitivity and specificity. Additionally, to confirm the efficacy seen in the phenotypic assay, qPCR analysis provides molecular evidence of the induced phenotype, offering a more comprehensive understanding of the biological processes at play. Since the progression of cardiac hypertrophy is associated with a reversion to the fetal gene program, cardiomyocytes begin expressing immature isoforms and stress-response proteins to compensate for increased workload and maintain cardiac function<sup>[19, 20]</sup>. The most prominent markers of this fetal reprogramming are the natriuretic peptides ANP and BNP, encoded by the *Nppa* and *Nppb* genes, respectively. Their expression is strongly upregulated in hypertrophic and failing hearts, making them key molecular indicators of hypertrophy.

Notably, this was the first time qPCR was implemented in our group for analysing gene expression in NRCMs. Establishing this protocol not only strengthens the assay pipeline but also broadens the analytical scope, allowing both phenotypic and molecular confirmation of hypertrophic responses.

In a first step, the hypertrophic induction of *Nppa* and *Nppb* in the mixed cardiac cell culture was assessed to confirm whether the stimulation of gene expression could be detected. To achieve this, cells were stimulated with a combination of 100  $\mu$ M PE and 50 ng/ml LIF, using a higher PE concentration than in the phenotypic assay. This adjustment was necessary because the stimulation period for qPCR analysis was limited to 24 h, requiring a stronger stimulus to increase the dynamic range of gene expression changes.

One key limitation of the qPCR approach was the high number of cells required for sufficient mRNA extraction. For reliable quantification, at least  $6 \times 10^5$  -  $1 \times 10^6$  cells had to be lysed per sample, which corresponds to a 400-fold higher cell number compared to the phenotypic assay, significantly reducing the throughput of the qPCR assay. Given that only about 7 million

cells could be extracted on average from each P5 rat heart, this limitation meant that fewer conditions could be tested per experiment compared to the high-throughput phenotypic assay.

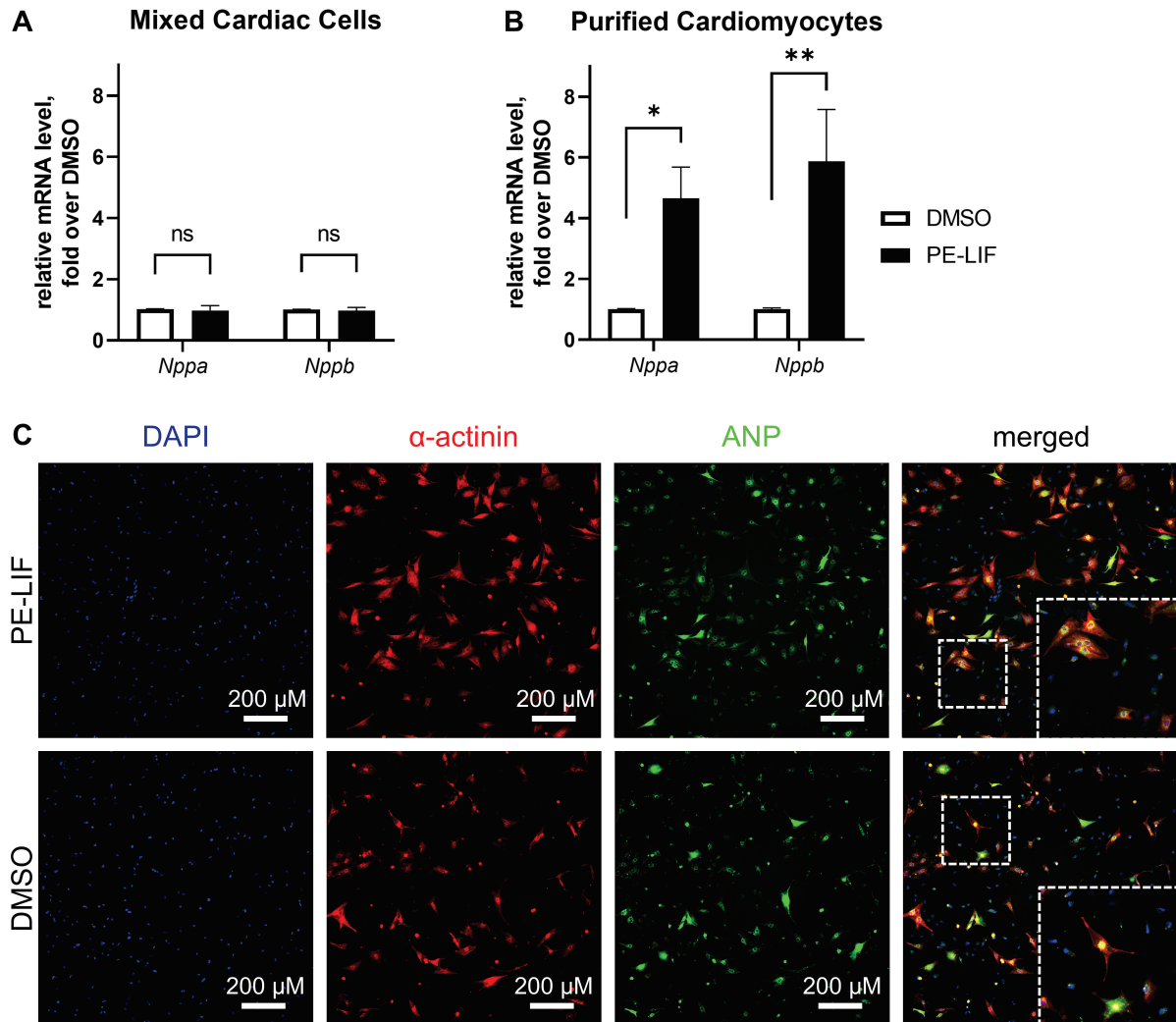


**Figure 15: Orthogonal assay readouts to validate PE-LIF-induced hypertrophy phenotypes.** (A, B) Cells were stimulated three days after seeding with 100  $\mu$ M PE and 50 ng/ml LF for 24 h and the gene expression levels of *Nppa* and *Nppb* were analysed by qPCR, using *Rpl32* as housekeeping gene. In mixed cardiac cell culture, (A) stimulation showed no induction of *Nppa* and *Nppb*, suggesting an interference from non-cardiomyocyte cells. In contrast, purified cardiomyocytes (B) showed a significant upregulation of both genes following stimulation, confirming the expected hypertrophic response. (C) Immunostaining for ANP in mixed cardiac cultures revealed that non-cardiomyocytes also displayed ANP signals, indicating a potential source of background expression that may obscure cardiomyocyte-specific expression changes. (n = 3, normalised to DMSO, mean  $\pm$  SEM, one-way ANOVA, \*  $p \leq 0.05$ , \*\*  $p \leq 0.01$ , \*\*\*  $p \leq 0.001$ , \*\*\*\*  $p \leq 0.0001$ )

Interestingly, despite 24 h of PE and LIF stimulation, neither *Nppa* nor *Nppb* expression was elevated in the mixed cardiac cell culture, remaining at levels comparable to the DMSO control. To investigate whether this was due to the presence of non-cardiomyocyte cells, the same stimulation protocol was applied to purified cardiomyocytes. This resulted in a significant increase in both *Nppa* and *Nppb* expression. Since these genes are widely reported to be



exclusively expressed in cardiomyocytes<sup>[109, 110]</sup>, this unexpected result raised questions about the influence of stromal cells on gene expression detection in the mixed culture.

To clarify these observations, an immunostaining experiment for ANP was performed under the same stimulation conditions as the phenotypic assay. The results revealed that ANP expression varied greatly among cardiomyocytes: some cells were strongly stained, indicating high expression, while others showed only weak perinuclear staining. Surprisingly, stromal cells also displayed an ANP signal, with an intensity comparable to weakly stained cardiomyocytes. This suggested that in a mixed cardiac culture, the presence of ANP-positive stromal cells could interfere with the qPCR-based detection of hypertrophy-related gene expression, masking cardiomyocyte-specific changes.

In conclusion, *Nppa* and *Nppb* expressions are not reliable markers in mixed cardiac cultures, as stromal cells overshadow cardiomyocyte-specific expression. To ensure accurate qPCR-based confirmation of hypertrophic responses, subsequent experiments were conducted exclusively on purified cardiomyocytes.

### 5.1.6 A “Therapeutic Assay” Approach: Rescue of the Hypertrophy Phenotype

*In vitro* models of cardiac hypertrophy typically follow a preventive treatment concept, in which disease phenotypes are induced simultaneously with the administration of a potential therapeutic compound. While this approach provides valuable insights into the pathophysiological mechanisms and potential cardioprotective interventions, it does not fully reflect the clinical reality. In patients, cardiac hypertrophy develops gradually over time and is often only diagnosed once pathological remodelling has progressed. Consequently, therapeutic interventions in a clinical setting primarily aim to reverse or at least delay disease progression rather than prevent its onset. To better mimic this therapeutic context, a phenotypic rescue model was developed, in which hypertrophy was established before administering potential treatments in order to assess whether pathological changes in cardiomyocytes can be reversed or rescued.

A major challenge in designing such an assay is the intrinsic time constraints imposed by NRCMs. Over time, NRCMs undergo dedifferentiation in 2D culture, a process driven by the loss of native biochemical and mechanical stimuli. This leads to significant morphological and functional changes within approximately one week in culture<sup>[111]</sup>.

This limited time window makes a carefully optimised protocol necessary, ensuring that cardiomyocytes develop a stable hypertrophic phenotype before treatment while still allowing sufficient time for potential therapeutic effects to manifest.

To determine the optimal timing for treatment application, it was first necessary to establish a time profile over 96 h of hypertrophic development in NRCMs. Cells were seeded and allowed to adhere for 24 h, after which hypertrophic stimulation was applied. Subsequently,

cells were fixed and analysed at 24-hour intervals (i.e., at 24, 48, 72 and 96 h post-stimulation) to monitor the progression of morphological changes. Two well-characterised hypertrophic stimuli were selected based on previous experiments: PE in combination with LIF, which had demonstrated the strongest hypertrophic effects and was therefore chosen as a positive control, and ET-1, a widely used hypertrophic stimulant that had shown consistent results in this assay. By mapping the kinetics of hypertrophic response, this approach aimed to define a precise time point at which the pathological phenotype is established, thus enabling the subsequent assessment of potential therapeutic compounds for phenotypic rescue.

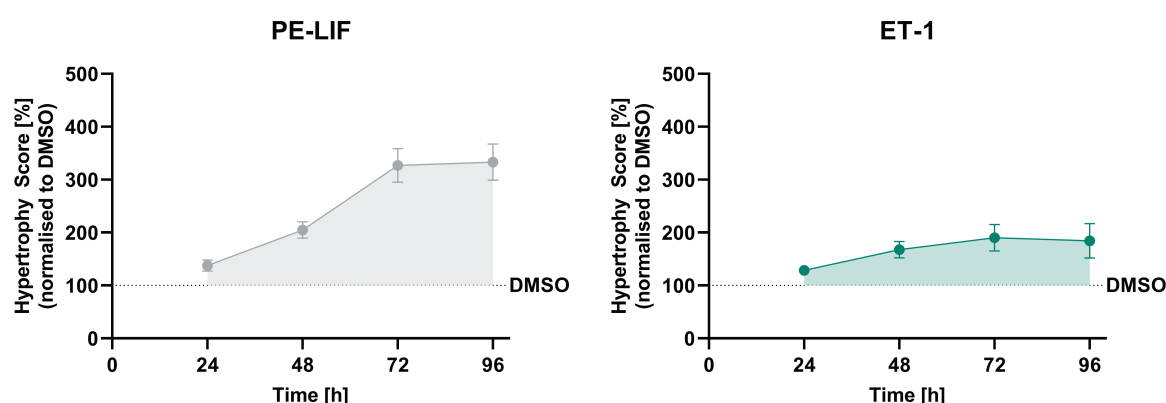


**Figure 16: Time profile of hypertrophic stimulation.** Mixed cardiac cells were stimulated with either PE-LIF (20  $\mu$ M and 50 ng/ml) or ET-1 (200 nM), and hypertrophic progression was monitored over a 96-hour period, with assessments every 24 h. While only a slight increase in the Hypertrophy Score was observed at 24 h, a distinct hypertrophic phenotype developed by 48 h, reaching its peak at 72 h, after which no further increase was detected. (n = 3, mean  $\pm$  SEM)

The results of the time profile analysis, as shown in Figure 16, confirm PE-LIF as a stronger stimulant of cardiac hypertrophy compared to ET-1, consistent with findings from the assay validation in Chapter 5.1.2. After 24 h of stimulation, only minor changes in the Hypertrophy Score were observed, suggesting the early onset of hypertrophic remodelling. By 48 h, the hypertrophic phenotype was clearly established, with further progression observed until 72 h, where hypertrophy reached its maximum. No additional increases were detected between 72 and 96 h, indicating that in this assay, cardiomyocyte hypertrophy is fully developed after 72 h.

For the “therapeutic assay” approach, 48 h and 72 h after hypertrophic stimulation were identified as suitable time points for compound administration. However, given the 96-hour timeframe of the assay, this approach allows for only 48 or 24 h of exposure to the anti-hypertrophic treatment, respectively. This limited duration may not be sufficient for the compounds to fully reverse the disease phenotype.

To evaluate whether the preventive activity of previously tested compounds could be translated into a therapeutic setting, three anti-hypertrophic agents were selected for further analysis: the GRK5 inhibitor **4a** from Chapter 5.2.3 as well as the glutaminase inhibitor **CB-839** and the glutamine reuptake inhibitor **V-9302**, both discussed in Chapter 5.3.3. In this setup, hypertrophy was first induced with PE-LIF, followed by compound administration at 24 h, 48 h or 72 h post-stimulation. The compounds' ability to reverse the established hypertrophic phenotype was then evaluated.

As shown in the results in Figure 17, the GRK5 inhibitor **4a** demonstrated only a modest, dose-dependent reduction in hypertrophy when added 24 h post-stimulation, with Hypertrophy Scores not returning to baseline DMSO levels. At later treatment initiation points (48 h and 72 h), **4a** failed to elicit a therapeutic effect even at concentrations that were effective in the preventive setting. These findings suggest that GRK5 inhibition may be more effective in preventing, rather than reversing, hypertrophy. However, possible compound instability over the multi-day experiment may also have contributed to the diminished effect, warranting follow-up experiments using freshly prepared solutions and stability profiling under assay conditions.

**CB-839**, which had previously shown strong dose-dependent preventive effects against PE-LIF-induced hypertrophy, failed to achieve a full therapeutic response. Although early administration (24 h) resulted in a partial reduction of Hypertrophy Scores, a consistent dose-response relationship was no longer observed and values remained between PE-LIF and DMSO controls across all concentrations and time points. Of note, early administration of **CB-839** showed stronger effects than later ones.

In contrast, **V-9302** showed a clear dose-dependent reduction in hypertrophy across all treatment windows. However, its anti-hypertrophic effect at high concentrations coincided with pronounced cytotoxicity in both cardiomyocytes and non-cardiomyocytes, indicating that the observed phenotype was driven by toxicity rather than targeted reversal. At lower, non-toxic concentrations, **V-9302** still produced a partial therapeutic effect, though efficacy declined with later treatment initiation, suggesting time-dependent sensitivity of the hypertrophic phenotype to metabolic interference.

In summary, this study highlights the challenges of therapeutically reversing established cardiac hypertrophy and underscores the importance of early intervention. Among the tested compounds, **V-9302** showed the strongest therapeutic activity, albeit with a narrow safety margin. **CB-839** retained partial efficacy at early intervention points but was unable to fully reverse hypertrophy, and the GRK5 inhibitor **4a** proved ineffective once hypertrophy was established. These findings illustrate that while GRK5 and glutamine metabolism remain promising targets, the timing, specificity and safety profile of candidate compounds are critical for therapeutic success.

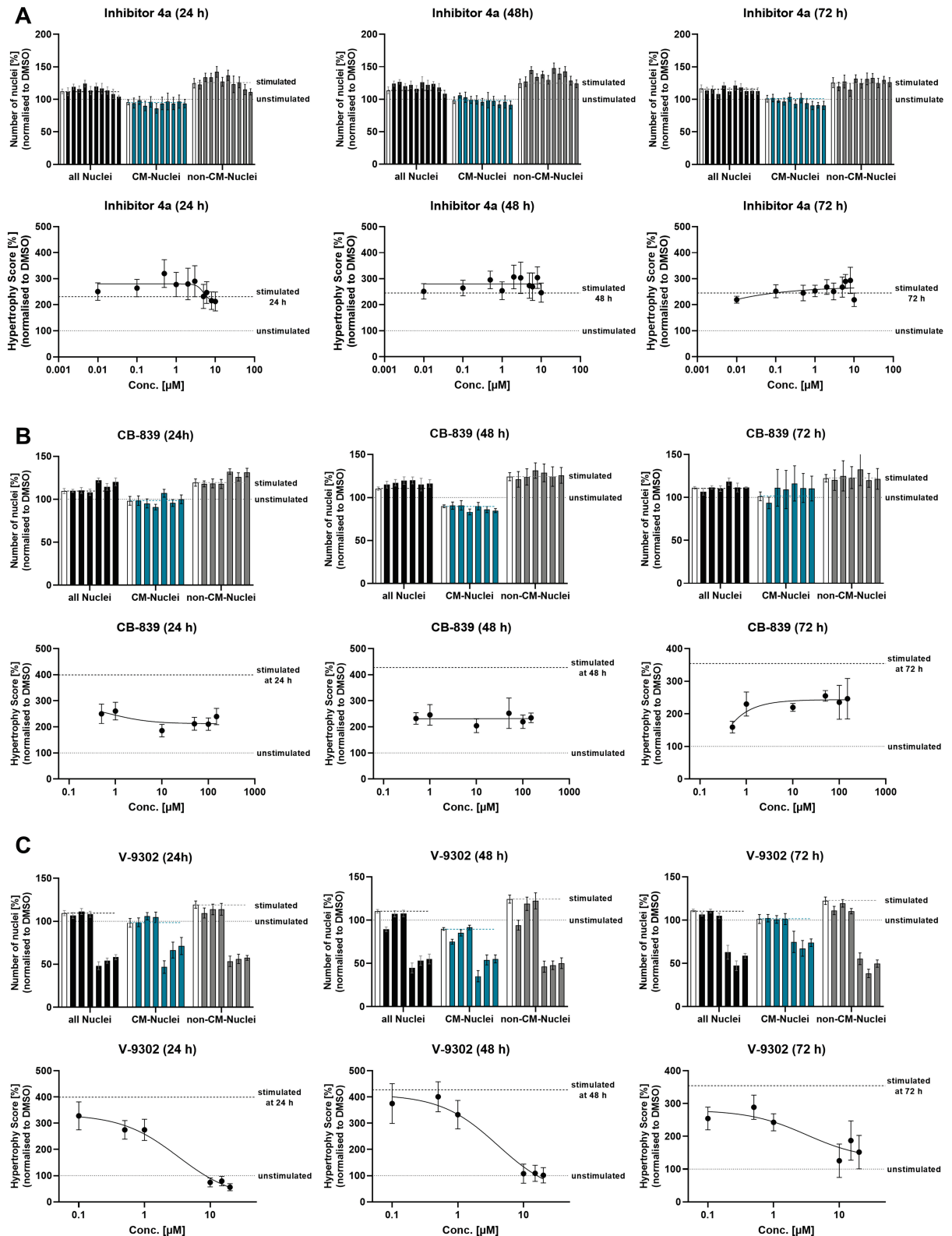


**Figure 17: Therapeutic approach to reverse the hypertrophy phenotype.** Mixed cardiac cells were stimulated with PE-LIF (20  $\mu$ M and 50 ng/ml) 24 h after seeding to induce cardiac hypertrophy. **(A)** The GRK5 inhibitor **4a** ( $n = 2$ ), **(B)** the glutaminase 1 inhibitor **CB-839** ( $n = 3$ ) and **(C)** the glutamine reuptake inhibitor **V-9302** ( $n = 3$ ) were added at 24, 48 and 72 h after hypertrophic stimulation to evaluate their potential to reverse the hypertrophic phenotype. All conditions were terminated by fixation and analysed at 96 h post-stimulation. (Mean  $\pm$  SEM)

### 5.1.7 Summary

In this chapter, a novel high-content image analysis pipeline was developed and applied to a mixed cardiac cell culture derived from neonatal rat cardiomyocytes, enabling an unbiased and quantitative assessment of hypertrophic responses in a model with high physiological relevance. By incorporating multiple cell types, this approach accounts for intercellular communication, enhancing both the sensitivity and translational value of the assay. Robust *in vitro* models are critical to improve the success of drug candidates advancing through preclinical stages and ultimately reaching clinical application. This is particularly important for first-in-class drugs or novel targets, which require early validation, usually in rodent, *in vivo* models. Using neonatal rat cardiomyocytes thus provides a biologically aligned platform for target-centric screening with increased translational probability, especially when paired with well-designed assays delivering robust, mechanistically meaningful outputs.

Although the dynamic range was slightly lower compared to assays using purified cardiomyocytes, strong hypertrophic morphological changes were still detectable. While adrenergic stimulation, especially  $\alpha$ -adrenergic stimulation with PE, resulted in comparable effects in both mixed cardiac cells and purified cardiomyocytes, only the latter responded to cytokine-induced hypertrophy by LIF and TGF $\beta$ -1. This raises the question of whether hypertrophic effects observed exclusively in purified cardiomyocytes truly reflect *in vivo* cardiac biology, given the heart's complex cellular composition. Furthermore, hypertrophic responses were detectable at both tested cell densities, but lower density cultures exhibited a greater dynamic range, likely due to increased space for cellular expansion and improved segmentation accuracy.

A custom and automated CellProfiler pipeline was established, significantly expanding the analytical capabilities and throughput of the assay. Unlike conventional assays which primarily focus on cardiomyocyte size, this approach also incorporates changes in nuclear area, cellular intensity and texture. A composite 'Hypertrophy Score' integrating the three most discriminative features enabled comprehensive phenotypic characterisation and facilitated direct condition comparisons. The automated nature of the image analysis ensures high reproducibility and unbiased measurement of compound effects, while the use of open-source software maintains accessibility for various research groups, regardless of laboratory equipment. Additionally, the assay demonstrated strong robustness across different imaging platforms. Despite differences in image quality between systems, the pipeline produced consistent Hypertrophy Scores, confirming robustness across platforms and suitability for diverse research environments.

In contrast, qPCR analysis of *Nppa* and *Nppb* expression proved unreliable in mixed cardiac cultures due to non-cardiomyocyte interference, necessitating the use of purified cardiomyocytes for accurate gene expression analysis in subsequent validation experiments.

In addition to advancing the phenotypic screening assay, this study investigated a therapeutic intervention approach aimed at reversing an already established hypertrophic phenotype rather than merely preventing its onset. This shift toward a disease-reversal model better reflects clinical reality, where hypertrophy is typically well-advanced by the time of diagnosis. The results demonstrated that the timing of therapeutic intervention is a critical factor influencing efficacy. While the glutamine reuptake inhibitor **V-9302** exhibited a dose-dependent reduction in hypertrophy, although with accompanying cytotoxicity at higher concentrations, the GRK5 inhibitor **4a** was ineffective once hypertrophy was fully developed. The glutaminase inhibitor **CB-839** showed only partial efficacy when administered early but failed to induce a full therapeutic response across later intervention time points. However, given that only three compounds were tested, further studies are required to determine whether these findings reflect broader target-specific effects. Additionally, validating both positive and negative outcomes of this *in vitro* therapeutic approach in *in vivo* models will be essential to ensure translational relevance and confirm efficacy in a more complex physiological environment. These findings highlight the challenges of reversing established cardiac hypertrophy and reinforce the importance of early therapeutic intervention to improve patient outcomes.

Moving forward, the image analysis pipeline can be adapted for other research questions or further improved by incorporating additional analysis modules. Unused features in the current pipeline may further refine hypertrophic fingerprints, aiding the detection of subtle phenotypic changes and refine the fingerprint. Additionally, incorporating quality control modules to exclude low-quality images or artifacts could further strengthen the results and reduce the likelihood of outliers in replicates. While expanding the analysis with additional measurements could enhance the depth of insights into cellular responses, it also increases processing time and necessitates efficient data handling. To address these challenges, custom R-based analysis pipelines, such as “C-MORE”<sup>[67]</sup>, could serve as a model for refining the workflow. Furthermore, artificial intelligence-driven image analysis presents an opportunity to improve cell segmentation and enhance the extraction of morphological changes, increasing both precision and scalability. The companion software CellProfiler Analyst provides a basic tool for training an algorithm to recognise morphological patterns; however, its transferability across experiments with varying image quality remains questionable. Additionally, the requirement for manual classification of cells during training introduces subjectivity, which may introduce bias into the automated analysis. Future studies should assess the reproducibility and reliability of such AI-driven approaches to ensure robust and unbiased phenotypic characterisation in cardiac hypertrophy research.

### 5.2 Targeting GRK5: A Novel Therapeutic Avenue in Cardiac Hypertrophy

#### 5.2.1 Role of GRKs in Cardiac Hypertrophy and Drug Targeting

The herein newly established hypertrophy assay, with its enhanced physiological relevance and extended imaging analysis, has demonstrated high sensitivity to adrenergic stimulation, one of the key drivers in the pathological development of cardiac hypertrophy. This makes it an ideal platform for drug discovery, particularly for evaluating novel compounds targeting the adrenergic signalling pathway. Among the key regulators of this pathway are G protein-coupled receptor kinases (GRK) 2 and 5, which play a crucial role in modulating  $\beta$ -adrenergic receptor signalling by promoting desensitisation and downstream regulation<sup>[80]</sup>. Dysregulation of these kinases, particularly in the context of chronic adrenergic overstimulation, has been strongly implicated in pathological cardiac remodelling. Hyperactivation of the sympathetic nervous system and sustained stimulation of  $\beta$ -adrenergic receptors drive maladaptive signalling cascades that promote hypertrophy and ultimately heart failure<sup>[14]</sup>. While current standard-of-care therapies primarily aim to reduce cardiac workload and alleviate symptoms, they do not directly address the underlying cellular and molecular mechanisms responsible for structural remodelling of the myocardium<sup>[32]</sup>. In contrast, GRK inhibition targets a central regulatory node in this pathogenic signalling, offering the potential not only to halt progression but also to reverse established hypertrophic changes. Thus, modulating GRK activity represents a mechanism-driven and disease-modifying therapeutic approach, positioning GRKs as compelling targets in the ongoing search for more effective treatments in heart failure<sup>[83]</sup>.

GRKs are key regulators of activated G protein-coupled receptors (GPCRs) on the cell surface. GPCRs are integral membrane proteins characterised by seven transmembrane domains, which undergo conformational changes upon agonist binding. This structural shift triggers the dissociation of heterotrimeric G proteins into their  $\alpha$  and  $\beta\gamma$  subunits, initiating downstream signalling cascades<sup>[112]</sup>. Activated GPCRs also stimulate GRKs, which phosphorylate the receptor, thereby preventing further coupling to heterotrimeric G proteins and terminating downstream G protein signalling. Additionally, phosphorylated GPCRs attract cytosolic  $\beta$ -arrestin, which mediates receptor internalisation via endocytosis. The receptor is then either degraded or recycled, allowing the cell to fine-tune its response. This mechanism plays a critical role in maintaining cardiac homeostasis by preventing excessive  $\beta$ -adrenergic receptor stimulation, a process that is upregulated in heart failure to enhance cardiac output<sup>[80]</sup>.

While GRKs are essential for normal cell function, dysregulation has been linked to the pathogenesis of various diseases, including heart failure<sup>[113]</sup>, Alzheimer's disease<sup>[114]</sup>, Parkinson's disease<sup>[115]</sup> and cancer<sup>[116, 117, 118]</sup>. Given their diverse roles, GRKs are being investigated as therapeutic targets, with a focus on selectively inhibiting individual isoforms to maximise efficacy while minimising adverse effects<sup>[119, 120]</sup>.

The GRK family consists of seven isoforms grouped into three subfamilies based on sequence homology: The rhodopsin kinase subfamily (GRK1/7, found in the retina), the  $\beta$ -adrenergic receptor kinases subfamily (GRK2/3, with GRK3 expressed in nasal epithelium) and the GRK4-like subfamily (GRK4/5/6, with GRK4 predominantly expressed in the testes)<sup>[112, 121, 122]</sup>. As a member of the AGC protein kinase family (which includes PKA, PKG and PKC), GRKs share structural similarities, with 32% sequence identity to protein kinase A (PKA)<sup>[119]</sup>. Among them, GRK2 and GRK5 are the most abundantly expressed GRKs in cardiac muscle, where they play a pivotal role in  $\beta$ -adrenergic receptor regulation, making them of particular relevance to cardiac research<sup>[119]</sup>.

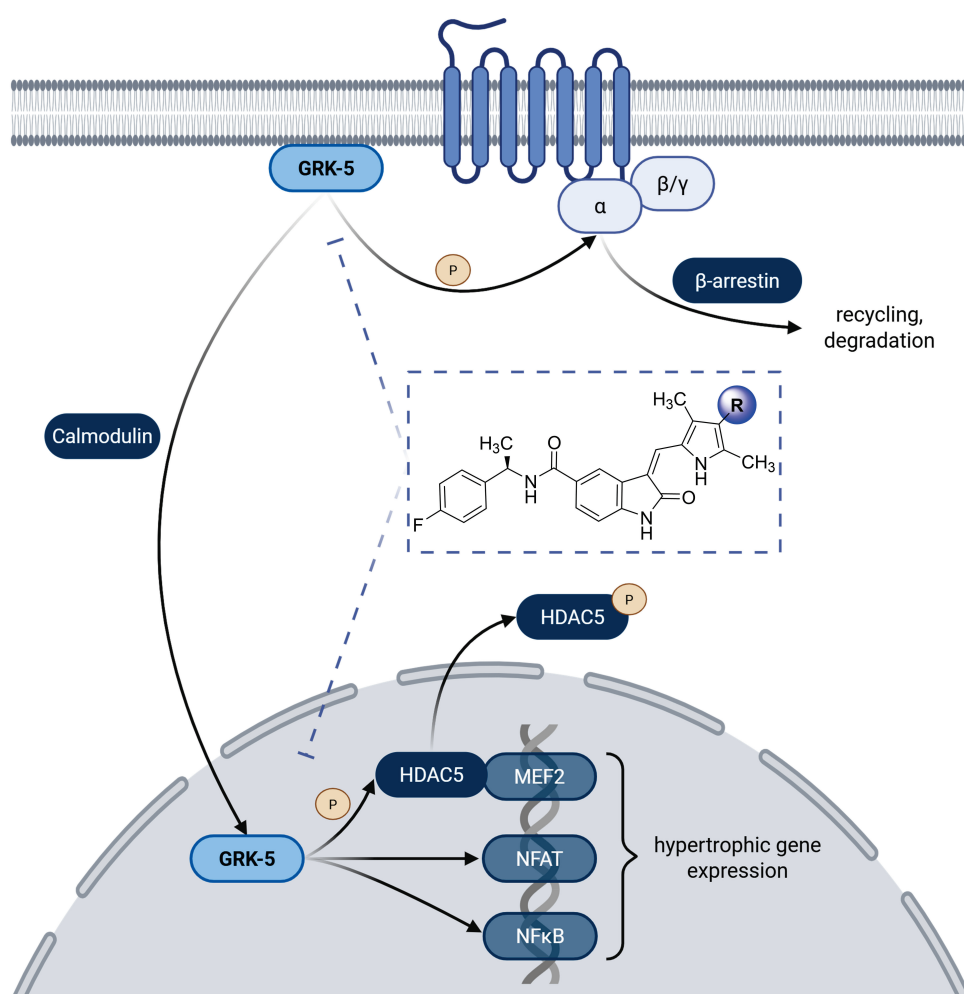


**Figure 18: Canonical and non-canonical signalling pathway of GRK5.** In the canonical pathway, GRKs regulate GPCR signalling by phosphorylating activated receptors, leading to  $\beta$ -arrestin recruitment, receptor internalisation and either degradation or re-sensitisation, maintaining cellular homeostasis. Non-canonical pathways involve GRK5 translocation to the nucleus in a  $\text{Ca}^{2+}$ /calmodulin-dependent manner, regulating transcription via NF $\kappa$ B, NFAT and promoting nuclear export of phosphorylated HDAC, leading to MEF2 activation and hypertrophic gene expression.



In the heart, GRK2 was first discovered in the 1980s<sup>[123, 124]</sup>, with its potential as a therapeutic target proposed in 1995<sup>[125]</sup>. GRK5 was later identified in the 1990s<sup>[126, 127]</sup>. While GRK2 primarily resides in the cytoplasm, it is recruited to the membrane upon GPCR activation<sup>[112]</sup>. Beyond its canonical role, GRK2 is also involved in non-canonical signalling pathways<sup>[82]</sup>, including mitochondrial localisation, where it promotes apoptosis and alters bioenergetics<sup>[128, 129, 130]</sup>. Additionally, GRK2 phosphorylates I $\kappa$ B, leading to its degradation and subsequent NF $\kappa$ B-mediated hypertrophic responses<sup>[131]</sup>. Another critical role of GRK2 is the phosphorylation of AKT, which inhibits glycogen synthase kinase 3 beta (GSK3 $\beta$ ). This prevents NFAT phosphorylation, allowing its nuclear translocation and activation of hypertrophic gene expression<sup>[92]</sup>.

In contrast, GRK5 is primarily membrane-associated but is also involved in nuclear signalling. It translocates to the nucleus in a Ca<sup>2+</sup>/calmodulin-dependent mechanism<sup>[81, 132]</sup>, where it influences hypertrophic gene transcription<sup>[82, 133]</sup>. The affected pathways include kinase-dependent nuclear export of histone deacetylases (HDACs), leading to de-repression of myocyte enhancer factor-2 (MEF2)<sup>[81, 132, 134]</sup>. Additionally, in a kinase-independent manner, GRK5 inhibits NF $\kappa$ B signalling<sup>[135]</sup> and NFAT activation<sup>[136]</sup>. Given these functions, specifically targeting the non-canonical nuclear activity of GRK5 could offer a more precise therapeutic approach, increasing potency while reducing adverse effects.

Both GRK2 and 5 are upregulated in failing hearts<sup>[83, 84]</sup>, with multiple animal studies highlighting their role in heart failure and pathological hypertrophy. Overexpression of GRK2 in mice led to reduced myocardial contractility, whereas expression of the GRK2 inhibiting peptide  $\beta$ -ARKct restored contractility<sup>[125]</sup>. Similarly, GRK5 deletion in mice significantly reduced hypertrophic remodelling, demonstrating its crucial role in pathological cardiac growth<sup>[85]</sup>.

Inhibiting GRK pharmacologically has also shown promise, both as monotherapy or as co-treatment with a GPCR-agonist, facilitating a therapeutic effect in lower doses with fewer off-target effects<sup>[137]</sup>. For example, paroxetine, a selective serotonin reuptake inhibitor, was identified as a GRK2 inhibitor, enhancing contraction amplitudes in hypertrophy-induced cardiomyocytes, though with a lower potency against GRK2 than serotonin transporters<sup>[138, 139]</sup>. Additionally, a drug screening identified amlexanox as an inhibitor of GRK5, able to block PE-induced phosphorylation of HDAC5 and consequent activation of MEF2 in NRCMs<sup>[140]</sup>. One example of ongoing GRK5-targeted drug discovery efforts is KR-39038. With an IC<sub>50</sub> value of 0.02  $\mu$ M, KR-39038 showed efficacy in Ang. II-induced NRCMs and in pressure-overloaded mice<sup>[141]</sup>. Furthermore, a compound designed by the Research Center for Medicinal Chemistry at the Korea Research Institute of Chemical Technology has demonstrated potent inhibition of both GRK2 and GRK5. However, it lacks selectivity for GRK5 over GRK2, highlighting the ongoing challenge in developing highly selective GRK5 inhibitors<sup>[142]</sup>.

For GRK inhibitors, the selectivity is of special importance due to the high sequence homology among GRKs and other kinases of the AGC protein family, leading to cross-reactivity and potential off-target toxicity. Achieving high selectivity is critical, as broad inhibition could disrupt normal cardiac function rather than specifically addressing pathological hypertrophy or heart failure<sup>[143]</sup>.

The Tesmer research group has pioneered the design of multiple GRK5-specific inhibitors with covalent, reversible covalent and non-covalent binding mechanisms, using sunitinib as a foundational scaffold. Sunitinib, a receptor tyrosine kinase inhibitor approved for the treatment of renal cell carcinoma, gastrointestinal stromal tumours and pancreatic neuroendocrine tumours<sup>[144]</sup>, demonstrated efficacy inhibiting GRK5, making it a promising starting point for further optimisation<sup>[120]</sup>. A selection of these promising inhibitors was kindly provided by the Tesmer group and subsequently tested in the high-content hypertrophy screening assay described in this study.

### 5.2.2 Target Validation of GRK5

While numerous GRK inhibitors have demonstrated activity in biochemical assays, only a few have been evaluated in cellular models<sup>[141, 145, 146]</sup>. Given that this study employs a novel, physiologically relevant mixed cardiac cell culture instead of the commonly used purified cardiomyocyte system, it was first necessary to validate GRK5 as a target in this assay system before implementing the high-content imaging analysis. Although GRK5 had previously been validated in purified cardiomyocyte cultures<sup>[147]</sup>, this validation aimed to confirm its role in cardiac hypertrophy within the mixed-cell model and to ensure that the adrenergic signalling pathway, including GRK5, is authentically represented to enable the detection of pharmacological modulation thereof.

To achieve this, GRK5 expression was reduced using small interfering RNA (siRNA) to determine whether GRK5 knockdown could prevent PE-LIF-induced hypertrophy. Cells transfected with GRK5-targeting siRNA were compared to those transfected with scrambled siRNA as a negative control. A change in the experiment from 384-well to a 6-well format was necessary to obtain sufficient protein for Western blot analysis, which was used to confirm the knockdown efficiency. Additionally, the cell density was increased (750,000 cells per well) to ensure adequate protein yield and to meet the siRNA transfection protocol requirements, which specify 80% cell confluency to reduce the toxic effect of transfection reagents. GRK5 protein levels analysed via Western blot under both DMSO control and PE-LIF stimulation conditions are shown in Figure 19. The results confirmed that the siRNA-mediated knockdown of GRK5 resulted in a reduction of protein levels to 38.5% and 18.7% in DMSO and PE-LIF treated cells as determined by semi-quantitative immunoblotting (relative to total protein per lane).

Notably, despite the transition from a 384-well to a 6-well format and the associated increase in cell density, the established CellProfiler pipeline remained fully applicable. Subsequent analysis demonstrated that PE-LIF stimulation significantly increased the Hypertrophy Score to 141.5%, confirming that hypertrophic development was both occurring and reliably detectable under these modified conditions. This underscores the robustness of the image analysis workflow, even when key culture parameters are altered.

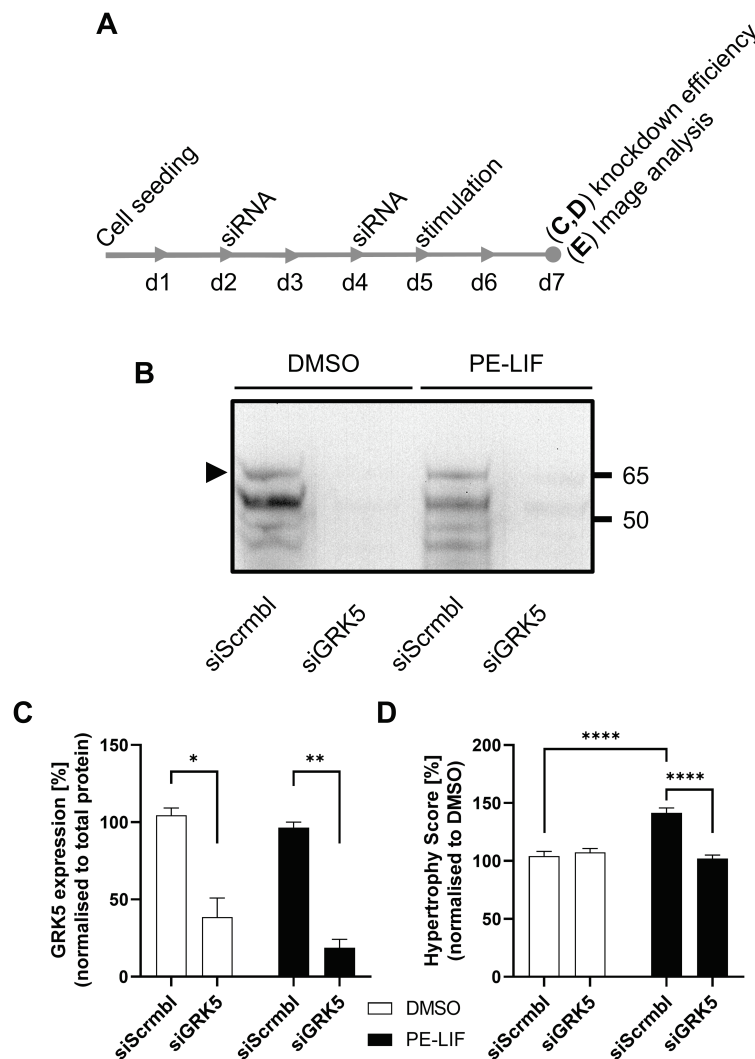


**Figure 19: Functional validation of GRK5 via siRNA knockdown.** (A) Experimental protocol for siRNA knockdown experiments. (B) Representative immunoblot for GRK5 expression. (C) siRNA knockdown of GRK5 in mixed cardiac cells significantly reduces GRK5 expression in both PE-LIF (20  $\mu$ M and 50 ng/ml) and DMSO-stimulated cells (n = 2). (D) Image-based quantification of the Hypertrophy Score reveals a significant hypertrophic response in PE-LIF-stimulated cells transfected with scrambled siRNA, whereas GRK5 knockdown effectively prevents hypertrophic development (n = 3). (Mean  $\pm$  SEM, unpaired t-test: \* p  $\leq$  0.05, \*\* p  $\leq$  0.01, \*\*\* p  $\leq$  0.001, \*\*\*\* p  $\leq$  0.0001)

Crucially, GRK5 knockdown successfully prevented PE-LIF-induced hypertrophy, restoring the Hypertrophy Score to baseline DMSO levels (102.1%), thus validating GRK5 as a functional target within the mixed cardiac cell model.

In summary, these findings further strengthen the role of GRK5 in hypertrophic development by demonstrating that its knockdown prevents key cellular changes associated with hypertrophy. Importantly, although some morphological variations occurred due to the modified assay conditions, the established CellProfiler pipeline successfully adapted to the new culture format and the Hypertrophy Score remained a robust and specific readout. This confirms the assay's capability to detect GRK5-dependent signalling changes with high sensitivity, even under altered experimental parameters. Therefore, this system is well-suited for further investigations into GRK5 modulation and the development of targeted inhibitors.

### 5.2.3 Assessment of Cellular Efficacy of GRK5 Inhibitors

Developing selective GRK5 inhibitors is challenging due to the high structural homology within the GRK family, making selectivity a key issue<sup>[119]</sup>. Since GRK2 has been the main focus in cardiovascular research, only a few selective GRK5 inhibitors have been reported<sup>[143]</sup>. Ideally, candidate compounds should exhibit high potency in the low nanomolar range, non-covalent binding properties, drug-like characteristics and high selectivity for the GRK5 isoform to minimise toxicity and adverse effects<sup>[143]</sup>.

The Tesmer research group addressed this challenge by screening a collection of known kinase inhibitors for their effects on GRK2 and GRK5, using a differential scanning fluorimetry assay. By comparing the thermal stability of these proteins in the presence and absence of inhibitors, they aimed to identify scaffolds with strong binding affinity. This approach led to the discovery of three inhibitors featuring a common pyrrole-pyrimidine scaffold<sup>[143]</sup>.

Structural studies have provided insights into potential selectivity mechanisms. Crystal structures of GRK2 and GRK5 revealed that GRK2 has a more spacious ATP-binding pocket, suggesting that steric clash-based approaches could be used to selectively target GRK5<sup>[119]</sup>. Furthermore, co-crystallisation of selected inhibitors with GRK2 and GRK1 identified the active site tether (AST) loop as a potential selectivity determinant for individual GRKs<sup>[143]</sup>. The crystal structure of GRK6 (like GRK5 a member of the GRK4 subfamily) further revealed a cysteine residue (Cys474) in the AST loop, located near the ATP-binding site. This discovery provided an opportunity to selectively target GRK5 via covalent inhibition, as Cys474 is unique to the GRK4 subfamily (GRK4/5/6)<sup>[148]</sup>. Building on these findings, covalent warheads were attached to pyrrole-pyrimidine inhibitors to target Cys474. However, the resulting inhibitors displayed only low micromolar affinity for GRK5, limiting their effectiveness<sup>[148]</sup>. To enhance potency, the focus shifted toward scaffolds with higher intrinsic GRK5 affinity, allowing sufficient residence time in the protein-inhibitor complex for the covalent bond to form.

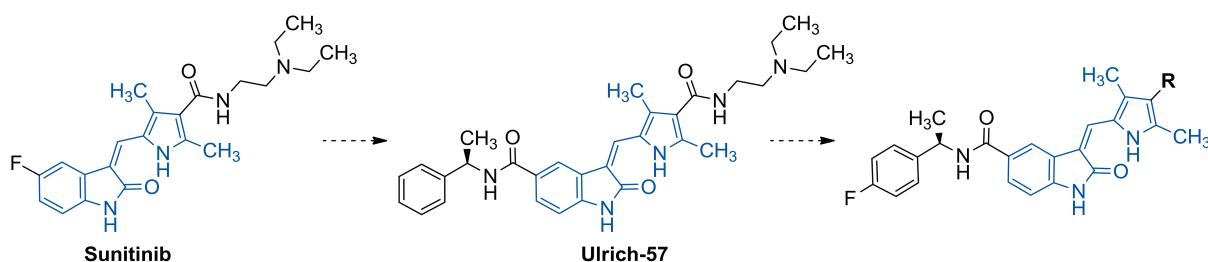


**Figure 20: Development of GRK5 inhibitor scaffold.** Sunitinib showed a moderate potency to inhibit GRK5 and was selected as the basic structure. With the modification of the indolinone in Ulrich-57, the potency and selectivity for GRK5 could be improved. In newer campaigns, the pyrrole moiety is diversified to further enhance potency and selectivity.

A breakthrough was the discovery of sunitinib's activity against GRK5, with an  $IC_{50}$  of  $0.83 \mu M$ <sup>[120]</sup>. Sunitinib, an FDA-approved receptor tyrosine kinase inhibitor used in cancer treatment, provided a valuable scaffold. A closely-related derivative, Ulrich-57, featuring the same indolinone scaffold as sunitinib, exhibited even higher potency in the low nanomolar range, with improved selectivity for GRK5 over GRK2, outperforming earlier pyrrole-pyrimidine-based inhibitors. Extensive structure-activity relationship (SAR) analysis confirmed that the indolinone scaffold, derived from sunitinib, forms two hydrogen bonds in the ATP-binding pocket, while the fluorophenyl group of Ulrich-57 interacts with the phosphate-binding loop<sup>[145]</sup>. Further structural analysis revealed that Ulrich-57's diethylamine moiety faced the AST loop, suggesting that replacing this group with covalent warheads targeting Cys474 could further enhance GRK5 selectivity. Interestingly, only the (*R*)-enantiomer of Ulrich-57 exhibited potency in inhibiting GRK5, making the (*S*)-enantiomer a useful negative control<sup>[120]</sup>.

To optimise selectivity and potency, Ulrich-57 was modified with a 2-haloacetyl-amido group<sup>[120]</sup>, leading to increased affinity in some derivatives. However, the haloacetamide moiety is highly reactive, raising concerns about potential toxicity. To lower these risks, a next generation of inhibitors was developed, featuring keto-amide derivatives, which form a reversible covalent hemithioacetal intermediate through nucleophilic attack by the Cys474 sulfur on the carbonyl group<sup>[149]</sup>. Simultaneously, 2-hydroxyamide derivatives were synthesised as a non-covalent control set, since the absence of a carbonyl moiety prevents covalent binding to Cys474. However, these modifications reduced selectivity over GRK2<sup>[149]</sup>.

Using the X-ray structure of hydroxyamide derivative **4a**, further modifications led to heterocyclic carboxamides. By introducing strategically positioned heteroatoms, substituents and rotatable bonds, these compounds mimicked non-covalent interactions seen in earlier inhibitors while achieving higher potency and selectivity. The enhanced steric clash with the AST loop of GRK2 contributed to this selectivity<sup>[145]</sup>. Testing these compounds against GRK5, GRK2 and GRK6 led to the identification of **5d** and **5k**, which exhibited good selectivity for

GRK5 over GRK2 but with surprisingly high affinity for GRK6<sup>[145]</sup>. Notably, GRK6 has recently emerged as a promising target for the treatment of multiple myeloma, making these compounds also of interest for oncological research.

While comprehensive *in vitro* activity and SAR data have been published for this class of GRK5 inhibitors, their cellular efficacy remains largely unexplored. To bridge this gap, the Tesmer research group kindly provided the following compounds for testing in this study's cardiac hypertrophy assay (see Figure 21): covalent binding inhibitor **3** ( $\alpha$ -ketoamide derivate) and non-covalent binding inhibitor **4a** (an  $\alpha$ -hydroxyamide derivate) with its inactive (*R*)-enantiomer **4b** as well as five heterocyclic carboxamide derivatives (**5b**, **5d**, **5i**, **5k**, **5m**). These compounds were evaluated for their cellular activity in the high-content imaging-based hypertrophy assay, providing valuable insights into their potential therapeutic application in cardiac disease.

The GRK5 inhibitors were tested against PE-LIF, the most potent hypertrophic stimulus identified in Chapter 5.1.2. This setup is particularly relevant because PE acts as an adrenergic stimulus and GRK5 is a central regulator of adrenergic signalling pathways involved in cardiac hypertrophy. Therefore, evaluating the effects of GRK5 inhibition under adrenergic stimulation provides direct insight into its therapeutic potential in modulating maladaptive cardiac signalling. After co-incubation with PE-LIF and the respective inhibitors for 96 h, mixed cardiac cells were fixed and stained with DAPI and  $\alpha$ -actinin to label nuclei and cardiomyocyte cytoplasm, respectively. Image-based analysis was performed using the previously developed CellProfiler pipeline.

To assess potential cardiotoxic effects, cardiomyocyte and non-cardiomyocyte nuclei were quantified. Inhibitor **5d** showed clear toxic effects, reducing non-cardiomyocyte numbers below DMSO baseline starting at 0.5  $\mu$ M. Cardiomyocytes were less sensitive but still showed reduced viability at  $\geq 2$   $\mu$ M. Of note, **5d** had the lowest GRK5 potency in the biochemical assay ( $IC_{50} = 50$   $\mu$ M), suggesting that its toxic effects were likely due to off-target activity. This is particularly important for interpreting the cellular phenotype, since toxic or stressed cells often exhibit reduced size and may falsely appear to respond positively in hypertrophy assays.

## 5. Results and Discussion

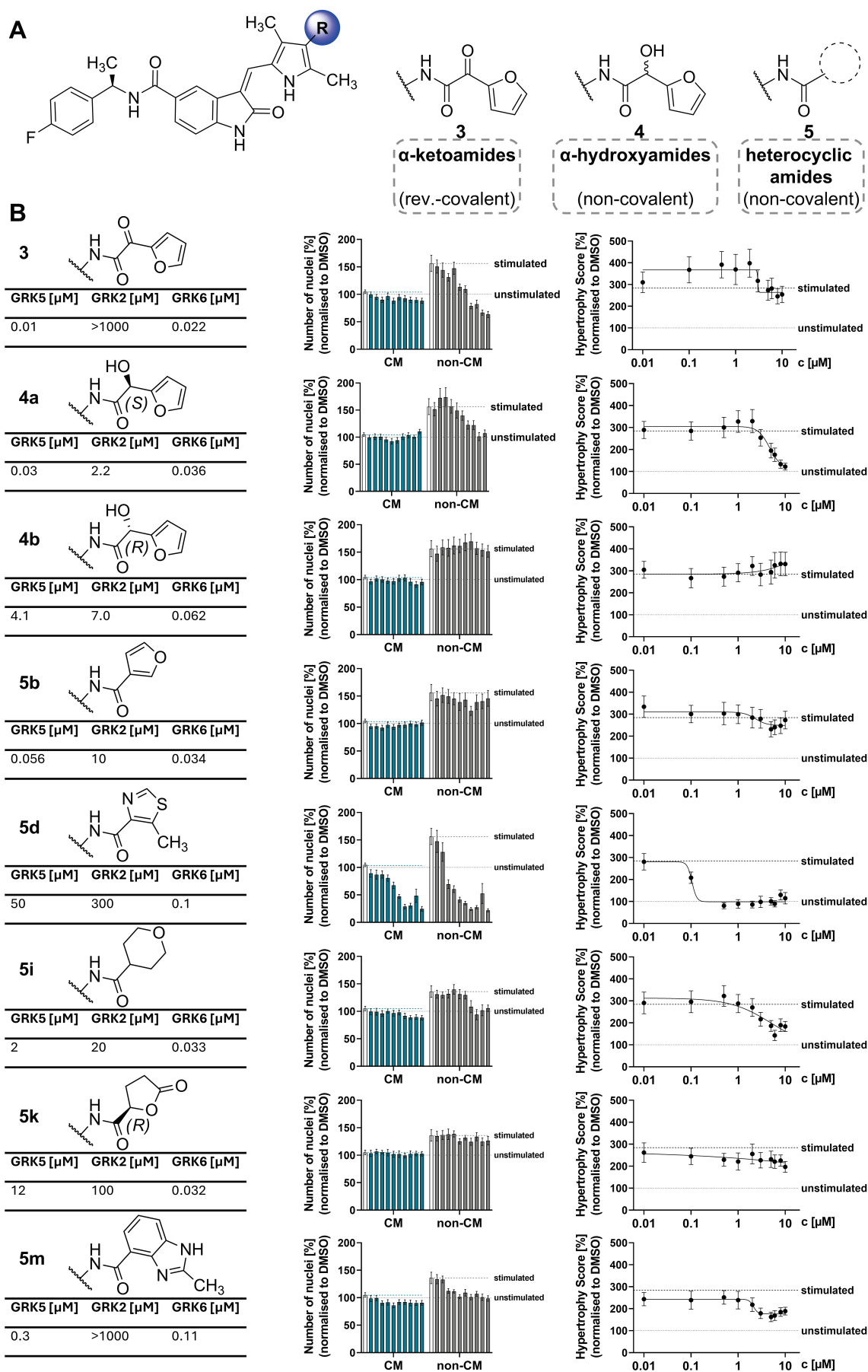


**Figure 21: Phenotypic characterisation and structure-activity relationships of GRK5-selective inhibitors.**

**(A)** GRK5 inhibitor scaffold optimised through three parallel medicinal chemistry campaigns targeting distinct binding modes: a covalent-binding series and two non-covalent series distinguished by different key moieties. Each campaign introduced specific structural modifications to refine potency, selectivity and pharmacological properties.

**(B)** Mixed cardiac cells were stimulated with PE-LIF (20  $\mu$ M, 50 ng/ml) and treated with GRK5 inhibitors, followed by 96 h incubation. Hypertrophic features of DAPI and  $\alpha$ -actinin stained cardiac cells were quantified using the established CellProfiler pipeline. Only inhibitor **5d** showed cardiotoxic effects, stronger for non-cardiomyocytes starting at 0.5  $\mu$ M. Inhibitors **3**, **4a** (but not antipode **4b**), **5i** and **5m** show an anti-proliferative effect for non-cardiomyocytes at higher concentrations. While inhibitor **4a** reduced the Hypertrophy Score to DMSO baseline, inhibitor **4b** showed no effect, confirming **4b** as the inactive optical antipode. The apparent anti-hypertrophic effect of **5d** is based on its cardiotoxicity. (n = 3, mean  $\pm$  SEM)

All other inhibitors did not exhibit overt toxicity but did show reductions in non-cardiomyocyte numbers, which likely reflects anti-proliferative activity. This effect was most pronounced for inhibitors **3** and **4a**, but absent for its (*R*)-enantiomer **4b**, confirming the latter's biochemical inactivity. Inhibitors **5i** and **5m** induced similar, though less pronounced, effects. Given the non-proliferative nature of post-mitotic cardiomyocytes, these reductions are most likely due to effects on proliferating cardiac fibroblasts. Cardiac fibroblasts are key contributors to pathological remodelling through proliferation and extracellular matrix deposition in response to stress. Their expansion is closely associated with the progression of cardiac hypertrophy<sup>[25]</sup>. Therefore, the observation that GRK5 inhibitors may affect fibroblast proliferation, in addition to counteracting cardiomyocyte hypertrophy, adds an important and previously unrecognised aspect to their therapeutic potential. Notably, this effect would have been missed in conventional assays relying solely on purified cardiomyocytes, thus underscoring the value of using a physiologically relevant assay system and highlighting the strength of the mixed cardiac cell culture model established in this thesis. Future studies should investigate whether this anti-proliferative effect arises from direct action on cardiac fibroblasts or whether it is mediated indirectly via paracrine signalling from cardiomyocytes. Understanding the mechanism behind this dual effect could provide further insights into the role of GRK5 in cardiac remodelling and inform therapeutic strategies for more targeted intervention.

The next step was the evaluation of the inhibitors' efficacy in preventing the PE-LIF-induced cardiac hypertrophy. In previous *in vitro* biochemical studies, **4a** had demonstrated high GRK5 potency ( $IC_{50}$  = 0.03  $\mu$ M), while its (*R*)-enantiomer **4b** was nearly inactive ( $IC_{50}$  = 4.1  $\mu$ M). These results were reflected in the cellular assay: **4a** significantly reduced the Hypertrophy Score from 3  $\mu$ M upward, while **4b** remained ineffective at all concentrations. Interestingly, both **4a** ( $IC_{50}$  = 0.036  $\mu$ M) and **4b** ( $IC_{50}$  = 0.062  $\mu$ M) also inhibited ubiquitously expressed GRK6 *in vitro* with comparable potency. Since **4b** showed no activity in this hypertrophy assay, the observed phenotype was not likely mediated by GRK6 inhibition, which is consistent with the minor role of GRK6 in cardiovascular pathophysiology<sup>[150]</sup>. Furthermore, while **4a** does



exhibit weak activity against GRK2 ( $IC_{50} = 2.2 \mu M$ ), this potency is insufficient to translate into significant cellular effects at the tested concentrations. In contrast, the strong activity of **4a** against GRK5 and the dose-dependent reduction in the Hypertrophy Score strongly suggest that the observed cellular effects are primarily due to selective GRK5 inhibition, rather than off-target effects on GRK2.

Inhibitor **5d** also appeared to be effective in suppressing hypertrophy, however, this effect was attributed to toxicity and stress rather than on-target efficacy, given the compound's low potency and toxic profile.

Inhibitors **5b** and **5k** showed no anti-proliferative effect in the previous cardiotoxicity evaluation, which is consistent with the lower anti-hypertrophic efficacy. In contrast, inhibitors **3**, **5i** and **5m** reduced the Hypertrophy Score to intermediate levels but did not reach the DMSO baseline. These compounds produced a partial effect that plateaued between the PE-LIF and DMSO controls. Given that not all compounds exhibited a clear dose-dependence,  $IC_{50}$  values were not reliable indicators of efficacy. Therefore, the measured effect at  $8 \mu M$  ( $I_{8 \mu M}$ ) was selected as a more robust comparison metric (see Figure 22A). Based on this analysis, **4a** emerged as the most potent cellular inhibitor and was selected for further validation by an orthogonal method.

To confirm the cellular efficacy of **4a** at the transcriptional level, a qPCR-based assay was performed (see Figure 22B). Purified cardiomyocytes were treated for 24 h with PE-LIF ( $100 \mu M$  /  $50 \text{ ng/ml}$ ) and **4a** ( $5 \mu M$  /  $10 \mu M$ ) in 6-well plates. The use of purified cardiomyocytes was critical to avoid confounding signals from proliferative non-cardiomyocytes, as previously investigated in this thesis (see Chapter 5.1.5). Gene expression of the hypertrophy markers *Nppa* and *Nppb* (encoding ANP and BNP) was quantified and normalised to the housekeeping gene *Rpl32* and the DMSO control. These markers are part of the fetal gene program that is upregulated in cardiac hypertrophy, where they exert cardioprotective effects such as natriuresis, vasodilatation and RAAS inhibition<sup>[29]</sup>.

The results in Figure 22B show that PE-LIF stimulation significantly induces the gene expression of *Nppa* and *Nppb*. Treatment with inhibitor **4a** significantly prevents the upregulation, keeping their expression at the DMSO control level. These results confirm the effectiveness of inhibitor **4a** not only in biochemical and phenotypic assays but also at the level of gene expression. Its potency, GRK5 selectivity and ability to counteract hypertrophy in cardiomyocytes make it a promising candidate for further *in vivo* validation or lead optimisation.

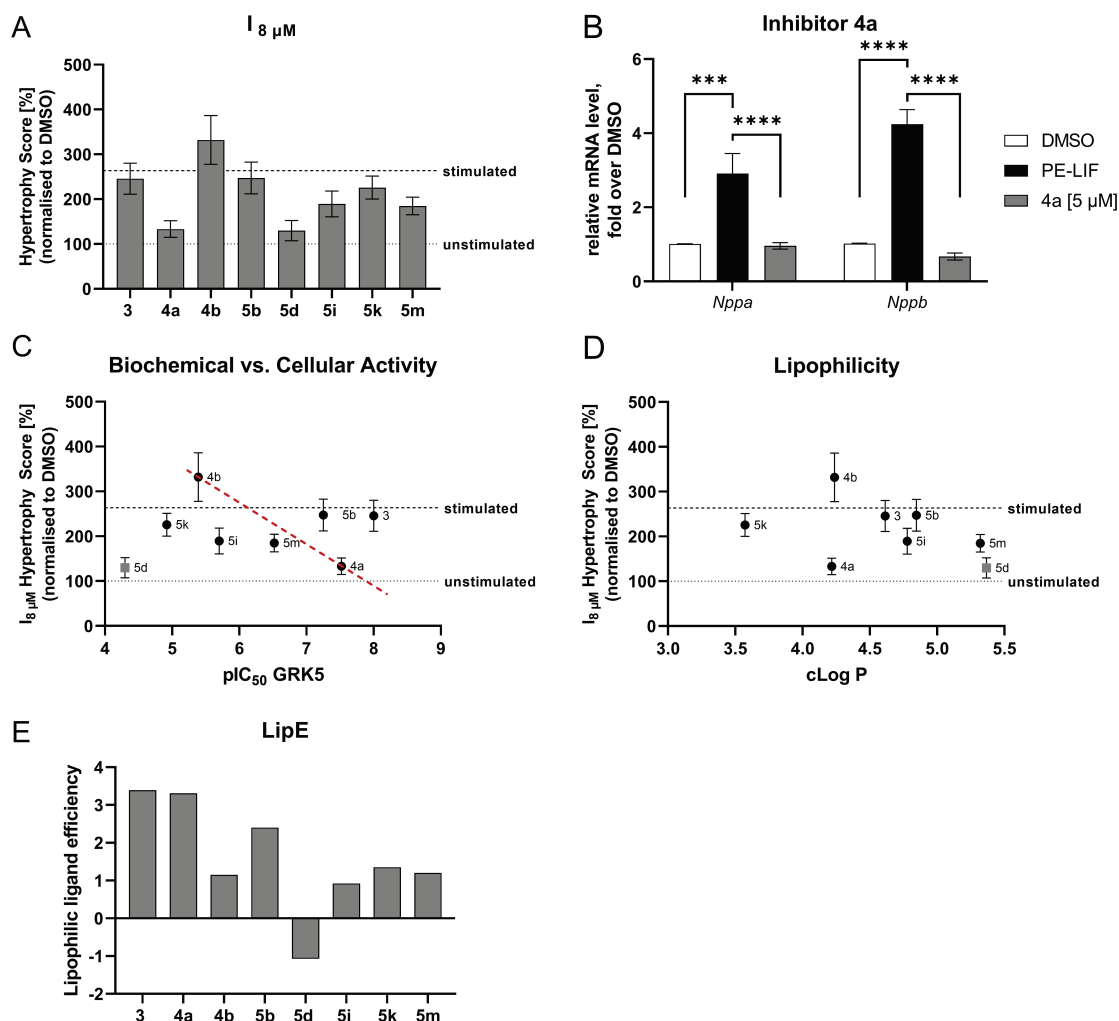


**Figure 22: Integrated evaluation of GRK5 inhibitor efficacy: biochemical potency, cellular activity and physicochemical properties.** (A) To compare the performance of different inhibitors, anti-hypertrophic efficacy at 8  $\mu M$  is used ( $I_{8 \mu M}$ ), revealing that inhibitor **4a** showed the highest cellular potency to prevent hypertrophic development. (B) Orthogonal qPCR assay confirms potency of inhibitor **4a**. Purified cardiomyocytes were incubated in 6-well plates for three days before PE-LIF (20  $\mu M$ , 50 ng/ml) stimulation and **4a** (5  $\mu M$ ) treatment for 24 h. Gene expression levels of *Nppa* and *Nppb* were normalised to *Rpl32* as a housekeeping gene ( $n = 4$ ). (C) Correlation between biochemical GRK5 potency ( $pIC_{50}$ ) and anti-hypertrophic efficacy in the cellular assay ( $I_{8 \mu M}$ ) reveals that compounds with low GRK5 activity show no cellular efficacy, while the potent inhibitor **4a** exhibits strong anti-hypertrophic effects. (D) Relationship between lipophilicity (cLogP) and cellular efficacy ( $I_{8 \mu M}$ ), exploring the impact of physicochemical properties on the translation from biochemical to cellular activity. cLogP values were calculated using Schrödinger's Maestro 14.3.129. (E) Based on the biochemical  $IC_{50}$  value for GRK5 potency and the cLogP values, the lipophilic efficiency (LipE) value was calculated. (Mean  $\pm$  SEM, one-way ANOVA: \*  $p \leq 0.05$ , \*\*  $p \leq 0.01$ , \*\*\*  $p \leq 0.001$ , \*\*\*\*  $p \leq 0.0001$ )

Despite similar biochemical potencies among most tested GRK5 inhibitors (except **5d**), their cellular efficacy varied substantially (see Figure 21). This discrepancy between biochemical and cellular activity is a common challenge in drug discovery. While high potency in simplified *in vitro* assays is a necessary starting point, compounds often exhibit diminished efficacy in

more complex cellular or *in vivo* environments due to factors such as limited membrane permeability, reduced intracellular target engagement, nonspecific protein binding and off-target interactions. If cellular potency is already insufficient, a compound's *in vivo* performance is likely to be further compromised, potentially disqualifying it from further development. This underscores the need for robust *in vitro* assays that more accurately reflect *in vivo* biology. The phenotypic assay established in this thesis addresses this gap by incorporating neonatal rat cardiomyocytes, highly relevant for rodent *in vivo* studies, and applying a high-content, image-based readout. Such physiologically meaningful and analytically powerful platforms are essential for improving the predictive value of early-stage testing and increasing the likelihood of successful *in vivo* target validation, particularly for novel molecular targets or first-in-class compounds.

To explore this discrepancy further, cellular efficacy ( $I_{8\ \mu\text{M}}$ ) was plotted against biochemical efficacy ( $\text{pIC}_{50}$  for GRK5) in Figure 22C. Compounds with poor GRK5 potency (**4b**, **5k**) lacked cellular efficacy, whereas those with high potency (**4a**) showed clear cellular effects. Interestingly, **5m** and **5i** had intermediate potencies and correspondingly moderate effects. However, inhibitors **3** and **5b** showed surprisingly poor cellular efficacy despite good GRK5 biochemical activity, prompting further analysis.

To identify possible explanations, the lipophilicity ( $\text{cLogP}$ ) of each compound was calculated using the Schrödinger Maestro software, providing an initial assessment in the absence of experimental data (see Figure 22D). While lipophilicity can enhance passive permeability, excessive values may lead to membrane trapping and increased nonspecific binding due to high unspecific hydrophobic interactions<sup>[151]</sup>, which are also key considerations in the Lipinski Rule of 5. The Rule of 5, which predicts the drug-likeness of a compound intended for oral administration, states that a drug has favourable pharmacokinetic characteristics if it has: a molecular weight of less than 500 Da, no more than 5 hydrogen bond donors, no more than 10 hydrogen bond acceptors and a  $\text{logP}$  (lipophilicity) value of less than 5<sup>[152]</sup>. While lipophilicity within these limits can improve membrane permeability, excessive lipophilicity, beyond this threshold, can increase the risk of off-target binding, leading to potential toxicity and poor pharmacokinetic properties<sup>[153]</sup>. To account for both potency and lipophilicity, the lipophilic efficiency (LipE) metric is often used in drug discovery programs to balance potency and lipophilicity. The LipE metric is calculated by subtracting the  $\text{cLogP}$  value from the negative logarithm of the  $\text{IC}_{50}$  value. A favourable range is considered to be a  $\text{LipE} > 5$ .<sup>[153]</sup> The results for the LipE values for the tested GRK5 inhibitors are shown in Figure 22E.

Inhibitors **3** and **5b** displayed particularly high  $\text{cLogP}$  values, which likely contributed to their low cellular efficacy despite good GRK5 inhibition *in vitro*. In contrast, **4a** had a lower  $\text{cLogP}$  and one of the highest LipE values, suggesting that its superior performance in cells may be due to a better balance between lipophilicity and potency. These findings underscore the

importance of physicochemical optimisation, beyond *in vitro* potency alone, in the development of GRK5 inhibitors for therapeutic application. Furthermore, this highlights how implementing physiologically relevant cellular models in the early stages of drug discovery can enhance translation to *in vivo* efficacy.

#### 5.2.4 Summary

Despite significant advances in cardiovascular medicine, effective treatments for cardiac hypertrophy, an early hallmark of heart failure, remain limited and current therapies often fail to reverse disease progression<sup>[32]</sup>. This underscores the urgent need for new therapeutic targets and strategies. GRK5 has emerged as a promising candidate due to its regulatory role in maladaptive cardiac signalling<sup>[83]</sup>. To support drug discovery in this area, physiologically relevant models are essential. The mixed cardiac cell assay established in this thesis addresses this need by capturing complex cell-cell interactions absent in purified cardiomyocyte cultures. Its robustness, scalability and sensitivity make it ideal for evaluating candidate compounds during lead optimisation and for improving the prediction of *in vivo* efficacy.

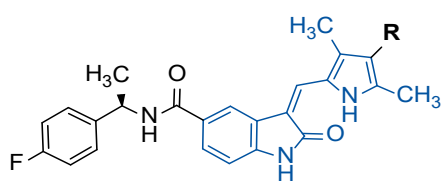
In this study, the role of GRK5 as a therapeutic target for cardiac hypertrophy was systematically investigated by combining genetic target validation, cellular compound profiling and detailed physicochemical analysis of selected inhibitors. GRK5's role in cardiac hypertrophy was reproducibly confirmed in the established assay using siRNA-mediated knockdown, which led to a reduction in hypertrophic markers. This result supported the assay's validity and provided important genetic evidence to guide GRK5-targeted lead optimisation.

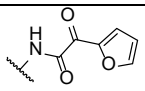
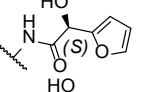
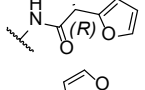
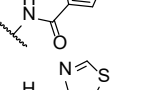
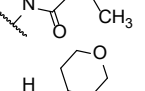
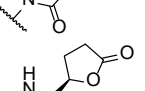
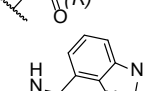
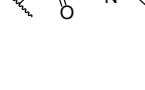
Building on this, a panel of chemically diverse GRK5 inhibitors, previously characterised for their *in vitro* biochemical potency, was evaluated.

Importantly, these data represent the first cellular efficacy results for this GRK5-selective inhibitor campaign in a physiologically relevant phenotypic model. To date, only CCG215022, a non-selective GRK2/GRK5 inhibitor, and KR-39038 have been tested in a cellular contexts<sup>[141, 154]</sup>. The present results provide critical proof-of-concept that selective GRK5 inhibition yields measurable anti-hypertrophic effects at the cellular level, underscoring GRK5's therapeutic relevance and laying the groundwork for target-focused lead optimisation and *in vivo* validation.

Several inhibitors showed potent anti-hypertrophic activity, most notably compound **4a**, which effectively prevented cardiomyocyte hypertrophy without inducing toxicity. Its inactive enantiomer, **4b**, served as a key control, confirming the stereospecificity of the effect and supporting the conclusion that GRK5 inhibition directly drives the observed phenotype. In contrast, the apparent efficacy of compound **5d** was attributed to cardiotoxicity, highlighting the necessity of parallel toxicity assessment to avoid false positives in phenotypic screening.

Table 15: Summary of GRK5 inhibitor evaluation.



	R	IC <sub>50</sub> GRK5 [μM]	IC <sub>50</sub> GRK2 [μM]	IC <sub>50</sub> GRK6 [μM]	I <sub>8</sub> μM CM-Nuclei [%]	I <sub>8</sub> μM non-CM- Nuclei [%]	I <sub>8</sub> μM Hypertrophy Score [%]	cLogP	LipE
3		0.010	>1000	0.022	89.78	66.70	245.58	4.615	3.385
4a		0.030	2.2	0.036	100.93	101.22	133.21	4.217	3.306
4b		4.100	7	0.062	91.31	153.81	332.08	4.238	1.149
5b		0.056	10	0.034	98.52	140.50	247.32	4.847	2.405
5d		50.000	300	0.100	48.41	52.48	129.78	5.368	-1.067
5i		2.000	20	0.033	89.56	101.77	189.50	4.779	0.920
5k		12.000	100	0.032	103.09	124.65	225.83	3.573	1.348
5m		0.300	>1000	0.110	90.27	100.86	184.70	5.322	1.201

Beyond the primary aim of confirming anti-hypertrophic activity, a secondary, therapeutically relevant effect emerged: compounds **3**, **4a**, **5i** and **5m** exhibited anti-proliferative activity on non-cardiomyocytes, likely cardiac fibroblasts. Since fibroblast proliferation and extracellular matrix deposition are central to maladaptive remodelling in hypertrophy and heart failure<sup>[25]</sup>, this finding suggests additional therapeutic potential. Such effects would likely be missed in purified cardiomyocyte assays, reinforcing the value of the mixed-cell model developed in this thesis. These results suggest that GRK5 inhibitors may exert pleiotropic effects on cardiac remodelling by targeting multiple pathogenic cell populations. Future studies should determine whether this anti-proliferative activity is due to direct GRK5 inhibition in fibroblasts or indirect effects mediated by paracrine cardiomyocyte signalling.

Complementing the efficacy data, physicochemical characterisation using cLogP and LipE calculations, based on computational estimates, highlighted the importance of balanced lipophilicity for translating biochemical potency into cellular activity. For instance, compound **4a**, with favourable lipophilicity, exhibited strong cellular efficacy, whereas compounds **3** and **5b**, despite potent *in vitro* GRK5 inhibition, were less active in cells, likely due to high cLogP.

These findings underscore the need to optimise both biochemical potency and drug-like properties, as intracellular target engagement is influenced by multiple factors, including membrane permeability, intracellular availability, off-target interactions and nonspecific binding.

Overall, this study advances the understanding of GRK5 as a therapeutic target in cardiac hypertrophy by providing robust genetic and pharmacological validation. It establishes a physiologically relevant assay that captures both therapeutic and adverse effects in a complex cellular context. The identification of potent, selective GRK5 inhibitors with favourable profiles, discovery of anti-proliferative effects on non-cardiomyocytes and incorporation of physicochemical analysis represents key contributions. Together, these findings lay a strong foundation for preclinical development and highlight the value of a multifaceted, validated screening approach in early drug discovery.

As a next step, *in vivo* validation of the most promising candidate, compound **4a**, would be highly desirable. Its potent anti-hypertrophic and anti-proliferative effects in the rodent-derived cell model, together with favourable physicochemical properties and a lack of cardiotoxicity, indicate a high probability of translational success in rodent models. The use of NRCMs further strengthens this likelihood, as species-specific differences are minimised. Moreover, selective *in vivo* characterisation of GRK5 is feasible based on these findings: **4a**'s biochemical potency for GRK2 is too low to contribute to its cellular potency and **4b**, despite high GRK6 activity *in vitro*, was inactive in the cellular assay, effectively devalidating GRK2 and GRK6 as relevant off-targets. A suitable model for *in vivo* testing is the TAC mouse, with mechanical hypertrophy induction. Demonstrating efficacy of **4a** in this model would confirm its robustness against both neurohumoral (cellular assay) and mechanical (TAC model) hypertrophic stimuli. The inclusion of **4b** as a control would further support the on-target mechanism of GRK5 inhibition.

Despite extensive research, no GRK5 inhibitor has yet reached market approval. This work introduces valuable new candidates and mechanistic insights to an underexplored therapeutic area. Given GRK5's key role in adrenergic signalling, maladaptive hypertrophy and fibrotic remodelling, its selective inhibition holds promise as a novel disease-modifying approach for heart failure, a condition still marked by high morbidity and mortality despite current therapies [2].

Furthermore, the broader biological role of GRK5, including nuclear roles in transcriptional regulation and epigenetic remodelling, suggests that inhibitors may affect additional disease-relevant pathways beyond cardiomyocyte hypertrophy. Further investigation into fibrotic, inflammatory and metabolic processes could expand the therapeutic potential of GRK5 targeting. In summary, this chapter provides a solid foundation for advancing GRK5 inhibitors and opens exciting new avenues for treating cardiac hypertrophy and heart failure.

### 5.3 L-2HG as a Hypertrophy Driver and Potential Therapeutic Target

#### 5.3.1 Interplay of L-2HG and Glutamine

Cardiac hypertrophy is a complex adaptive response to increased workload, initially serving as a compensatory mechanism, but without relief of heightened demand progresses to heart failure<sup>[7, 8, 9]</sup>. Alongside structural and functional remodelling, metabolic alterations occur, reflecting the heart's need to adapt its energy production to increased demands. A well-documented change is the reactivation of the fetal gene program, which shifts metabolism from fatty acid oxidation to glucose utilisation<sup>[20]</sup>. In cardiac hypertrophy, oxygen supply often becomes insufficient due to inadequate vascularisation, resulting in local hypoxia. In this context, the preferential use of glucose is advantageous, as it generates ATP with lower oxygen requirements than fatty acid oxidation<sup>[21]</sup>. However, this is only one aspect of the metabolic remodelling that occurs in cardiac mitochondria. Studies have shown that mitochondrial dysfunction is a key hallmark of heart failure, characterised by increased reactive oxygen species (ROS) production, reduced adenosine triphosphate synthesis and disrupted mitochondrial fusion-fission dynamics<sup>[155, 156, 157]</sup>. Notably, these energetic changes also drive structural remodelling by activating pro-hypertrophic signalling pathways<sup>[86, 156, 157]</sup>. As a result, mitochondrial dysfunction represents a promising therapeutic target for both cardiac hypertrophy and heart failure.

To identify key metabolic pathways altered in cardiac hypertrophy and heart failure, the group of Oliver Müller conducted extensive transcriptomic and metabolomic analyses on tissue samples from mice subjected to transverse aortic constriction (TAC). By sampling at different time points after the induction of pressure overload, they tracked progressive metabolic and gene expression changes from early compensatory hypertrophy to the transition into heart failure and, ultimately, end-stage heart failure. Their analysis of cardiac tissues revealed that 143 out of 439 analysed metabolites were dysregulated as early as two weeks after TAC, coinciding with the onset of hypertrophy. Among the upregulated metabolites was L-2-hydroxyglutarate (L-2HG), along with a decrease in its corresponding enzyme, L-2-hydroxyglutarate dehydrogenase (L-2HGDH)<sup>[86]</sup>.

2HG is a chiral metabolite produced in small quantities from  $\alpha$ -ketoglutarate ( $\alpha$ -KG) through poorly understood metabolic pathways<sup>[158, 159]</sup>. Within mitochondria, L-2HGDH catalyses its conversion back to  $\alpha$ -KG. This key tricarboxylic acid (TCA) cycle intermediate can originate from glutamine via glutaminase-mediated deamidation to glutamate and subsequent deamination by glutamate dehydrogenase or through glucose-derived carbon entering the TCA cycle (see Figure 23)<sup>[87, 160, 161]</sup>. 2HGDH acts thereby as a metabolic damage-control mechanism, maintaining balanced 2HG levels<sup>[160, 162]</sup>. This is critical, since its accumulation leads to 2-hydroxyglutaric aciduria, a neurometabolic disorder characterised by elevated

plasma levels of 2HG, neurological impairments and developmental abnormalities<sup>[160, 163]</sup>. Under hypoxic conditions, L-2HG production increases due to promiscuous activity of enzymes such as lactate dehydrogenase (LDH) and malate dehydrogenase (MDH)<sup>[158, 159, 163]</sup>. Beyond its accumulation, L-2HG has been shown to couple the energy metabolism of mitochondria and cytoplasm by cellular redox regulation<sup>[159]</sup>. In parallel, D-2HG functions as a well-established oncometabolite, building up in several cancers driven by mutations in isocitrate dehydrogenase 1 (IDH1), whereas L-2HG accumulates in clear cell renal carcinoma due to loss-of-function mutations in L-2HGDH<sup>[163]</sup>. Both stereoisomers share the ability to inhibit ATP synthase, thereby suppressing mitochondrial respiration and dampening mTOR signalling in a manner comparable to  $\alpha$ -KG<sup>[161, 164, 165]</sup>.

Higher levels of L-2HG have been shown to protect against oxidative stress following myocardial injury in low-flow ischemia and ischemia-reperfusion models<sup>[166]</sup>. In contrast, cellular  $\alpha$ -KG levels are decreased, while circulating levels and its receptor are increased<sup>[157, 165]</sup>. In fact, supplementation of  $\alpha$ -KG in mice subjected to TAC and Ang. II-induced cardiomyocytes exerted an anti-hypertrophic and protective effect, improving mitophagy and reducing intracellular ROS levels<sup>[165]</sup>. Also, glutamate dehydrogenase was significantly upregulated in isoprenaline-induced neonatal rat cardiomyocytes and its overexpression was sufficient to induce hypertrophy<sup>[167]</sup>.

These reports suggest an involvement of all three metabolites in cardiac hypertrophy, making the altered levels of L-2HG and L-2HGDH in the metabolomic analysis particularly interesting. In support of this hypothesis, the group of Oliver Müller showed that circulating L-2HG levels progressively increased with advancing heart failure in human patients, while L-2HGDH mRNA expression was significantly reduced in cardiac tissue from individuals with dilated cardiomyopathy (Ding et al., manuscript in preparation<sup>[168]</sup>). These clinical observations strengthen the relevance of L-2HG dysregulation in human cardiac disease and support its further investigation as a contributing factor in hypertrophic remodelling. Additionally, in an AAV-mediated overexpression study of L-2HGDH in neonatal rat cardiomyocytes, L-2HG levels were decreased as expected, since L-2HGDH is responsible for L-2HG clearance. L-2HGDH overexpression protected cardiomyocytes from L-2HG-induced hypertrophy, as shown by normalised fetal gene expression and cell area measurements. Additionally, L-2HG stimulation led to a time-dependent decrease in mitochondrial membrane potential, while AAV-mediated overexpression of L-2HGDH improved mitochondrial function. These *in vitro* findings were also validated in the *in vivo* model of mice subjected to TAC, showing improvements in systolic function, left ventricular mass, heart weight-to-tibia length ratio, fibrosis and normalisation of the fetal gene program upon AAV-mediated overexpression of L-2HGDH.

In summary, these results suggest that upregulation of L-2HGDH has a protective effect in cardiac hypertrophy and heart failure, presenting a novel therapeutic target. Either inhibiting



the pro-hypertrophic effects of L-2HG or upregulating L-2HGDH could represent a promising new strategy for cardiac hypertrophy management.

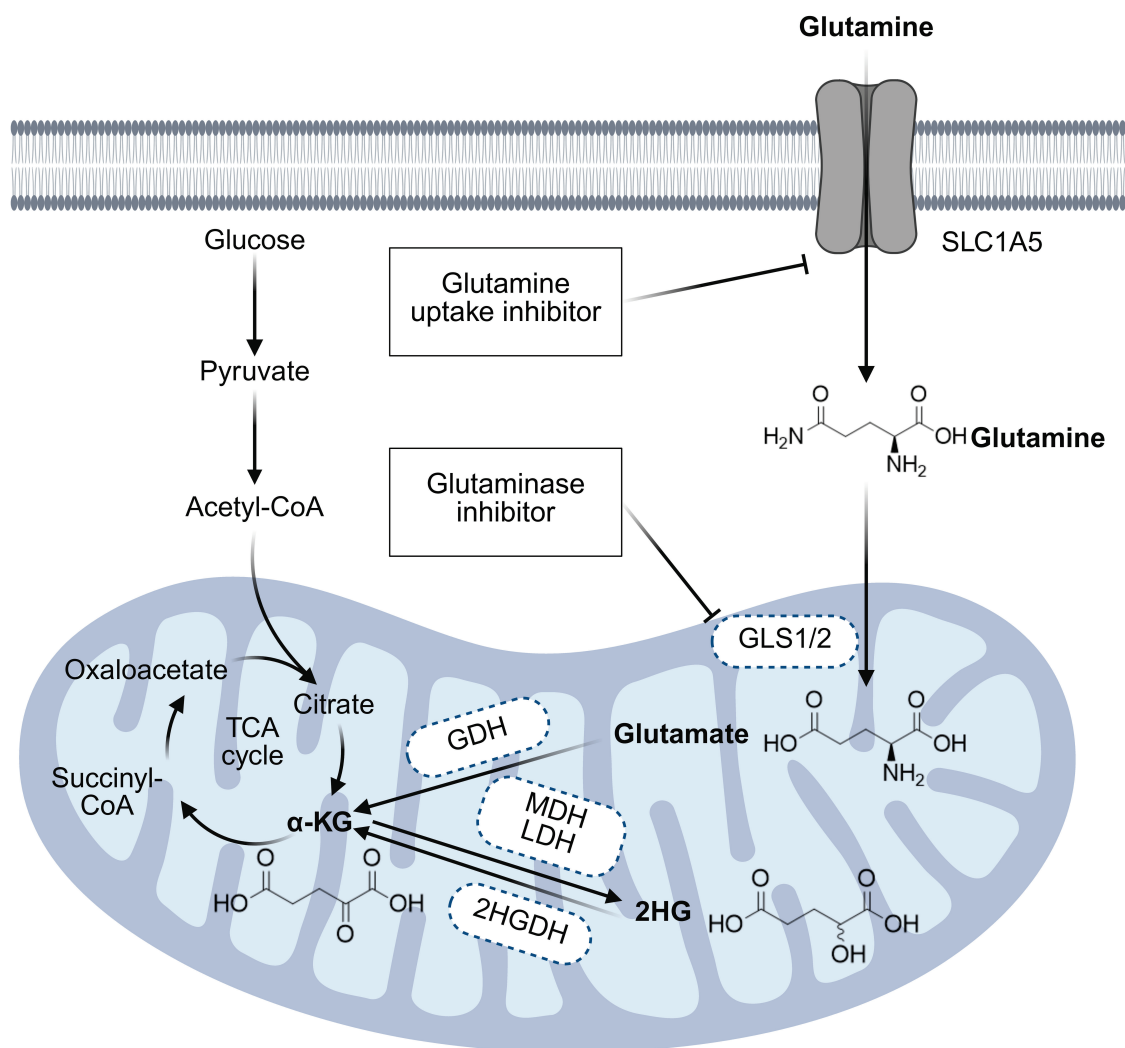


**Figure 23: Illustration of the metabolic interplay between  $\alpha$ -KG, 2HG and glutamine.** In cardiac hypertrophy, energy metabolism shifts towards glycolysis. Glucose degradation products enter the tricarboxylic acid (TCA) cycle, with  $\alpha$ -ketoglutarate ( $\alpha$ -KG) as a key metabolic intermediate. Promiscuous activity of malate dehydrogenase (MDH) and lactate dehydrogenase (LDH) leads to the conversion of  $\alpha$ -KG to L-2-hydroxyglutarate (L-2HG), while L-2-hydroxyglutarate dehydrogenase (L-2HGDH) converts it back to  $\alpha$ -KG to maintain balanced L-2HG levels. The main carbon source of L-2HG was found to be glutamine, linking the three metabolites. After the intake of glutamine over the solute carrier family 1 neural amino acid transporter member 5 (SLC1A5), glutamine is first converted to glutamate through glutaminase (GLS) 1 or 2 and subsequently to  $\alpha$ -KG by glutamate dehydrogenase (GDH).

Here, the hypertrophic effect of L-2HG was confirmed by establishing its phenotypic profile within the assay platform developed in this thesis. Given that glutamine serves as the major carbon source for both  $\alpha$ -KG and 2HG<sup>[169]</sup>, its potential role in cardiac hypertrophy was also investigated to determine whether the pro-hypertrophic effects of 2HG are metabolite-specific

or part of a broader metabolic reprogramming. Notably, glutamine had not been included as a culture medium supplement in any of the previous experiments. Since  $\alpha$ -KG is known to regulate mitochondrial function and energy metabolism, these findings could suggest that the balance between  $\alpha$ -KG and L-2HG may contribute to mitochondrial dysfunction in cardiac hypertrophy. The observed effects could further support the notion that targeting metabolic dysregulation, either by modulating L-2HG levels, enhancing L-2HGDH activity or influencing glutamine metabolism, could represent a promising therapeutic strategy for preventing mitochondrial dysfunction and its downstream consequences in heart failure.

### 5.3.2 Phenotypic Profiling of L-2HG and Glutamine

L-2HG has recently emerged as a metabolite of interest in the cardiac hypertrophy pathophysiology. While its accumulation has been implicated in mitochondrial dysfunction and altered redox balance, its role as a therapeutic target in cardiac hypertrophy remains insufficiently characterised. In a previous study by our group, it was demonstrated that L-2HG induces cardiac hypertrophy in purified neonatal rat cardiomyocytes and mice subjected to TAC (Ding et al., manuscript in preparation<sup>[168]</sup>). This finding raised further questions about how the phenotypic fingerprint of L-2HG compares within the newly developed assay platform to the established positive control combination of PE and LIF. The assay's ability to capture effects on cardiomyocytes in the presence of non-cardiomyocytes, or even direct effects on non-cardiomyocytes, offers additional insights into L-2HG's role. Moreover, its capability to model L-2HG-induced hypertrophy provides a robust foundation for systematic analysis of pharmacological interventions targeting this metabolism-driven disease model.

To address these questions, mixed cardiac cells were stimulated 24 h after seeding and incubated for an additional 96 h prior to fixation and phenotypic analysis. L-2HG was tested at three concentrations (1, 2 and 3 mM), selected based on reports of intracellular L-2HG levels reaching the low millimolar range under pathological conditions<sup>[159, 163]</sup>. In parallel, glutamine, commonly used as a cell culture supplement, was tested at the same concentrations to determine whether the hypertrophic effect observed for L-2HG is specific or potentially shared with upstream metabolic precursors. Notably, glutamine was absent from the culture media during the assay to minimise any hypertrophic effects arising from nutrient supplementation.

Figure 24 presents the comparative analysis of L-2HG and glutamine in relation to the established hypertrophic stimulus, PE-LIF. As previously demonstrated (Chapter 5.1.2), the combination of phenylephrine and LIF induced a broad hypertrophic response across cardiomyocyte-specific parameters, including increased cell area, intensity and a decreased texture. L-2HG similarly elicited a robust hypertrophic phenotype, prominently affecting the same morphological features of cardiomyocytes. In addition, L-2HG influenced nuclear parameters: while the number of cardiomyocyte nuclei was only slightly elevated (113%), a

notable increase was observed in non-cardiomyocyte nuclear count (124%), resulting in a total nuclear count of 119% compared to DMSO control.

In contrast, despite its structural similarity to L-2HG, glutamine did not replicate the hypertrophic profile. Only moderate increases in cell area and intensity were observed and cardiomyocyte texture remained unchanged. However, glutamine induced a strong proliferative effect in non-cardiomyocytes, with their nuclear count increasing to 561%, compared to a modest rise in cardiomyocyte nuclei (107%). Interestingly, the nuclear area showed similar trends: reduced in cardiomyocytes (89%) and slightly increased in non-cardiomyocytes (104%).

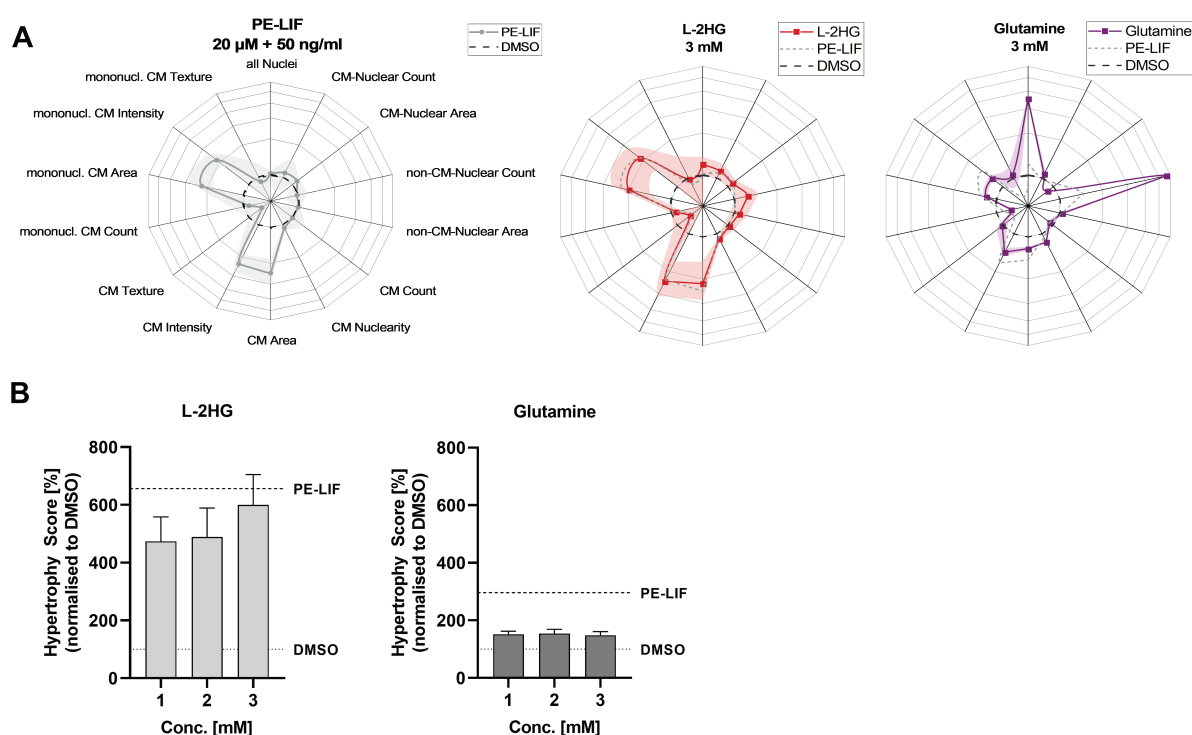


**Figure 24: Phenotypic fingerprint of L-2HG and Glutamine.** Mixed neonatal rat cardiac cells were stimulated 24 h after seeding with either L-2HG or glutamine. DMSO and the combination of PE-LIF served as negative and positive controls, respectively. Cells were fixed and stained for image analysis 96 h post-stimulation. **(A)** Radar plots illustrate the phenotypic profiles of each stimulation. L-2HG induced a hypertrophic phenotype comparable to PE-LIF, with pronounced effects on cardiomyocyte area, intensity and texture. In contrast, glutamine triggered a distinct response characterised by strong proliferation in non-cardiomyocytes and only moderate hypertrophic changes in cardiomyocytes. **(B)** Hypertrophy Scores calculated for both metabolites confirmed the superior hypertrophic effect of L-2HG compared to glutamine. (n = 3, normalised to DMSO, axis of radar plots ranges from 60-600%, mean  $\pm$  SEM)

Comparison of the Hypertrophy Scores revealed that L-2HG induced a disease-like phenotype nearly as strongly as PE-LIF, while glutamine only caused moderate changes. A notable difference in the dynamic range of the PE-LIF response was also apparent between experiments. This variability can be attributed to seasonal fluctuations in primary cell cultures

and biological variability of the donor animals. Specifically, glutamine was tested in experiments conducted later than those for L-2HG, during a period when also the well-established PE-LIF-induced Hypertrophy Score had dropped from 656% to 296%. These observations underline the importance of including positive controls in every experiment to account for shifts in cell responsiveness. It was also noted that primary cultures exhibited seasonal variation, with more moderate hypertrophic responses and smaller litter sizes commonly observed during winter and spring.

In summary, these findings highlight distinct roles for L-2HG and glutamine in modulating cellular responses within mixed primary cardiac cultures. L-2HG acts as a potent inducer of cardiomyocyte hypertrophy, potentially through mechanisms that promote growth and biosynthetic activity. Glutamine, in contrast, exerts a dual effect: mildly enhancing cardiomyocyte hypertrophy while strongly stimulating proliferation in non-cardiomyocytes, likely through its central role in metabolic pathways supporting cell growth and extracellular matrix production. This differential behaviour underscores the complexity of intercellular signalling within the cardiac system and the importance of considering both hypertrophic and proliferative effects when evaluating treatment responses. Notably, the proliferative response to glutamine could only be seen in the co-culture of cardiomyocytes with non-cardiomyocytes, underlining the importance of using co-culture models to preserve the physiological relevance of *in vitro* studies.

### 5.3.3 Targeting the Glutamine Metabolism

Having established the hypertrophic and proliferative effects of L-2HG and glutamine in mixed cardiac cultures, attention was next directed toward the glutamine metabolic pathway as a potential therapeutic target. Glutamine serves as a central carbon source for the generation of both  $\alpha$ -ketoglutarate and L-2HG<sup>[169]</sup>, metabolites that have been implicated in hypertrophic signalling. Given the pathway's metabolic relevance and its pharmacological tractability, a set of small-molecule inhibitors originally developed for oncological diseases was selected for repurposing in this context. These compounds target key enzymes involved in glutamine uptake and metabolism. The primary objective was to determine whether inhibition of glutamine metabolism could mitigate L-2HG-induced hypertrophy and whether these inhibitors would also be effective in the hypertrophic setting induced by PE-LIF stimulation. The following experiments explore the potential of these glutamine-targeting compounds to attenuate pathological cardiomyocyte remodelling.

Glutamine has emerged as a central focus in oncological research due to its critical role in supporting the elevated bioenergetic and biosynthetic demands of rapidly proliferating tumour cells. As the most abundant amino acid in mammalian cells, glutamine serves as a versatile substrate, providing carbon and nitrogen for the synthesis of amino acids, lipids and

nucleotides. Additionally, it plays a key role in maintaining redox homeostasis. Cancer cells, in particular, exhibit an increased reliance on glutamine to fuel anabolic processes and sustain proliferation, a phenomenon often referred to as "glutamine addiction". This heightened consumption is frequently accompanied by upregulation of enzymes involved in glutaminolysis, especially glutaminase (GLS), which catalyses the conversion of glutamine to glutamate<sup>[170, 171]</sup>.

Glutamine is processed by two isoforms of glutaminase: kidney-type glutaminase (GLS1) and liver-type glutaminase (GLS2). GLS1 itself includes two splice variants, kidney isoform of glutaminase (KGA) and glutaminase C (GAC), with distinct regulatory and functional properties<sup>[170]</sup>. The uptake of glutamine into the cell is primarily mediated by the solute carrier family 1 neutral amino transporter (SLC1A5)<sup>[170]</sup>.

Several pharmacological inhibitors have been developed to target glutamine metabolism in cancer<sup>[172]</sup>. **CB-839 (telaglenastat)** is a first-in-class, reversible, allosteric inhibitor of GLS1 that binds between homodimers of the enzyme, promoting the formation of an inactive tetrameric complex<sup>[169]</sup>. **CB-839** is an optimised analogue of bis-2-(5-phenylacetamido-1,3,4-thiadiazol-2-yl)ethyl sulfide (BPTES), a GLS1 inhibitor with poor potency<sup>[173]</sup> and poor solubility<sup>[170]</sup>. It exhibits high selectivity for GLS1, with a biochemical IC<sub>50</sub> of 15 nM, though its solubility is limited to 0.4 µM<sup>[169, 174]</sup>. Despite this, **CB-839** demonstrated efficacy in both *in vitro* and *in vivo* tumour models<sup>[169]</sup> and is currently undergoing clinical evaluation in phase 2 trials<sup>[175]</sup>.

Building on **CB-839**, **IPN60090** was developed through structure-based optimisation, heralding the next-generation of GLS1 inhibitors with improved metabolic stability and solubility (40 µM) while maintaining potency (IC<sub>50</sub> 31 nM)<sup>[174]</sup>. Like its predecessor, it is also being tested in clinical trials, both as monotherapy and in combination regimens<sup>[174]</sup>.

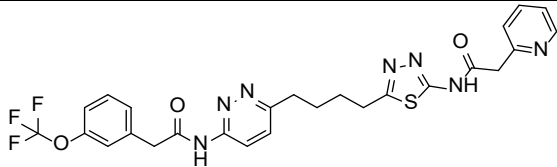
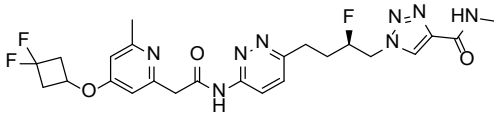
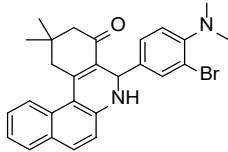
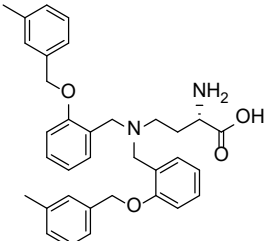
**Compound 968** represents an alternative approach, acting as a reversible allosteric inhibitor that selectively targets the GAC splice variant of GLS1. It demonstrates moderate potency with a biochemical IC<sub>50</sub> of 2.5 µM<sup>[176, 177, 178]</sup>.

In addition to enzyme inhibition, targeting glutamine uptake itself has also gained interest. **V-9302** is the first small-molecule antagonist of the glutamine transporter SLC1A5, with an IC<sub>50</sub> of 9.6 µM in human cells<sup>[170]</sup>. However, its specificity has been questioned, as it was also found to inhibit the uptake of isoleucine, suggesting potential off-target effects<sup>[179]</sup>.

Together, these inhibitors provide a pharmacological toolbox for dissecting the role of glutamine metabolism in disease and offer promising candidates for therapeutic repurposing beyond oncology, including in cardiac pathologies such as hypertrophy. Importantly, this collection of compounds spans a range of selectivities for different glutaminase isoforms and splice variants, offering a valuable toolset to illuminate the specific contributions of individual GLS1 forms, such as KGA and GAC, to pathological processes. This distinction could prove

particularly informative in elucidating the precise role of specific glutaminase isoform activity in the development and progression of cardiac hypertrophy.

**Table 16: Glutamine metabolism-targeting inhibitors.**

	Structure	Target	IC <sub>50</sub> [μM]
<b>CB-839</b>		GLS1 (both splice variants)	0.015
<b>IPN60090</b>		GLS1 (both splice variants)	0.031
<b>Compound 968</b>		GLS1 (GAC specific)	2.5
<b>V-9302</b>		SLC1A5	9.6

To explore this therapeutic potential, the selected glutaminase and glutamine uptake inhibitors were evaluated in the established mixed cardiac cell model. Their effects on cardiomyocyte viability and hypertrophic growth were assessed following stimulation with either PE-LIF or L-2HG, representing two distinct hypertrophic stimuli. While L-2HG primarily drives hypertrophy through metabolic remodelling and glutamine pathway alterations, PE-LIF triggers hypertrophy via classical neurohumoral signalling pathways. Thus, it was of particular interest to investigate whether glutamine metabolism-targeting inhibitors could also modulate hypertrophic responses induced by PE-LIF, suggesting broader applicability beyond L-2HG-driven models. Additionally, cardiotoxic effects were carefully monitored to ensure that reductions in hypertrophy were not secondary to impaired cell viability.

Mixed cardiac cells were therefore stimulated (PE-LIF with 20 μM / 50 ng/ml or L-2HG with 3 mM) and treated with respective inhibitors for 96 h. DAPI and α-actinin stained cells were analysed with the established CellProfiler pipeline, with the results for PE-LIF stimulation shown in Figure 25 and for L-2HG in Figure 26.

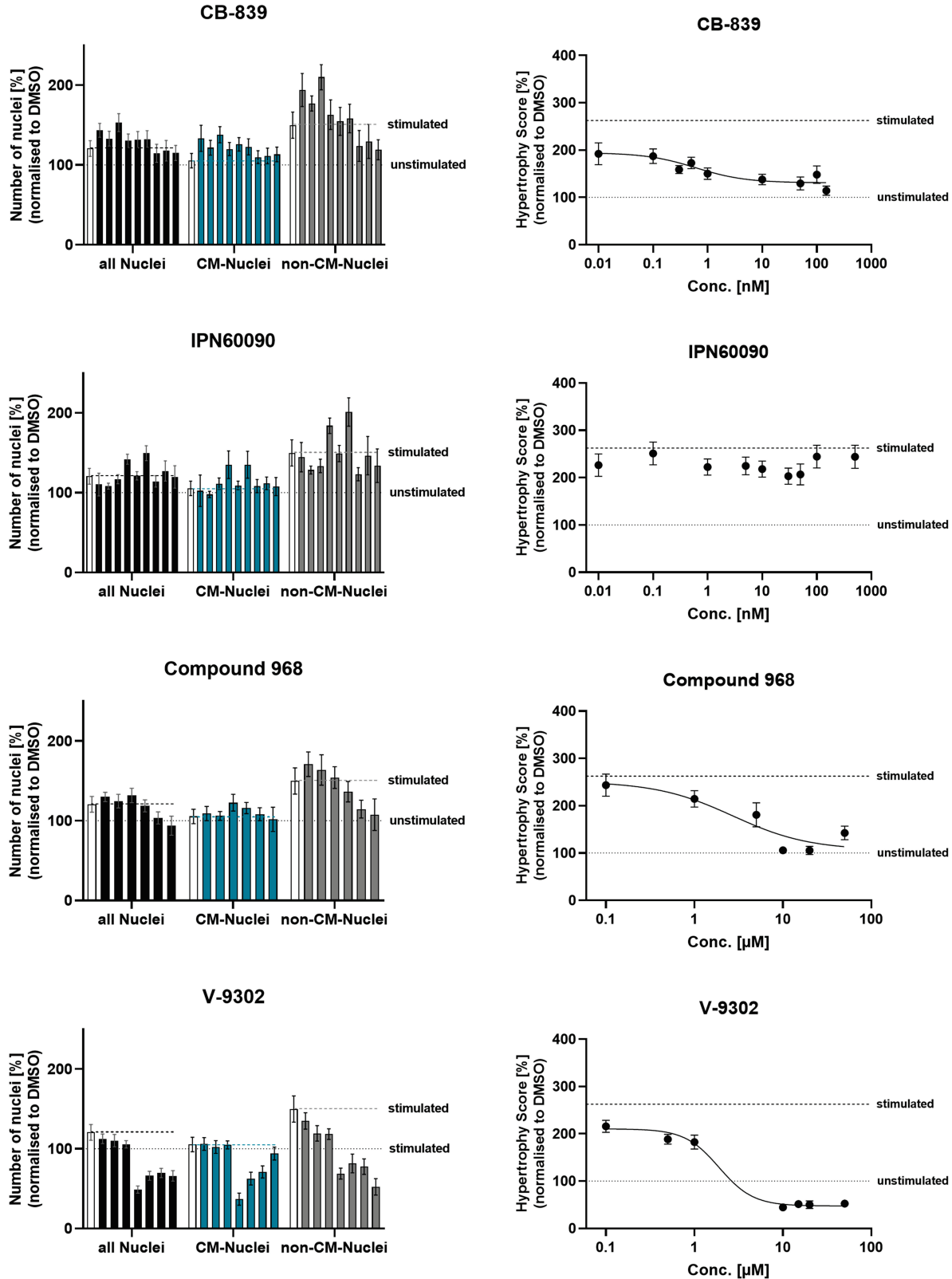


**Figure 25: Phenotypic characterisation of glutamine metabolism-targeting inhibitors against PE-LIF.** Mixed cardiac cells were stimulated with PE-LIF (20 μM / 50 ng/ml) and treated with inhibitors for 96 h. Hypertrophic features and nuclear counts of DAPI and α-actinin stained cardiac cells were quantified using the established CellProfiler pipeline. Image analysis results were normalised to DMSO control (= 100%). (n = 3, mean ± SEM)

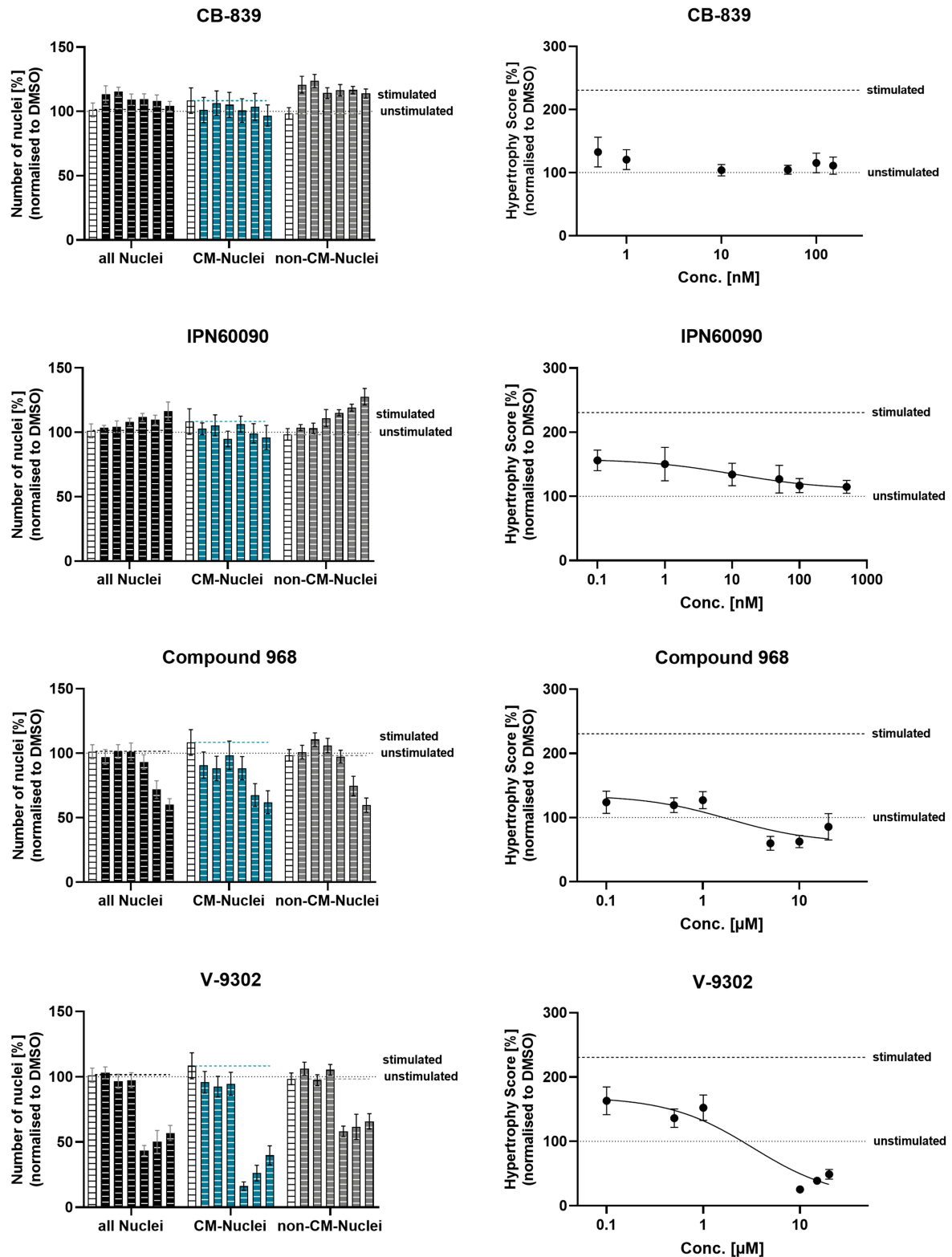


**Figure 26: Phenotypic characterisation of glutamine metabolism-targeting inhibitors against L-2HG.** Mixed cardiac cells were stimulated with L-2HG (3 mM) and treated with inhibitors for 96 h. Hypertrophic features and nuclear counts of DAPI and  $\alpha$ -actinin stained cardiac cells were quantified using the established CellProfiler pipeline. Image analysis results were normalised to DMSO control (= 100%). (n = 3, mean  $\pm$  SEM)



In the phenotypic high-content assay, similar anti-proliferative effects to those observed in the GRK5 inhibitor experiments (Chapter 5.2.3) were seen with several glutaminase inhibitors. Specifically, **CB-839**, **IPN60090** and **Compound 968** all reduced non-cardiomyocyte proliferation under PE-LIF stimulation to DMSO control level, whereas **V-9302** was poorly tolerated and exhibited toxicity in higher concentrations towards both cardiomyocytes and non-cardiomyocytes, reducing counts below DMSO control level. Interestingly, these anti-proliferative effects were less pronounced when the inhibitors were tested against L-2HG-induced hypertrophy. Here, **CB-839** and **IPN60090** showed no anti-proliferative effect on non-cardiomyocytes. **IPN60090** even induced a slight increase in non-cardiomyocyte proliferation. Surprisingly, **Compound 968** caused toxicity only against L-2HG in both cell populations, although not to the same extent as **V-9302**.

Turning to the anti-hypertrophic efficacy of the inhibitors, **CB-839** and **IPN60090** would be expected to perform similarly, considering that **IPN60090** was developed based on **CB-839** and both target the same isoform of glutaminase. However, under PE-LIF stimulation, only **CB-839** exhibited a clear dose-dependent inhibition of hypertrophic growth, even reducing the Hypertrophy Score down to DMSO control levels at higher concentrations. In contrast, **IPN60090** did not significantly prevent hypertrophy, with scores remaining similar to PE-LIF stimulated controls across all tested concentrations. **Compound 968** demonstrated a robust, dose-dependent inhibition of hypertrophic development, combining both anti-proliferative and anti-hypertrophic effects. **V-9302**, while capable of reducing the Hypertrophy Score below DMSO control levels, did so at concentrations that were already toxic to the cells. At non-toxic concentrations, **V-9302** only partially reduced hypertrophy, achieving scores between those of PE-LIF and DMSO controls.

When comparing the results between PE-LIF and L-2HG stimulation, some unexpected differences became apparent. In the L-2HG model, **IPN60090**, despite its lack of efficacy against PE-LIF-induced hypertrophy, was able to prevent hypertrophy in a clear, dose-dependent manner. **CB-839** maintained the phenotype at DMSO control levels across all tested concentrations, displaying consistent activity independent of the stimulus. **V-9302** exhibited the same pattern as observed with PE-LIF: strong reduction of Hypertrophy Scores at toxic concentrations and only partial efficacy at non-toxic doses. **Compound 968**, although inducing cardiotoxicity at higher concentrations, was still able to significantly reduce the Hypertrophy Score below DMSO control levels, while lower, non-toxic concentrations normalised the Hypertrophy Scores to DMSO levels.

Taken together, the screening of glutaminase and glutamine uptake inhibitors revealed distinct profiles with varying degrees of anti-proliferative, cardiotoxic and anti-hypertrophic effects. While some compounds, such as **CB-839** and **Compound 968**, effectively reduced hypertrophic growth and non-cardiomyocyte proliferation, others showed limited efficacy or

induced cytotoxicity, particularly at higher concentrations. Notably, **CB-839** and **Compound 968** attenuated hypertrophic responses also when cells were stimulated with PE-LIF, a physiological inducer acting primarily through adrenergic pathways and thus independent of glutamine metabolism. This observation suggests a broader metabolic dependency in hypertrophic signalling, in which glutamine availability may serve as a general permissive factor for pathological remodelling.

The anti-hypertrophic effects of the glutamine metabolism inhibitors observed in the phenotypic assay were further validated by qPCR analysis of hypertrophic gene expression (see Figure 27). To avoid signal interference from non-cardiomyocytes, purified cardiomyocytes were cultured and stimulated with 3 mM L-2HG. L-2HG stimulation significantly increased the expression levels of the hypertrophic markers *Nppa* and *Nppb*, both encoding for the cardioprotective natriuretic peptides ANP and BNP, respectively. Treatment with **CB-839** (75 nM), **IPN60090** (1  $\mu$ M), **Compound 968** (10  $\mu$ M) and **V-9302** (10  $\mu$ M) effectively prevented the upregulation of these genes, further confirming the anti-hypertrophic potential of targeting glutamine metabolism.

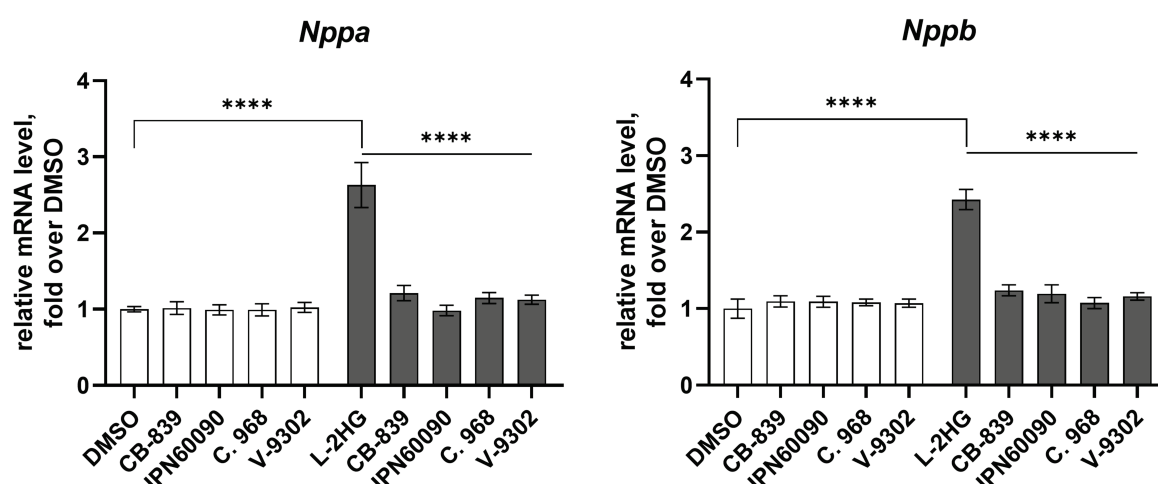


**Figure 27: Confirmation of anti-hypertrophic effects of glutamine metabolism-targeting inhibitors via qPCR analysis.** Purified cardiomyocytes were cultured in 6-well plates for three days prior to stimulation with 3 mM L-2HG (grey) or DMSO (white) and simultaneous treatment with selected inhibitors for 24 h. Tested concentrations were: **CB-839** (75 nM), **IPN60090** (1  $\mu$ M), **Compound 968** (10  $\mu$ M) and **V-9302** (10  $\mu$ M). Gene expression levels were normalised to DMSO control and *Rp32* as housekeeping gene. (n = 3, mean  $\pm$  SEM, one-way ANOVA: \* p  $\leq$  0.05, \*\* p  $\leq$  0.01, \*\*\* p  $\leq$  0.001, \*\*\*\* p  $\leq$  0.0001)

In summary, these results suggest that selectively targeting the GAC splice variant of GLS1 with **Compound 968**, showing toxic effects at higher concentrations against L-2HG stimulation, exerts different effects compared to broader inhibition of GLS1 splice variants by **CB-839** and **IPN60090**. Given that the GAC isoform has been reported to exhibit the highest

enzymatic activity among GLS1 variants<sup>[180]</sup>, targeting glutamine metabolism through GAC likely results in a more pronounced effect.

Moreover, the divergence in inhibitor efficacy between PE-LIF and L-2HG stimulation highlights the complexity of hypertrophic signalling pathways and indicates that glutaminase dependency may vary depending on the upstream hypertrophic stimulus. Notably, inhibition of glutamine uptake at the transporter level with **V-9302** resulted in generally stronger effects compared to direct glutaminase inhibition. However, these effects were accompanied by substantial toxicity towards both cardiomyocytes and non-cardiomyocytes. This observation suggests that the more broadly and upstream glutamine metabolism is disrupted, the stronger and potentially more destructive the cellular responses become. As a conditionally essential nutrient, glutamine plays a central role in cellular energy production, redox balance and biosynthesis. Thus, blocking its uptake represents a drastic intervention that can compromise fundamental metabolic processes. These findings underscore that both the degree and the point of interference within the glutamine metabolic pathway critically influence not only therapeutic efficacy but also the risk of cellular toxicity. A more targeted, downstream intervention may offer a more favourable approach to therapeutically modulate L-2HG regulation. The additional confirmation of anti-hypertrophic effects via qPCR strengthens the robustness of these findings and underscores the promise of glutamine metabolism as a therapeutic target for cardiac hypertrophy.

### 5.3.4 Summary

In this chapter, the role of L-2HG in cardiac hypertrophy was investigated in detail. With the known shift towards increased glucose consumption and mitochondrial dysfunction as key hallmarks of hypertrophic cardiomyocytes, targeting cardiac metabolism has emerged as a promising therapeutic strategy<sup>[20]</sup>. Building on previous findings that identified elevated levels of L-2HG as a characteristic metabolic alteration in cardiac hypertrophy<sup>[168]</sup>, this study aimed to clarify the functional contribution of L-2HG to disease progression. Recognising the close metabolic relationship between L-2HG and glutamine, the primary carbon donor for 2HG biosynthesis<sup>[169]</sup>, the investigation was extended to also examine glutamine metabolism as a therapeutic avenue.

Initial experiments confirmed that both L-2HG and glutamine can independently promote hypertrophic changes in mixed cardiac cell cultures. Notably, L-2HG proved to be a particularly strong hypertrophic stimulus, reaching an effect size comparable to that of PE-LIF, which was selected as the physiological positive control for this assay. Since PE triggers adrenergic overstimulation, a highly relevant mechanism in human cardiac hypertrophy, this finding underscores the pathophysiological importance of L-2HG and highlights it as a promising target for therapeutic intervention. Interestingly, while L-2HG predominantly triggered direct

hypertrophic growth in cardiomyocytes, glutamine mainly stimulated the proliferation of non-cardiomyocytes, suggesting that both metabolites may contribute to cardiac remodelling through distinct yet complementary mechanisms.

Building on these findings, a selection of small-molecule inhibitors was assembled for targeting this metabolic dysfunction. As no drug candidates currently exist that directly target L-2HG or its metabolising enzyme L-2HGDH, this study turned to glutamine metabolism as an alternative therapeutic entry point. The chosen compounds, including GLS1 inhibitors **CB-839**, **IPN60090**, **Compound 968** and the glutamine uptake inhibitor **V-9302**, represent a diverse set of pharmacological tools. They have already advanced into preclinical or early clinical testing for oncological indications, where glutamine metabolism plays a similarly crucial role. This repurposing approach aimed to evaluate whether modulation of glutamine pathways could also impact pathological cardiac remodelling. Importantly, the selected inhibitors covered a range of specificities for glutaminase isoforms (**CB-839** and **IPN60090** targeting GLS1) and splice variants (**Compound 968** targeting the GAC splice variant of GLS1), offering the possibility to dissect the contributions of different branches of glutamine metabolism to hypertrophy and proliferation<sup>[172]</sup>.

When tested in mixed cardiac cell culture, these compounds revealed distinct profiles: **CB-839** and **Compound 968** demonstrated both anti-proliferative effects on non-cardiomyocytes and inhibition of hypertrophic growth. In contrast, **IPN60090**, though based on the same scaffold and also inhibiting GLS1 like **CB-839**, showed only moderate anti-proliferative effects and failed to prevent hypertrophic development after PE-LIF stimulation. These differences in cellular efficacy may be attributed to variations in physicochemical properties between the compounds. **V-9302**, a glutamine uptake inhibitor targeting a step even further upstream, induced pronounced toxicity across both cardiomyocyte and non-cardiomyocyte populations, highlighting the central role of glutamine metabolism for cellular viability. Interestingly, the inhibitory effects were not uniform across different hypertrophic stimuli: when hypertrophy was induced by L-2HG instead of PE-LIF, some compounds displayed altered efficacy, suggesting stimulus-specific differences in metabolic vulnerability. **IPN60090** showed dose-dependent efficacy in preventing L-2HG-induced hypertrophy, while **Compound 968** exhibited toxicity at higher concentrations, possibly due to higher enzymatic activity of targeted GAC-splice isoform.

At the molecular level, qPCR analysis confirmed that all selected inhibitors successfully prevented the L-2HG-induced upregulation of the hypertrophic marker genes *Nppa* and *Nppb* in purified cardiomyocytes, providing robust evidence that pharmacological targeting of glutamine metabolism can counteract hypertrophic signalling pathways.

Together, these results underscore that while targeting glutamine metabolism offers a promising strategy to counteract pathological cardiac remodelling, the essential role of

glutamine in fundamental cellular processes imposes a narrow therapeutic window where efficacy and toxicity must be carefully balanced. Notably, Yoshikawa et al. reported in 2022 that glutamine metabolism is altered in Angiotensin II-infused mice and demonstrated that pharmacological inhibition of GLS1 with BPTES could attenuate hypertrophic development both *in vivo* and *in vitro*<sup>[77]</sup>. However, BPTES possesses relatively low potency and poor solubility compared to more advanced glutaminase inhibitors such as **CB-839**, making it less suitable for clinical translation and limiting its utility for characterising GLS1 inhibition as a therapeutic strategy for cardiac hypertrophy<sup>[169, 181]</sup>. Furthermore, Yoshikawa et al. relied on manual quantification of cardiomyocyte size, a method that is less precise and reproducible than the automated image-based phenotypic screening approaches employed in this study. Thus, while their findings further support the concept of targeting glutamine metabolism in cardiac hypertrophy, the present work provides a more detailed and translationally relevant analysis of this therapeutic avenue. Importantly, their successful demonstration of efficacy in an *in vivo* animal model highlights the translational potential of glutamine-targeted therapies and reinforces the relevance of the *in vitro* findings presented in this study.

Overall, this work illustrates both the promise and the complexity of repurposing glutamine metabolism inhibitors for the treatment of cardiac hypertrophy. Targeting glutaminase activity or glutamine uptake introduces a novel class of potential therapeutic agents distinct from current standard treatments. However, significant challenges remain, as the essential function of glutamine in cellular energy production and redox balance across many tissues presents a major barrier to systemic application. This likely explains why, despite encouraging preclinical data, no glutamine metabolism-targeting drug has yet achieved full market approval. Nonetheless, clinical interest remains high, as highlighted by the FDA Fast Track designation granted to **CB-839 (telaglenastat)** in 2023 for the treatment of metastatic renal cell carcinoma in combination with cabozantinib<sup>[182]</sup>.

Future research will need to prioritise the validation of these findings in *in vivo* models of cardiac hypertrophy, both to confirm therapeutic efficacy and to better characterise potential systemic toxicities. Moreover, combination therapies, such as the simultaneous targeting of glutamine metabolism and adrenergic overstimulation pathways, may offer synergistic benefits, enhancing therapeutic outcomes while mitigating adverse effects. By refining targeting strategies and optimising therapeutic regimens, the glutamine metabolism axis could become an important new frontier in the fight against cardiac hypertrophy.

## 5.4 Cardiodepressive Effects of Colon Cancer Patients' Blood Serum

### 5.4.1 Translational Research: The Tumour-Heart Axis

Translational research bridges the gap between basic scientific discoveries and their clinical applications, ensuring that findings from laboratory studies lead to substantial improvements in patient care. It plays a crucial role in refining diagnostic and therapeutic strategies while considering the cost-effectiveness and accessibility. The phrase "bench to bedside" is often used in this context, highlighting the process of applying experimental findings to clinical practice. Although definitions of translational research vary, its core objective remains the enhancement and acceleration of public health and addressing unmet clinical needs<sup>[88, 183]</sup>.

Unlike basic research, which primarily seeks to expand fundamental knowledge without an immediate clinical application, translational research is problem-driven. It focuses on developing new diagnostic tools, treatment strategies and preventive measures<sup>[88]</sup>. This approach is particularly relevant for complex, multifactorial diseases such as CVDs, where early detection and intervention can significantly alter disease progression and improve patient outcomes.

CVDs remain the leading cause of morbidity and mortality worldwide<sup>[2]</sup>. Despite advances in therapeutic strategies, many patients are diagnosed at late stages when irreversible cardiac damage has already occurred. Moreover, reversing pathological cardiac remodelling, particularly hypertrophy, remains challenging with current therapeutic options<sup>[32]</sup>. This highlights the urgent need to identify novel risk factors and early biomarkers that facilitate timely diagnosis and disease prevention, ideally before irreversible structural changes develop. While well-established causes, such as conditions that impose volume or pressure overload on the heart, are known to induce mechanically driven cardiac hypertrophy, other pathological conditions and comorbidities also contribute to disease development.

One emerging area of interest is the connection between malignancies and cardiac dysfunction. While the cardiotoxic effects of oncological treatments, such as chemotherapy, are well documented<sup>[184]</sup>, an increasing number of studies suggest that tumours themselves may exert direct cardiodepressive effects. Both cancer and CVDs share common risk factors, including unhealthy lifestyle habits such as smoking, excessive alcohol consumption, obesity and physical inactivity<sup>[185, 186]</sup>. Additionally, genetics, ethnicity, age and family history are significant contributors to the development of both diseases<sup>[187]</sup>. Beyond these shared risk factors, several overlapping pathological mechanisms have been identified, including chronic inflammation, dysregulated metabolism and hyperactivation of neurohumoral regulatory systems, like the sympathetic nervous system and RAAS<sup>[186, 188]</sup>. Furthermore, cancer cachexia, a severe syndrome of loss of weight and muscle mass associated with malignancies<sup>[189]</sup>, has been linked to cardiac dysfunction and heart failure. Interestingly, this

effect appears to be bidirectional, as heart failure itself has been shown to induce cachexia<sup>[186, 189, 190]</sup>.

Although shared risk factors and common pathological mechanisms may explain part of the correlation between cancer and CVDs, it is also possible that currently unidentified circulating tumour-derived factors play a key role in linking both diseases. Several proteins known to be elevated in heart failure have been shown to promote proliferation in colon cancer cells<sup>[191]</sup>. This concept, often referred to as the “tumour-heart axis”, describes the potential interplay between tumour-derived factors and cardiac function. In particular, colorectal carcinoma has been implicated in promoting cardiodepressive effects through mechanisms that remain largely unexplored. Epidemiological studies have highlighted a striking association between colorectal cancer and cardiovascular disease. Patients with colorectal cancer have a two- to fourfold increased risk of developing CVDs compared to the general population<sup>[89]</sup>. This correlation is particularly pronounced in older patients, where the incidence of newly developed CVDs reaches 57%, compared to just 22% in age-matched controls<sup>[192]</sup>.

Investigating the tumour-heart-axis is essential for understanding the broader impact of malignancies on cardiovascular health and for identifying potential biomarkers or therapeutic targets to influence tumour-induced cardiac dysfunction. Additionally, a better understanding of this correlation can increase the awareness among healthcare professionals, encouraging a more integrated approach to patient care that bridges the fields of oncology and cardiology. It also supports clinical management, enhances risk stratification and can inform oncological treatment decisions based on the cardiovascular side effect profile of a given therapy. Ultimately, a deeper understanding of tumour-induced cardiac dysfunction and the identification of prognostic factors may contribute to reducing mortality rates associated with these two leading causes of death worldwide<sup>[90, 185]</sup>.

### 5.4.2 Screening Results of Serum Samples

This project aimed to explore the tumour-heart axis using the *in vitro* assay platform established in the herein presented thesis. To investigate whether tumours located in the colon secrete circulating factors into the bloodstream that may influence cardiac function, serum samples obtained from colon cancer patients were tested on both mixed cardiac cell cultures and purified cardiomyocytes. The objective was to assess their potential cardiodepressive effects and determine whether these effects correlate with patient characteristics such as age and sex, as well as tumour-specific factors including localisation, size and lymph node involvement. Identifying a direct link between colon cancer and cardiac dysfunction could pave the way for analysing blood samples from cancer patients for tumour-derived circulating factors as a diagnostic tool. Additionally, this study evaluates the sensitivity of the developed assay in detecting biological samples with cardiodepressive properties, further validating its potential

as a tool for translational research beyond hypertrophy-related outcomes. Notably, this application shifts the assay's output from an increase in nuclear and cellular parameters, as seen in hypertrophy, to a decrease indicative of a cardiodepressive effect. This suggests that the assay may serve as a versatile phenotypic platform for assessing cardiomyopathy, irrespective of whether the outcome is hypertrophic or atrophic.

Testing biological samples such as blood serum in cell culture experiments introduces unique challenges. Small molecules are typically dissolved in DMSO, a common and chemically-defined vehicle, where assay noise and toxicity becomes a concern only beyond concentrations of 0.5-1%. In contrast, biological samples exhibit inherent variability. For example, fetal bovine serum (FBS), a common supplement in cell culture media, contains a complex mixture of growth factors, proteins, vitamins and hormones. However, its composition varies between batches, introducing potential experimental inconsistencies<sup>[193]</sup>. In addition to this variability, biological samples pose a risk of contaminating the cell culture and, particularly in the case of patient-derived material, may carry infectious diseases. Although clinical evaluations are performed prior to biobank inclusion to rule out known diseases, a residual infection risk for researchers remains and must be considered when handling such samples. A crucial consideration for this assay, which was developed to detect cardiac hypertrophy, is that FBS has a well-documented hypertrophic effect on primary cardiomyocytes in a dose-dependent manner. This can either amplify hypertrophic stimulants or obscure the effects of weaker stimulants<sup>[60]</sup>. Consequently, the use of FBS in hypertrophy assays must be carefully controlled.

When testing human blood serum for its potential cardiotoxic effects, the challenge lies in distinguishing between general serum-induced, hypertrophic changes and patient-specific cardiodepressive responses. To address this, an initial experiment was conducted using both FBS and human blood serum from healthy donors across a wide concentration range. Serum from eight healthy volunteers was collected and blinded to ensure anonymity. The goal was to identify a concentration window where serum could be tested on primary cardiomyocytes without inducing pronounced baseline effects, thereby allowing the detection of patient-specific responses in subsequent experiments.

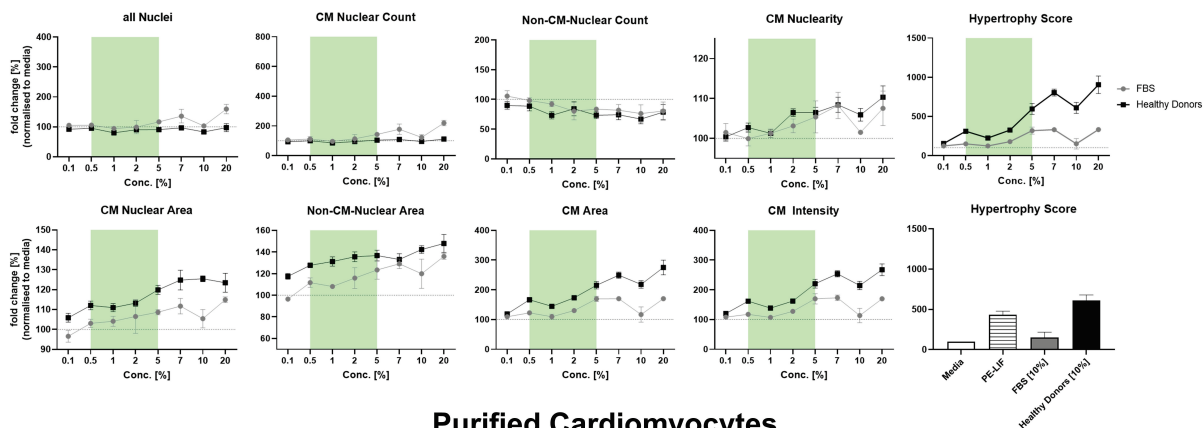
The results, presented in Figure 28, show the phenotypic analysis of both mixed cardiac cells and purified cardiomyocytes treated with FBS or serum from healthy control donors at concentrations ranging from 0.1% to 20%. Serum was diluted in culture medium without the usual FBS supplementation and treated cells were incubated for 96 h.

The image analysis revealed that total nuclear counts, including cardiomyocyte and non-cardiomyocyte cells, remained unchanged at lower concentrations. At higher serum concentrations, nuclear counts of cardiomyocytes increased, though with high variability, while non-cardiomyocyte nuclear numbers slightly decreased below media control levels.



Additionally, cardiomyocyte nuclearity increased from 5% onwards. This suggests two possible explanations: either the growing cardiomyocyte area led to an inaccurate distinction between nuclear subpopulations, resulting in the misassignment of stromal nuclei to cardiomyocytes, or serum treatment selectively promoted cardiomyocyte maturation with development of binucleation.

### Mixed Cardiac Cells



### Purified Cardiomyocytes

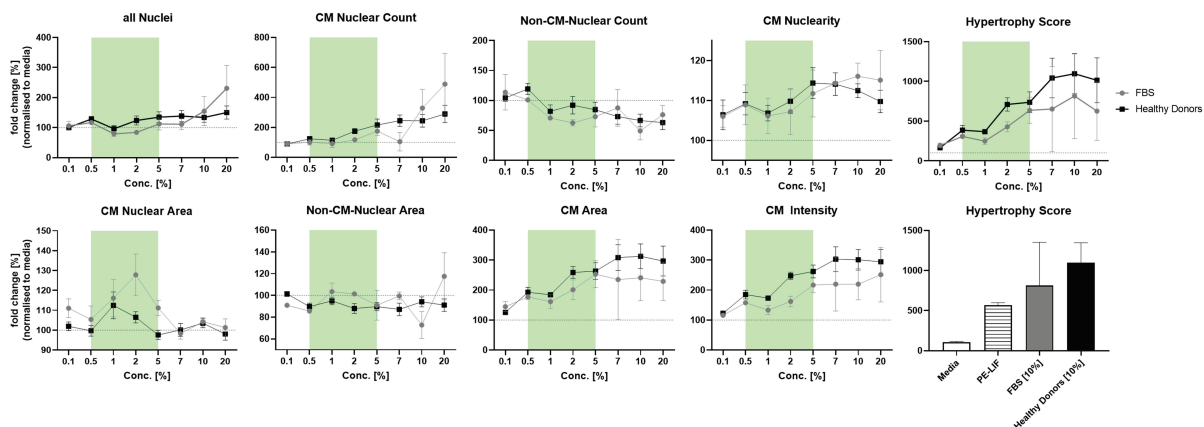


**Figure 28: Dose-finding for serum sample screening.** FBS and human blood serum from healthy donors were tested at a wide concentration range on both mixed cardiac cells and purified cardiomyocytes over four days. Morphological characteristics were analysed using the CellProfiler pipeline established in this study. While proliferative effects were observed only in cardiomyocytes, hypertrophic parameters increased in a dose-dependent manner. Notably, cardiomyocyte nuclear area was only increased in mixed cardiac cells, emphasising the need to test patient samples in both culture approaches. The concentration ranges from 0.5% to 5% (marked in green) was selected for subsequent patient sample screening. (n = 2-3, normalised to DMSO, mean  $\pm$  SEM)

A notable difference between the two culture approaches was observed in nuclear area measurements. While the nuclear area increased in mixed cardiac cells, no such effect was seen in purified cardiomyocytes. This highlights a previously observed trend (see Chapter 5.1.2) where cardiomyocytes in co-culture responded differently to external stimulants, such as cytokine exposure. The crucial role of intercellular signalling in modulating cardiomyocyte

responses further underscores the necessity of including both culture approaches in the subsequent screening of patient samples.

Of note, the analysis of the non-cardiomyocyte population in purified cardiomyocyte cultures is included for completeness. However, due to the Percoll gradient centrifugation yielding an average cardiomyocyte purity of 79%, the remaining non-cardiomyocyte fraction is relatively small and susceptible to variability.

Since FBS is known to induce hypertrophy, all hypertrophic parameters, including cellular area, intensity and the combined Hypertrophy Score, increased as expected in a dose-dependent manner, starting at 2%. Interestingly, human serum from healthy adult donors induced stronger effects than FBS, possibly due to compositional differences related to donor maturity, as FBS is derived from fetal calves. This may also explain the higher Hypertrophy Scores observed with human serum compared to the PE-LIF positive control. The complex and mature composition of adult human serum appears to exert a more pronounced phenotypic effect in both mixed cardiac cells and purified cardiomyocytes compared to the chemically defined PE-LIF combination.

Overall, pronounced serum-induced effects were observed starting at 5%, while the lowest tested concentration (0.1%) showed no significant effects compared to the media baseline. Based on these findings, the concentration range for subsequent patient sample screening was set between 0.5% and 5% (marked green in Figure 28). Higher concentrations (above 5%) were expected to overstimulate cells, potentially masking tumour-derived cardiodepressive effects. Conversely, the absence of effects at 0.1% suggests that this concentration was too low to cause a measurable response. The chosen range of 0.5% to 5% ensures that both weak hypertrophic responses at lower concentrations and more pronounced effects at higher concentrations are captured. A cardiodepressive effect could manifest either as a reduction in hypertrophic responses below media control levels or as a shift in moderate hypertrophy towards baseline values.

In the next step, blood serum samples from 30 colon cancer patients were kindly provided by the biomaterial bank (BMB) of the Comprehensive Cancer Center (CCC) within the popgen 2.0 network (P2N). The popgen 2.0 network is supported by the Medical Faculty of the University of Kiel. The BMB-CCC provides researchers with biomaterial from cancer patients as well as control cohorts from patients with other diseases to advance cancer research, including its prevention, diagnosis and treatment. All patients were informed about the storage and use of their biomaterial samples and the associated pseudonymised clinical data for research purposes. Informed consent was obtained prior to sample collection, with the declaration of consent provided in Appendix 7.2. Before the release of materials, the ethics committee of the Medical Faculty of the Christian-Albrechts-University Kiel reviewed the intended use of the samples and approved this study.

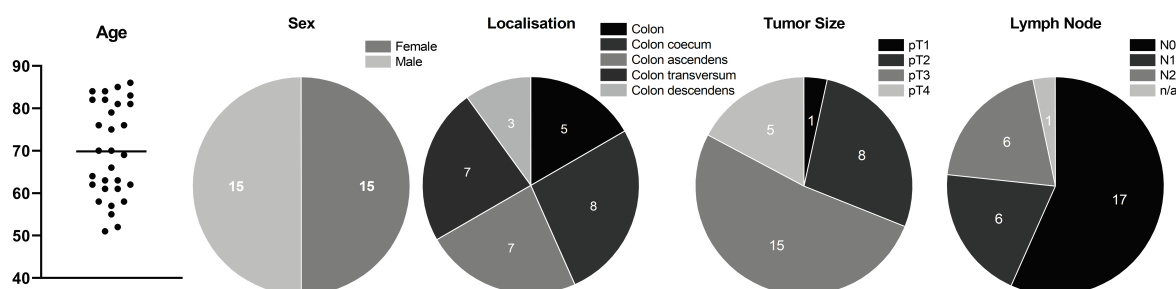


**Figure 29: Demographic and tumour-specific information of the patient cohort.** Serum samples from 30 patients were provided by the biomaterial bank and the corresponding anonymised clinical data are summarised. (p=pathological examination, T=tumour stage, N=lymph node)

The anonymised patient data provided by the biomaterial bank is summarised in Figure 29. The cohort consists of an equal number of male and female donors, with an average age of 70 years. Tumour characteristics, including localisation, size and lymph node involvement, were available for each sample. Based on the TNM staging system, tumour size (T), evaluated by pathological (p) examination, is classified from pT1 to pT4. The majority of samples ( $n = 15$ ) are classified as pT3, indicating more extensive tumour growth with potential infiltration into surrounding tissues. Lymph node involvement (N) is classified from N0 to N3, depending on the number and distance of affected nodes. In this cohort, 17 patients were classified as N0, indicating no detectable lymph node metastases. Information of lymph node involvement was not available for one patient.

Regarding tumour localisation, the distribution was as follows: coecum ( $n = 8$ ), ascending colon ( $n = 7$ ), transverse colon ( $n = 7$ ) and descending colon ( $n = 3$ ). For five patients, only the general localisation within the colon was provided. Information regarding the presence of distant metastases (M) was not available. Overall, this cohort represents a broad spectrum of colon cancer cases. However, the limited sample size ( $n = 30$ ) may reduce the statistical power of this screening. As the BMB-CCC is still in the process of collecting samples, the available serum was restricted to the current cohort at the time of this study.

To assess potential cardiodepressive effects, serum samples from colon cancer patients were incubated with both mixed cardiac cell cultures and purified cardiomyocytes for 96 h and the effects were compared to ones from serum of healthy donors. Due to the limited volume of each patient sample, testing was conducted in technical triplicate and experimental duplicates for mixed cardiac cells, while purified cardiomyocytes were tested in a single experiment.

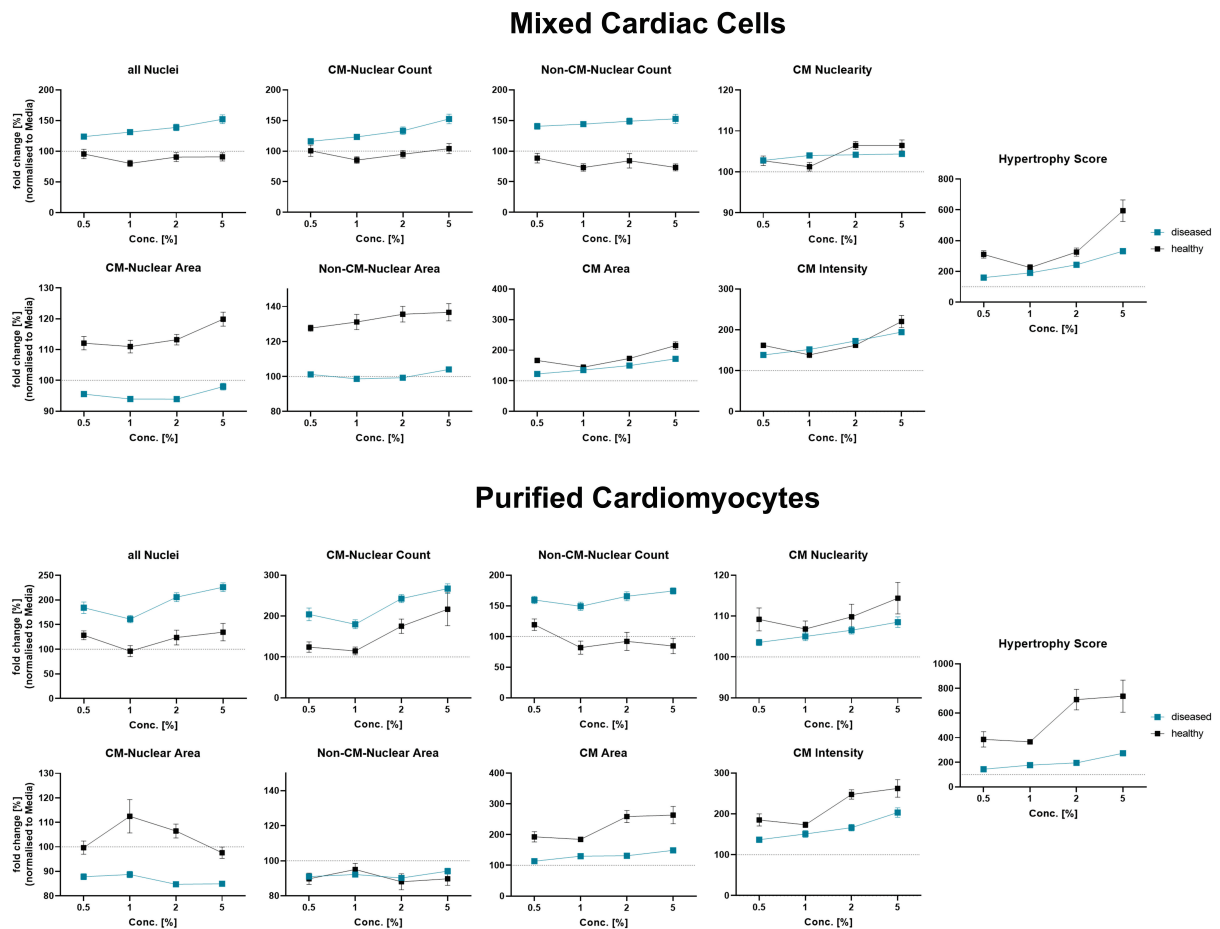


**Figure 30: Morphological response to serum from colon cancer patients.** Analysis of mixed cardiac cells and purified cardiomyocytes treated with serum from colon cancer patients and healthy donors. Hypertrophic and proliferative parameters were assessed to evaluate the potential cardiodepressive effects of patient serum. ( $n = 1-2$ , normalised to DMSO, mean  $\pm$  SEM)

Image analysis (results are presented in Figure 30) revealed a notably higher nuclear count across all three cell subpopulations in samples treated with patient serum, demonstrating a dose-dependent increase. This was surprising, since a proliferative effect after treatment with serum from healthy donors was only observed at higher concentrations and exclusively in cardiomyocytes. This suggests that tumour-associated factors present in the serum may induce a proliferative response. However, in contrast to this increase in cell number, the nuclear area of both cardiomyocyte and non-cardiomyocyte cells was reduced following treatment with patient serum. In particular, cardiomyocyte nuclear area significantly decreased below medium control, indicating a stressed cellular state despite enhanced proliferation. This suggests a cardiodepressive effect in which cardiomyocyte growth is impaired, potentially as a response to circulating tumour-derived factors. These trends were consistently observed in both mixed cardiac cells and purified cardiomyocytes. The only exception was the nuclear area of stromal cells in purified cardiomyocyte cultures, which did not show a significant difference between patient and control serum. A possible explanation might be the reduced presence of

stromal cells (approx. 21%) following cardiomyocyte purification. While the remaining stromal cells still exhibited a proliferative response, their lower abundance may have prevented the detection of significant changes in nuclear area.

Further analysis of hypertrophic parameters revealed that cardiomyocyte area, intensity and the overall Hypertrophy Score were decreased in response to patient serum, showing an atrophy-related effect. However, despite this reduction, values remained above medium control, indicating that while hypertrophic effects were reduced, they were not eliminated. Notably, patient serum did not induce the same increase in these parameters at 2% and 5% concentrations, which was typically observed with serum from healthy donors. This suggests that circulating tumour-derived factors may interfere with or counteract the hypertrophic effect of blood serum. The observed effects were particularly pronounced in purified cardiomyocytes, suggesting that non-cardiomyocyte cells may play a buffering role, either modifying the cardiodepressive effect or providing a protective response that partially compensates for the tumour-induced changes. These findings align with previous observations in cancer cachexia, where systemic factors contribute to muscle atrophy, including in the heart<sup>[190]</sup>.

If tumour-derived factors are indeed responsible for the impaired morphology of cardiomyocytes seen in this study, identifying these circulating biomarkers could provide valuable insights into cancer-induced cardiac dysfunction. Additionally, they may enable early risk assessment for cardiovascular complications in colon cancer patients and could serve as potential therapeutic targets to prevent or treat tumour-associated cardiac dysfunction.

### 5.4.3 Correlation of Patient Data with Cardiac Response

The previous findings confirm the hypothesised link between malignancies and cardiovascular health, supporting the notion that tumour-derived factors influence cardiomyocyte morphology. To further characterise this connection, a correlation analysis was performed, linking the assay results to patient-specific data, including tumour size, localisation, lymph node involvement, age and sex. Identifying statistical associations between these parameters could strengthen the evidence for a tumour-heart axis and provide deeper insights into how colon cancer may contribute to cardiac dysfunction. Furthermore, understanding these associations may help identify vulnerable patients who are at higher risk of developing CVDs alongside colon cancer and adapt their treatment according to the cardiovascular side effect profile.

To achieve this, patient-specific data were correlated with the phenotypic parameters most affected by patient serum treatment: total nuclei numbers, nuclear area of cardiomyocytes, cardiomyocyte area and intensity, as well as the composite Hypertrophy Score. The Pearson correlation coefficient ( $r$ ) for each combination is presented in Figure 31. A correlation coefficient close to 1 represents a strong positive correlation, whereas a coefficient near 0

indicates no correlation. A negative correlation suggests that as one variable increases, the other decreases. In this context, a negative correlation was expected, as a more severe disease state, like larger tumour size or lymph node involvement, would likely result in a stronger cardiodepressive effect. Similarly, an age-related decline in cardiac function was anticipated. Female patients were assigned the value 1 and male patients the value 2, meaning a negative correlation would indicate a stronger cardiodepressive effect in males and vice versa. Tumour localisation was arranged from the colon coecum to the descending colon to investigate whether tumours in the posterior colon were associated with worse cardiac outcomes.

The correlation analysis provided further insight into the relationship between tumour characteristics and the cardiodepressive effects observed in the assay. In mixed cardiac cell cultures, age exhibited the strongest and most significant negative correlation with cardiac function, suggesting that older patients may be at a higher risk for tumour-associated CVDs. This finding aligns with epidemiological studies that report a higher incidence of CVDs in older colorectal cancer patients<sup>[192]</sup>. Additionally, male patients showed a tendency for greater cardiovascular impairment compared to female patients, particularly at 1% serum concentration, as indicated by a decrease in cardiomyocyte area and nuclear count. However, this effect was not consistently observed across all serum concentrations.

Interestingly, at 0.5% serum concentration, both total nuclei count and Hypertrophy Score correlated positively with tumour localisation, while nuclear area showed a negative correlation. This suggests that tumour location may influence different aspects of cardiomyocyte morphology, though this trend weakened at higher serum concentrations. Tumour size did not show a consistent effect on cardiomyocyte parameters across different serum concentrations, indicating that its impact might be more complex or dependent on additional factors. A weak negative correlation with lymph node involvement was detected at 5% serum concentration, accompanied by a proliferative response. However, at lower concentrations, this effect was less pronounced or inconsistent.

In purified cardiomyocyte cultures, tumour size demonstrated a notable negative correlation with cardiomyocyte parameters, an effect not observed in mixed cardiac cells. This suggests that stromal cells in mixed cultures may buffer or mitigate tumour-induced cardiodepressive effects. Interestingly, at 5% serum concentration, tumour size appeared to have a positive effect on cardiomyocyte nuclear area, despite all other hypertrophic parameters being negatively correlated. Lymph node involvement was associated with a general negative impact on cardiac function at 0.5% serum concentration, whereas in mixed cardiac cells, this effect was only observed at 5% serum concentration. Here, at higher concentrations, the influence of lymph node involvement became less pronounced, with the exception of a possible toxic effect on total nuclear count.

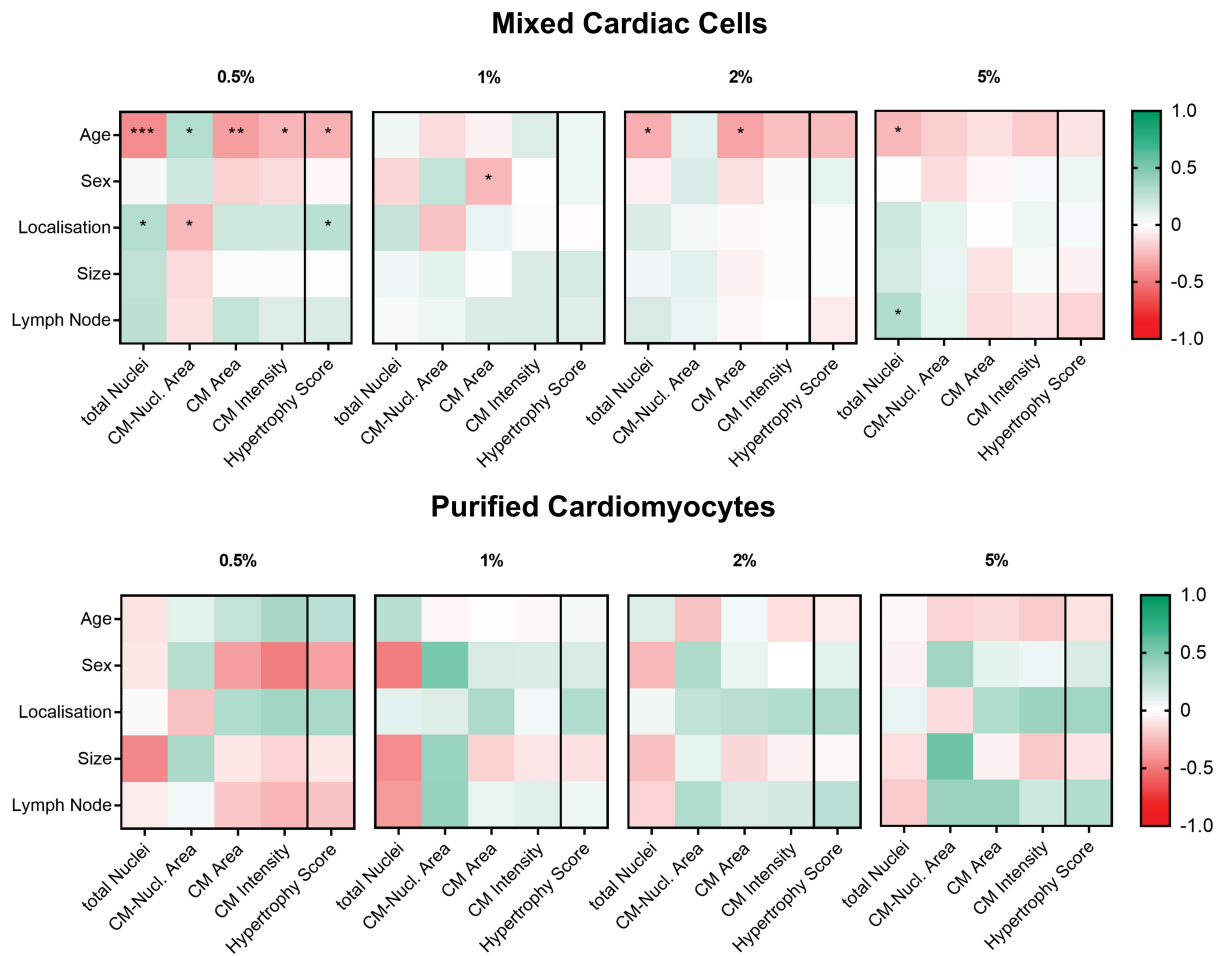


**Figure 31: Heatmap of correlation coefficients between patient data and morphological parameters.** Pearson correlation coefficients ( $r$ ) representing the relationship between demographic and tumour-specific patient data and the most influential phenotypic parameters by patients' serum are shown. Shown are results for mixed cardiac cells ( $n = 2$ ) and purified cardiomyocytes ( $n = 1$ ). (Mean, two-tailed test: \*  $p \leq 0.05$ , \*\*  $p \leq 0.01$ , \*\*\*  $p \leq 0.001$ , \*\*\*\*  $p \leq 0.0001$ ).

The negative impact of age on cardiac function became more apparent at higher serum concentrations (2% and 5%) in purified cardiomyocytes, suggesting that age-related cardiac decline may become more pronounced under stronger external stimulation. Similar to mixed cardiac cells, there was a trend indicating that male patients were at higher risk for tumour-associated cardiac dysfunction. However, this trend was not consistently observed across all tested concentrations and parameters.

Representative correlation plots are displayed in Figure 32, illustrating key relationships between patient-specific data and morphological changes at selected serum concentrations. However, it is important to note that the lack of biological replicates (i.e., only technical replicates) in purified cardiomyocyte experiments weakened the statistical power of this analysis. Additionally, certain cohort characteristics, such as pT3 tumours, were overrepresented, potentially introducing a bias in the dataset.

Despite these limitations, several significant correlations were identified, suggesting preliminary trends. While no single demographic or tumour-associated factor showed a consistent correlation across both cell culture approaches or all serum concentrations, a general negative association of patient age, tumour size and lymph node involvement with cardiac function was observed. Moreover, serum from male patients tended to induce stronger cardiodepressive effects, indicating that male colon cancer patients might be at greater risk for cardiac dysfunction. In contrast, tumour localisation along the colon tract did not show a uniform trend, suggesting that factors beyond anatomical positioning might be more influential in driving cardiac changes. These findings highlight the need for larger patient cohorts and more detailed serum biomarker analyses to further elucidate the relationship between colon cancer and cardiac function.



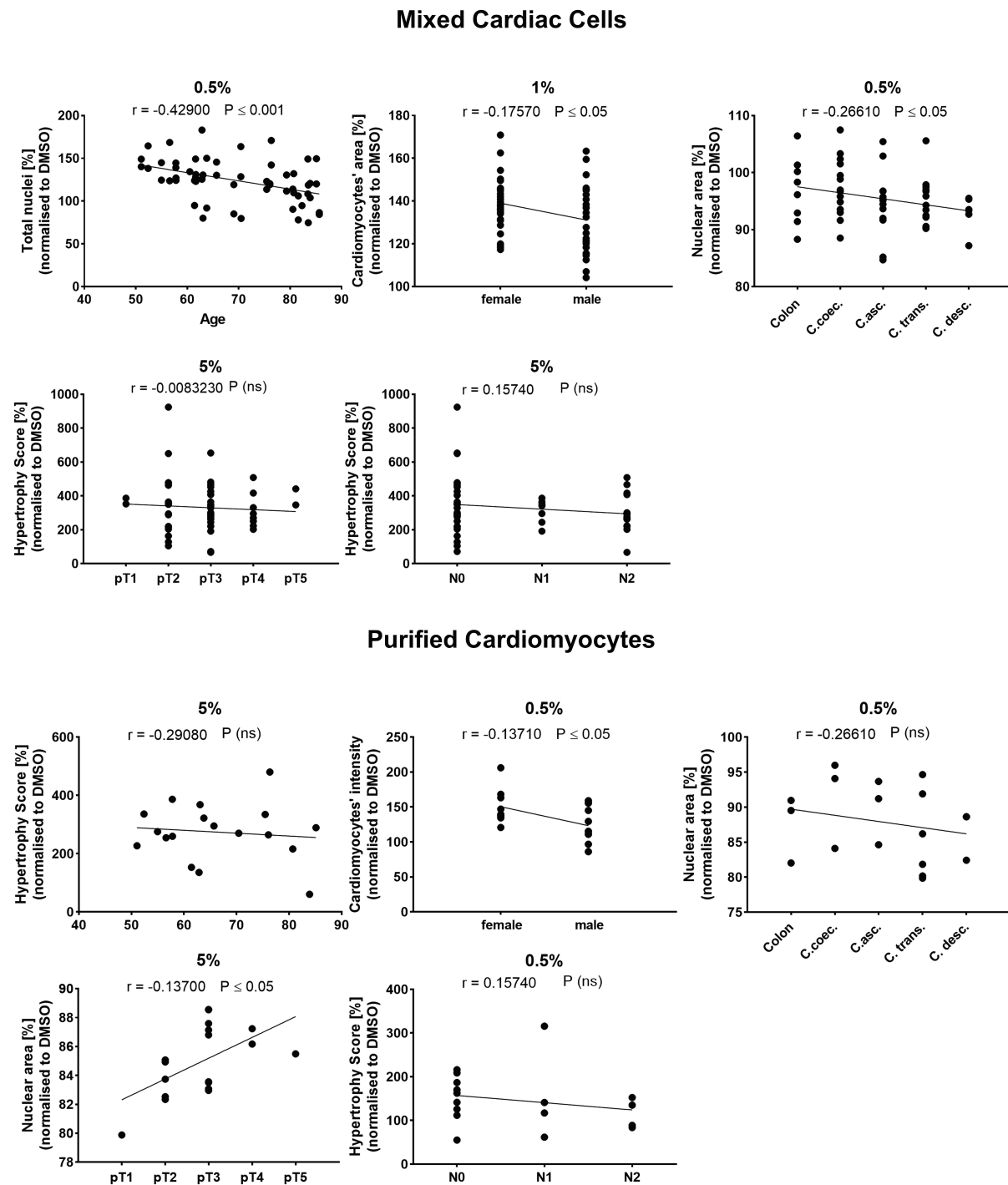


**Figure 32: Representative correlations plots for patients' data to morphological changes.** Representative correlation plots are shown, illustrating the relationship between patient-specific data and morphological parameters at selected serum concentrations. The full dataset for mixed cardiac cells is available in Appendix 7.3.1 and for purified cardiomyocytes in Appendix 7.3.2. Pearson correlation coefficients ( $r$ ) and  $p$ -values were calculated for each correlation. (Mean, two-tailed test: \*  $p \leq 0.05$ , \*\*  $p \leq 0.01$ , \*\*\*  $p \leq 0.001$ , \*\*\*\*  $p \leq 0.0001$ )

#### 5.4.4 Summary

In this study, the established cardiac hypertrophy assay was utilised to characterise the cardiomyocyte phenotype following treatment with blood serum from colon cancer patients, thereby investigating the tumour-heart axis. Epidemiological studies have reported an increased risk of CVDs in colon cancer patients<sup>[89]</sup>. Thus, this assay aimed to detect potential cardiodepressive effects of patient serum. Demonstrating a resulting cardiac dysfunction after exposure to patient serum would support the hypothesis that tumour-derived factors in circulation mediate adverse effects on the heart.

As an initial step, an assay baseline was established by testing blood serum from healthy donors and FBS to assess the general influence of biological samples on cardiomyocyte phenotype. Since both exhibited significant hypertrophic effects at concentrations of 5% and above, a concentration range between 0.5% and 5% was selected for the subsequent screening of 30 patient samples.

Comparison of patient and healthy donor samples revealed a dose-dependent proliferative effect across all cellular subpopulations in response to patient serum. However, all previously established hypertrophic parameters showed a decrease in response to patient serum, suggesting that colon cancer influences cardiomyocyte morphology in a cardiodepressive manner. The pronounced hypertrophic response observed with healthy donor serum at 2% and 5% was distinctly diminished following treatment with patient serum, suggesting that tumour-derived factors in circulation may exert anti-hypertrophic or atrophic effects. The analysis of both mixed cardiac cells and purified cardiomyocytes revealed a stronger cardiodepressive effect in the purified cardiomyocyte cultures, indicating that stromal cells play a crucial role in cardiomyocyte health, potentially buffering the effects of circulating tumour-derived factors or mediating protective pathways.

To further strengthen the suggested tumour-heart-axis, patient-specific data were correlated with cardiomyocyte morphology. This analysis indicated that tumour size and lymph node involvement were associated with a stronger cardiodepressive effect. Additionally, serum from male and older patients showed a greater tendency to induce adverse cardiac effects. While some correlations reached statistical significance, the small cohort size ( $n = 30$ ) and limited number of replicates represent a constraint, potentially leading to an over- or underestimation of specific associations. Unequal representation of patient characteristics may introduce additional bias, emphasising the need for larger, well-balanced cohorts in future studies to validate these findings.

While this study supports the hypothesised tumour-heart axis, it leaves open the question of which tumour-derived factors mediate cardiac dysfunction and the observed atrophic cardiomyocyte phenotype. Identifying such circulating biomarkers could offer valuable tools for early risk assessment and targeted interventions in colon cancer patients. A promising

approach involves proteomic or metabolomic profiling to compare molecular signatures between patients and healthy controls. Candidate factors could then be prioritised by referencing known mediators of cardiac atrophy, such as inflammatory cytokines, oncometabolites and markers of metabolic or oxidative stress<sup>[194]</sup>. Consequently, these prioritised candidates could be tested in functional assays like the established hypertrophy assay of this work.

A successful example for biomarker identification in cardiovascular research is the brain natriuretic peptide (BNP), a well-established marker for heart failure. Initially identified through differential screening of heart tissue<sup>[195]</sup>, BNP was later validated as a circulating biomarker, reflecting cardiac stress and ventricular dysfunction. A similar strategy, screening for proteins, RNAs or metabolic factors uniquely elevated in colon cancer patients with pronounced cardiac effects, could lead to the discovery of novel tumour-associated cardiotoxic markers. Such findings might not only improve cardiovascular risk management in cancer patients but also provide new therapeutic targets to counteract tumour-induced cardiac dysfunction.

Future studies should focus on expanding patient cohorts, integrating multi-omics approaches and refining *in vitro* models to better mimic the complex interactions between tumour-derived factors and cardiac tissue. Advancing the understanding of the tumour-heart axis may pave the way for earlier detection, risk stratification and improved management of cardiovascular complications in cancer patients.

## 6. Conclusion and Outlook

Cardiovascular diseases remain the leading cause of mortality worldwide<sup>[1, 2]</sup>, with cardiac hypertrophy representing a critical pathological process contributing to heart failure. Drug innovation in cardiology has lagged behind other medical fields, such as oncology, resulting in a weak pipeline for novel therapeutics<sup>[34, 35]</sup>. To revitalise drug discovery towards new targets and modalities for treating cardiac hypertrophy, currently established preclinical assays require improvement to enhance the probability of identifying or optimising high-quality drug candidates. Notably, a meaningful *in vitro* assay based on rodent cells is vital for successful *in vivo* translation of early lead structures along with pharmacological target and mode-of-action validation in rodent disease models, as typically employed in the first place.

Within the herein presented thesis, a hypertrophy assay platform was established that recapitulates the complex, physiologically more relevant mix of cardiac cells from neonatal rat hearts in culture and in high-throughput-compatible formats. This *in vitro* model maintains intercellular and paracrine signalling, thereby more closely mimicking the complex composition of the organ. Different hypertrophy-inducing stimuli were systematically assessed in the new system, resulting in distinct, well-defined disease phenotypes. To do this, a custom automated CellProfiler pipeline was developed for high-content image analysis that expanded the morphological scope of the phenotypic assay beyond simple cell area measurement. By integrating multiple phenotypic parameters into a 'Hypertrophy Score' metric, the assay enabled direct and robust comparisons of different tested conditions. This open-source software pipeline is not only widely applicable, regardless of available equipment or computational power, but can also be easily adapted or further expanded for individual aims and applications.

In a first application, this assay platform was employed to enable the very first reported cellular efficacy profiling of a small-molecular GRK5-selective inhibitor set. Regulating the maladaptive signalling of adrenergic stimulation in the heart, GRK5 has emerged as a promising therapeutic target due to its role in promoting pro-hypertrophic gene expression<sup>[80]</sup>. Its involvement in phenylephrine- (PE-) driven cardiac hypertrophy development was successfully confirmed in the new assay system via siRNA-mediated knockdown, providing genetic evidence to support pharmacological targeting of GRK5. A chemotype-specific collection of GRK5 inhibitors<sup>[145]</sup> was chosen based on their *in vitro* biochemical potencies and isoform selectivities to investigate cellular efficacy translation. Inhibitor **4a** emerged as the most promising candidate, demonstrating strong anti-hypertrophic effects ( $IC_{50} = 4.7 \mu M$ ) that were confirmed in an orthogonal biomarker assay (qPCR). Importantly, the optical antipode **4b**, which exhibited similar biochemical potency for GRK2 and GRK6 but no GRK5 activity, showed no cellular effect, thus ruling out GRK2 and GRK6 as off-targets and confirming that GRK5 inhibition alone is sufficient to treat cardiac hypertrophy. Interestingly, several of the tested

inhibitors, including **4a**, also exhibited anti-proliferative effects in the non-cardiomyocyte population, suggesting a potential benefit against fibrotic remodelling. Notably, this effect would have been missed in a conventional assay setup using purified cardiomyocytes, underlining the biological strength and added value of the established mixed cell culture model. By linking biochemical potency, calculated lipophilicity and cellular efficacy, this work contributes important insights and offers a proof-of-concept for the therapeutic relevance of GRK5. It provides relevant cellular data for further lead optimisation, which is now possible via profiling hundreds of lead derivatives from GRK5-centric medicinal chemistry campaigns. Hence, the assay platform is a powerful tool to accelerate *in vivo* validation of GRK5 and distinct inhibitor chemotypes. The successful development of a clinical GRK5 inhibitor holds promise as a novel approach for treating cardiac hypertrophy at the level of tissue remodelling.

The second application of the new assay platform investigated the contribution of L-2-hydroxyglutamate (L-2HG) to cardiac hypertrophy, providing novel insights into the metabolic vulnerabilities of hypertrophic cardiomyocytes. Previous findings of upregulated L-2HG levels in cardiac hypertrophy patients and its stimulatory capacity in purified cardiomyocytes were successfully confirmed in this mixed cardiac cell model<sup>[86]</sup>. L-2HG stimulation resulted in a profound hypertrophic phenotype, comparable to the positive controls using adrenergic (i.e., PE) and cytokine (i.e., LIF) stimulation. Pharmacological targeting of L-2HG is challenging due to the lack of small-molecule modulators that directly affect L-2HG formation or turnover. Therefore, the focus was shifted to glutamine, a closely linked metabolite. While glutamine stimulation induced a rather minor hypertrophic response, it caused strong proliferation in the non-cardiomyocyte population, suggesting a more pronounced role in cardiac fibrosis. These findings indicated that both metabolites contribute to pathological cardiac remodelling through distinct yet complementary mechanisms. A panel of glutamine metabolism inhibitors, originally developed for oncological therapy, was repurposed to target L-2HG-driven hypertrophy. The GLS1 inhibitors **CB-839 (telaglenastat)**, its next-generation analogue **IPN90060** and **Compound 968** showed robust anti-hypertrophic effects, confirmed by orthogonal biomarker analysis (qPCR), and additional anti-proliferative activity, similar to GRK5 inhibitor **4a**. In contrast, upstream intervention by targeting glutamine uptake with **V-9302** induced broad toxicity, highlighting the importance of selecting an optimal intervention point when perturbing essential metabolic pathways. Differences in toxicity at higher concentrations and variable efficacy against L-2HG or PE-LIF stimulation identified **CB-839** as the most promising candidate for *in vivo* validation. Since **CB-839** is already being evaluated in clinical trials for various cancers, its known safety profile, combined with these encouraging cellular efficacy data, lays the groundwork for further exploration of metabolic intervention as a therapeutic strategy for cardiac hypertrophy.

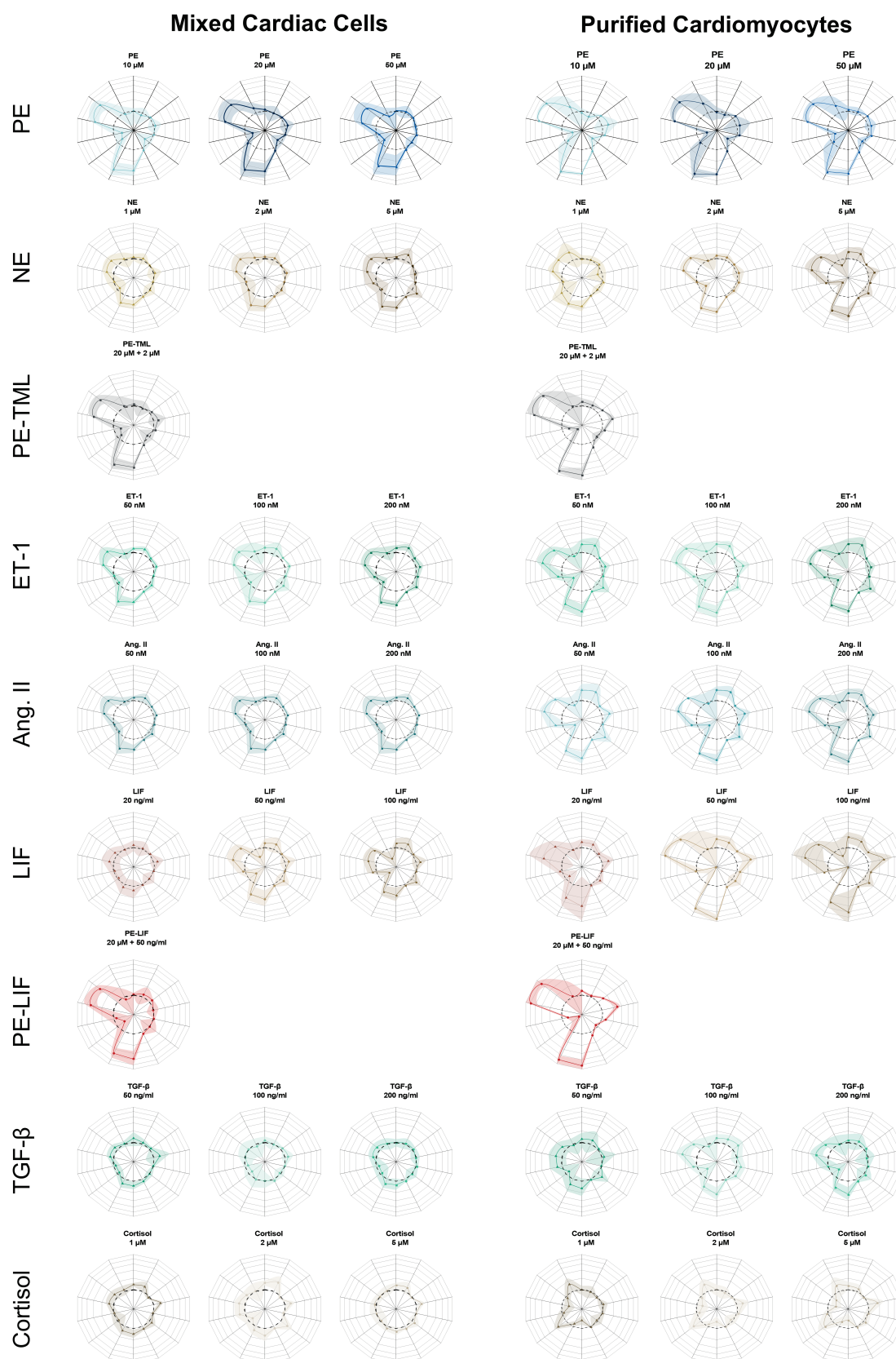
Lastly, the translational scope of the developed assay platform was further expanded by a screening approach to investigate the tumour-heart axis. Blood serum from a cohort of colorectal cancer patients was evaluated for its cardiodepressive effects, shifting the original assay readout from a hypertrophic to an atrophic phenotype. While serum from healthy donors induced an expected hypertrophic response, attributed to the nutrient content, serum from cancer patients reduced hallmark hypertrophic growth features, suggesting the presence of tumour-derived circulating factors that negatively affect cardiomyocytes. Comparative analysis between the purified cardiomyocyte model and the newly established mixed cardiac cell culture revealed that cardiomyocytes were particularly vulnerable to these effects in the absence of non-cardiomyocytes, highlighting the protective or buffering role of stromal cells within the cardiac microenvironment. Notably, tumour size, lymph node involvement and male sex correlated with stronger cardiodepressive effects, pointing to a potential stratification of colon cancer patients at higher risk for developing CVDs. Although the low availability of patient serum ( $n = 30$ ) limits the statistical power of these results, the presented study highlights the assay's adaptability to diverse cardiovascular research questions. Future efforts to identify the responsible circulating factors could enable the discovery of novel biomarkers for early diagnosis or risk stratification, as well as guide the selection of oncological therapies with reduced cardiotoxic side effects. Candidate factors could subsequently be re-tested on this assay platform to confirm their involvement in tumour-induced cardiac dysfunction.

This thesis established a novel and versatile high-throughput screening platform that combines physiologically relevant mixed cardiac cell cultures with a high-content image analysis pipeline, substantially advancing both biological relevance and analytical depth. Its robust phenotypic characterisation makes it a powerful tool for both hypothesis-driven investigation and exploratory drug discovery. Key achievements include the identification of GRK5 inhibitor **4a** as a promising candidate for *in vivo* validation, new insights into targeting metabolic remodelling as a strategy for cardiac hypertrophy and the strong cellular evidence linking colorectal cancer to cardiodepressive effects. Together, these contributions advance our understanding of cardiovascular disease mechanisms and therapeutic opportunities. By integrating disease modelling, targeted pathway intervention and translational insights, this work paves the way for more effective, mechanism-based drug discovery, ultimately aiming to improve the lives of patients affected by cardiovascular diseases.



## 7. Appendix

### 7.1 Radar Plots Hypertrophy stimulants





## 7.2 Declaration of Consent for Blood Serum Biobank

### Einwilligungserklärung und Datenschutzerklärung

**Patient:** \_\_\_\_\_  
Name, Vorname

**Geburtsdatum:** \_\_\_\_\_  
Tag/Monat/Jahr

Bitte lesen Sie folgenden Text aufmerksam durch, kreuzen Sie Zutreffendes an und unterschreiben Sie die Einwilligungserklärung.

Ich willige ein, dass meine Biomaterialien wie nachstehend angegeben sowie meine Daten, wie in der zugehörigen Informationsschrift beschrieben ist, vom Universitätsklinikum Schleswig Holstein, Campus Kiel, bzw. der Biobank BMB-CCC im Institut für Experimentelle Tumorforschung gewonnen bzw. erhoben und dort aufbewahrt bzw. gespeichert und für medizinische Forschungszwecke verwendet werden. Ich willige ein, dass die Zwecke der medizinischen Forschung, für die meine Biomaterialien und Daten verwendet werden, nicht eingegrenzt werden.

**Ich willige ein, dass die nachfolgend aufgeführten Biomaterialien gewonnen und in der Biobank BMB-CCC gesammelt werden (falls nicht gewünscht, bitte „Nein“ ankreuzen):**

- |   |                                      |
|---|--------------------------------------|
| - Gewebeproben aus meinem entfernten Gewebe | <input type="checkbox"/> <b>Nein</b> |
| - maximal 50 ml Blut                        | <input type="checkbox"/> <b>Nein</b> |
| - maximal 10 ml Knochenmarkblut             | <input type="checkbox"/> <b>Nein</b> |
| - Urin-, Stuhl- sowie Speichelproben        | <input type="checkbox"/> <b>Nein</b> |

Insbesondere willige ich ein, dass wie in der Informationsschrift beschrieben

- das Universitätsklinikum Schleswig Holstein, Campus Kiel, personenbezogene Daten, insbesondere Angaben über meine Gesundheit, von mir erhebt, gegebenenfalls weitere personenbezogene Daten aus meinen Krankenunterlagen entnimmt und die Daten pseudonymisiert (d. h. kodiert) speichert. Meine Biomaterialien und Daten dürfen unbefristet für medizinische Forschungszwecke verwendet werden.
- die Biomaterialien pseudonymisiert an die Biobank BMB-CCC im Institut für Experimentelle Tumorforschung, Universitätsklinikum Schleswig Holstein, Campus Kiel, weitergegeben und dort aufbewahrt werden. Das Eigentum an den Biomaterialien übertrage ich an das Universitätsklinikum Schleswig Holstein.
- die Biomaterialien zusammen mit den vorgenannten Daten pseudonymisiert an Universitäten, öffentliche Forschungseinrichtungen und forschende Privatunternehmen zu Zwecken der medizinischen Forschung weitergegeben werden dürfen.

Dies schließt unter Umständen auch die Weitergabe in Länder außerhalb der Europäischen Union (EU) ein. Dies ist generell zulässig, wenn ein Angemessenheitsbeschluss der Europäischen Kommission vorliegt oder die Gewährleistung eines angemessenen Schutzniveaus vertraglich vereinbart und umgesetzt wird.

## Einwilligungserklärung und Datenschutzerklärung

**Darüber hinaus willige ich in die Weitergabe meiner Biomaterialien und Daten in Länder außerhalb der EU auch in den Fällen ein, in denen kein Angemessenheitsbeschluss der Europäischen Kommission vorliegt und keine Gewährleistung eines angemessenen Schutzniveaus vertraglich vereinbart oder umgesetzt wird. Über die möglichen Risiken einer solchen Weitergabe bin ich aufgeklärt worden (Ziffer 7c in der Informationsschrift).**

☐ Ja

☐ Nein

**Ich willige ein, dass ich evtl. zu einem späteren Zeitpunkt erneut kontaktiert werde,** um zum Beispiel weitere Daten oder Biomaterialien von mir zu erbitten oder um meine Erlaubnis zu erhalten, dass meine Daten und Biomaterialien mit weiteren Daten aus anderen Quellen verknüpft werden dürfen.

☐ Ja

☐ Nein

Ich habe die Patienteninformation zu dieser Einwilligungserklärung erhalten. Mir wurden Kopien beider Dokumente zum Verbleib bei mir ausgehändigt. Das Original der Einwilligungserklärung verbleibt beim Universitätsklinikum Schleswig-Holstein, Campus Kiel.

Ich habe beide Dokumente gelesen und verstanden. Dadurch wurde ich ausreichend über das Ziel und den Verlauf der Biobank BMB-CCC, die Chancen und Risiken meiner Teilnahme, die Nutzung und eventuelle Weitergabe meiner Daten und Biomaterialien und die durch meine Teilnahme für mich entstehenden Rechte und Pflichten aufgeklärt.

Ich hatte ausreichend Zeit für meine Entscheidung. Ich bin darüber aufgeklärt worden, dass ich meine Einwilligung gegenüber dem UKSH, Campus Kiel, oder der Biobank BMB-CCC, Institut für Experimentelle Tumorforschung ohne Angabe von Gründen jederzeit widerrufen kann. Beim Widerruf werden auf mein Verlangen die verbliebenen Biomaterialien und die erhobenen Daten vernichtet bzw. gelöscht oder anonymisiert. Eine Datenlöschung erfolgt im Rahmen der technischen Möglichkeiten und soweit die Verwirklichung des Forschungsvorhabens nicht unmöglich gemacht oder unangemessen beeinträchtigt wird. Daten aus bereits durchgeführten Analysen können nicht mehr gelöscht werden.

**Ort, Datum:** \_\_\_\_\_  
vom Patienten einzutragen

**Unterschrift des Patienten:** \_\_\_\_\_

**Name der aufklärenden Person:** \_\_\_\_\_  
in Druckbuchstaben

**Unterschrift der aufklärenden Person:** \_\_\_\_\_

## 7.3 Full Data set: Correlation of Patient Data with Cardiac Response

## 7.3.1 Mixed Cardiac Cells

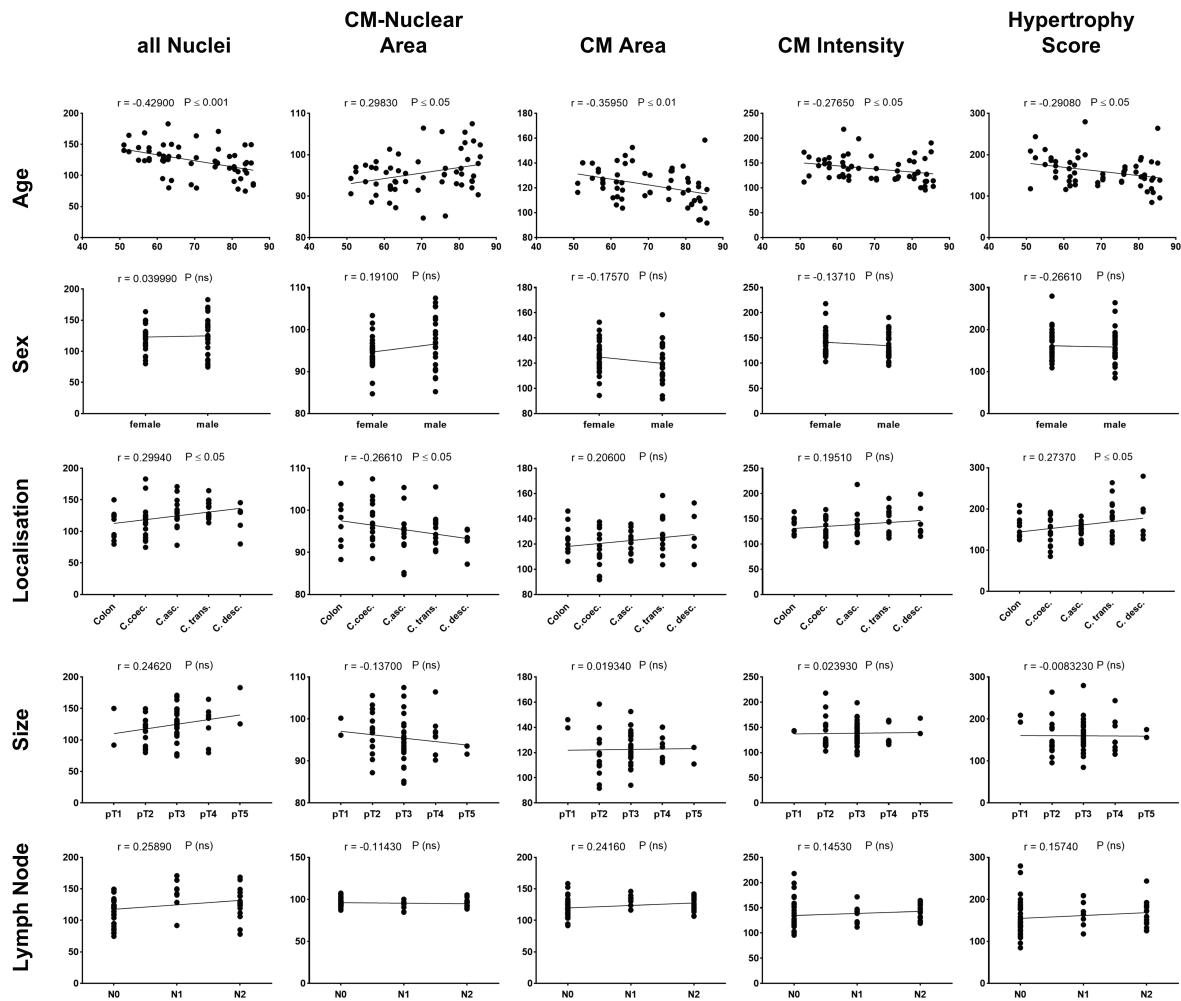


**Figure 33: Correlation for serum concentration of 0.5%.** Correlations plots for patients' data to morphological changes. Mixed cardiac cells were treated with 0.5% patients' blood serum for four days. Pearson correlation coefficients (r) and p-values were calculated for each correlation. (Mean, two-tailed test: \*  $p \leq 0.05$ , \*\*  $p \leq 0.01$ , \*\*\*  $p \leq 0.001$ , \*\*\*\*  $p \leq 0.0001$ )

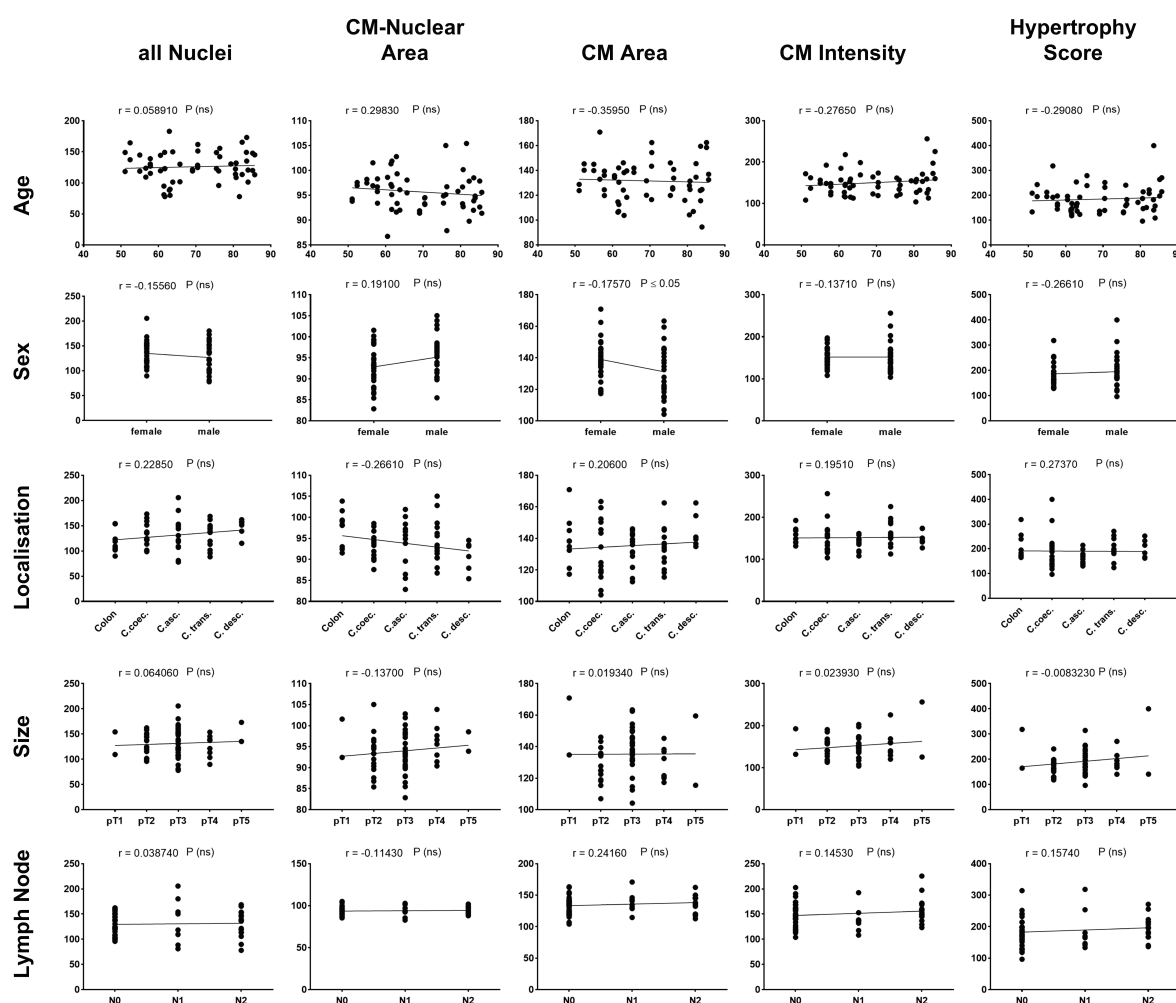


**Figure 34: Correlation for serum concentration of 1%.** Correlations plots for patients' data to morphological changes. Mixed cardiac cells were treated with 1% patients' blood serum for four days. Pearson correlation coefficients (r) and p-values were calculated for each correlation. (Mean, two-tailed test: \*  $p \leq 0.05$ , \*\*  $p \leq 0.01$ , \*\*\*  $p \leq 0.001$ , \*\*\*\*  $p \leq 0.0001$ )

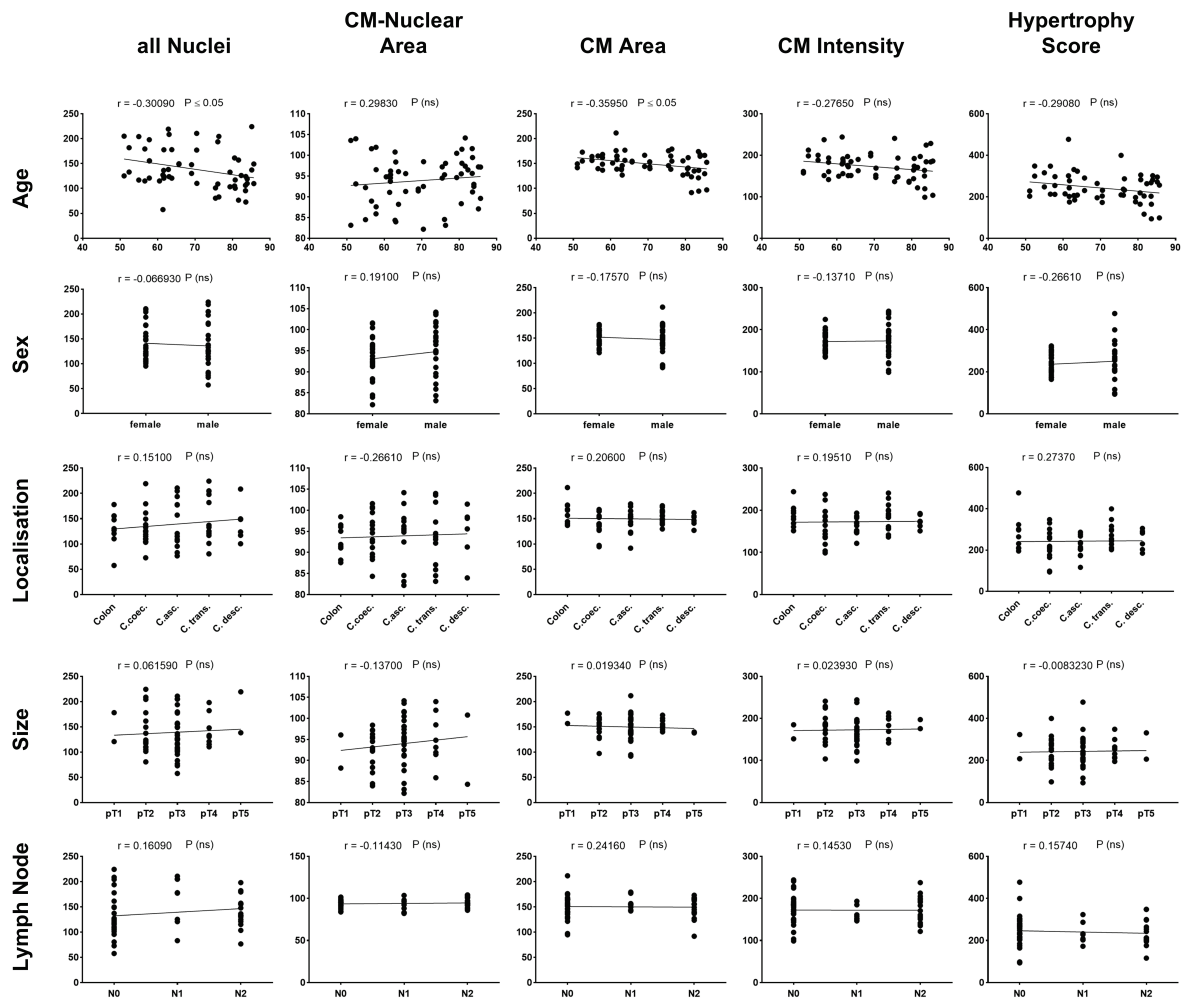


**Figure 35: Correlation for serum concentration of 2%.** Correlations plots for patients' data to morphological changes. Mixed cardiac cells were treated with 2% patients' blood serum for four days. Pearson correlation coefficients (r) and p-values were calculated for each correlation. (Mean, two-tailed test: \*  $p \leq 0.05$ , \*\*  $p \leq 0.01$ , \*\*\*  $p \leq 0.001$ , \*\*\*\*  $p \leq 0.0001$ )

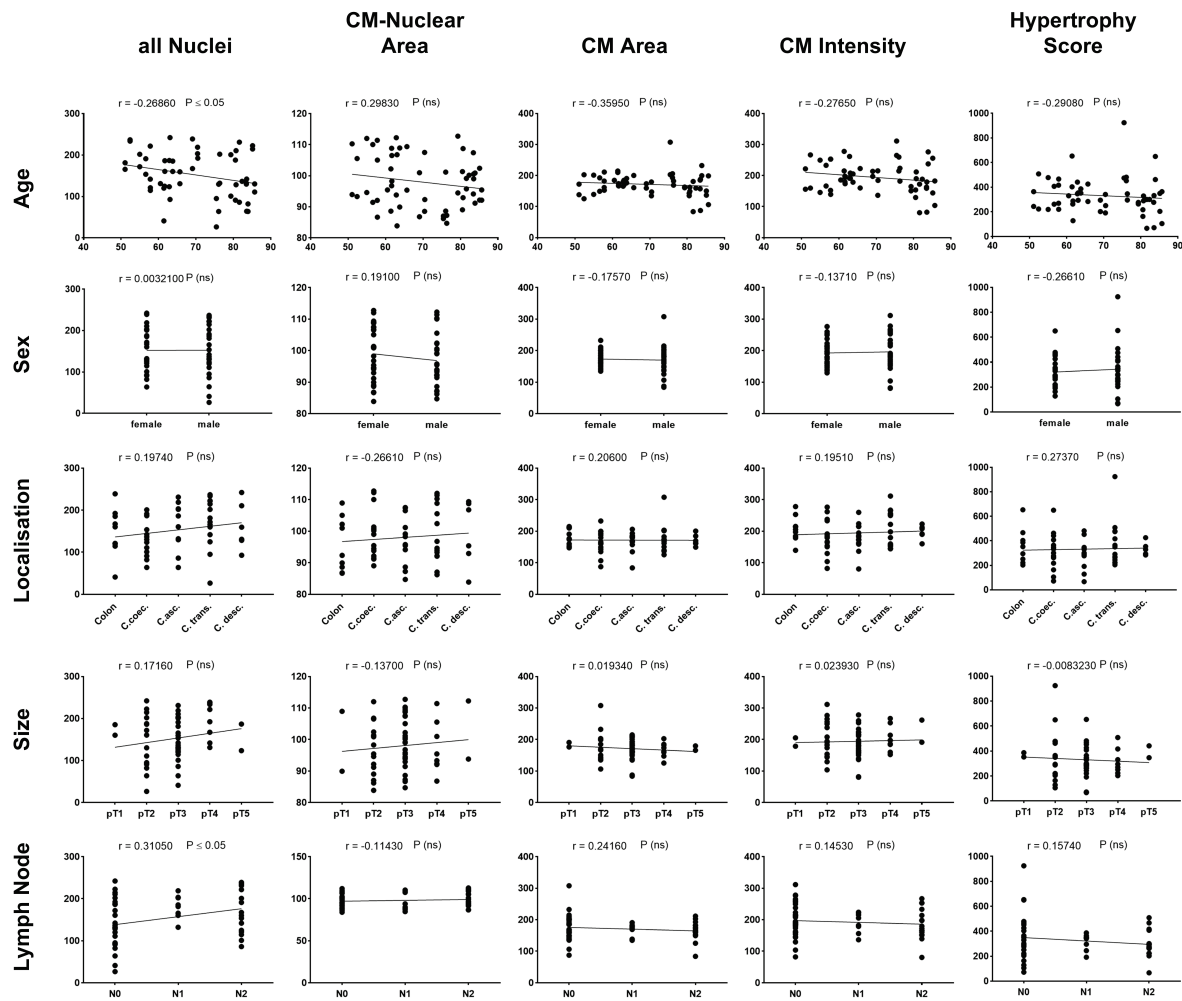


**Figure 36: Correlation for serum concentration of 5%.** Correlations plots for patients' data to morphological changes. Mixed cardiac cells were treated with 5% patients' blood serum for four days. Pearson correlation coefficients (r) and p-values were calculated for each correlation. (Mean, two-tailed test: \*  $p \leq 0.05$ , \*\*  $p \leq 0.01$ , \*\*\*  $p \leq 0.001$ , \*\*\*\*  $p \leq 0.0001$ )

## 7.3.2 Purified Cardiomyocytes

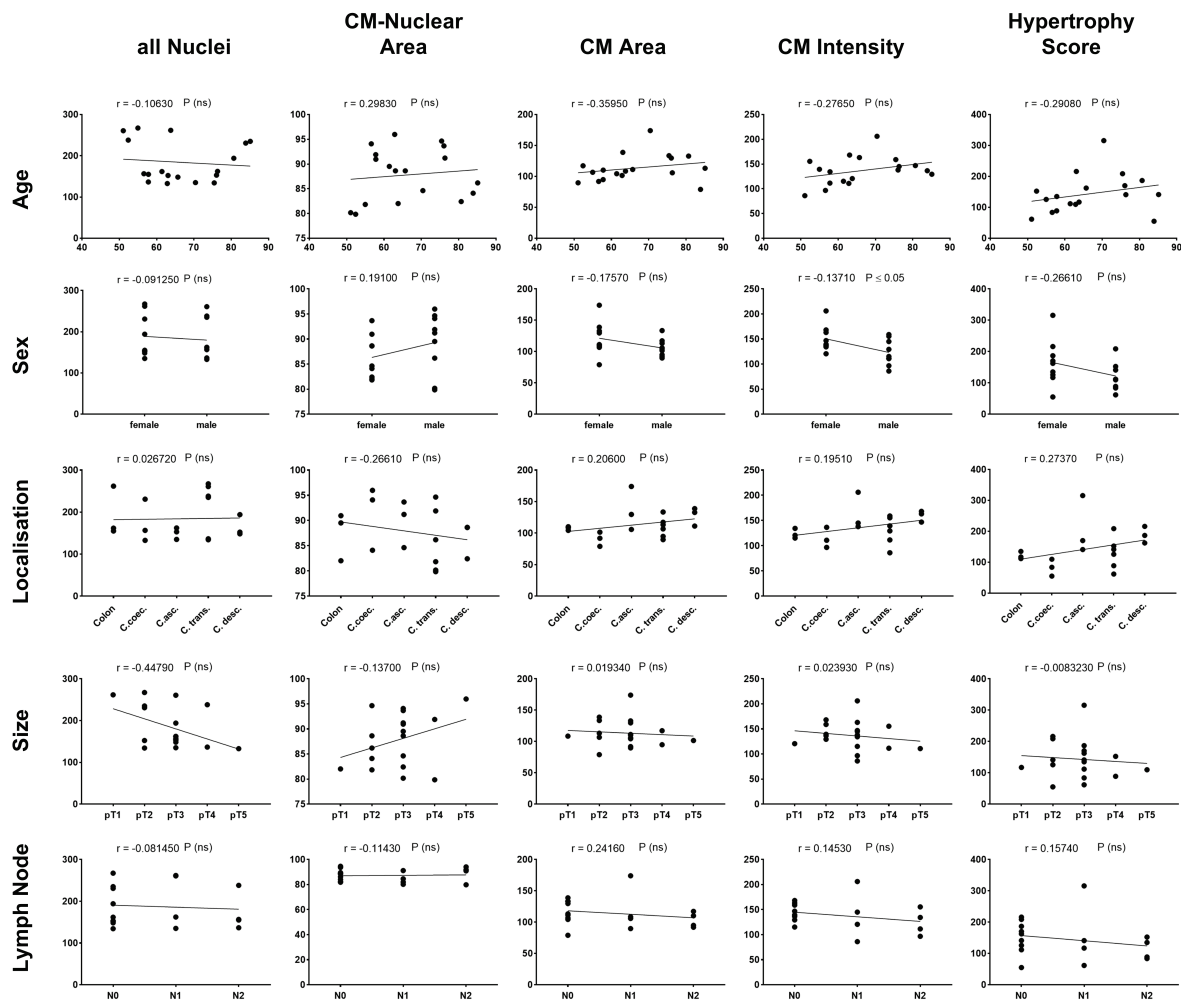


**Figure 37: Correlation for serum concentration of 0.5%.** Correlations plots for patients' data to morphological changes. Purified cardiomyocytes were treated with 0.5% patients' blood serum for four days. Pearson correlation coefficients (r) and p-values were calculated for each correlation. (Mean, two-tailed test: \*  $p \leq 0.05$ , \*\*  $p \leq 0.01$ , \*\*\*  $p \leq 0.001$ , \*\*\*\*  $p \leq 0.0001$ )

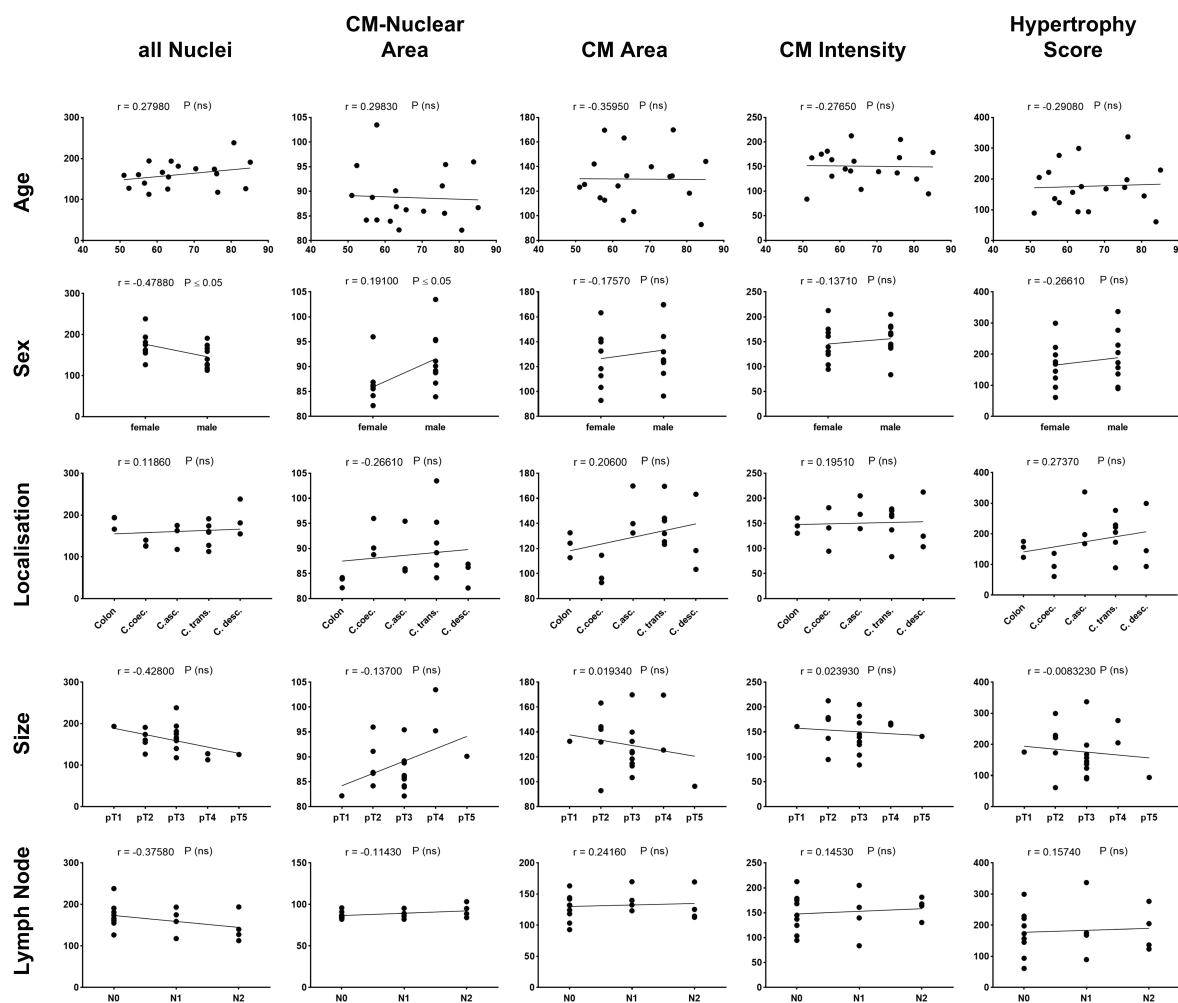


**Figure 38: Correlation for serum concentration of 1%.** Correlations plots for patients' data to morphological changes. Purified cardiomyocytes were treated with 1% patients' blood serum for four days. Pearson correlation coefficients (r) and p-values were calculated for each correlation. (Mean, two-tailed test: \*  $p \leq 0.05$ , \*\*  $p \leq 0.01$ , \*\*\*  $p \leq 0.001$ , \*\*\*\*  $p \leq 0.0001$ )



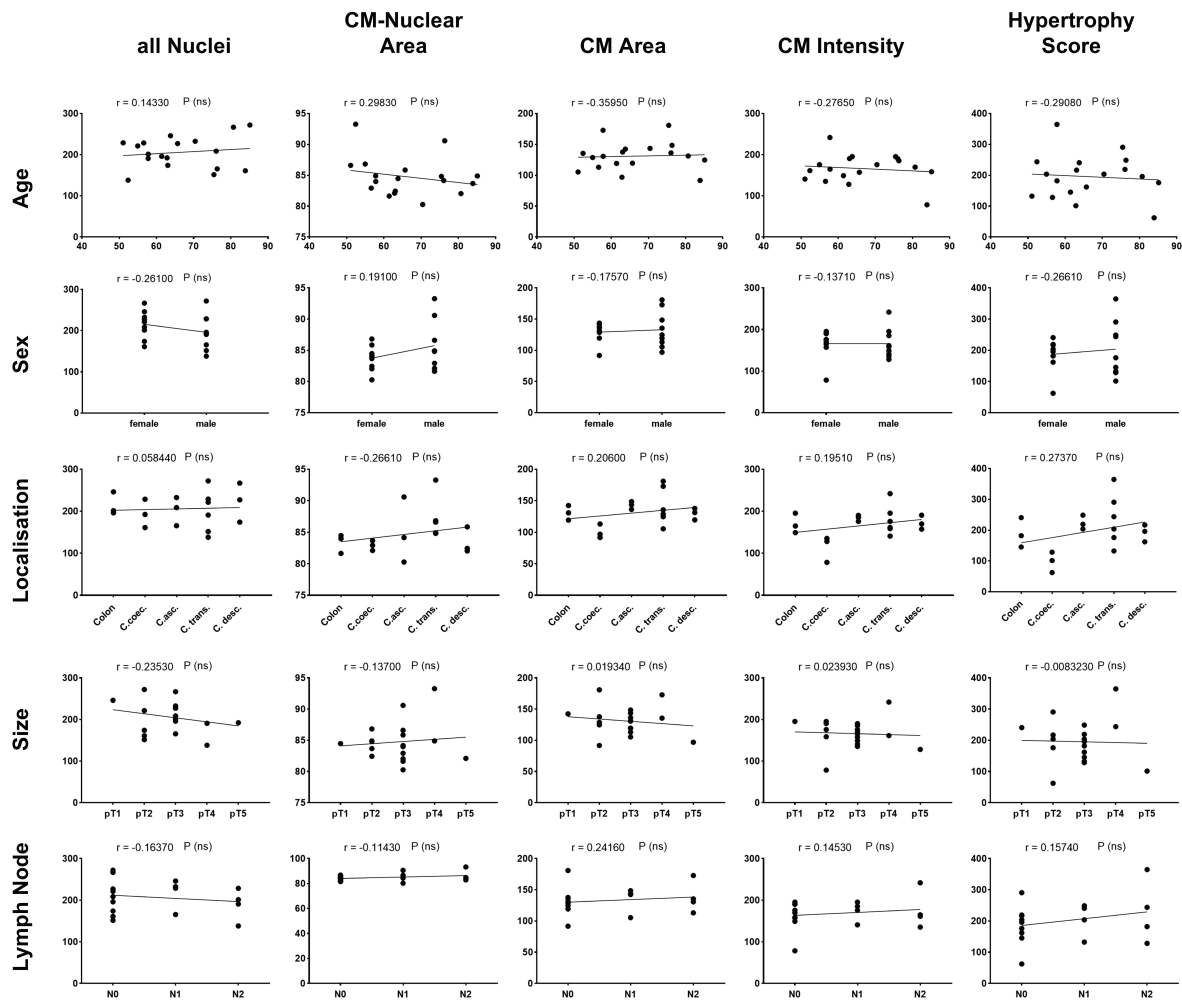


**Figure 39: Correlation for serum concentration of 2%.** Correlations plots for patients' data to morphological changes. Purified cardiomyocytes were treated with 2% patients' blood serum for four days. Pearson correlation coefficients (r) and p-values were calculated for each correlation. (Mean, two-tailed test: \*  $p \leq 0.05$ , \*\*  $p \leq 0.01$ , \*\*\*  $p \leq 0.001$ , \*\*\*\*  $p \leq 0.0001$ )

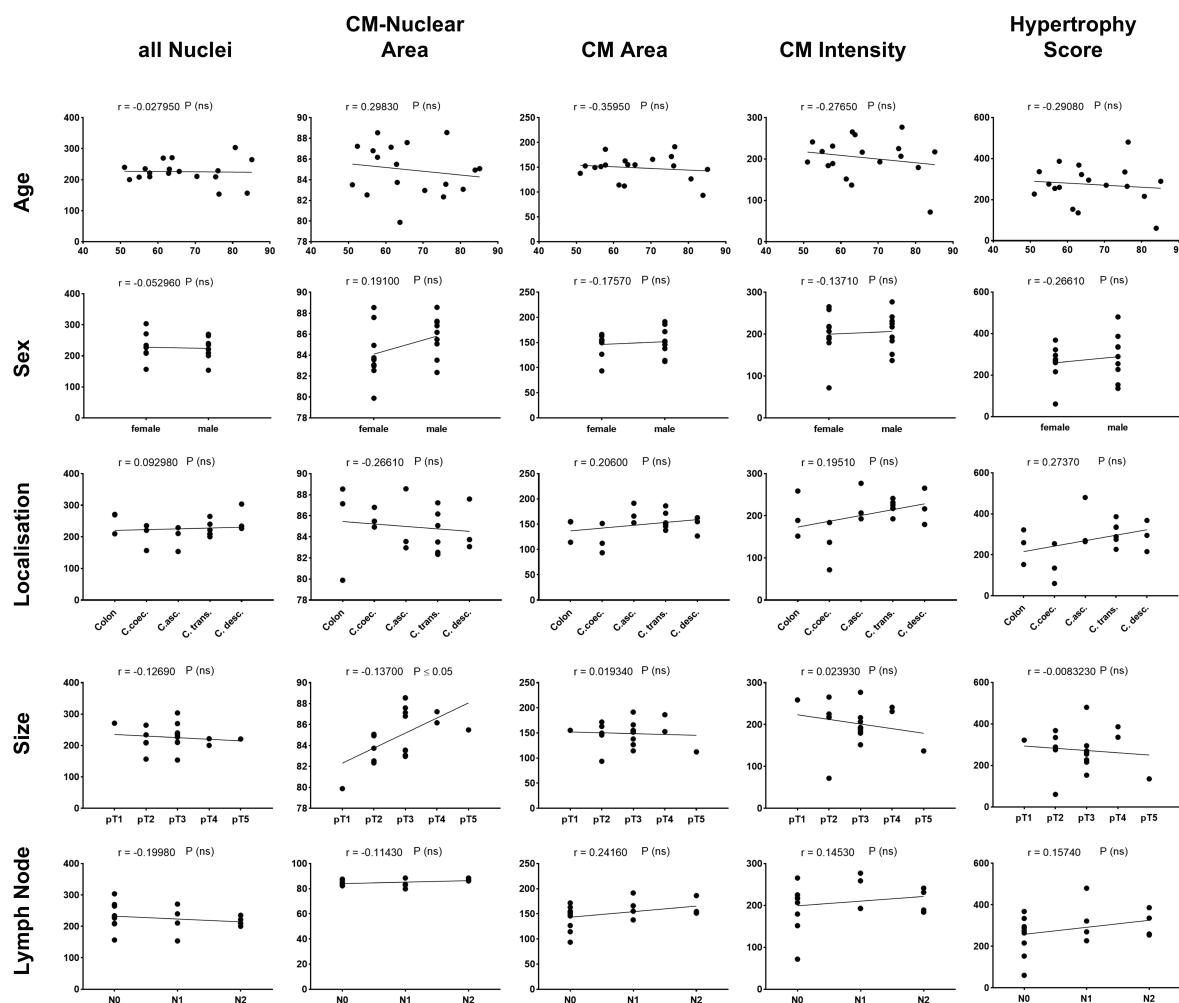


**Figure 40: Correlation for serum concentration of 5%.** Correlations plots for patients' data to morphological changes. Purified cardiomyocytes were treated with 5% patients' blood serum for four days. Pearson correlation coefficients (r) and p-values were calculated for each correlation. (Mean, two-tailed test: \*  $p \leq 0.05$ , \*\*  $p \leq 0.01$ , \*\*\*  $p \leq 0.001$ , \*\*\*\*  $p \leq 0.0001$ )



## 8. References

- [1] Townsend, N.; Kazakiewicz, D.; Lucy Wright, F.; Timmis, A.; Huculeci, R.; Torbica, A.; Gale, C. P.; Achenbach, S.; Weidinger, F.; Vardas, P.: Epidemiology of cardiovascular disease in Europe; *Nat Rev Cardiol.* **2022** *19* (2) 133–143.
- [2] Martin, T. G.; Juarros, M. A.; Leinwand, L. A.: Regression of cardiac hypertrophy in health and disease: mechanisms and therapeutic potential; *Nat Rev Cardiol.* **2023** *20* (5) 347–363.
- [3] Timmis, A.; Aboyans, V.; Vardas, P.; Townsend, N.; Torbica, A.; Kavousi, M.; Boriani, G.; Huculeci, R.; Kazakiewicz, D.; Scherr, D.; Karagiannis, E.; Cvijic, M.; Kapłon-Cieślicka, A.; Ignatiuk, B.; Raatikainen, P.; Smedt, D. de; Wood, A.; Dudek, D.; van Belle, E.; Weidinger, F.: European Society of Cardiology: the 2023 atlas of cardiovascular disease statistics; *Eur Heart J.* **2024** *45* (38) 4019–4062.
- [4] Srivastava, D.; Olson, E. N.: A genetic blueprint for cardiac development; *Nature.* **2000** *407* (6801) 221–226.
- [5] Luttun, A.; Carmeliet, P.: De novo vasculogenesis in the heart; *Cardiovasc Res.* **2003** *58* (2) 378–389.
- [6] Maillet, M.; van Berlo, J. H.; Molkentin, J. D.: Molecular basis of physiological heart growth: fundamental concepts and new players; *Nat Rev Mol Cell Biol.* **2013** *14* (1) 38–48.
- [7] Oka, T.; Akazawa, H.; Naito, A. T.; Komuro, I.: Angiogenesis and cardiac hypertrophy: maintenance of cardiac function and causative roles in heart failure; *Circ Res.* **2014** *114* (3) 565–571.
- [8] Nakamura, M.; Sadoshima, J.: Mechanisms of physiological and pathological cardiac hypertrophy; *Nat Rev Cardiol.* **2018** *15* (7) 387–407.
- [9] Caturano, A.; Vetrano, E.; Galiero, R.; Salvatore, T.; Docimo, G.; Epifani, R.; Alfano, M.; Sardù, C.; Marfella, R.; Rinaldi, L.; Sasso, F. C.: Cardiac hypertrophy: from pathophysiological mechanisms to heart failure development; *Rev Cardiovasc Med.* **2022** *23* (5) 165.
- [10] Grossman, W.; Jones, D.; McLaurin, L. P.: Wall stress and patterns of hypertrophy in the human left ventricle; *J Clin Invest.* **1975** *56* (1) 56–64.
- [11] Teekakirikul, P.; Zhu, W.; Huang, H. C.; Fung, E.: Hypertrophic Cardiomyopathy: An Overview of Genetics and Management; *Biomolecules.* **2019** *9* (12) 878.
- [12] Packer, M.: The neurohormonal hypothesis: a theory to explain the mechanism of disease progression in heart failure; *J Am Coll Cardiol.* **1992** *20* (1) 248–254.
- [13] Hartupee, J.; Mann, D. L.: Neurohormonal activation in heart failure with reduced ejection fraction; *Nat Rev Cardiol.* **2017** *14* (1) 30–38.

- [14] Lympelopoulou, A.; Rengo, G.; Koch, W. J.: Adrenergic nervous system in heart failure: pathophysiology and therapy; *Circ Res.* **2013** 113 (6) 739–753.
- [15] Palandri, C.; Santini, L.; Argirò, A.; Margara, F.; Doste, R.; Bueno-Orovio, A.; Olivotto, I.; Coppini, R.: Pharmacological management of hypertrophic cardiomyopathy: from bench to bedside; *Drugs.* **2022** 82 (8) 889–912.
- [16] Colombo, G.; Biering-Sorensen, T.; Ferreira, J. P.; Lombardi, C. M.; Bonelli, A.; Garascia, A.; Metra, M.; Inciardi, R. M.: Cardiac remodelling in the era of the recommended four pillars heart failure medical therapy; *ESC Heart Fail.* **2025** 12 (2) 1029–1044.
- [17] Levine, B.; Kalman, J.; Mayer, L.; Fillit, H. M.; Packer, M.: Elevated circulating levels of tumor necrosis factor in severe chronic heart failure; *N Engl J Med.* **1990** 323 (4) 236–241.
- [18] Mann, D. L.: Innate immunity and the failing heart: the cytokine hypothesis revisited; *Circ Res.* **2015** 116 (7) 1254–1268.
- [19] Hannan, R. D.; Jenkins, A.; Jenkins, A. K.; Brandenburger, Y.: Cardiac hypertrophy: a matter of translation; *Clin Exp Pharmacol Physiol.* **2003** 30 (8) 517–527.
- [20] Taegtmeyer, H.; Sen, S.; Vela, D.: Return to the fetal gene program: a suggested metabolic link to gene expression in the heart; *Ann N Y Acad Sci.* **2010** 1188 191–198.
- [21] Tran, D. H.; Wang, Z. V.: Glucose metabolism in cardiac hypertrophy and heart failure; *J Am Heart Assoc.* **2019** 8 (12) e012673.
- [22] Pandya, K.; Smithies, O.:  $\beta$ -MyHC and cardiac hypertrophy: size does matter; *Circ Res.* **2011** 109 (6) 609–610.
- [23] Chou, C.; Chin, M. T.: Pathogenic Mechanisms of Hypertrophic Cardiomyopathy beyond Sarcomere Dysfunction; *Int J Mol Sci.* **2021** 22 (16) 8933.
- [24] Yoshimura, M.; Yasue, H.; Ogawa, H.: Pathophysiological significance and clinical application of ANP and BNP in patients with heart failure; *Can. J. Physiol. Pharmacol.* **2001** 79 (8) 730–735.
- [25] Camelliti, P.; Borg, T. K.; Kohl, P.: Structural and functional characterisation of cardiac fibroblasts; *Cardiovasc Res.* **2005** 65 (1) 40–51.
- [26] Nicin, L.; Schroeter, S. M.; Glaser, S. F.; Schulze-Brüning, R.; Pham, M.-D.; Hille, S. S.; Yekelchik, M.; Kattih, B.; Abplanalp, W. T.; Tombor, L.; Müller, O. J.; Braun, T.; Meder, B.; Reich, C.; Arsalan, M.; Holubec, T.; Walther, T.; Emrich, F.; Krishnan, J.; Zeiher, A. M.; John, D.; Dimmeler, S.: A human cell atlas of the pressure-induced hypertrophic heart; *Nat Cardiovasc Res.* **2022** 1 (2) 174–185.
- [27] Seferović, P. M.; Vardas, P.; Jankowska, E. A.; Maggioni, A. P.; Timmis, A.; Milinković, I.; Polovina, M.; Gale, C. P.; Lund, L. H.; Lopatin, Y.; Lainscak, M.; Savarese, G.; Huculeci, R.; Kazakiewicz, D.; Coats, A. J.: The Heart Failure Association atlas: heart

- failure epidemiology and management statistics 2019; *Eur J Heart Fail.* **2021** 23 (6) 906–914.
- [28] Arbelo, E.; Protonotarios, A.; Gimeno, J. R.; Arbustini, E.; Barriales-Villa, R.; Basso, C.; Bezzina, C. R.; Biagini, E.; Blom, N. A.; Boer, R. A. de; Winter, T. de; Elliott, P. M.; Flather, M.; Garcia-Pavia, P.; Haugaa, K. H.; Ingles, J.; Jurcut, R. O.; Klaassen, S.; Limongelli, G.; Loeys, B.; Mogensen, J.; Olivotto, I.; Pantazis, A.; Sharma, S.; van Tintelen, J. P.; Ware, J. S.; Kaski, J. P.: 2023 ESC guidelines for the management of cardiomyopathies; *Eur Heart J.* **2023** 44 (37) 3503–3626.
- [29] Lueder, T. G. von; Sangaralingham, S. J.; Wang, B. H.; Kompa, A. R.; Atar, D.; Burnett, J. C.; Krum, H.: Renin-angiotensin blockade combined with natriuretic peptide system augmentation: novel therapeutic concepts to combat heart failure; *Circ Heart Fail.* **2013** 6 (3) 594–605.
- [30] McDonagh, T. A.; Metra, M.; Adamo, M.; Gardner, R. S.; Baumbach, A.; Böhm, M.; Burri, H.; Butler, J.; Čelutkienė, J.; Chioncel, O.; Cleland, J. G.; Coats, A. J.; Crespo-Leiro, M. G.; Farmakis, D.; Gilard, M.; Heymans, S.; Hoes, A. W.; Jaarsma, T.; Jankowska, E. A.; Lainscak, M.; Lam, C. S.; Lyon, A. R.; McMurray, J. J.; Mebazaa, A.; Mindham, R.; Muneretto, C.; Francesco Piepoli, M.; Price, S.; Rosano, G. M.; Ruschitzka, F.; Kathrine Skibelund, A.: 2021 ESC guidelines for the diagnosis and treatment of acute and chronic heart failure; *Eur Heart J.* **2021** 42 (36) 3599–3726.
- [31] Fak, A. S.; Okucu, M.; Tezcan, H.; Bodur, G.; Oktay, A.: The effects of amlodipine on left ventricular mass and diastolic function in concentric and eccentric left ventricular hypertrophy; *J Cardiovasc Pharmacol Ther.* **1996** 1 (2) 95–100.
- [32] Cuspidi, C.; Meani, S.; Valerio, C.; Fusi, V.; Sala, C.; Maisaidi, M.; Zanchetti, A.: Effects of angiotensin II receptor blockade-based therapy with losartan on left ventricular hypertrophy and geometry in previously treated hypertensive patients; *Blood Press.* **2006** 15 (2) 107–115.
- [33] Jiang, Y.; Liu, P.; Qiu, Z.; Zhou, M.; Cheng, M.; Yang, T.: The U.S. FDA approved cardiovascular drugs from 2011 to 2023: A medicinal chemistry perspective; *Eur J Med Chem.* **2024** 275 116593.
- [34] Mullard, A.: 2023 FDA approvals; *Nat Rev Drug Discov.* **2024** 23 (2) 88–95.
- [35] McClellan, M.; Brown, N.; Califf, R. M.; Warner, J. J.: Call to action: urgent challenges in cardiovascular disease: a presidential advisory from the American Heart Association; *Circulation.* **2019** 139 (9) e44–e54.
- [36] Ghadermarzi, S.; Li, X.; Li, M.; Kurgan, L.: Sequence-served markers of drug targets and potentially druggable human proteins; *Front Genet.* **2019** 10 (1) 1075.

- [37] Xie, X.; Yu, T.; Li, X.; Zhang, N.; Foster, L. J.; Peng, C.; Huang, W.; He, G.: Recent advances in targeting the "undruggable" proteins: from drug discovery to clinical trials; *Signal Transduct Target Ther.* **2023** 8 (1) 335.
- [38] Sliwoski, G.; Kothiwale, S.; Meiler, J.; Lowe, E. W.: Computational methods in drug discovery; *Pharmacol Rev.* **2014** 66 (1) 334–395.
- [39] Swinney, D. C.: Phenotypic vs. target-based drug discovery for first-in-class medicines; *Clin Pharmacol Ther.* **2013** 93 (4) 299–301.
- [40] Swinney, D. C.; Anthony, J.: How were new medicines discovered?; *Nat Rev Drug Discov.* **2011** 10 (7) 507–519.
- [41] Sadri, A.: Is target-based drug discovery efficient? Discovery and "off-target" mechanisms of all drugs; *J Med Chem.* **2023** 66 (18) 12651–12677.
- [42] Vincent, F.; Nueda, A.; Lee, J.; Schenone, M.; Prunotto, M.; Mercola, M.: Phenotypic drug discovery: recent successes, lessons learned and new directions; *Nat Rev Drug Discov.* **2022** 21 (12) 899–914.
- [43] Vincent, F.; Loria, P. M.; Weston, A. D.; Stepan, C. M.; Doyonnas, R.; Wang, Y.-M.; Rockwell, K. L.; Peakman, M.-C.: Hit triage and validation in phenotypic screening: considerations and strategies; *Cell Chem Biol.* **2020** 27 (11) 1332–1346.
- [44] Moffat, J. G.; Rudolph, J.; Bailey, D.: Phenotypic screening in cancer drug discovery - past, present and future; *Nat Rev Drug Discov.* **2014** 13 (8) 588–602.
- [45] Swinney, D. C.; Lee, J. A.: Recent advances in phenotypic drug discovery; *F1000Res.* **2020** 9 944.
- [46] Sinha, S.; Vohora, D.: Pharmaceutical medicine and translational clinical research; *Elsevier/Academic Press*. London **2018**.
- [47] Yamaguchi, S.; Kaneko, M.; Narukawa, M.: Approval success rates of drug candidates based on target, action, modality, application, and their combinations; *Clin Transl Sci.* **2021** 14 (3) 1113–1122.
- [48] Zuppinger, C.: 3D cardiac cell culture: a critical review of current technologies and applications; *Front Cardiovasc Med.* **2019** 6 87.
- [49] Savoji, H.; Mohammadi, M. H.; Rafatian, N.; Toroghi, M. K.; Wang, E. Y.; Zhao, Y.; Korolj, A.; Ahadian, S.; Radisic, M.: Cardiovascular disease models: a game changing paradigm in drug discovery and screening; *Biomaterials.* **2019** 198 3–26.
- [50] Janssen, P. M.; Elnakish, M. T.: Modeling heart failure in animal models for novel drug discovery and development; *Expert Opin Drug Discov.* **2019** 14 (4) 355–363.
- [51] Rockman, H. A.; Ross, R. S.; Harris, A. N.; Knowlton, K. U.; Steinhilber, M. E.; Field, L. J.; Ross, J.; Chien, K. R.: Segregation of atrial-specific and inducible expression of an atrial natriuretic factor transgene in an *in vivo* murine model of cardiac hypertrophy; *Proc Natl Acad Sci U S A.* **1991** 88 (18) 8277–8281.

- [52] Lindpaintner, K.; Kreutz, R.; Ganten, D.: Genetic variation in hypertensive and 'control' strains. What are we controlling for anyway?; *Hypertension*. **1992** 19 (5) 428–430.
- [53] Doggrell, S. A.; Brown, L.: Rat models of hypertension, cardiac hypertrophy and failure; *Cardiovasc Res*. **1998** 39 (1) 89–105.
- [54] Garg, P.; Assadi, H.; Jones, R.; Chan, W. B.; Metherall, P.; Thomas, R.; van der Geest, R.; Swift, A. J.; Al-Mohammad, A.: Left ventricular fibrosis and hypertrophy are associated with mortality in heart failure with preserved ejection fraction; *Sci Rep*. **2021** 11 (1) 617.
- [55] Sergeeva, I. A.; Christoffels, V. M.: Regulation of expression of atrial and brain natriuretic peptide, biomarkers for heart development and disease; *Biochim Biophys Acta*. **2013** 1832 (12) 2403–2413.
- [56] Rinwa, P.; Eriksson, M.; Cotgreave, I.; Bäckberg, M.: 3R-Refinement principles: elevating rodent well-being and research quality; *Lab Anim Res*. **2024** 40 (1) 11.
- [57] Bourque, K.; Hawey, C.; Jones-Tabah, J.; Pétrin, D.; Martin, R. D.; Ling Sun, Y.; Hébert, T. E.: Measuring hypertrophy in neonatal rat primary cardiomyocytes and human iPSC-derived cardiomyocytes; *Methods*. **2022** 203 447–464.
- [58] Onódi, Z.; Visnovitz, T.; Kiss, B.; Hambalkó, S.; Koncz, A.; Ágg, B.; Váradi, B.; Tóth, V. É.; Nagy, R. N.; Gergely, T. G.; Gergő, D.; Makkos, A.; Pelyhe, C.; Varga, N.; Reé, D.; Apáti, Á.; Leszek, P.; Kovács, T.; Nagy, N.; Ferdinandy, P.; Buzás, E. I.; Görbe, A.; Giricz, Z.; Varga, Z. V.: Systematic transcriptomic and phenotypic characterization of human and murine cardiac myocyte cell lines and primary cardiomyocytes reveals serious limitations and low resemblances to adult cardiac phenotype; *J Mol Cell Cardiol*. **2022** 165 19–30.
- [59] HARARY, I.; FARLEY, B.: *In vitro* studies of single isolated beating heart cells; *Science*. **1960** 131 (3414) 1674–1675.
- [60] Simpson, P.; McGrath, A.; Savion, S.: Myocyte hypertrophy in neonatal rat heart cultures and its regulation by serum and by catecholamines; *Circ Res*. **1982** 51 (6) 787–801.
- [61] Blondel, B.; Roijen, I.; Cheneval, J. P.: Heart cells in culture: a simple method for increasing the proportion of myoblasts; *Experientia*. **1971** 27 (3) 356–358.
- [62] Yang, D.; Xi, J.; Xing, Y.; Tang, X.; Dai, X.; Li, K.; Li, H.; Lv, X.; Lu, D.; Wang, H.: A new method for neonatal rat ventricular myocyte purification using superparamagnetic iron oxide particles; *Int J Cardiol*. **2018** 270 293–301.
- [63] LaFramboise, W. A.; Scalise, D.; Stoodley, P.; Graner, S. R.; Guthrie, R. D.; Magovern, J. A.; Becich, M. J.: Cardiac fibroblasts influence cardiomyocyte phenotype *in vitro*; *Am J Physiol Cell Physiol*. **2007** 292 (5) C1799-808.
- [64] Cartledge, J. E.; Kane, C.; Dias, P.; Tesfom, M.; Clarke, L.; Mckee, B.; Al Ayoubi, S.; Chester, A.; Yacoub, M. H.; Camelliti, P.; Terracciano, C. M.: Functional crosstalk



- between cardiac fibroblasts and adult cardiomyocytes by soluble mediators; *Cardiovasc Res.* **2015** 105 (3) 260–270.
- [65] Xing-Fei Deng, D. Gregg Rokosh, Paul C. Simpson: Autonomous and growth factor–induced hypertrophy in cultured neonatal mouse cardiac myocytes; *Circ Res.* **2000** 87 (9) 781–788.
- [66] Kijima, K.; Matsubara, H.; Murasawa, S.; Maruyama, K.; Mori, Y.; Ohkubo, N.; Komuro, I.; Yazaki, Y.; Iwasaka, T.; Inada, M.: Mechanical stretch induces enhanced expression of angiotensin II receptor subtypes in neonatal rat cardiac myocytes; *Circ Res.* **1996** 79 (4) 887–897.
- [67] Furkel, J.; Knoll, M.; Din, S.; Bogert, N. V.; Seeger, T.; Frey, N.; Abdollahi, A.; Katus, H. A.; Konstandin, M. H.: C-MORE: a high-content single-cell morphology recognition methodology for liquid biopsies toward personalized cardiovascular medicine; *Cell Rep Med.* **2021** 2 (11) 100436.
- [68] Komuro, J.; Tokuoka, Y.; Seki, T.; Kusumoto, D.; Hashimoto, H.; Katsuki, T.; Nakamura, T.; Akiba, Y.; Kuoka, T.; Kimura, M.; Yamada, T.; Fukuda, K.; Funahashi, A.; Yuasa, S.: Development of non-bias phenotypic drug screening for cardiomyocyte hypertrophy by image segmentation using deep learning; *Biochem Biophys Res Commun.* **2022** 632 181–188.
- [69] Goncalves, G. K.; Scalzo, S.; Alves, A. P.; Agero, U.; Guatimosim, S.; Reis, A. M.: Neonatal cardiomyocyte hypertrophy induced by endothelin-1 is blocked by estradiol acting on GPER; *Am J Physiol Cell Physiol.* **2018** 314 (3) C310–C322.
- [70] Zhang, C.; Shan, X.-L.; Liao, Y.-L.; Zhao, P.; Guo, W.; Wei, H.-C.; Lu, R.: Effects of stachydrine on norepinephrine-induced neonatal rat cardiac myocytes hypertrophy and intracellular calcium transients; *BMC Complement Altern Med.* **2014** 14 474.
- [71] Jentzsch, C.; Leierseder, S.; Loyer, X.; Flohrschütz, I.; Sassi, Y.; Hartmann, D.; Thum, T.; Laggerbauer, B.; Engelhardt, S.: A phenotypic screen to identify hypertrophy-modulating microRNAs in primary cardiomyocytes; *J Mol Cell Cardiol.* **2012** 52 (1) 13–20.
- [72] Musunuru, K.; Sheikh, F.; Gupta, R. M.; Houser, S. R.; Maher, K. O.; Milan, D. J.; Terzic, A.; Wu, J. C.: Induced pluripotent stem cells for cardiovascular disease modeling and precision medicine: a scientific statement from the American Heart Association; *Circ Genom Precis Med.* **2018** 11 (1) e000043.
- [73] Eder, A.; Vollert, I.; Hansen, A.; Eschenhagen, T.: Human engineered heart tissue as a model system for drug testing; *Adv Drug Deliv Rev.* **2016** 96 214–224.
- [74] Hansen, A.; Eder, A.; Bönstrup, M.; Flato, M.; Mewe, M.; Schaaf, S.; Aksehirlioglu, B.; Schwoerer, A. P.; Uebeler, J.; Eschenhagen, T.: Development of a drug screening platform based on engineered heart tissue; *Circ Res.* **2010** 107 (1) 35–44.

- [75] Schmidt, C.; Deyett, A.; Ilmer, T.; Haendeler, S.; Torres Caballero, A.; Novatchkova, M.; Netzer, M. A.; Ceci Ginistrelli, L.; Mancheno Juncosa, E.; Bhattacharya, T.; Mujadzic, A.; Pimpale, L.; Jahnel, S. M.; Cirigliano, M.; Reumann, D.; Tavernini, K.; Papai, N.; Hering, S.; Hofbauer, P.; Mendjan, S.: Multi-chamber cardioids unravel human heart development and cardiac defects; *Cell*. **2023** *186* (25) 5587-5605.e27.
- [76] Iwaki, K.; Sukhatme, V. P.; Shubeita, H. E.; Chien, K. R.: Alpha- and beta-adrenergic stimulation induces distinct patterns of immediate early gene expression in neonatal rat myocardial cells. fos/jun expression is associated with sarcomere assembly; Egr-1 induction is primarily an alpha 1-mediated response; *Journal of Biological Chemistry*. **1990** *265* (23) 13809–13817.
- [77] Yoshikawa, S.; Nagao, M.; Toh, R.; Shinohara, M.; Iino, T.; Irino, Y.; Nishimori, M.; Tanaka, H.; Satomi-Kobayashi, S.; Ishida, T.; Hirata, K.-I.: Inhibition of glutaminase 1-mediated glutaminolysis improves pathological cardiac remodeling; *Am J Physiol Heart Circ Physiol*. **2022** *322* (5) H749-H761.
- [78] Yuan, L.; Qiu, L.; Ye, Y.; Wu, J.; Wang, S.; Wang, X.; Zhou, N.; Zou, Y.: Heat-shock transcription factor 1 is critically involved in the ischaemia-induced cardiac hypertrophy via JAK2/STAT3 pathway; *J Cell Mol Med*. **2018** *22* (9) 4292–4303.
- [79] Liu, Y.; Shen, H.-J.; Wang, X.-Q.-Y.; Liu, H.-Q.; Zheng, L.-Y.; Luo, J.-D.: EndophilinA2 protects against angiotensin II-induced cardiac hypertrophy by inhibiting angiotensin II type 1 receptor trafficking in neonatal rat cardiomyocytes; *J Cell Biochem*. **2018** *119* (10) 8290–8303.
- [80] Pierce, K. L.; Lefkowitz, R. J.: Classical and new roles of beta-arrestins in the regulation of G-protein-coupled receptors; *Nat Rev Neurosci*. **2001** *2* (10) 727–733.
- [81] Gold, J. I.; Martini, J. S.; Hullmann, J.; Gao, E.; Chuprun, J. K.; Lee, L.; Tilley, D. G.; Rabinowitz, J. E.; Bossuyt, J.; Bers, D. M.; Koch, W. J.: Nuclear translocation of cardiac G protein-coupled receptor kinase 5 downstream of select Gq-activating hypertrophic ligands is a calmodulin-dependent process; *PLoS One*. **2013** *8* (3) e57324.
- [82] Lieu, M.; Koch, W. J.: GRK2 and GRK5 as therapeutic targets and their role in maladaptive and pathological cardiac hypertrophy; *Expert Opin Ther Targets*. **2019** *23* (3) 201–214.
- [83] Dzimir, N.; Muiya, P.; Andres, E.; Al-Halees, Z.: Differential functional expression of human myocardial G protein receptor kinases in left ventricular cardiac diseases; *Eur J Pharmacol*. **2004** *489* (3) 167–177.
- [84] Lymperopoulos, A.; Rengo, G.; Koch, W. J.: Adrenal adrenoceptors in heart failure: fine-tuning cardiac stimulation; *Trends Mol Med*. **2007** *13* (12) 503–511.

- [85] Gold, J. I.; Gao, E.; Shang, X.; Premont, R. T.; Koch, W. J.: Determining the absolute requirement of G protein-coupled receptor kinase 5 for pathological cardiac hypertrophy; *Circ Res.* **2012** *111* (8) 1048–1053.
- [86] Müller, O. J.; Heckmann, M. B.; Ding, L.; Rapti, K.; Rangrez, A. Y.; Gerken, T.; Christiansen, N.; Rennefahrt, U. E.; Witt, H.; González Maldonado, S.; Ternes, P.; Schwab, D. M.; Ruf, T.; Hille, S.; Remes, A.; Jungmann, A.; Weis, T. M.; Kreußer, J. S.; Gröne, H.-J.; Backs, J.; Schatz, P.; Katus, H. A.; Frey, N.: Comprehensive plasma and tissue profiling reveals systemic metabolic alterations in cardiac hypertrophy and failure; *Cardiovasc Res.* **2019** *115* (8) 1296–1305.
- [87] Shelar, S.; Shim, E.-H.; Brinkley, G. J.; Kundu, A.; Carobbio, F.; Poston, T.; Tan, J.; Parekh, V.; Benson, D.; Crossman, D. K.; Buckhaults, P. J.; Rakheja, D.; Kirkman, R.; Sato, Y.; Ogawa, S.; Dutta, S.; Velu, S. E.; Emberley, E.; Pan, A.; Chen, J.; Huang, T.; Absher, D.; Becker, A.; Kunick, C.; Sudarshan, S.: Biochemical and epigenetic insights into L-2-hydroxyglutarate, a potential therapeutic target in renal cancer; *Clin Cancer Res.* **2018** *24* (24) 6433–6446.
- [88] Rubio, D. M.; Schoenbaum, E. E.; Lee, L. S.; Schteingart, D. E.; Marantz, P. R.; Anderson, K. E.; Platt, L. D.; Baez, A.; Esposito, K.: Defining translational research: implications for training; *Academic medicine: journal of the Association of American Medical Colleges.* **2010** *85* (3) 470–475.
- [89] Brown, J. C.; Caan, B. J.; Prado, C. M.; Weltzien, E.; Xiao, J.; Cespedes Feliciano, E. M.; Kroenke, C. H.; Meyerhardt, J. A.: Body composition and cardiovascular events in patients with colorectal cancer: a population-based retrospective cohort study; *JAMA Oncol.* **2019** *5* (7) 967–972.
- [90] Cuthbert, C. A.; Hemmelgarn, B. R.; Xu, Y.; Cheung, W. Y.: The effect of comorbidities on outcomes in colorectal cancer survivors: a population-based cohort study; *J Cancer Surviv.* **2018** *12* (6) 733–743.
- [91] Carrillo García, C.; Becker, C.; Forster, M.; Lohmann, S.; Freitag, P.; Laufer, S.; Sievers, S.; Fleischmann, B. K.; Hesse, M.; Schade, D.: High-throughput screening platform in postnatal heart cells and chemical probe toolbox to assess cardiomyocyte proliferation; *J Med Chem.* **2022** *65* (2) 1505–1524.
- [92] Schlegel, P.; Reinkober, J.; Meinhardt, E.; Tscheschner, H.; Gao, E.; Schumacher, S. M.; Yuan, A.; Backs, J.; Most, P.; Wieland, T.; Koch, W. J.; Katus, H. A.; Raake, P. W.: G protein-coupled receptor kinase 2 promotes cardiac hypertrophy; *PLoS One.* **2017** *12* (7) e0182110.
- [93] Laemmli, U. K.: Cleavage of structural proteins during the assembly of the head of bacteriophage T4; *Nature.* **1970** *227* (5259) 680–685.

- [94] Ladner, C. L.; Yang, J.; Turner, R. J.; Edwards, R. A.: Visible fluorescent detection of proteins in polyacrylamide gels without staining; *Anal Biochem.* **2004** 326 (1) 13–20.
- [95] Pfaffl, M. W.: A new mathematical model for relative quantification in real-time RT-PCR; *Nucleic Acids Res.* **2001** 29 (9) e45.
- [96] Carpenter, A. E.; Jones, T. R.; Lamprecht, M. R.; Clarke, C.; Kang, I. H.; Friman, O.; Guertin, D. A.; Chang, J. H.; Lindquist, R. A.; Moffat, J.; Golland, P.; Sabatini, D. M.: CellProfiler: image analysis software for identifying and quantifying cell phenotypes; *Genome Biol.* **2006** 7 (10) R100.
- [97] Logan, D. J.; Shan, J.; Bhatia, S. N.; Carpenter, A. E.: Quantifying co-cultured cell phenotypes in high-throughput using pixel-based classification; *Methods.* **2016** 96 6–11.
- [98] Stirling, D. R.; Swain-Bowden, M. J.; Lucas, A. M.; Carpenter, A. E.; Cimini, B. A.; Goodman, A.: CellProfiler 4: improvements in speed, utility and usability; *BMC Bioinformatics.* **2021** 22 (1) 433.
- [99] Chahine, M. N.; Mioulane, M.; Sikkil, M. B.; O’Gara, P.; Dos Remedios, C. G.; Pierce, G. N.; Lyon, A. R.; Földes, G.; Harding, S. E.: Nuclear pore rearrangements and nuclear trafficking in cardiomyocytes from rat and human failing hearts; *Cardiovasc Res.* **2015** 105 (1) 31–43.
- [100] Barki-Harrington, L.; Perrino, C.; Rockman, H. A.: Network integration of the adrenergic system in cardiac hypertrophy; *Cardiovasc Res.* **2004** 63 (3) 391–402.
- [101] Matsui, H.; Fujio, Y.; Kunisada, K.; Hirota, H.; Yamauchi-Takahara, K.: Leukemia inhibitory factor induces a hypertrophic response mediated by gp130 in murine cardiac myocytes; *Res Commun Mol Pathol Pharmacol.* **1996** 93 (2) 149–162.
- [102] Kodama, H.; Fukuda, K.; Pan, J.; Makino, S.; Baba, A.; Hori, S.; Ogawa, S.: Leukemia inhibitory factor, a potent cardiac hypertrophic cytokine, activates the JAK/STAT pathway in rat cardiomyocytes; *Circ Res.* **1997** 81 (5) 656–663.
- [103] Wagner, M. A.; Siddiqui, M. A.: The JAK-STAT pathway in hypertrophic stress signaling and genomic stress response; *JAKSTAT.* **2012** 1 (2) 131–141.
- [104] Murata, M.; Fukuda, K.; Ishida, H.; Miyoshi, S.; Koura, T.; Kodama, H.; Nakazawa, H. K.; Ogawa, S.: Leukemia inhibitory factor, a potent cardiac hypertrophic cytokine, enhances L-type Ca<sup>2+</sup> current and Ca<sup>2+</sup>i transient in cardiomyocytes; *J Mol Cell Cardiol.* **1999** 31 (1) 237–245.
- [105] Hirano, T.: IL-6 in inflammation, autoimmunity and cancer; *Int Immunol.* **2021** 33 (3) 127–148.
- [106] Remes, A.; Wagner, A. H.; Schmiedel, N.; Heckmann, M.; Ruf, T.; Ding, L.; Jungmann, A.; Senger, F.; Katus, H. A.; Ullrich, N. D.; Frey, N.; Hecker, M.; Müller, O. J.: AAV-mediated expression of NFAT decoy oligonucleotides protects from cardiac hypertrophy and heart failure; *Basic Res Cardiol.* **2021** 116 (1) 38.

- [107] Gunnes, G.; Valheim, M.; Press, C. M.; Tverdal, A.; Storset, A.: Comparison of flow cytometry and image morphometry in the quantitative analysis of cell population markers in the lymph node of sheep; *Vet Immunol Immunopathol.* **2003** *94* (3-4) 177–183.
- [108] Tromans-Coia, C.; Jamali, N.; Abbasi, H. S.; Giuliano, K. A.; Hagimoto, M.; Jan, K.; Kaneko, E.; Letzsch, S.; Schreiner, A.; Sexton, J. Z.; Suzuki, M.; Trask, O. J.; Yamaguchi, M.; Yanagawa, F.; Yang, M.; Carpenter, A. E.; Cimini, B. A.: Assessing the performance of the Cell Painting assay across different imaging systems; *Cytometry A.* **2023** *103* (11) 915–926.
- [109] Celik, S.; Sadegh, M. K.; Morley, M.; Roselli, C.; Ellinor, P. T.; Cappola, T.; Smith, J. G.; Gidlöf, O.: Antisense regulation of atrial natriuretic peptide expression; *JCI Insight.* **2019** *4* (19) e130978.
- [110] Man, J.; Barnett, P.; Christoffels, V. M.: Structure and function of the Nppa-Nppb cluster locus during heart development and disease; *Cell Mol Life Sci.* **2018** *75* (8) 1435–1444.
- [111] Nguyen, P. D.; Hsiao, S. T.; Sivakumaran, P.; Lim, S. Y.; Dilley, R. J.: Enrichment of neonatal rat cardiomyocytes in primary culture facilitates long-term maintenance of contractility *in vitro*; *Am J Physiol Cell Physiol.* **2012** *303* (12) C1220-8.
- [112] Sato, P. Y.; Chuprun, J. K.; Schwartz, M.; Koch, W. J.: The evolving impact of g protein-coupled receptor kinases in cardiac health and disease; *Physiol Rev.* **2015** *95* (2) 377–404.
- [113] Wang, J.; Gareri, C.; Rockman, H. A.: G-Protein-coupled receptors in heart disease; *Circ Res.* **2018** *123* (6) 716–735.
- [114] Obrenovich, M. E.; Palacios, H. H.; Gasimov, E.; Leszek, J.; Aliev, G.: The GRK2 overexpression is a primary hallmark of mitochondrial lesions during early Alzheimer disease; *Cardiovasc Psychiatry Neurol.* **2009** *2009* 327360.
- [115] Bychkov, E. R.; Gurevich, V. V.; Joyce, J. N.; Benovic, J. L.; Gurevich, E. V.: Arrestins and two receptor kinases are upregulated in Parkinson's disease with dementia; *Neurobiol Aging.* **2008** *29* (3) 379–396.
- [116] Kim, J. I.; Chakraborty, P.; Wang, Z.; Daaka, Y.: G-protein coupled receptor kinase 5 regulates prostate tumor growth; *J Urol.* **2012** *187* (1) 322–329.
- [117] Chakraborty, P. K.; Zhang, Y.; Coomes, A. S.; Kim, W.-J.; Stupay, R.; Lynch, L. D.; Atkinson, T.; Kim, J. I.; Nie, Z.; Daaka, Y.: G protein-coupled receptor kinase GRK5 phosphorylates moesin and regulates metastasis in prostate cancer; *Cancer Res.* **2014** *74* (13) 3489–3500.
- [118] Jiang, L.-P.; Fan, S.-Q.; Xiong, Q.-X.; Zhou, Y.-C.; Yang, Z.-Z.; Li, G.-F.; Huang, Y.-C.; Wu, M.-G.; Shen, Q.-S.; Liu, K.; Yang, C.-P.; Chen, Y.-B.: GRK5 functions as an oncogenic factor in non-small-cell lung cancer; *Cell Death Dis.* **2018** *9* (3) 295.

- [119] Waldschmidt, H. V.; Homan, K. T.; Cruz-Rodríguez, O.; Cato, M. C.; Waninger-Saroni, J.; Larimore, K. M.; Cannavo, A.; Song, J.; Cheung, J. Y.; Kirchhoff, P. D.; Koch, W. J.; Tesmer, J. J.; Larsen, S. D.: Structure-based design, synthesis, and biological evaluation of highly selective and potent G protein-coupled receptor kinase 2 inhibitors; *J Med Chem.* **2016** *59* (8) 3793–3807.
- [120] Rowlands, R. A.; Chen, Q.; Bouley, R. A.; Avramova, L. V.; Tesmer, J. J.; White, A. D.: Generation of highly selective, potent, and covalent G protein-coupled receptor kinase 5 inhibitors; *J Med Chem.* **2021** *64* (1) 566–585.
- [121] Pitcher, J. A.; Freedman, N. J.; Lefkowitz, R. J.: G protein-coupled receptor kinases; *Annu Rev Biochem.* **1998** *67* 653–692.
- [122] Hullmann, J.; Traynham, C. J.; Coleman, R. C.; Koch, W. J.: The expanding GRK interactome: implications in cardiovascular disease and potential for therapeutic development; *Pharmacol Res.* **2016** *110* 52–64.
- [123] Benovic, J. L.; Strasser, R. H.; Caron, M. G.; Lefkowitz, R. J.: Beta-adrenergic receptor kinase: identification of a novel protein kinase that phosphorylates the agonist-occupied form of the receptor; *Proc Natl Acad Sci U S A.* **1986** *83* (9) 2797–2801.
- [124] Benovic, J. L.; Mayor, F.; Staniszewski, C.; Lefkowitz, R. J.; Caron, M. G.: Purification and characterization of the beta-adrenergic receptor kinase; *Journal of Biological Chemistry.* **1987** *262* (19) 9026–9032.
- [125] Koch, W. J.; Rockman, H. A.; Samama, P.; Hamilton, R. A.; Bond, R. A.; Milano, C. A.; Lefkowitz, R. J.: Cardiac function in mice overexpressing the beta-adrenergic receptor kinase or a beta ARK inhibitor; *Science.* **1995** *268* (5215) 1350–1353.
- [126] Premont, R. T.; Koch, W. J.; Inglese, J.; Lefkowitz, R. J.: Identification, purification, and characterization of GRK5, a member of the family of G protein-coupled receptor kinases; *Journal of Biological Chemistry.* **1994** *269* (9) 6832–6841.
- [127] Kunapuli, P.; Benovic, J. L.: Cloning and expression of GRK5: a member of the G protein-coupled receptor kinase family; *Proc Natl Acad Sci U S A.* **1993** *90* (12) 5588–5592.
- [128] Woodall, M. C.; Ciccarelli, M.; Woodall, B. P.; Koch, W. J.: G protein-coupled receptor kinase 2: a link between myocardial contractile function and cardiac metabolism; *Circ Res.* **2014** *114* (10) 1661–1670.
- [129] Fusco, A.; Santulli, G.; Sorriento, D.; Cipolletta, E.; Garbi, C.; Dorn, G. W.; Trimarco, B.; Feliciello, A.; Iaccarino, G.: Mitochondrial localization unveils a novel role for GRK2 in organelle biogenesis; *Cell Signal.* **2012** *24* (2) 468–475.
- [130] Sato, P. Y.; Chuprun, J. K.; Ibeti, J.; Cannavo, A.; Drosatos, K.; Elrod, J. W.; Koch, W. J.: GRK2 compromises cardiomyocyte mitochondrial function by diminishing fatty acid-mediated oxygen consumption and increasing superoxide levels; *J Mol Cell Cardiol.* **2015** *89* (Pt B) 360–364.

- [131] Sorriento, D.; Santulli, G.; Franco, A.; Cipolletta, E.; Napolitano, L.; Gambardella, J.; Gomez-Monterrey, I.; Campiglia, P.; Trimarco, B.; Iaccarino, G.; Ciccarelli, M.: Integrating GRK2 and NFkappaB in the pathophysiology of cardiac hypertrophy; *J Cardiovasc Transl Res.* **2015** 8 (8) 493–502.
- [132] Johnson, L. R.; Scott, M. G.; Pitcher, J. A.: G protein-coupled receptor kinase 5 contains a DNA-binding nuclear localization sequence; *Mol Cell Biol.* **2004** 24 (23) 10169–10179.
- [133] Traynham, C. J.; Hullmann, J.; Koch, W. J.: Canonical and non-canonical actions of GRK5 in the heart; *J Mol Cell Cardiol.* **2016** 92 196–202.
- [134] Martini, J. S.; Raake, P.; Vinge, L. E.; DeGeorge, B. R.; Chuprun, J. K.; Harris, D. M.; Gao, E.; Eckhart, A. D.; Pitcher, J. A.; Koch, W. J.: Uncovering G protein-coupled receptor kinase-5 as a histone deacetylase kinase in the nucleus of cardiomyocytes; *Proc Natl Acad Sci U S A.* **2008** 105 (34) 12457–12462.
- [135] Sorriento, D.; Ciccarelli, M.; Santulli, G.; Campanile, A.; Altobelli, G. G.; Cimini, V.; Galasso, G.; Astone, D.; Piscione, F.; Pastore, L.; Trimarco, B.; Iaccarino, G.: The G-protein-coupled receptor kinase 5 inhibits NFkappaB transcriptional activity by inducing nuclear accumulation of IkappaB alpha; *Proc Natl Acad Sci U S A.* **2008** 105 (46) 17818–17823.
- [136] Hullmann, J. E.; Grisanti, L. A.; Makarewich, C. A.; Gao, E.; Gold, J. I.; Chuprun, J. K.; Tilley, D. G.; Houser, S. R.; Koch, W. J.: GRK5-mediated exacerbation of pathological cardiac hypertrophy involves facilitation of nuclear NFAT activity; *Circ Res.* **2014** 115 (12) 976–985.
- [137] Homan, K. T.; Tesmer, J. J.: Molecular basis for small molecule inhibition of G protein-coupled receptor kinases; *ACS Chem Biol.* **2015** 10 (1) 246–256.
- [138] Thal, D. M.; Homan, K. T.; Chen, J.; Wu, E. K.; Hinkle, P. M.; Huang, Z. M.; Chuprun, J. K.; Song, J.; Gao, E.; Cheung, J. Y.; Sklar, L. A.; Koch, W. J.; Tesmer, J. J.: Paroxetine is a direct inhibitor of g protein-coupled receptor kinase 2 and increases myocardial contractility; *ACS Chem Biol.* **2012** 7 (11) 1830–1839.
- [139] Homan, K. T.; Wu, E.; Wilson, M. W.; Singh, P.; Larsen, S. D.; Tesmer, J. J.: Structural and functional analysis of g protein-coupled receptor kinase inhibition by paroxetine and a rationally designed analog; *Mol Pharmacol.* **2014** 85 (2) 237–248.
- [140] Homan, K. T.; Wu, E.; Cannavo, A.; Koch, W. J.; Tesmer, J. J.: Identification and characterization of amlexanox as a G protein-coupled receptor kinase 5 inhibitor; *Molecules.* **2014** 19 (10) 16937–16949.
- [141] Lee, J. H.; Seo, H. W.; Ryu, J. Y.; Lim, C. J.; Yi, K. Y.; Oh, K.-S.; Lee, B. H.: KR-39038, a novel GRK5 inhibitor, attenuates cardiac hypertrophy and improves cardiac function in heart failure; *Biomol Ther (Seoul).* **2020** 28 (5) 482–489.

- [142] Cho, S. Y.; Lee, B. H.; Jung, H.; Yun, C. S.; Du Ha, J.; Kim, H. R.; Chae, C. H.; Lee, J. H.; Seo, H. W.; Oh, K.-S.: Design and synthesis of novel 3-(benzodioxazol-2-yl)-5-(1-(piperidin-4-yl)-1H-pyrazol-4-yl)pyridin-2-amine derivatives as selective G-protein-coupled receptor kinase-2 and -5 inhibitors; *Bioorg Med Chem Lett.* **2013** 23 (24) 6711–6716.
- [143] Homan, K. T.; Larimore, K. M.; Elkins, J. M.; Szklarz, M.; Knapp, S.; Tesmer, J. J.: Identification and structure-function analysis of subfamily selective G protein-coupled receptor kinase inhibitors; *ACS Chem Biol.* **2015** 10 (1) 310–319.
- [144] Motzer, R. J.; Escudier, B.; Gannon, A.; Figlin, R. A.: Sunitinib: ten years of successful clinical use and study in advanced renal cell carcinoma; *Oncologist.* **2017** 22 (1) 41–52.
- [145] Ghosh, A. K.; Chen, Y.; Gadi, R. K.; Sonawane, A.; Gamage, S. P.; Tesmer, J. G.: Design, synthesis, and X-ray structural studies of a series of highly potent, selective, and drug-like G protein-coupled receptor kinase 5 inhibitors; *Eur J Med Chem.* **2025** 282 117024.
- [146] Xu, G.; Gaul, M. D.; Liu, Z.; DesJarlais, R. L.; Qi, J.; Wang, W.; Krosky, D.; Petrounia, I.; Milligan, C. M.; an Hermans; Lu, H.-R.; Huang, D. Z.; Xu, J. Z.; Spurlino, J. C.: Hit-to-lead optimization and discovery of a potent, and orally bioavailable G protein coupled receptor kinase 2 (GRK2) inhibitor; *Bioorg Med Chem Lett.* **2020** 30 (23) 127602.
- [147] Yeh, S.-T.; Zambrano, C. M.; Koch, W. J.; Purcell, N. H.: PH domain leucine-rich repeat protein phosphatase 2 (PHLPP2) regulates G-protein-coupled receptor kinase 5 (GRK5)-induced cardiac hypertrophy *in vitro*; *J Biol Chem.* **2018** 293 (21) 8056–8064.
- [148] Rowlands, R. A.; Cato, M. C.; Waldschmidt, H. V.; Bouley, R. A.; Chen, Q.; Avramova, L.; Larsen, S. D.; Tesmer, J. J.; White, A. D.: Structure-based design of selective, covalent G protein-coupled receptor kinase 5 inhibitors; *ACS Med Chem Lett.* **2019** 10 (12) 1628–1634.
- [149] Chen, Y.; Sonawane, A.; Manda, R.; Gadi, R. K.; Tesmer, J. J.; Ghosh, A. K.: Development of a new class of potent and highly selective G protein-coupled receptor kinase 5 inhibitors and structural insight from crystal structures of inhibitor complexes; *Eur J Med Chem.* **2024** 264 115931.
- [150] Yang, J.; van Villar, A. M.; Armando, I.; Jose, P. A.; Zeng, C.: G Protein-coupled receptor kinases: crucial regulators of blood pressure; *J Am Heart Assoc.* **2016** 5 (7) e003519.
- [151] Lee, Y.; Choi, S. Q.: Quantitative analysis for lipophilic drug transport through a model lipid membrane with membrane retention; *Eur J Pharm Sci.* **2019** 134 176–184.
- [152] Lipinski, C. A.; Lombardo, F.; Dominy, B. W.; Feeney, P. J.: Experimental and computational approaches to estimate solubility and permeability in drug discovery and development settings; *Adv Drug Deliv Rev.* **1997** 23 (1-3) 3–25.



- [153] Johnson, T. W.; Gallego, R. A.; Edwards, M. P.: Lipophilic efficiency as an important metric in drug design; *J Med Chem.* **2018** 61 (15) 6401–6420.
- [154] Homan, K. T.; Waldschmidt, H. V.; Glukhova, A.; Cannavo, A.; Song, J.; Cheung, J. Y.; Koch, W. J.; Larsen, S. D.; Tesmer, J. J.: Crystal Structure of G Protein-coupled Receptor Kinase 5 in Complex with a Rationally Designed Inhibitor; *J Biol Chem.* **2015** 290 (34) 20649–20659.
- [155] Knowlton, A. A.; Le Chen; Malik, Z. A.: Heart failure and mitochondrial dysfunction: the role of mitochondrial fission/fusion abnormalities and new therapeutic strategies; *J Cardiovasc Pharmacol.* **2014** 63 (3) 196–206.
- [156] Doenst, T.; Nguyen, T. D.; Abel, E. D.: Cardiac metabolism in heart failure: implications beyond ATP production; *Circ Res.* **2013** 113 (6) 709–724.
- [157] Ritterhoff, J.; Tian, R.: Metabolism in cardiomyopathy: every substrate matters; *Cardiovasc Res.* **2017** 113 (4) 411–421.
- [158] Intlekofer, A. M.; Dematteo, R. G.; Venneti, S.; Finley, L. W.; Lu, C.; Judkins, A. R.; Rustenburg, A. S.; Grinaway, P. B.; Chodera, J. D.; Cross, J. R.; Thompson, C. B.: Hypoxia induces production of L-2-hydroxyglutarate; *Cell Metab.* **2015** 22 (2) 304–311.
- [159] Oldham, W. M.; Clish, C. B.; Yang, Y.; Loscalzo, J.: Hypoxia-mediated increases in L-2-hydroxyglutarate coordinate the metabolic response to reductive stress; *Cell Metab.* **2015** 22 (2) 291–303.
- [160] Rzem, R.; van Schaftingen, E.; Veiga-da-Cunha, M.: The gene mutated in L-2-hydroxyglutaric aciduria encodes L-2-hydroxyglutarate dehydrogenase; *Biochimie.* **2006** 88 (1) 113–116.
- [161] Fu, X.; Chin, R. M.; Vergnes, L.; Hwang, H.; Deng, G.; Xing, Y.; Pai, M. Y.; Li, S.; Ta, L.; Fazlollahi, F.; Chen, C.; Prins, R. M.; Teitell, M. A.; Nathanson, D. A.; Lai, A.; Faull, K. F.; Jiang, M.; Clarke, S. G.; Cloughesy, T. F.; Graeber, T. G.; Braas, D.; Christofk, H. R.; Jung, M. E.; Reue, K.; Huang, J.: 2-hydroxyglutarate inhibits ATP synthase and mTOR signaling; *Cell Metab.* **2015** 22 (3) 508–515.
- [162] Linster, C. L.; van Schaftingen, E.; Hanson, A. D.: Metabolite damage and its repair or pre-emption; *Nat Chem Biol.* **2013** 9 (2) 72–80.
- [163] Du, X.; Hu, H.: The roles of 2-Hydroxyglutarate; *Front Cell Dev Biol.* **2021** 9 651317.
- [164] Carboneau, M.; M Gagné, L.; Lalonde, M.-E.; Germain, M.-A.; Motorina, A.; Guiot, M.-C.; Secco, B.; Vincent, E. E.; Tumber, A.; Hulea, L.; Bergeman, J.; Oppermann, U.; Jones, R. G.; Laplante, M.; Topisirovic, I.; Petrecca, K.; Huot, M.-É.; Mallette, F. A.: The oncometabolite 2-hydroxyglutarate activates the mTOR signalling pathway; *Nat Commun.* **2016** 7 12700.

- [165] An, D.; Zeng, Q.; Zhang, P.; Ma, Z.; Zhang, H.; Liu, Z.; Li, J.; Ren, H.; Xu, D.: Alpha-ketoglutarate ameliorates pressure overload-induced chronic cardiac dysfunction in mice; *Redox Biol.* **2021** *46* 102088.
- [166] He, H.; Mulhern, R. M.; Oldham, W. M.; Xiao, W.; Lin, Y.-D.; Liao, R.; Loscalzo, J.: L-2-Hydroxyglutarate Protects Against Cardiac Injury via Metabolic Remodeling; *Circ Res.* **2022** *131* (7) 562–579.
- [167] Lin, Z.-R.; Li, Z.-Z.; Cao, Y.-J.; Yu, W.-J.; Ye, J.-T.; Liu, P.-Q.: GDH promotes isoprenaline-induced cardiac hypertrophy by activating mTOR signaling via elevation of  $\alpha$ -ketoglutarate level; *Naunyn Schmiedebergs Arch Pharmacol.* **2022** *395* (11) 1373–1385.
- [168] Ding, L.; Kamlage, B.; Rangrez, A.; Rennefahrt, U.; Folberth, J.; Ternes, P.; Schatz, P.; Hille, S.; Heckmann, M.; Jungmann, A.; Rapti, K.; Ruf, T.; Li, X.; Weis, T.; Meder, B.; Schwaninger, M.; Frank, D.; Katus, H. A.; Frey, N.; Remes, A.; Müller, O. J.: L-2-hydroxyglutarate dehydrogenase is a novel metabolic target protecting from cardiac remodeling and heart failure; *in preparation*.
- [169] Gross, M. I.; Demo, S. D.; Dennison, J. B.; Chen, L.; Chernov-Rogan, T.; Goyal, B.; Janes, J. R.; Laidig, G. J.; Lewis, E. R.; Li, J.; Mackinnon, A. L.; Parlati, F.; Rodriguez, M. L.; Shwonek, P. J.; Sjogren, E. B.; Stanton, T. F.; Wang, T.; Yang, J.; Zhao, F.; Bennett, M. K.: Antitumor activity of the glutaminase inhibitor CB-839 in triple-negative breast cancer; *Mol Cancer Ther.* **2014** *13* (4) 890–901.
- [170] Li, L.; Meng, Y.; Li, Z.; Dai, W.; Xu, X.; Bi, X.; Bian, J.: Discovery and development of small molecule modulators targeting glutamine metabolism; *Eur J Med Chem.* **2019** *163* 215–242.
- [171] Katt, W. P.; Lukey, M. J.; Cerione, R. A.: A tale of two glutaminases: homologous enzymes with distinct roles in tumorigenesis; *Future Med Chem.* **2017** *9* (2) 223–243.
- [172] Xu, X.; Meng, Y.; Li, L.; Xu, P.; Wang, J.; Li, Z.; Bian, J.: Overview of the development of glutaminase inhibitors; *J Med Chem.* **2019** *62* (3) 1096–1115.
- [173] Ramachandran, S.; Pan, C. Q.; Zimmermann, S. C.; Duvall, B.; Tsukamoto, T.; Low, B. C.; Sivaraman, J.: Structural basis for exploring the allosteric inhibition of human kidney type glutaminase; *Oncotarget.* **2016** *7* (36) 57943–57954.
- [174] Soth, M. J.; Le, K.; Di Francesco, M. E.; Hamilton, M. M.; Liu, G.; Burke, J. P.; Carroll, C. L.; Kovacs, J. J.; Bardenhagen, J. P.; Bristow, C. A.; Cardozo, M.; Czako, B.; Stanchina, E. de; Feng, N.; Garvey, J. R.; Gay, J. P.; Do, M. K.; Greer, J.; Han, M.; Harris, A.; Herrera, Z.; Huang, S.; Giuliani, V.; Jiang, Y.; Johnson, S. B.; Johnson, T. A.; Kang, Z.; Leonard, P. G.; Liu, Z.; McAfoos, T.; Miller, M.; Morlacchi, P.; Mullinax, R. A.; Palmer, W. S.; Pang, J.; Rogers, N.; Rudin, C. M.; Shepard, H. E.; Spencer, N. D.; Theroff, J.; Wu, Q.; Xu, A.; Yau, J. A.; Draetta, G.; Toniatti, C.; Heffernan, T. P.; Jones,

- P.: Discovery of IPN60090, a clinical stage selective glutaminase-1 (GLS-1) inhibitor with excellent pharmacokinetic and physicochemical properties; *J Med Chem.* **2020** 63 (21) 12957–12977.
- [175] Lee, C.-H.; Motzer, R.; Enamekhoo, H.; Matrana, M.; Percent, I.; Hsieh, J. J.; Hussain, A.; Vaishampayan, U.; Liu, S.; McCune, S.; Patel, V.; Shaheen, M.; Bendell, J.; Fan, A. C.; Gartrell, B. A.; Goodman, O. B.; Nikolinakos, P. G.; Kalebasty, A. R.; Zakharia, Y.; Zhang, Z.; Parmar, H.; Akella, L.; Orford, K.; Tannir, N. M.: Telaglenastat plus everolimus in advanced renal cell carcinoma: a randomized, double-blinded, placebo-controlled, phase II ENTRATA trial; *Clin Cancer Res.* **2022** 28 (15) 3248–3255.
- [176] Wang, J.-B.; Erickson, J. W.; Fuji, R.; Ramachandran, S.; Gao, P.; Dinavahi, R.; Wilson, K. F.; Ambrosio, A. L.; Dias, S. M.; Dang, C. V.; Cerione, R. A.: Targeting mitochondrial glutaminase activity inhibits oncogenic transformation; *Cancer Cell.* **2010** 18 (3) 207–219.
- [177] Han, T.; Guo, M.; Zhang, T.; Gan, M.; Xie, C.; Wang, J.-B.: A novel glutaminase inhibitor-968 inhibits the migration and proliferation of non-small cell lung cancer cells by targeting EGFR/ERK signaling pathway; *Oncotarget.* **2017** 8 (17) 28063–28073.
- [178] Cederkvist, H.; Kolan, S. S.; Wik, J. A.; Sener, Z.; Skålhegg, B. S.: Identification and characterization of a novel glutaminase inhibitor; *FEBS Open Bio.* **2022** 12 (1) 163–174.
- [179] Bröer, A.; Fairweather, S.; Bröer, S.: Disruption of amino acid homeostasis by novel ASCT2 inhibitors involves multiple targets; *Front Pharmacol.* **2018** 9 785.
- [180] Xu, L.; Yin, Y.; Li, Y.; Chen, X.; Chang, Y.; Zhang, H.; Liu, J.; Beasley, J.; McCaw, P.; Zhang, H.; Young, S.; Groth, J.; Wang, Q.; Locasale, J. W.; Gao, X.; Tang, D. G.; Dong, X.; He, Y.; George, D.; Hu, H.; Huang, J.: A glutaminase isoform switch drives therapeutic resistance and disease progression of prostate cancer; *Proc Natl Acad Sci U S A.* **2021** 118 (13) e2012748118.
- [181] Shukla, K.; Ferraris, D. V.; Thomas, A. G.; Stathis, M.; Duvall, B.; Delahanty, G.; Alt, J.; Rais, R.; Rojas, C.; Gao, P.; Xiang, Y.; Dang, C. V.; Slusher, B. S.; Tsukamoto, T.: Design, synthesis, and pharmacological evaluation of bis-2-(5-phenylacetamido-1,2,4-thiadiazol-2-yl)ethyl sulfide 3 (BPTES) analogs as glutaminase inhibitors; *J Med Chem.* **2012** 55 (23) 10551–10563.
- [182] Ternyila, D.: FDA grants CB-839 fast track designation for mRCC; *Targeted Oncology.* **May 3 2018.**
- [183] Fort, D. G.; Herr, T. M.; Shaw, P. L.; Gutzman, K. E.; Starren, J. B.: Mapping the evolving definitions of translational research; *J Clin Transl Sci.* **2017** 1 (1) 60–66.
- [184] Mudd, T. W.; Khalid, M.; Guddati, A. K.: Cardiotoxicity of chemotherapy and targeted agents; *Am J Cancer Res.* **2021** 11 (4) 1132–1147.

- [185] Johnson, C. B.; Davis, M. K.; Law, A.; Sulpher, J.: Shared risk factors for cardiovascular disease and cancer: implications for preventive health and clinical care in oncology patients; *Can J Cardiol.* **2016** 32 (7) 900–907.
- [186] Kadowaki, H.; Akazawa, H.; Shindo, A.; Ueda, T.; Ishida, J.; Komuro, I.: Shared and reciprocal mechanisms between heart failure and cancer - an emerging concept of heart-cancer axis; *Circ J.* **2024** 88 (2) 182–188.
- [187] Zhang, C.; Cheng, Y.; Luo, D.; Wang, J.; Liu, J.; Luo, Y.; Zhou, W.; Zhuo, Z.; Guo, K.; Zeng, R.; Yang, J.; Sha, W.; Chen, H.: Association between cardiovascular risk factors and colorectal cancer: a systematic review and meta-analysis of prospective cohort studies; *EClinicalMedicine.* **2021** 34 100794.
- [188] Boer, R. A. de; Hulot, J.-S.; Tocchetti, C. G.; Aboumsallem, J. P.; Ameri, P.; Anker, S. D.; Bauersachs, J.; Bertero, E.; Coats, A. J.; Čelutkienė, J.; Chioncel, O.; Dodion, P.; Eschenhagen, T.; Farmakis, D.; Bayes-Genis, A.; Jäger, D.; Jankowska, E. A.; Kitsis, R. N.; Konety, S. H.; Larkin, J.; Lehmann, L.; Lenihan, D. J.; Maack, C.; Moslehi, J. J.; Müller, O. J.; Nowak-Sliwinska, P.; Piepoli, M. F.; Ponikowski, P.; Pudil, R.; Rainer, P. P.; Ruschitzka, F.; Sawyer, D.; Seferovic, P. M.; Suter, T.; Thum, T.; van der Meer, P.; van Laake, L. W.; Haehling, S. von; Heymans, S.; Lyon, A. R.; Backs, J.: Common mechanistic pathways in cancer and heart failure. A scientific roadmap on behalf of the Translational Research Committee of the Heart Failure Association (HFA) of the European Society of Cardiology (ESC); *Eur J Heart Fail.* **2020** 22 (12) 2272–2289.
- [189] Kazemi-Bajestani, S. M.; Becher, H.; Fassbender, K.; Chu, Q.; Baracos, V. E.: Concurrent evolution of cancer cachexia and heart failure: bilateral effects exist; *J Cachexia Sarcopenia Muscle.* **2014** 5 (2) 95–104.
- [190] Murphy, K. T.: The pathogenesis and treatment of cardiac atrophy in cancer cachexia; *Am J Physiol Heart Circ Physiol.* **2016** 310 (4) H466-77.
- [191] Meijers, W. C.; Maglione, M.; Bakker, S. J.; Oberhuber, R.; Kieneker, L. M.; Jong, S. de; Haubner, B. J.; Nagengast, W. B.; Lyon, A. R.; van der Vegt, B.; van Veldhuisen, D. J.; Westenbrink, B. D.; van der Meer, P.; Silljé, H. H.; Boer, R. A. de: Heart failure stimulates tumor growth by circulating factors; *Circulation.* **2018** 138 (7) 678–691.
- [192] Kenzik, K. M.; Balentine, C.; Richman, J.; Kilgore, M.; Bhatia, S.; Williams, G. R.: New-onset cardiovascular morbidity in older adults with stage I to III colorectal cancer; *J Clin Oncol.* **2018** 36 (6) 609–616.
- [193] van der Valk, J.; Brunner, D.; Smet, K. de; Fex Svenningsen, A.; Honegger, P.; Knudsen, L. E.; Lindl, T.; Noraberg, J.; Price, A.; Scarino, M. L.; Gstraunthaler, G.: Optimization of chemically defined cell culture media-replacing fetal bovine serum in mammalian *in vitro* methods; *Toxicol In Vitro.* **2010** 24 (4) 1053–1063.

- [194]** Anker, M. S.; Rassaf, T.; Zamorano, J. L.; Khan, M. S.; Landmesser, U.: Cardiac wasting and cancer; *Eur Heart J.* **2024** *45* (34) 3135–3137.
- [195]** Sudoh, T.; Kangawa, K.; Minamino, N.; Matsuo, H.: A new natriuretic peptide in porcine brain; *Nature.* **1988** *332* (6159) 78–81.

## **Erklärung zu §8 der Promotionsordnung**

Hiermit erkläre ich, dass ich die vorliegende Dissertation – abgesehen von der fachlichen Beratung durch meinen Betreuer – selbstständig und ausschließlich unter Verwendung der angegebenen Hilfsmittel angefertigt habe. Sie beruht auf eigenständigen wissenschaftlichen Leistungen und wurde unter Beachtung der Regeln guter wissenschaftlicher Praxis der Deutschen Forschungsgemeinschaft erstellt.

Ich versichere ferner, dass mir bislang kein akademischer Grad entzogen wurde und dass diese Arbeit weder vollständig noch in Teilen bereits im Rahmen eines anderen Prüfungsverfahrens eingereicht wurde oder dort vorgelegen hat.

---

Pia Steinkuhl